

**Brønsted Acid-initiated Formal [1,3]-Rearrangement
Reaction of β -Substituted Ene-Aldimines**

ブレンステッド酸を開始剤とする
 β 置換エン-アルジミンの形式的[1,3]-転位反応

Chanantida JONGWOHAN

SOKENDAI

(The Graduate University for Advanced Studies)

**School of Physical Sciences
Department of Functional Molecular Science**

TABLE OF CONTENTS

ACKNOWLEDGMENTS.....	vi
LIST OF SCHEMES.....	viii
LIST OF TABLES.....	xii
LIST OF FIGURES.....	xiv
LIST OF ABBREVIATIONS.....	xvi

CHAPTER 1. GENERAL INTRODUCTION

1.1	Introduction: Homoallylic amines.....	1
1.2	Regioselective synthesis of homoallylic amines.....	1
1.2.1	Addition reaction of allyl metal reagents to imines.....	2
1.2.2	Sigmatropic rearrangement reaction of ene-imines.....	5
1.2.3	Discovery of Brønsted acid-initiated formal [1,3]- rearrangement reaction of ene-aldimines.....	7
1.3	Scope of this thesis.....	8
1.4	References.....	12

CHAPTER 2. BRØNSTED ACID-INITIATED REARRANGEMENT

REACTION OF ENE-ALDIMINES FOR CONSTRUCTION OF 2,4,4-SUBSTITUTED HOMOALLYLIC AMINES

2.1.	Introduction.....	14
2.2	Brønsted acid-initiated rearrangement reaction of ene-aldimines.....	14
2.2.1	Reaction optimization under normal heating method.....	14
2.2.2	Reaction optimization by the use of microwave reactor.....	18
2.2.3	Reaction scope.....	20
2.2.4	Utilities of formal [1,3]-rearrangement products.....	20
2.3	Conclusion.....	21
2.4	Experimental sections.....	22

2.4.1	General method	22
2.4.2	Procedure of rearrangement reaction of ene-aldimines.....	22
2.4.3	Characterization of rearrangement products	23
2.4.4	Procedure and characterization of derivatives	28
2.4.5	Synthesis and characterization of starting materials	34
2.5	References	41

**CHAPTER 3. MECHANISTIC STUDIES ON BRØNSTED ACID-INITIATED
REARRANGEMENT REACTION OF ENE-ALDIMINES**

3.1	Introduction	42
3.2	Crossover experiment studies.....	42
3.2.1	Crossover experiment study of substrates	42
3.2.2	Crossover experiment study of products	43
3.3	Speculation of reaction mechanism	43
3.4	Experimental and computational studies for generation of 2-azaallenium cation	44
3.4.1	Experimental study on the effect of the 2-OH of aryl group on benzylidene	44
3.4.2	Computational study for structure of 2-azaallenium cation	44
3.4.3	Conformation and stability of ene-aldimine substrates.....	45
3.4.4	DFT calculation of 2-azania-[3,3]-sigmatopic rearrangement	46
3.5	Proposed chain reaction mechanism.....	47
3.5.1	Proposed mechanism in initiation step.....	47
3.5.2	Proposed mechanism in propagation step	47
3.5.3	Experimental study using model ene-aldimine substrate	48
3.5.4	Computation and discussion for initiation step.....	49
3.5.5	Computation and discussion for propagation step	51
3.6	Conclusion.....	57

3.7	Experimental sections	57
3.7.1	General method	57
3.7.2	Procedure and characterization of crossover experiments	58
3.7.3	Procedure and characterization of starting materials	60
3.7.4	DFT calculation.....	61
3.8	References	63

CHAPTER 4. BRØNSTED ACID-INITIATED ASYMMETRIC

REARRANGEMENT REACTION OF CHIRAL ENE-ALDIMINES

4.1	Introduction	65
4.2	Design and synthesis of chiral substrates.....	65
4.2.1	<i>E</i> -Olefin substrates	65
4.2.2	<i>Z</i> -Olefin substrates	67
4.3	Chirality transfer studies	69
4.4	Proposed mechanism	71
4.5	Conclusion.....	74
4.6	Experimental sections	74
4.6.1	Procedure and characterization of chirality transfer experiments	74
4.6.2	Procedure and characterization of starting materials	77
4.7	References	94

CHAPTER 5. CATALYTIC ASYMMETIC FORMAL [1,3]-REARRANGEMENT OF ENE-ALDIMINE INITIATED BY CHIRAL BRØNSTED ACID

5.1	Introduction	95
5.2	Catalytic asymmetric formal [1,3]-rearrangement initiated by (1 <i>S</i>)-(+)-10-champhorsulfonic acid	96
5.3	Catalytic asymmetric formal [1,3]-rearrangement initiated by	

(<i>R</i>)-BINOL-derived phosphoric acid	97
5.3.1 Substituent effect at the 3,3'-position of chiral phosphoric acid	98
5.3.2 Reaction optimization in the presence of chiral phosphoric acid	99
5.3.3 Screening of (<i>R</i>)-BINOL-derived phosphoric acids.....	100
5.3.4 Catalyst loading of (<i>R</i>)-BINOL phosphoric acid	102
5.4 Mechanistic consideration in interaction mode.....	102
5.4.1 Substituents effect of benzylidene unit.....	103
5.4.2 Absolute configuration of the ene-aldimine product.....	104
5.4.3 Proposed transition state.....	106
5.5 Conclusion.....	107
5.6 Experimental sections	107
5.6.1 General method.....	107
5.6.2 Procedure for catalytic asymmetric rearrangement reaction of ene-aldimines.....	108
5.6.3 Characterization of rearrangement products.....	108
5.6.4 Procedure and characterization of derivatives	109
5.7 References	114

CHAPTER 6. SUMMARY AND PERSPECTIVES

6.1 Summary	115
6.2 Perspectives.....	118

APPENDIX

A. NMR charts	119
B. DFT calculation Table	183
C. Crystal data reports	191

ACKNOWLEDGEMENT

This thesis summarizes my Ph.D. research from April 2016 to September 2019 at the Department of Functional Molecular Science, School of Physical Sciences, The SOKENDAI (Graduate University for Advanced Studies) under the supervision of Dr. Norie Momiyama, Associate Professor of SOKENDAI.

First and foremost, I would like to express the deepest gratitude to my supervisor Associate Professor Norie Momiyama for her patience, guidance, encouragement, immense knowledge, and continuous support of my research.

Besides my supervisor, I would like to thank the rest of my thesis committee: Professor Yasuhiro Uozumi, Professor Masahiro Ehara, Associate professor Toshiyasu Suzuki, and Professor Masaharu Nakamura (Kyoto University), not only for their insightful comments and encouragement, but also for the hard questions which incited me to widen my research from various perspectives.

I would like to sincerely thank Associate Professor Toshiyasu Suzuki, Dr. Yasushi Honda (West-Japan Office, HPC SYSTEMS, Inc.), and Mr. Kiyohiro Adachi (the University of Tokyo) for collaborative studies in mechanistic studies, which are part of my research. I have learned a lot and always motivated by their spirit of enthusiasm and professionalism in pursuing scientific research. This thesis would not have been possible without their support.

My sincere thanks also go to current members and alumni of Momiyama group, Dr. Takeshi Fujinami, Dr. Naoya Ohtsuka, Mr. Tatsuaki Hori, Mr. Yuto Sugahara, Mr. Shunya Oishi, Ms. Hino Ota, and Mr. Masayuki Kato, Assistant Professor Atsuto Izumiseki, Dr. Katsunori Yamanishi, Dr. Akina Yoshizawa, Mr. Taku Watanabe, Mr. Fumio Nakashima, and Mr. Yu Masui for their warm friendship and precious and stimulating discussion. I appreciate the kind help from secretary, Ms. Yoko Watanabe, for administrative works. I wish to thank Ms. Pawittra Chaibuth and Dr. Warothon Paisuwan (Chulalongkorn University) for the collaborative work and friendship from the short-term visitors.

I would like to thank Professor Shigeyuki Masaoka (Osaka University), Assistant Professor Mio Kondo, Associate Professor Shuhei Higashibayashi (Keio University), Assistant Professor Takuya Kurahashi, Assistant Professor Koji Yamamoto (Gunma University), other members as well as invited speakers for the fruitful discussion during the joint seminar in the first two years.

I appreciate for the help from the Graduate Student Affairs Section, Ms. Shinobu Okuda, Ms. Akiko Kabeya, and Ms. Makiko Tanaka. I would like to thank IMS instrument center for mass analysis of chemical compounds in this research, as well as Uozumi group for research facilities.

I would like to thank for the financial support from IMS RA, FRA, and JASSO scholarship throughout my Ph.D. study.

I very appreciate the invaluable friendship from my international friends, Dr. Lee Sze Koon, Mr. Ruan De Villiers, Ms. Zlata Polyakova, Dr. Haruko Miura, Dr. Matthias Meißner, Dr. Yousef Yari Kamrani, Dr. Reinhard Peter Kaiser, and Mr. Benjamin Cagnon, for supporting and accompany though all my life in general during my stay in Japan. I thank to my Thai's friends including my housemate Ms. Methanee Hiranyakorn, Dr. Tianchai Chooppawa, Mr. Akasit Visootsat, and Ms. Wiyada Saenawa, for all the fun we have had in the last few years.

Last but not least, I would like to thank for the mental care, support, and encouragement from my family and crucial persons in my life, Mr. Thus La-ongnuan, Mr. Mark Kilby, Mr. Sattawat Dueansawang, Ms. Napaporn Janseeta, Ms. Jariya Nonsing, Ms. Sujitra Bootdama, and Ms. Wiphawadee Krutin.

LIST OF SCHEMES

Chapter 1

Scheme 1.	Synthesis of 1,2-substituted homoallylic amines using allyl metal reagents	2
Scheme 2.	Stereoselective 1,2-substituted homoallylic amines by allylation of imines with chiral allyl silanes	2
Scheme 3.	Synthesis of homoallylic amines by the reaction of aldehyde-derived imines with allyl silane.....	3
Scheme 4.	(<i>R</i>)-DIFLUOROPHOS·AgF complex-catalyzed crotylation reaction to synthesize 1,2-substituted homoallylic amino compounds	3
Scheme 5.	Chiral Brønsted acid-catalyzed crotylation reaction of imines with crotyl trimethyl silanes	3
Scheme 6.	Synthesis of 1,2,2- and 1,4,4-substituted homoallylic amines by allylic barium reagents	4
Scheme 7.	Synthesis of 1,4,4-substituted homoallylic amines by allyl zinc reagent.....	5
Scheme 8.	2-Azonia-[3,3]-sigmatropic rearrangement of chiral ene-iminiums.....	6
Scheme 9.	Brønsted acid-catalyzed Aza-Cope rearrangement of α - and β -substituted chiral ene-imine	6
Scheme 10.	2-Azonia-[3,3]-sigmatropic rearrangement of branched homoallylic nitrones.....	7
Scheme 11.	Discovery of Brønsted acid-initiated formal [1,3]-rearrangement reaction of ene-aldimines	8
Scheme 12.	Development of formal [1,3]-rearrangement of β -substituted ene-aldimines to synthesize 2,4,4-substituted homoallylic amines.....	9
Scheme 13.	Crossover experiments of substrates, and products.....	10
Scheme 14.	Asymmetric formal [1,3]-rearrangement of chiral ene-aldimines with tetrahydronaphthalene unit at the β -position.....	11
Scheme 15.	Catalytic asymmetric formal [1,3]-rearrangement of ene-aldimine Promoted by chiral Brønsted acid.....	12

Chapter 2

Scheme 1.	Reproducibility and potential utilities of the formal [1,3]-rearrangement reaction of β -dimethyl- and β -diphenyl-substituted ene-aldimines	14
Scheme 2.	Synthesis and preparation of ene-aldimine substrate.....	15
Scheme 3.	Synthesis of 2,4,4-substituted homoallylic amines.....	21
Scheme 4.	Synthesis of aza-spiro compound	21
Scheme 5.	Synthesis of β -amino acid precursor.....	21
Scheme 6.	Reaction of new rearrangement and derivatization	28
Scheme 7.	Synthesis of (<i>E</i>)- <i>tert</i> -butyl (2,2-alkyl or 2-cycloalkyl pent-3-en-1-yl)carbamate starting material.....	34
Scheme 8.	Synthesis of (<i>E</i>)- <i>tert</i> -butyl (2,2-phenyl pent-3-en-1-yl)carbamate starting material	37
Scheme 9.	Synthesis of (<i>Z</i>)- <i>tert</i> -butyl-(2,2-dialkyl or 2-cycloalkyl alk-3-ene-1-yl) carbamate	38

Chapter 3

Scheme 1.	Crossover experiment of substrates	43
Scheme 2.	Crossover experiment of products	43
Scheme 3.	Formal [1,3]-rearrangement reaction of ene-aldimine possessing no methyl group at the terminal olefin	44
Scheme 4.	Experimental studies on β -substituents of ene-aldimine substrate under normal heating condition. (a) Comparison of cyclohexyl with methyl group, (b) examination of benzaldehyde-derived β -cyclohexyl ene-aldimine.	49
Scheme 5.	Synthesis of deuterated substrates d^2 -(<i>E</i>)- 1a	60

Chapter 4

Scheme 1.	Synthesis of (<i>S,E</i>)- and (<i>R,E</i>)- 1 chiral substrates.....	66
Scheme 2.	Protection of (<i>E</i>)- 4 and determination of absolute configurations	67
Scheme 3.	Synthesis of (<i>S,Z</i>)- and (<i>R,Z</i>)- R1 chiral substrates	68
Scheme 4.	Synthesis of optically pure derivatives (<i>Z</i>)- 2	68
Scheme 5.	Hydrogenation reaction of (<i>S,E</i>)- 2 to hydrogenated (<i>R</i>)- 3	69
Scheme 6.	Hydrogenation reaction of protected (<i>R,Z</i>)- 2 to give hydrogenated product (<i>S</i>)- 3	69
Scheme 7.	Asymmetric formal [1,3]-rearrangements of (<i>E</i>)-chiral ene-aldimines.....	69
Scheme 8.	Derivatization of chirality transfer products (<i>S,E</i>)- 4 and (<i>R,E</i>)- 4	70
Scheme 9.	Asymmetric formal [1,3]-rearrangements of (<i>Z</i>)-chiral ene-aldimines	71
Scheme 10.	Synthesis of (<i>E</i>)-chiral substrates	77
Scheme 11.	Synthesis of (<i>Z</i>)-chiral substrates	82
Scheme 12.	Synthesis of (<i>R,Z</i>)- 6 and (<i>S,Z</i>)- 6 substrates.....	85

Chapter 5

Scheme 1.	Asymmetric formal [1,3]-rearrangement of chiral substrate.....	95
Scheme 2.	Enantioselective synthesis of homoallylic amines promoted by chiral Brønsted acid	95
Scheme 3.	Hydrolysis and optical resolution of rearrangement product 2a	105
Scheme 4.	Protection of (<i>S</i>)- 3a for determination of retention time	105
Scheme 5.	Protection of (<i>S</i>)- and (<i>R</i>)- 3a and determination of absolute configurations	105
Scheme 6.	Reaction of formal [1,3]-rearrangement of ene-aldimine and derivatization.....	108
Scheme 7.	Derivatization of formal [1,3]-rearrangement product	109

Chapter 6

Scheme 1.	Rearrangement reaction of ene-imine. (a) General design in previous reports, (b) our design of β -substituted ene-alimine substrate and our discovery of formal [1,3]-rearrangement.....	115
Scheme 2.	Development of formal [1,3]-rearrangement of β -substituted ene-aldimines to synthesize 2,4,4-substituted homoallylic amines....	116
Scheme 3.	Crossover experiment of (a) substrates (b) products	117
Scheme 4.	Asymmetric formal [1,3]-rearrangement of chiral ene-aldimines with tetrahydronaphthalene unit at the β -position	118
Scheme 5.	Enantioselective formal [1,3]-rearrangement of ene-alimine promoted by chiral Brønsted acid.....	118

LIST OF TABLES

Chapter 2

Table 1.	Study of electronic effects on benzylidene unit	16
Table 2.	Solvent screening.....	16
Table 3.	Study on temperature and catalyst loading under normal heating.....	17
Table 4.	Screening of Brønsted acid	17
Table 5.	Reactions with (±)-CSA and TFA catalysts in microwave reactor	18
Table 6.	Optimization of reaction condition under microwave reactor.....	19
Table 7.	Applicability of Brønsted acid under microwave condition	19

Chapter 3

Table 1.	N1-OH and its isomer	61
Table 2.	R1 and P1	61
Table 3.	Initiation step.....	61
Table 4.	Propagation step in Path A	61
Table 5.	TS10 in the propagation step in Path B	62
Table 6.	TS11 in the propagation step in Path B	62
Table 7.	<i>Syn</i> -pathway of the propagation step in Path B	62
Table 8.	<i>Anti</i> -pathway of the propagation step in Path B	62
Table 9.	H1–N and C1–N distances (Å) between N1 and R1 in TS10-syn	63

Chapter 5

Table 1.	Catalytic asymmetric formal [1,3]-rearrangement initiated by (+)-CSA	97
Table 2.	Substituent effect of chiral phosphoric acid.....	98
Table 3.	Reaction optimization in the presence of (<i>R</i>)-BINOL-derived phosphoric acid B-3	99
Table 4.	Electronic effect of BINOL Brønsted acids	100

Table 5.	Catalyst loading studies	102
Table 6.	Electronic and steric effects on benzylidene unit	103

LIST OF FIGURES

Chapter 1

- Figure 1. Homoallylic amines for synthesis of nitrogen-containing compounds 1
- Figure 2. Brønsted acid-catalyzed Aza-Cope rearrangement of ene-imines and ene-aldimines 7

Chapter 2

- Figure 1. Substrate scope of (*E*)- and (*Z*)-ene-aldimine 20

Chapter 3

- Figure 1. Intermolecular reaction *via* generation of 2-azaallenium cation 43
- Figure 2. Conformational stability of 2-azaallenium and *o*-quinonoid 45
- Figure 3. DFT calculations for conformational stabilities of (a) ene-aldimine substrate (**R1**), (b) protonated ene-aldimine substrate (**R1-H⁺**) 46
- Figure 4. Concerted chair transition state in 2-azonia-[3,3]-sigmatropic rearrangement under protonation, (a) α -substituted ene-imine, (b) β -substituted ene-aldimine (**R1**) 47
- Figure 5. Proposed mechanism in initiation step in chain reaction mechanism 47
- Figure 6. Proposed mechanism in propagation step 48
- Figure 7. Free energy diagram for the initiation steps 50
- Figure 8. DFT calculation of reaction pathway of initiation step. (a) initiation, (b) optimized geometries for the initiation step 50
- Figure 9. Free energy diagram for the initiation and propagation steps;

	(a) Path A , (b) Path B	51
Figure 10.	DFT calculation of reaction pathway for propagation step in Path A . (a) Propagation step; (b) optimized geometries	52
Figure 11.	DFT calculation of the <i>syn</i> -pathway in Path B , (a) The <i>syn</i> -pathway of the propagation step from R1 (<i>1b</i>); (b) optimized geometries for the propagation steps of the <i>syn</i> -pathway	55
Figure 12.	DFT calculation of the <i>anti</i> -pathway in Path B	56
Figure 13.	¹ H NMR chart of crossover experiment of substrates from 8.50 ppm to 4.50 ppm.....	59
Figure 14.	¹ H NMR chart of crossover experiment of products from 8.50 ppm to 4.50 ppm.....	59

Chapter 4

Figure 1.	Design of chiral substrates	65
Figure 2.	ORTEP diagram of derivatized rearrangement products.....	70
Figure 3.	DFT calculation for azonia-[3,3]-sigmatropic rearrangement step in asymmetric formal [1,3]-rearrangement of (<i>R,E</i>)- 1 substrate	72
Figure 4.	DFT calculation for azonia-[3,3]-sigmatropic rearrangement step in asymmetric formal [1,3]-rearrangement of (<i>R,Z</i>)- 1 substrate	72
Figure 5.	Plausible mechanisms of ene-aldimine rearrangement reaction	74
Figure 6.	ORTEP diagram of (<i>R,Z</i>)- 2 substrate by Sponge X-ray analysis.....	91

Chapter 5

Figure 1.	Working hypothesis of catalytic asymmetric formal [1,3]-rearrangement by chiral counteranion.....	96
Figure 2.	Interaction mode in transition state for (a) (<i>S</i>)-product, (b) (<i>R</i>)-product.....	106
Figure 3.	Proposed transition state of substituent at 4- and 5-position on benzylidene unit	107

LIST OF ABBREVIATIONS

Ar	aryl
aq	Aqua
BINOL	binaphthol
Bn	benzyl
Boc	<i>tert</i> -butoxycarbonyl
<i>n</i> -Bu	normal butyl
<i>t</i> -Bu	tertiary butyl
cat.	catalyst
Cp	cyclopentadienyl
DCM	dichloromethane
DCE	dichloroethane
DMPU	1,3-Dimethyl-3,4,5,6-tetrahydro-2(1H)-pyrimidinone
DMF	dimethylformamide
DMSO	dimethylsulfoxide
ee	enantiomeric excess
Et	ethyl
EtOAc	ethyl acetate
h	hour
HPLC	high-performance liquid chromatography
Hz	Herz
LDA	lithium diisopropylamide
M	molar
MS	molecular sieve
Me	methyl
min	minute
NMR	nuclear magnetic resonance
Ph	phenyl

<i>i</i> -Pr	<i>iso</i> propyl
Py	pyridine
rt	room temperature
R _t	retention time
Tf	trifluoromethanesulfonyl
TFA	trifluoroacetic acid
THF	tetrahydrofuran
TLC	thin layer chromatography
Ts	<i>p</i> -toluenesulfonyl
TS	transition state

CHAPTER 1

GENERAL INTRODUCTION

1.1 Introduction: Homoallylic amines

Homoallylic amines have been known as key precursors in the synthesis of natural products and nitrogen heterocycles,¹⁻³ because amino allylic moiety is readily converted into functionally useful compounds (Figure 1). For example, γ -amino carboxylic acids were synthesized from homoallylic amines as intermediates *via* hydroboration with $\text{BH}_3\cdot\text{SMe}_2$, oxidation by the use of alkaline H_2O_2 , protection with *tert*-butyl decarbonate, and oxidation in final step.⁴ Anti-Markovnikov hydroamination reaction of homoallylic amines gave diamines in the presence of rhodium complex catalyst.⁵ In addition, treatment of homoallylic amines with iodine afforded pyrrolidines *via* iodo cyclization, and palladium-catalyzed aerobic oxidation of homoallyl amino compounds proceeded to yield ketones.⁶⁻⁷

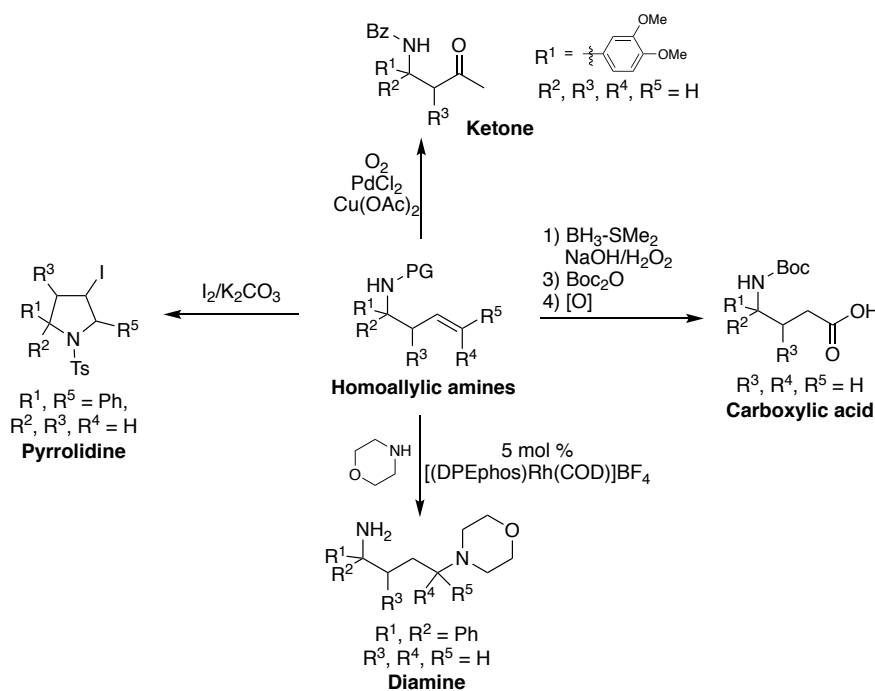


Figure 1. Homoallylic amines for synthesis of nitrogen-containing compounds

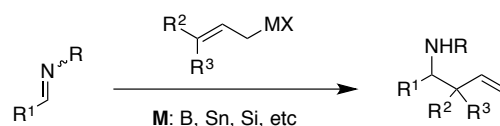
1.2 Regioselective synthesis of homoallylic amines

Based on the utilities of homoallylic amino groups, regio- and stereoselective homoallylic amine syntheses have been an important subject, and various methodologies have been developed. Allylation reaction of imines and rearrangement reaction of ene-imine

are representative transformations and easily access substituted homoallylic amino compounds.

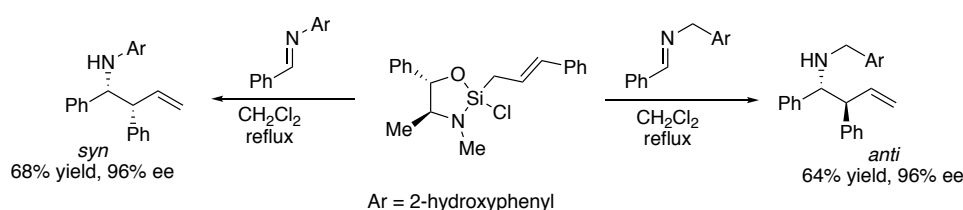
1.2.1 Addition reaction of allyl metal reagents to imines

Addition reaction of allyl metal reagents to imines is a typical approach for synthesis of homoallylic amino compounds recent years. During the past fifty years, a variety of allyl metal reagents have been reported. For example, allyl boranes, allyl tins, and allyl silanes have been available for the synthesis of 1,2-substituted homoallylic amines (Scheme 1).⁸⁻¹⁰ Due to their stability and less-toxicity, allyl silane is one of the most popular reagents for this transformation; therefore, regioselective reactions using allyl silane reagents are focused in following paragraph.



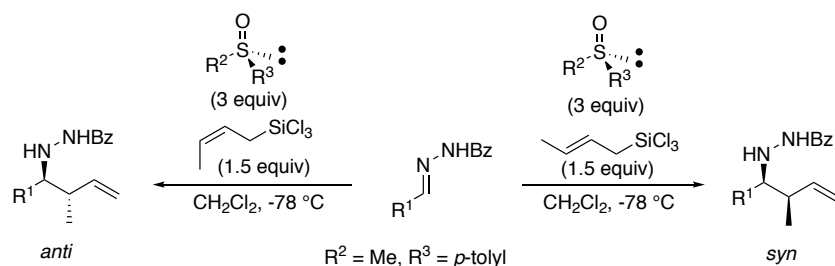
Scheme 1. Synthesis of 1,2-substituted homoallylic amines using allyl metal reagents

Leighton and co-workers developed methodology for highly stereoselective synthesis of 1,2-substituted homoallylic amines by the use of chiral allyl silane reagents (Scheme 2). An aromatic substituent on imine nitrogen provided *syn* homoallylic amines while *anti* homoallylic amines were obtained from an aliphatic substituent.¹¹⁻¹²



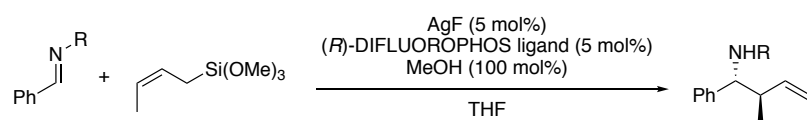
Scheme 2. Stereoselective 1,2-substituted homoallylic amines by allylation of imines with chiral allyl silanes

In 2003, Kobayashi and co-workers reported synthesis of homoallylic amines from aldehyde-derived imines with allyl trichlorosilane. When *trans*-crotyl silane was used, the *syn* homoallylic amines were obtained; while *cis*-crotyl silane provided *anti* homoallylic amines (Scheme 3).¹³



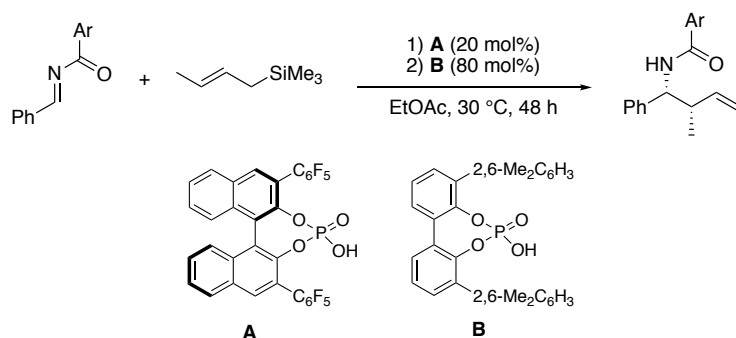
Scheme 3. Synthesis of homoallylic amines by the reaction of aldehyde-derived imines with allyl silane

Catalytic asymmetric reaction for synthesis of 1,2-substituted homoallylic amines was first reported by Yamamoto.¹⁴ The reaction of aldehyde-derived imines with (*Z*)-crotyl trimethoxysilane provided desired *anti*-1,2-substituted homoallylic amines with high stereoselectivities in the presence of (*R*)-DIFLUOROPHOS·AgF complex (Scheme 4).



Scheme 4. (*R*)-DIFLUOROPHOS·AgF complex-catalyzed crotylation reaction to synthesized 1,2-substituted homoallylic amino compounds

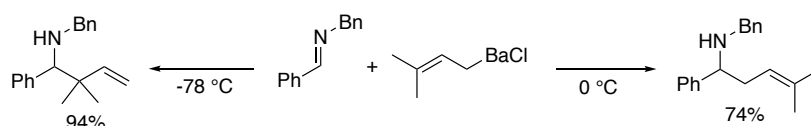
Similarly, Momiyama, Terada, and co-workers developed chiral Brønsted acid-catalyzed allylation of imines with allyl trimethylsilane to control stereochemistry of homoallylic amino compounds. The reaction of *N*-acyl imine and *trans*-crotyl trimethyl silane gave 1,2-substituted homoallylic amino compounds in good yields with high enantioselectivities (Scheme 5).¹⁵



Scheme 5. Chiral Brønsted acid-catalyzed crotylation reaction of imines with crotyl trimethyl silanes

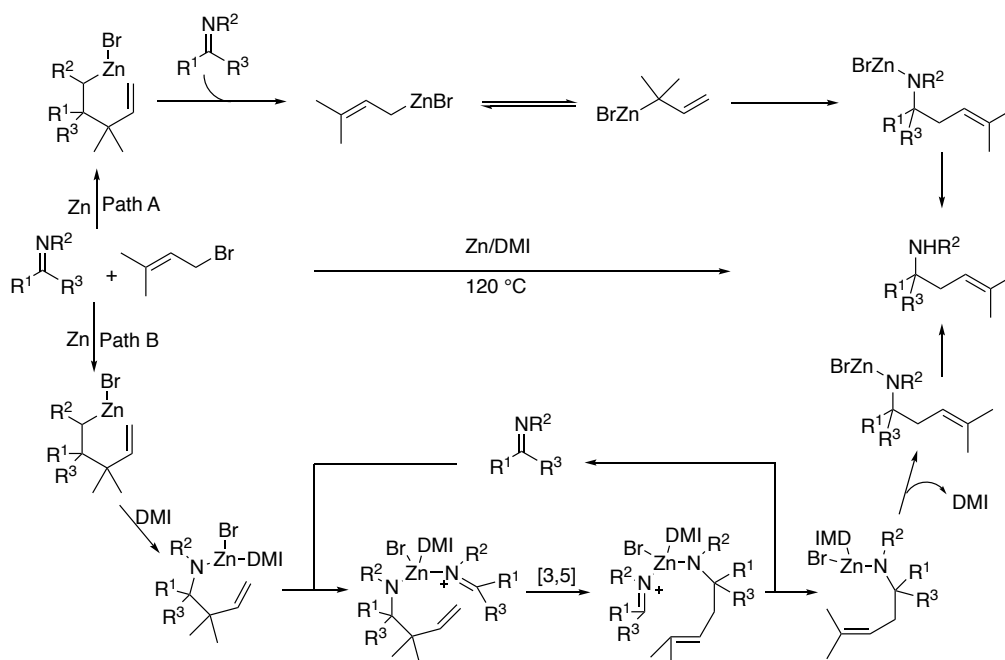
As an aforementioned series of allylation reactions, allyl silanes have been used to provide regio- and stereoselective 1,2-substituted homoallylic amino compounds. On the other hand, 1,4- or 1,4,4-substituted homoallylic amines have been rarely synthesized by allyl silane reagents; therefore, other allyl metal reagents were used for 1,4- or 1,4,4-substituted homoallylic amine syntheses.

In 1996, Yamamoto and co-workers developed allylation of benzyl-protected imine with allyl barium reagent to synthesize either 1,2,2- or 1,4,4-substituted homoallylic amines by simply changing reaction temperature. The allylation reaction at 0 °C gave 1,4,4-substituted homoallylic amine as product. On the other hand, when the reaction was conducted at -78 °C, 1,2,2-substituted homoallylic amine product was obtained (Scheme 6).¹⁶



Scheme 6. Synthesis of 1,2,2- and 1,4,4-substituted homoallylic amines by allylic barium reagents

Zhao and co-workers developed prenylation reaction of imines and *in situ*-generated allyl zinc reagent to synthesize 1,4,4-substituted homoallylic amines (Scheme 7). Two possible pathways are proposed: in path A, 1,2- or α -addition occurred to give prenylation product, in path B, [3,5]-rearrangement of nitrogen-zinc complex took place, and then decoordination provided 1,4,4-substituted homoallylic amino compound.¹⁷

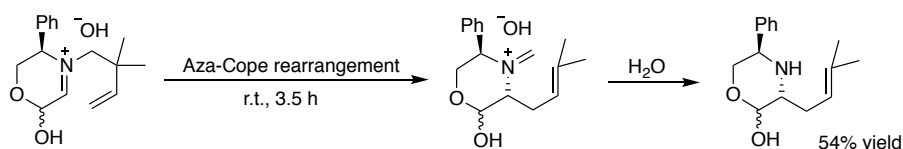


Scheme 7. Synthesis of 1,4,4-substituted homoallylic amines by allyl zinc reagent

1.2.2 Sigmatropic rearrangement reaction of ene-imines

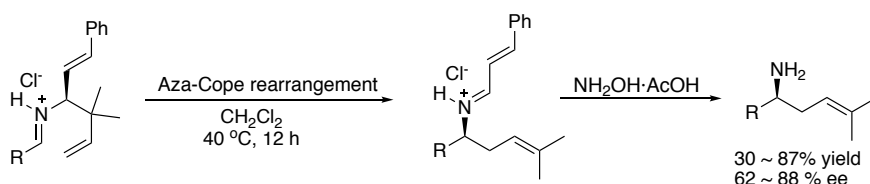
Allylation reactions of allyl metal reagents to imines have been successfully developed for synthesis of substituted homoallylic amino compounds. However, due to specific feature of each allyl metal reagents, there are still limitations of these approaches for 1,4- and 1,4,4-homoallylic amines; therefore, rearrangement reactions have been developed to synthesize 1,4- or 1,4,4-substituted homoallylic amino compounds.¹⁸

2-Azonia-[3,3]-Sigmatropic rearrangement and Aza-Cope rearrangement of ene-imines have been recognized as useful and straightforward methods to access homoallylic amines. Couty and co-workers developed 2-azonia-[3,3]-sigmatropic rearrangement of chiral ene-iminium (Scheme 8).¹⁹ The reaction of this chiral ene-iminium substrate was performed under aqueous medium condition to give [3,3]-rearrangement intermediate, the germinal methyl groups sterically promoted the rearrangement reaction to iminium intermediate or [3,3]-rearrangement intermediate with more stable of internal double bond. The intermediate was hydrolyzed under water solution affording cyclic 1,4,4-substituted product.



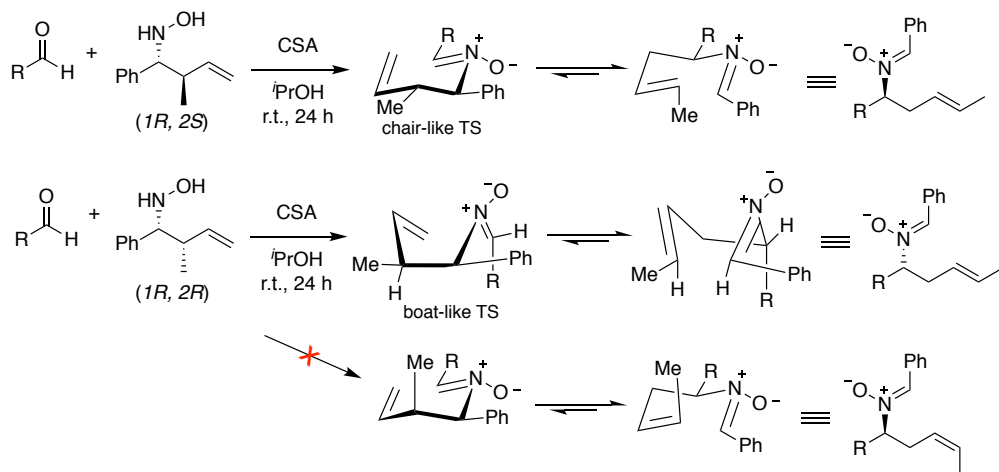
Scheme 8. 2-Azonia-[3,3]-sigmatropic rearrangement of chiral ene-iminiums

Additionally, Gonzalez-Gomez and co-workers reported 2-azonia-[3,3]-sigmatropic rearrangement reaction of acyclic ene-iminiums with α - and β -substituents (Scheme 9).²⁰ 2-Azonia-[3,3]-sigmatropic rearrangement of the chiral ene-iminium substrates underwent to provide 1,4,4-substituted homoallylic amines in dichloromethane. Further treatment of the desired products with $\text{NH}_2\text{OH}\cdot\text{AcOH}$ gave acyclic 1,4,4-substituted homoallylic amine derivatives.



Scheme 9. Brønsted acid-catalyzed Aza-Cope rearrangement of α - and β -substituted chiral ene-imine

Similarly, chiral hydroxy amines were used to synthesize 1,4-substituted homoallylic nitrones in the presence of Brønsted acid. Chiral nitron was generated *in situ*, and 2-azonia-[3,3]-sigmatropic rearrangement proceeded to give 1,4-substituted homoallylic nitrones with high stereoselectivities (Scheme 10).²¹ In the presence of (\pm)-10-camphor sulfonic acid (CSA) catalyst, (*R*)-*trans*-1,4-substituted homoallylic nitron was obtained from (*1R,2S*)-branched homoallylic hydroxyl amine as a reagent. On the other hand, (*S*)-*cis*-1,4-substituted homoallylic nitron product was obtained from (*1R,2R*)-branched homoallylic nitron under the same condition (when R group is the third priority). The reaction proceeded through chair-like transition state when *anti*-substrates were used, in contrast, boat-like transition state was proposed in the case of *syn*-substrates due to unfavorable 1,3-diaxial interaction.



Scheme 10. 2-Azonia-[3,3]-sigmatropic rearrangement of branched homoallylic nitrones

1.2.3 Discovery of Brønsted acid-initiated formal [1,3]-rearrangement reaction of ene-aldimines

As mentioned above, to synthesize 1,4- or 1,4,4-substituted homoallylic amines, aza-Cope rearrangement of imines and their analog have been preferred rather than allylation of imines with allylic metal reagents. Chiral auxiliary next to imino- or nitronium nitrogen is responsible to control stereoselectivity of the rearrangement products. To develop catalytic asymmetric version of these synthesis, Brønsted acid-catalyzed aza-Cope rearrangement of β -substituted ene-aldimines would be a potential approach for the synthesis of optically active 1,4- or 1,4,4-homoallyl amines. Although chiral Brønsted acid-catalyzed aza-Cope rearrangement of ene-aldimines were successfully developed (Figure 2a),²²⁻²⁴ there has been no report of catalytic asymmetric reaction for the synthesis of 1,4- or 1,4,4-substituted homoallylic amines (Figure 2b).

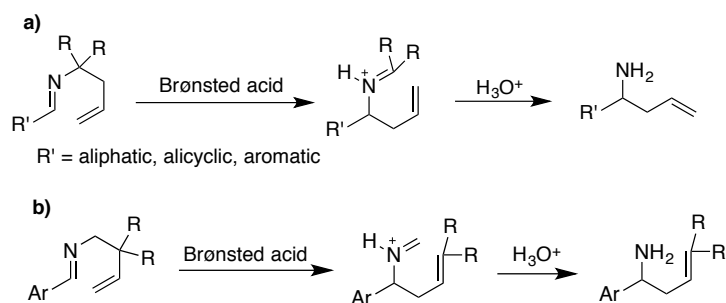
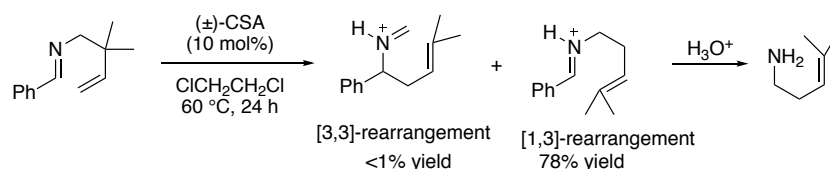


Figure 2. Brønsted acid-catalyzed aza-cope rearrangement (a) α -substituted ene-imines, (b) β -substituted ene-aldimines

At this point, Momiyama and co-workers designed β -substituted ene-aldimines and conducted the reaction in the presence of CSA as Brønsted acid catalyst. They discovered that the reaction did not provide [3,3]-rearrangement products, instead, only [1,3]-rearrangement products were obtained (Scheme 11).²⁵



Scheme 11. Discovery of Brønsted acid-initiated formal [1,3]-rearrangement reaction of ene-aldimines

1.3 Scope of this thesis

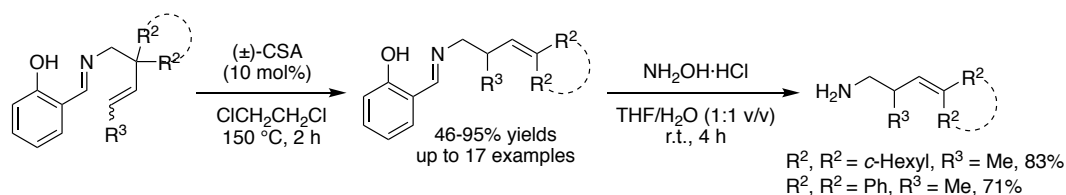
On the basis of aforementioned background and the newly discovered formal [1,3]-rearrangement of β -substituted ene-aldimine, it is envisioned that this formal [1,3]-rearrangement reaction would be applicable to synthesize 2,4,4-substituted homoallylic amines by further introducing the substituent at the terminal olefin. Importantly, although 1- and other positions-substituted homoallylic amines have been synthesized by previously developed methods, homoallylic amines containing substituents at the 2-position but not the 1-position cannot be easily synthesized. Therefore, this study for doctoral thesis is aimed to develop the newly discovered formal [1,3]-rearrangement to synthesize 2,4,4-substituted homoallylic amines and their derivatives.

In chapter 2, experimental results for reaction developments are summarized (Scheme 12). The investigation of electronic effects on aryl group, solvent, Brønsted acid, and reaction temperature were carried out in this study.

Brønsted acids, such as trifluoro acetic acid (TFA), phosphoric acid diphenyl ester, and CSA efficiently promoted the reaction in acetonitrile (MeCN) and 1,2-dichloroethane as solvents under normal or microwave heating method. Importantly, 1 mol% catalyst loading was realized when microwave heating method was used. After optimizing formal [1,3]-rearrangement reaction, scope of substrate was evaluated. It was demonstrated that a variety of substituents on ene-aldimine substrates were tolerated and gave corresponding rearrangement products in good to excellent yields.

To establish the utilities of this rearrangement reaction, ene-imine products were subjected into hydrolysis condition to afford 2,4,4-substituted homoallylic amines. Furthermore, the obtained 2,4,4-homoallylic amines were used for the synthesis of a spiro compound and a β -amino acid precursor.

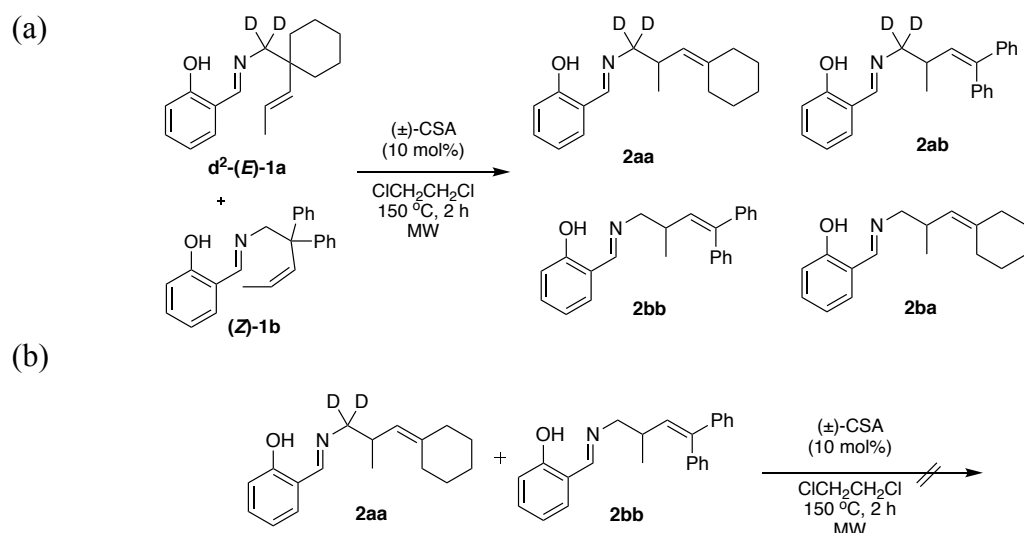
Details on reaction optimization, substrate scope, and derivatization will be described in chapter 2.



Scheme 12. Development of formal [1,3]-rearrangement of β -substituted ene-aldimines to synthesize 2,4,4-substituted homoallylic amines

In chapter 3, experimental results for the mechanistic studies are summarized. Furthermore, details of reaction mechanism are proposed and discussed based on experimental and computational studies.

This rearrangement reaction has not been reported so far, and the reaction mechanism has been unclear. Therefore, the studies were conducted to clarify the mechanism of this reaction. To think about the reaction pathway: either intra- or intermolecular, crossover experiments of substrates was initially examined. It was revealed that two normal- and two crossover rearrangement products were observed in a ratio of *ca.* 1:1:1:1 (Scheme 13). When the two normal rearrangement products were subjected in the presence of (\pm)-CSA under the heating condition, the reaction did not give the crossover products. These results suggest that $\text{C}(\alpha)\text{-C}(\beta)$ cleavage occurs during the irreversible rearrangement process, in other words, $\text{C}(\alpha)\text{-C}(\beta)$ cleavage does not proceed after the product formation. Therefore, intermolecular pathway is proposed for this formal [1,3]-rearrangement reaction.



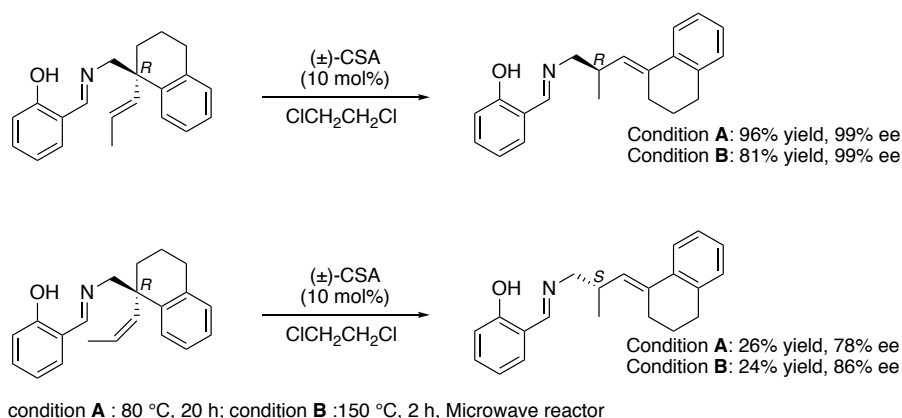
Scheme 13. Crossover experiments of (a) substrates and (b) products

To propose details of reaction mechanism, collaborative study was carried out with Dr. Honda in HPC SYSTEMS and Prof. Suzuki in IMS, where enormous DFT calculations were conducted.

Detailed reaction mechanism, chain reaction mechanism of 2-azaallenium cation as a chain carrier, was proposed based on DFT calculations. Further discussions for the chain reaction mechanism is also summarized in chapter 3.

In chapter 4, studies on asymmetric formal [1,3]-rearrangement of chiral ene-aldimine substrates is summarized. According to the one of proposed mechanism in propagation step, asymmetric formal [1,3]-rearrangement of chiral ene-aldimine substrates may proceed with highly chirality transfer ratio. Furthermore, as far as we know, highly asymmetric formal [1,3]-rearrangements of ene-aldimines have not been reported. Therefore, this study gives not only a great insight into the reaction mechanism of propagation step but also opens the new entry for asymmetric rearrangement reaction of ene-imines.

On the basis of the results in chapter 2, tetrahydronaphthalene was chosen as substituent on chiral substrate, and this chiral substrate was synthesized from commercially available 1-cyano-1,2,3,4-tetrahydronaphthalene. The chirality transfer experiments clearly showed that chirality at 2-position was transferred, and good to excellent enantioselectivities were obtained in the cases of both *E*- and *Z*-olefin substrates (Scheme 14).

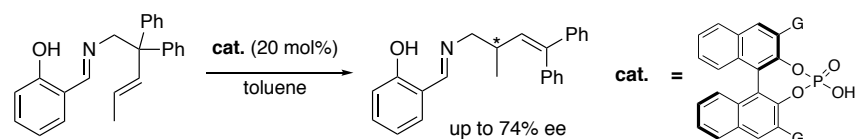


Scheme 14. Asymmetric formal [1,3]-rearrangement of chiral ene-aldimines with tetrahydronaphthalene unit at the β -position

Absolute configurations of the ene-aldimine substrates and products were determined by single crystal X-ray diffraction analysis, derivatization, and crystal sponge method. These results supported the reaction pathway that begins with C–N bond formation in the propagation step. Moreover, DFT calculation by Prof. Suzuki showed good agreement with the experimental results of stereochemistries.

In chapter 5, examinations of catalytic asymmetric formal [1,3]-rearrangement are described. During the study on chapter 2, 3, and 4, development of the new rearrangement was realized in the presence of racemic Brønsted acid such as (\pm)-CSA. It is no doubt that catalytic asymmetric version of this reaction by chiral catalyst is ultimate challenge during the course of this study. According to the plausible mechanism in chapter 4, a well-designed chiral counter anion as chiral catalysts may give the asymmetric induction.

At this point, chiral Brønsted acids were selected as one of candidates for this study. It was found that although (+)-CSA did not give any asymmetric induction at all, chiral phosphoric acid with substituents at the 3,3'-position provided moderate enantioselectivities of the ene-aldimine products (Scheme 15). Detailed studies on catalyst substituents and solvent effects will be summarized in chapter 5.



Scheme 15. Catalytic asymmetric formal [1,3]-rearrangement of ene-aldimine promoted by chiral Brønsted acid

In chapter 6, studies for this thesis are summarized, and perspective of the formal [1,3]-rearrangement of ene-aldimines is described.

1.4 References

1. Puentes, C. O.; Kouznetsov, V. J. *Heterocycl. Chem.* **2002**, *39*, 595-614.
2. Yus, M.; González-Gómez, J. C.; Foubelo, F. *Chem. Rev.* **2013**, *113*, 5595-5698.
3. Pandey, M. K.; Bisai, A.; Pandey, A.; Singh, V. K. *Tetrahedron Lett.* **2005**, *46*, 5039-5041.
4. Ramachandran, P. V.; Biswas, D. *Org. Lett.* **2007**, *9*, 3025-3027.
5. Ensign, S. C.; Vanable, E. P.; Kortman, G. D.; Weir, L. J.; Hull, K. L. *J. Am. Chem. Soc.* **2015**, *137*, 13748-13751.
6. Davis, F. D.; Song, M.; Augustine, A. *J. Org. Chem.* **2006**, *71*, 2779-2786.
7. Friestad, G.; Korapala, C. S.; Ding, H. *J. Org. Chem.* **2006**, *71*, 281-289.
8. Bosque, I.; Foubelo, F.; Gomez, J. C. *Org. Biomol. Chem.* **2013**, *11*, 7507-7515.
9. Sugiura, M.; Hirano, K.; Kobayashi, S. *J. Am. Chem. Soc.* **2004**, *126*, 7182-7183.
10. Shibata, I.; Miyamoto, S.; Tsunoi, S.; Sakamoto, K. Baba, A. *Eur. J. Org. Chem.* **2009**, 3508-3511.
11. Huber, J. D.; Leighton, J. L. *J. Am. Chem. Soc.* **2007**, *129*, 14552-14553.
12. Huber, J. D.; Perl, N. R.; Leighton, J. L. *Angew. Chem. Int. Ed.* **2008**, *47*, 3037-3039.
13. Kobayashi, S.; Ogawa, C.; Konishi, H.; Sugiura, M. *J. Am. Chem. Soc.* **2003**, *125*, 6610-6611.
14. Naodovic, M.; Wadamoto, M.; Yamamoto, H. *Eur. J. Org. Chem.* **2009**, 5129-5131.
15. Momiyama, N.; Nishimoto, H.; Terada, M. *Org. Lett.* **2011**, *13*, 2126-2129.
16. Yanagisawa, A.; Ogasawara, K.; Yasue, K., Yamamoto, H. *Chem. Commun.* **1996**, 367-368.
17. Zhao, L.; Zhang, S.; Jin, H.; Wan, L.; Dou, F. *Org. Lett.* **2012**, *14*, 886-889.
18. Jemison, R.; Laird, T.; Ollis, W. D.; Sutherland, L. O. *J. Chem. Soc. Perkin I.* **1980**, 1458-1461.
19. Agami, C.; Couty, F.; Poursoulis, M. *Synlett.* **1992**, 847-848.
20. Bosque, I.; Foubelo, F.; Gomez, J. C. *Org. Biomol. Chem.* **2013**, *11*, 7505-7515.
21. Cheng, H.; Seow, A.; Loh, T. *Org. Lett.* **2008**, *10*, 2805-2807.
22. Sugiura, M.; Mori, C.; Kobayashi, S. *J. Am. Chem. Soc.* **2006**, *128*, 11038-11039.
23. Rueping, M.; Antonchick, A. P. *Angew. Chem. Int. Ed.* **2008**, *47*, 10090-10093.
24. Ren, H.; Wulff, W. D. *J. Am. Chem. Soc.* **2011**, *133*, 5656-5659.
25. Jongwohan, C.; Honda, Y.; Suzuki, T.; Fujinami, T.; Adachi, K.; Momiyama, N. *Org. Lett.*

2019, accepted (DOI: 10.1021/acs.orglett.9b01533).

CHAPTER 2

BRØNSTED ACID-INITIATED REARRANGEMENT REACTION OF ENE-ALDIMINES FOR SYNTHESIS OF 2,4,4-SUBSTITUTED HOMOALLYLIC AMINES

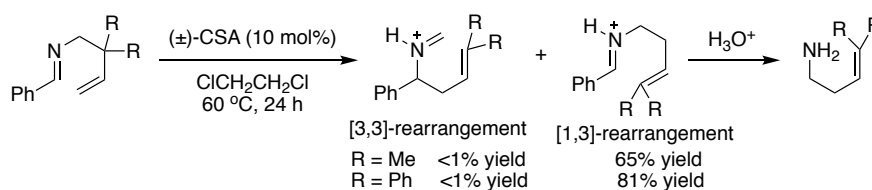
2.1 Introduction

As described in 1.2.3, the rearrangement reaction of β -substituted ene-aldimines gave the products by the formal [1,3]-rearrangement instead of those by 2-azonia-[3,3]-sigmatropic rearrangement. This result was in contrast to previous reports.¹⁻³ As far as we know, this formal [1,3]-rearrangement of ene-aldimine has not been reported. Therefore, this transformation has been studied in detail by exploring substituents, optimizing reaction condition, and investigating substrate scope. Furthermore, to establish the utilities of this reaction, derivatizations of rearrangement products were conducted.

2.2 Brønsted acid-initiated formal [1,3]-rearrangement reaction of ene-aldimines

2.2.1 Reaction optimization under normal heating method

To start this study, reproducibility and potential utilities were examined in the rearrangement reaction of β -dimethyl- and β -diphenyl-substituted ene-aldimine (Scheme 1). It was found that the formal [1,3]-rearrangement was reproducible, and the reaction of β -diphenyl-substituted ene-aldimine also gave the formal [1,3]-rearrangement product in a good yield.

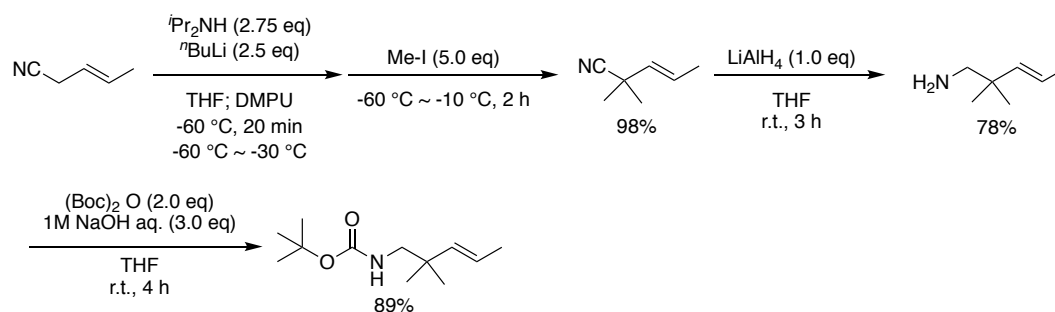


Scheme 1. Reproducibility and potential utilities of the formal [1,3]-rearrangement reaction of β -dimethyl- and β -diphenyl-substituted ene-aldimines

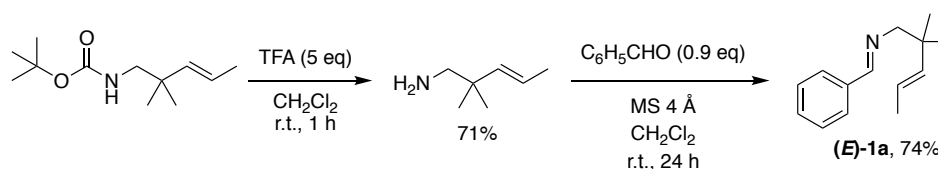
On the basis of these results, this formal [1,3]-rearrangement was applied for synthesis of 2,4,4-substituted homoallylic amines. For this purpose, (*E*)-*tert*-butyl (2,2-dimethylpent-3-en-1-yl)carbamate was initially synthesized (Scheme 2a), and the benzaldehyde-derived ene-aldimine (*E*)-**1a** was prepared from *tert*-butoxycarbonyl (Boc)

deprotection of carbamate followed by condensation of amine with benzaldehyde (Scheme 2b).

(a)

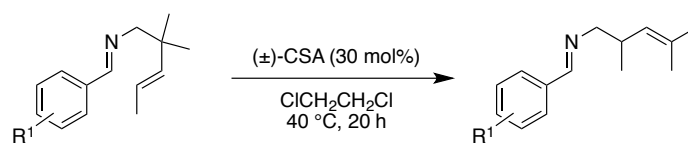


(b)



Scheme 2. Synthesis and preparation of ene-aldimine substrate; (a) synthesis of (*E*)-*tert*-butyl (2,2-dimethylpent-3-en-1-yl)carbamate, and (b) preparation of benzaldehyde-derived ene-aldimine (*E*)-**1a**

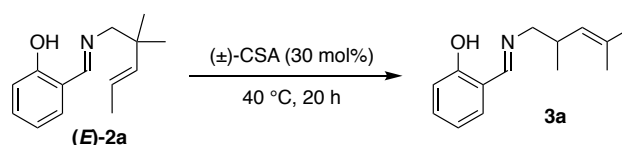
The reaction of (*E*)-**1a** was initially conducted in the presence of (\pm)-10-camphorsulfonic acid (CSA) at 40 °C for 20 h. It was revealed that the formal [1,3]-rearrangement product was obtained in 24% yield (Table 1, entry 1), as same as in Scheme 1, the reaction of (*E*)-**1a** did not give [3,3]-rearrangement product. Next, the substituents on benzylidene unit were investigated to evaluate electronic effect for reaction progress; therefore, 4-Cl, 4-OMe, 2-OH, and 2-OMe as R¹ were chosen as representative substituents on aryl group (Table 1). It was found that 2-hydroxyl substituent provided rearrangement product in a similar yield to the case of no substituent (Table 1, entry 1 vs. 4). Chlorine substituent could also allow to rearrangement product; however, yield was only in 7% (Table 1, entry 2). In the viewpoint of chemical yields and handling, 2-hydroxyl substituent was used for next investigations.

Table 1. Study of electronic effects on benzylidene unit

Entry	R ¹	Yield (%) ^a
1	H	24
2	4-Cl	7
3	4-OMe	0
4	2-OH	26
5	2-OMe	<1

^aDetermined by ¹H NMR using dibromomethane as an internal standard

Based on the results of investigation for substituents on benzylidene, the salicylaldehyde-derived ene-aldimine (*E*)-**2a** was used for solvent screening. The reactions were performed in 1,2-dichloroethane (ClCH₂CH₂Cl), toluene, tetrahydrofuran (THF), ethyl acetate (EtOAc), and acetonitrile (MeCN). The results showed that MeCN and ClCH₂CH₂Cl were available for this reaction (Table 2).

Table 2. Solvent screening

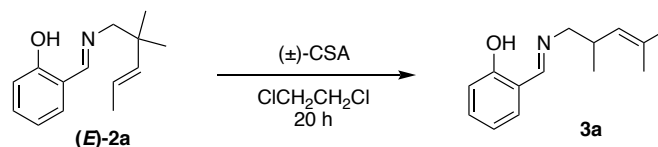
Entry	Solvent	Yield (%) ^a
1	ClCH ₂ CH ₂ Cl	26
2	toluene	<1
3	THF	<1
4	EtOAc	<1
5	MeCN	76

^aDetermined by ¹H NMR using dibromomethane as an internal standard

Next, reaction temperature was investigated in ClCH₂CH₂Cl with 30 mol% of (±)-CSA (Table 3, entries 1-3). At the 80 °C, reaction provided the formal [1,3]-rearrangement product in the highest yield (entry 3). Moreover, catalyst loading was studied in the presence of 10 mol% and 5 mol% (Table 3, entries 4 and 5). It was revealed that reaction provided the desired product in good yield at 80 °C under 5 mol% of CSA, (Table 3, entry 5). These

results indicated that low catalyst loading was possible when the reaction was performed at higher temperature.

Table 3. Study on temperature and catalyst loading under normal heating

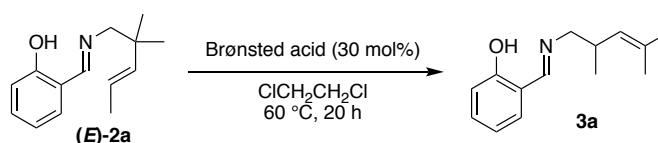


Entry	Temperature (°C)	Catalyst loading (mol%)	Yield (%) ^a
1	40	30	26
2	60	30	62
3	80	30	81
4	80	10	74
5	80	5	60

^aDetermined by ¹H NMR using dibromomethane as an internal standard

Finally, a variety of Brønsted acid catalysts was evaluated at 60 °C. In this investigation, the reaction proceeded in the case of Brønsted acids having low pK_a: trifluoroacetic acid (TFA), phosphoric acid diphenyl ester, and (±)-CSA (Table 4, entries 1-3). In contrast, higher pK_a Brønsted acids, such as benzoic acid (PhCO₂H) and acetic acid (MeCO₂H), did not facilitate the reaction (entries 4 and 5). These results indicated that acidity of Brønsted acid was very important for this reaction.

Table 4. Screening of Brønsted acid



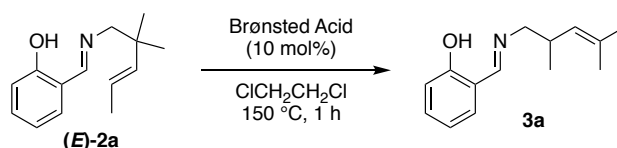
Entry	Brønsted acid	Yield (%) ^a
1	TFA	80
2	Phosphoric acid diphenyl ester	48
3	(±)-CSA	62
4	PhCO ₂ H	<1
5	MeCO ₂ H	<1

^aDetermined by ¹H NMR using dibromomethane as an internal standard

2.2.2 Reaction optimization by the use of microwave reactor

Higher reaction temperature in the presence of TFA and (±)-CSA improved the chemical yields of the reactions. It was speculated that the microwave reactor was possible to carry out the reaction at higher temperature and effective to increase the reaction yields. Therefore, microwave reactor was used to conduct the reaction in the presence of TFA and (±)-CSA. It was found that the reactions afforded desired products in appropriate yields in both cases (Table 5, entries 1 and 2).

Table 5. Reactions with (±)-CSA and TFA catalysts in microwave reactor

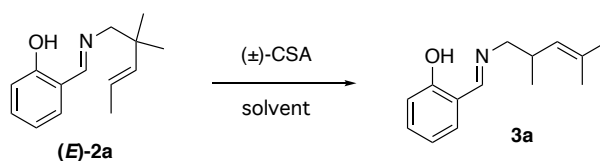


Entry	Brønsted acid	Yield (%) ^a
1	(±)-CSA	89
2	TFA	73

^aDetermined by ¹H NMR using dibromomethane as an internal standard

According to the results of normal heating and microwave conditions, although TFA and (±)-CSA showed good reaction efficiency, (±)-CSA was chosen to further studies due to stability and handling. Reaction time and temperature were further optimized under microwave condition. At 150 °C, for 2 h, and with 10 mol% of (±)-CSA, the reaction gave superior results compared to all other conditions in ClCH₂CH₂Cl (Table 6, entry 4). Since reaction gave the great yield in MeCN under normal heating condition (Table 2, entry 5), the reaction was performed in MeCN as solvent under microwave condition; however, the yield was lower than that in ClCH₂CH₂Cl (Table 6, entry 5).

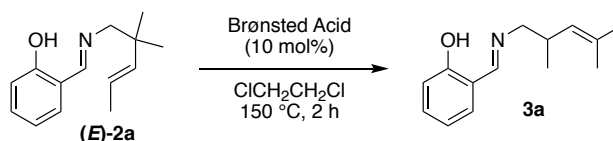
As mentioned earlier, low catalyst loading was possible when the reaction was conducted at high temperature. Therefore, the reactions were evaluated with 10 to 5, 3, 2, and 1 mol% of CSA, prolonging the reaction time for 3, 4, and 12 h (Table 6, entries 7-10). It was revealed that 1 mol% of catalyst loading was possible without deterioration of the yield (Table 6, entry 10).

Table 6. Optimization of reaction condition under microwave reactor

Entry	Temperature (°C)	Time (h)	Catalyst loading (mol%)	Solvent	Yield (%) ^a
1	100	1	10	ClCH ₂ CH ₂ Cl	72
2	120	1	10	ClCH ₂ CH ₂ Cl	87
3	150	1	10	ClCH ₂ CH ₂ Cl	89
4	150	2	10	ClCH ₂ CH ₂ Cl	92
5	150	2	10	MeCN	81
6	150	3	5	ClCH ₂ CH ₂ Cl	92
7	150	3	3	ClCH ₂ CH ₂ Cl	92
8	150	4	2	ClCH ₂ CH ₂ Cl	91
9	150	12	1	ClCH ₂ CH ₂ Cl	89

^aDetermined by ¹H NMR using dibromomethane as an internal standard

Under the optimized reaction condition using microwave reactor, applicability of Brønsted acid catalysts was examined (Table 7). Among various Brønsted acid catalysts, (±)-CSA gave the best yield (Table 7, entry 1), although all other Brønsted acid catalysts also provided rearrangement products in good to high yields (Table 7, entries 2-5).

Table 7. Applicability of Brønsted acid under microwave condition

Entry	Brønsted acid	Yield (%) ^a
1	(±)-CSA	92
2	TFA	91
3	MeCO ₂ H	74
4	Diphenyl phosphoric acid	75
5	<i>p</i> -TsOH·H ₂ O	90

^aDetermined by ¹H NMR using dibromomethane as an internal standard

2.2.3 Reaction scope

With optimized condition in hands, the scope of ene-aldimine substrates was investigated. The dialkyl substituted product **3a** was obtained from (*E*)-**2a** and (*Z*)-**2a** in excellent yields. Even though cyclobutyl and cyclopentyl substituted ene-aldimines ((*E*)-**2b** and (*E*)-**2c**) yielded rearrangement product **3b** and **3c** in moderate yields under 10 mol% catalyst loading, the cyclohexyl substituted R^2 ((*E*)-**2d** and (*Z*)-**2d**) smoothly proceeded to formal [1,3]-rearrangement product **3d** in excellent yields by the used of 2 mol% (\pm)-CSA. Moreover, acyclic and aromatic substituted substrates R^2 ((*E*)-**2e** - **2h** and (*Z*)-**2h**) could also give corresponding rearrangement product in excellent yields under 2 mol% of catalyst loading. Although (\pm)-CSA 10 mol% was necessary to obtain good yields for ethyl and isopropyl substituted R^3 ((*Z*)-**2i** - **2m**), the (\pm)-CSA 2 mol% was also applicable in some cases, for example (*E*)-**2k** and (*E*)-**2m**.

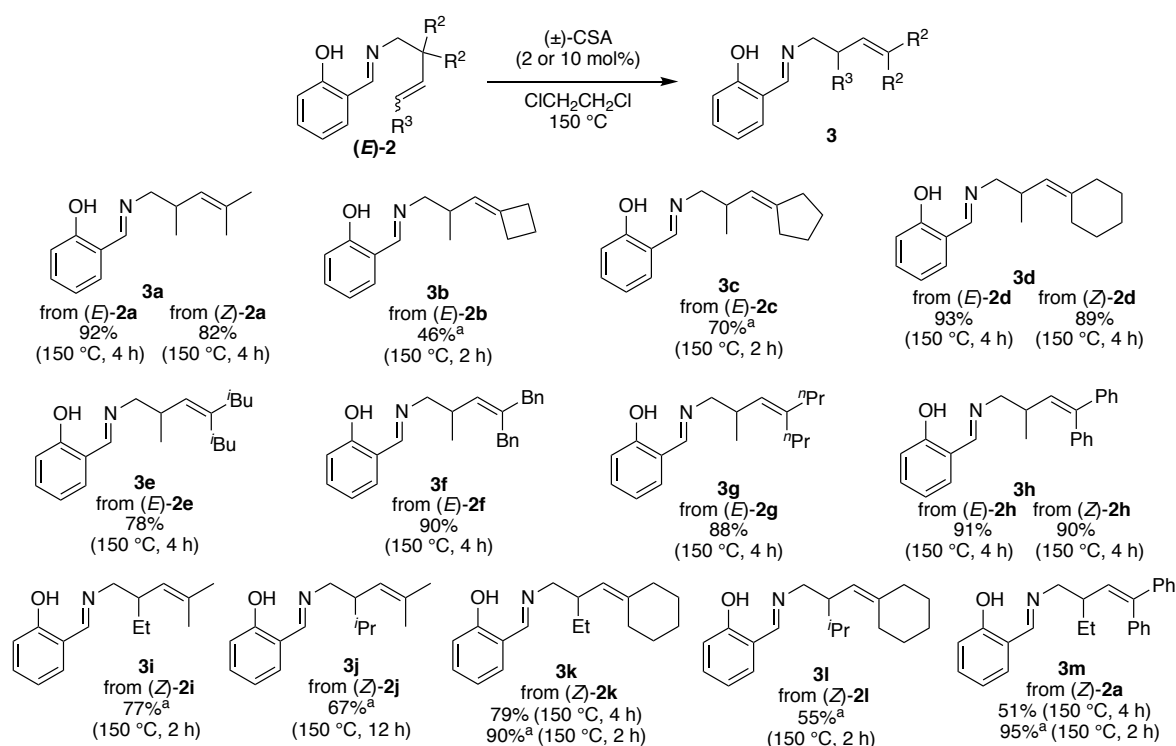
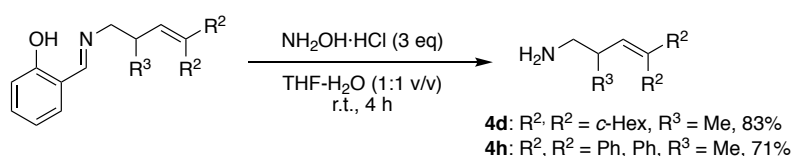


Figure 1. Substrate scope of (*E*)- and (*Z*)-ene-aldimine. Reaction was conducted in the presence of (\pm)-CSA 2 mol % under microwave heating, ^a(\pm)-CSA 10 mol % was used.

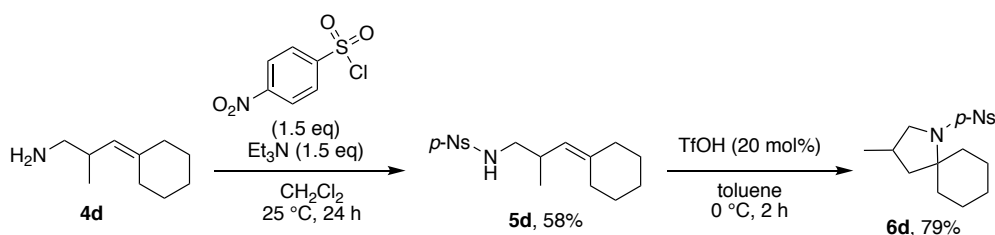
2.2.4 Utilities of formal [1,3]-rearrangement products

The rearrangement products (**3a**-**3m**) are important synthetic intermediates that could be converted to the previously inaccessible 2,4,4-homoallylic primary amines. Therefore, to establish the synthetic utility of such compounds, products **3d** and **3h** were subjected into

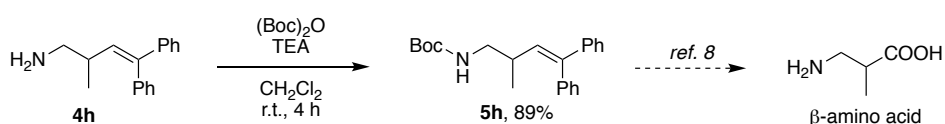
hydrolysis condition. The treatment of **3d** and **3h** with hydroxylamine hydrochloride ($\text{NH}_2\text{OH}\cdot\text{HCl}$) provided 2,4,4-substituted homoallylic primary amines in good yields (Scheme 3).⁴ In addition, 2,4,4-substituted homoallylic primary amine **4d** was protected with *p*-nosylchloride to form the *p*-nosylate **5d** before intramolecular hydroamination with substoichiometric amounts of triflic acid affording spiropyrrolidine **6d** (Scheme 4).⁵⁻⁷ In addition, the homoallylic primary amine **4h** was transformed into the *tert*-butoxycarbonyl (Boc) protected amine **5h** in excellent yield by the treatment with $(\text{Boc})_2\text{O}$, which is a useful intermediate for β -amino acid synthesis (Scheme 5).⁸



Scheme 3. Synthesis of 2,4,4-substituted homoallylic amines



Scheme 4. Synthesis of aza-spiro compound



Scheme 5. Synthesis of β -amino acid precursor

2.3 Conclusion

The formal [1,3]-rearrangement reaction was developed by optimizing reaction condition in both normal and microwave condition. The $\text{ClCH}_2\text{CH}_2\text{Cl}$ and MeCN solvents and a variety of Brønsted acids were used for this new transformation, and the broadened substrates were available under these conditions. The 2,4,4-substituted homoallylic primary amines, which were inaccessible by previous reports, were successfully synthesized. Moreover, our rearrangement products were applicable to synthesize aza-spiro compounds and a β -amino acid precursor.

2.4 Experimental sections

2.4.1 General method

All reactions were carried out under an atmosphere of standard grade nitrogen gas (oxygen <10 ppm) in flame-dried glassware with magnetic stirring. Toluene and tetrahydrofuran were used as anhydrous in solvent line system KANTO. Benzene and 1,2-dichloroethane (ClCH₂CH₂Cl) were purchased from commercial supplier as anhydrous solvents. Benzaldehyde, 4-methoxybenzaldehyde, 2-methoxybenzaldehyde, 4-chlorobenzaldehyde, and 2-hydroxybenzaldehyde were distilled before use. Other reagents were purchased from commercial suppliers and used without further purification. Purification of reaction products was carried out by flash column chromatography on silica gel 60 (spherical, neutral, 100-210 μm; Merck). Analytical thin layer chromatography (TLC) was performed on E. Merck precoated (0.25 mm) silica gel 60-F254 plates. Visualization was accomplished with UV light, potassium permanganate solution in water, and phosphomolybdic acid solution in ethanol by heating. Microwave reaction was performed in a CEM Discover or Biotage Initiator Microwave system. ¹H NMR spectra were recorded on a ECA-400 (400 MHz) spectrometer at ambient temperature. CDCl₃ NMR solvents were purchased from CIL, and it was dried over activated MS 4Å before used. Data are reported as follows: chemical shifts are reported in ppm from tetramethylsilane on the δ scale, with solvent resonance employed as internal standard (CDCl₃ 7.26 ppm, DMSO-d₆ 2.49 ppm), multiplicity (b = broad, s = singlet, d = doublet, dd = doublet of doublet, t = triplet, q = quartet, and m = multiplet), integration, coupling constant (Hz) and assignment. ¹³C NMR spectra were recorded on a JEOL ECA-400 (100 MHz), spectrometer at ambient temperature. Chemical shifts are reported in ppm from tetramethylsilane on the δ scale, with solvent resonance employed as internal standard (CDCl₃ 77.0 ppm). Mass spectra were obtained on Applied Biosystem Voyager DE-STR in Instrument center of IMS.

2.4.2 Procedure of rearrangement reaction of ene-aldimines

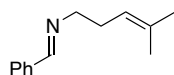
Normal heating condition: To a (±)-10-camphorsulfonic acid (10 mol%) was added the solution of ene-imine in ClCH₂CH₂Cl (0.1 M) at room temperature. Then, the reaction was stirred at an indicated temperature for an indicated time. After cooled to room temperature, the reaction was quenched with NEt₃. After stirred at room temperature for 15 min, the resulting mixture was extracted with CH₂Cl₂ (5 mL x 3). The organic layer was washed with brine (10 mL x 3), and aqueous layer was extracted with CH₂Cl₂ (20 mL x 3).

The combined organic extracts were dried over Na₂SO₄ and concentrated under reduced pressure after filtration to give the ene-imine as product.

Microwave condition: A test tube for microwave reaction apparatus (0.2-0.5 mL) should be used. To a (±)-10-camphorsulfonic acid (10 mol%) was added the solution of ene-imine in 1 ClCH₂CH₂Cl (0.5 M) at room temperature with sealed reaction vessel, and then the resulting solution was stirred at an indicated temperature in a microwave reactor with 600 rpm (75-400 W.) for an indicated time. The reaction was quenched with NEt₃. After stirred for 15 min, the resulting mixture was extracted with CH₂Cl₂ (5 mL x 3). The organic layer was washed with brine (10 mL x 3), and aqueous layer was extracted with CH₂Cl₂ (20 mL x 3). The combined organic extracts were dried over Na₂SO₄ and concentrated under reduced pressure after filtration to give the ene-imine as product.

2.4.3 Characterization of rearrangement products

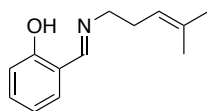
Because of stability of rearrangement products, the characterization data are only provided by ¹H NMR.



(*E*)-*N*-benzylidene-4-methylpent-3-en-1-amine

TLC R_f = 0.30 (4:1 hexane:ethyl acetate).

¹H NMR (CDCl₃, 400 MHz) δ 8.26 (s, 1H, N=CH), 7.78-7.63 (m, 3H, Ar-H), 7.46-7.36 (m, 2H, Ar-H), 4.92 (t, 2H, *J* = 7.1 Hz, CH=C), 3.62 (t, 2H, *J* = 7.0 Hz, N-CH₂), 2.37 (q, 2H, *J* = 7.1 Hz, N-CH₂-CH₂), 1.72 (s, 3H, CH₃), 1.65 (s, 3H, CH₃).

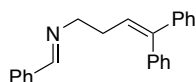


(*E*)-2-(((4-methylpent-3-en-1-yl)imino)methyl)phenol

TLC R_f = 0.54 (10:1 hexane:ethyl acetate).

¹H NMR (CDCl₃, 400 MHz) δ 8.30 (s, 1H, CH=N), 7.32-7.22 (m, 3H, Ar-H), 6.95 (d, 1H, *J* = 8.2 Hz, Ar-H), 6.86 (td, 1H, *J* = 7.4, 1.1 Hz, Ar-H), 5.17-5.13 (m, 1H, CH₂-CH=C), 3.58

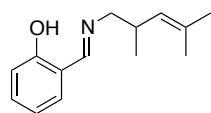
(td, 2H, $J = 7.0, 1.1$ Hz, N-CH₂), 2.38 (q, 2H, $J = 7.0$ Hz, CH₂-CH₂-CH), 1.70 (s, 3H, C-CH₃), 1.61 (s, 3H, C-CH₃)



(E)-N-(4,4-diphenylbut-3-en-1-yl)-1-phenylmethanimine

TLC R_f = 0.45 (10:1 hexane:ethyl acetate).

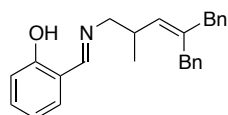
¹H NMR (CDCl₃, 400 MHz) δ 7.73-7.69 (m, 2H, Ar-H), 7.39-7.17 (m, 13H, Ar-H), 6.14 (t, 1H, $J = 7.6$ Hz, CH=C), 3.73-3.69 (m, 2H, NH-CH₂), 2.58-2.51 (m, 2H, CH₂-CH₂).



(E)-2-(((2,4-dimethylpent-3-en-1-yl)imino)methyl)phenol

TLC R_f = 0.55 (3:1 hexane:ethyl acetate).

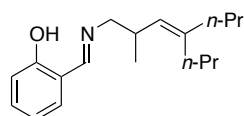
¹H NMR (CDCl₃, 400 MHz) δ 8.26 (s, 1H, N=CH), 7.26-7.22 (m, 2H, Ar-H), 6.9 (d, 1H, $J = 8.2$ Hz, Ar-H), 6.85 (t, 1H, $J = 7.4$ Hz, Ar-H), 4.95 (d, 1H, $J = 9.4$ Hz, CH=C), 3.48-3.40 (m, 1H, N-CH₂-CH), 2.76-2.73 (m, 1H, CH-CH₃), 1.68 (s, 3H, C-CH₃), 1.60 (d, 3H, $J = 0.9$ Hz, C-CH₃).



(E)-2-(((4-benzyl-2-methyl-5-phenylpent-3-en-1-yl)imino)methyl)phenol

TLC R_f = 0.55 (3:1 hexane:ethyl acetate).

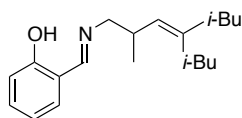
¹H NMR (CDCl₃, 600 MHz) δ 8.36 (s, 1H, N=CH), 7.36 (t, 1H, $J = 10.0$ Hz, Ar-H), 7.32-7.29 (m, 1H, Ar-H), 7.26 (d, 1H, $J = 10.0$ Hz, Ar-H), 7.22 (t, 1H, $J = 10.0$ Hz, Ar-H), 5.22 (d, 1H, $J = 9.6$ Hz, CH=C), 3.73-3.45 (m, 2H, N-CH₂), 3.35 (dd, 4H, CH₂-Ph), 3.05-2.95 (m, 1H), 1.13 (d, 3H, $J = 5.1$ Hz).



(E)-2-(((2-methyl-4-propylhept-3-en-1-yl)imino)methyl)phenol

TLC $R_f = 0.55$ (3:1 hexane:ethyl acetate).

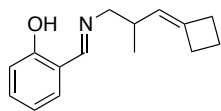
$^1\text{H NMR}$ (CDCl_3 , 600 MHz) δ 8.26 (s, 1H, $\text{N}=\text{CH}$), 7.31-7.21 (m, 2H, Ar- H), 6.90 (d, 1H, $J = 10.0$ Hz, Ar- H), 6.85 (t, 1H, $J = 10.0$ Hz, Ar- H), 4.94 (d, 1H, $J = 10.0$ Hz, $\text{CH}=\text{C}$), 3.51-3.41 (m, 2H, N- CH_2), 2.81-2.74 (m, 1H, N- CH_2 - CH), 2.04-1.87 (m, 4H), 1.41-1.30 (m, 4H), 1.02 (d, 3H, $J = 6.4$ Hz, CH_3), 0.90-0.81 (m, 6H).



(*E*)-2-(((4-isobutyl-2,6-dimethylhept-3-en-1-yl)imino)methyl)phenol

TLC $R_f = 0.55$ (3:1 hexane:ethyl acetate).

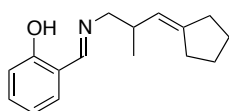
$^1\text{H NMR}$ (CDCl_3 , 400 MHz) δ 8.26 (s, 1H, $\text{N}=\text{CH}$), 7.30-7.26 (m, 1H, Ar- H), 7.22 (dd, 1H, $J = 7.7, 1.7$ Hz, Ar- H), 6.94 (d, 1H, $J = 8.2$ Hz, Ar- H), 6.85 (td, 1H, $J = 7.4, 0.9$ Hz, Ar- H), 4.97 (d, 1H, $J = 9.6$ Hz, $\text{CH}=\text{C}$), 4.94-4.90 (m, 2H, N- CH_2), 2.86-2.79 (m, 1H, N- CH_2 - CH), 1.61-1.95 (m, 6H, C- CH_2 - $\text{CH}(\text{CH}_3)_2$), 0.87-0.81 (m, 9H, CH- CH_3), 0.87-0.81 (m, 9H), 0.76 (d, 3H, $J = 6.6$ Hz, CH_2 - CH - CH_3).



(*E*)-2-(((3-cyclobutylidene-2-methylpropyl)imino)methyl)phenol

TLC $R_f = 0.55$ (3:1 hexane:ethyl acetate).

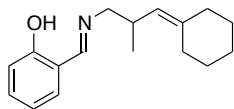
$^1\text{H NMR}$ (CDCl_3 , 600 MHz) δ 8.32 (s, 1H, $\text{N}=\text{CH}$), 7.32-7.25 (m, 2H, Ar- H), 6.90 (d, 1H, $J = 10.0$ Hz, Ar- H), 7.87 (t, 1H, $J = 10.0$ Hz, Ar- H), 4.92 (dt, 1H, $J = 10.0$ Hz, $\text{CH}=\text{C}$), 3.73-3.41 (m, 2H, N- CH_2), 2.64-2.57 (m, 1H, N- CH_2 - CH), 1.83 (d, 2H, $J = 9.6$ Hz), 1.02 (d, 3H, $J = 6.6$ Hz, CH_3).



(*E*)-2-(((3-cyclopentylidene-2-methylpropyl)imino)methyl)phenol

TLC $R_f = 0.55$ (3:1 hexane:ethyl acetate).

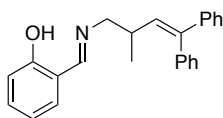
^1H NMR (CDCl_3 , 600 MHz) δ 8.26 (s, 1H, $\text{N}=\text{CH}$), 7.31-7.21 (m, 2H, Ar- H), 7.94 (d, 1H, $J = 10.0$ Hz, Ar- H), 7.85 (t, 1H, $J = 10.0$ Hz, Ar- H), 5.08 (d, 1H, $J = 9.6$ Hz, $\text{CH}=\text{C}$), 3.52-3.40 (m, 2H, N- CH_2), 2.64-2.57 (m, 1H, N- CH_2 - CH), 2.22-2.10 (m, 4H), 1.64-1.52 (m, 4H), 1.03 (d, 3H, $J = 6.8$ Hz, CH_3).



(*E*)-2-(((3-cyclohexylidene-2-methylpropyl)imino)methyl)phenol

TLC $R_f = 0.55$ (3:1 hexane:ethyl acetate).

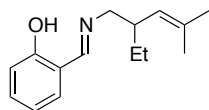
^1H NMR (CDCl_3 , 400 MHz) δ 8.25 (s, 1H, $\text{N}=\text{CH}$), 7.31-7.21 (m, 2H, Ar- H), 6.90 (d, 1H, $J = 10.0$ Hz, Ar- H), 6.85 (t, 1H, $J = 10.0$ Hz, Ar- H), 4.88 (d, 1H, $J = 9.2$ Hz, $\text{CH}=\text{C}$), 3.73-3.37 (m, 2H, N- CH_2), 2.82-2.75 (m, 1H, N- CH_2 - CH), 2.09 (dt, 4H), 1.48-1.30 (m, 6H), 1.02 (d, 3H, $J = 9.2$ Hz, CH_3).



(*E*)-2-(((2-methyl-4,4-diphenylbut-3-en-1-yl)imino)methyl)phenol

TLC $R_f = 0.18$ (10:1 hexane:ethyl acetate).

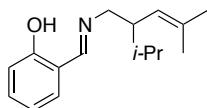
^1H NMR (CDCl_3 , 400 MHz) δ 8.26 (s, 1H, $\text{N}=\text{CH}$), 7.30-7.10 (m, 12H, Ar- H), 6.97-6.93 (m, 1H, Ar- H), 6.88-6.84 (m, 1H, Ar- H), 5.93 (d, 1H, $J = 10.3$ Hz, $\text{CH}=\text{C}$), 3.57-3.54 (m, 2H, N- CH_2), 2.76-2.67 (m, 1H, N- CH_2 - CH), 1.12 (d, 3H, $J = 6.9$ Hz, CH_3).



(*E*)-2-(((2-ethyl-4-methylpent-3-en-1-yl)imino)methyl)phenol

TLC $R_f = 0.50$ (10:1 hexane:ethyl acetate).

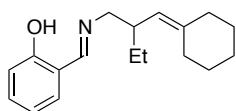
^1H NMR (CDCl_3 , 400 MHz) δ 8.25 (d, 1H, $J = 3.9$ Hz, $\text{N}=\text{CH}$), 7.31-7.21 (m, 2H, Ar- H), 6.95 (dd, 1H, $J = 8.0, 3.2$ Hz, Ar- H), 6.87-6.82 (m, 1H, Ar- H), 4.89 (dt, 1H, $J = 9.8, 1.3$ Hz, $\text{CH}-\text{CH}=\text{C}$), 3.59-3.54 (m, 1H, NH- CH_2), 3.43-3.38 (m, 1H, NH- CH_2), 2.56-2.46 (m, 1H, $\text{CH}_2-\text{CH}-\text{CH}$), 1.71-1.69 (m, 3H, CH- CH_3), 1.58 (d, 3H, $J = 1.1$ Hz, 2H, CH- CH_3), 1.32-1.22 (m, 1H, CH- CH_2-CH_3), 0.99-0.94 (m, 1H, CH- CH_2-CH_3), 0.85-0.90 (m, 3H, CH_2-CH_3).



(E)-2-(((2-isopropyl-4-methylpent-3-en-1-yl)imino)methyl)phenol

TLC R_f = 0.50 (10:1 hexane:ethyl acetate).

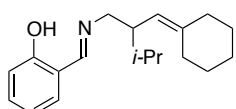
^1H NMR (CDCl_3 , 400 MHz) δ 8.27 (d, 1H, J = 24.0 Hz, $\text{N}=\text{CH}$), 7.32-7.21 (m, 2H, Ar- H), 6.95 (dd, 1H, J = 8.2, 5.5 Hz, Ar- H), 6.89-6.83 (m, 1H, Ar- H), 4.978-4.946 (m, 1H, $\text{CH}=\text{C}$), 4.495-4.493 (d, 2H, J = 9.6 Hz, $\text{NH}-\text{CH}_2-\text{CH}$), 1.56 (s, 3H, C- CH_3), 1.56-1.53 (m, 1H, $\text{CH}-\text{CH}-\text{CH}_3$), 0.94 (d, 3H, J = 6.9 Hz, CH_2-CH_3).



(E)-2-(((2-(cyclohexylidenemethyl)butyl)imino)methyl)phenol

TLC R_f = 0.45 (10:1 hexane:ethyl acetate).

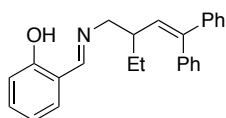
^1H NMR (CDCl_3 , 400 MHz) δ 8.24 (s, 1H, $\text{N}=\text{CH}$), 7.30-7.26 (m, 1H, Ar- H), 7.24-7.29 (m, 1H, Ar- H), 6.96-6.92 (m, 1H, Ar- H), 6.86-6.82 (m, 1H, Ar- H), 4.80 (d, 1H, J = 10.0 Hz, $\text{CH}=\text{C}$), 3.58-3.52 (m, 1H, $\text{N}-\text{CH}_2$), 3.42-3.37 (m, 1H, $\text{N}-\text{CH}_2$), 2.59-2.52 (m, 1H, $\text{N}-\text{CH}_2-\text{CH}$), 2.16-2.00 (m, 4H), 1.67-1.34 (m, 7H), 1.29-1.19 (m, 1H), 0.89 (t, 3H, J = 7.6 Hz, CH_2-CH_3).



(E)-2-(((2-(cyclohexylidenemethyl)-3-methylbutyl)imino)methyl)phenol

TLC R_f = 0.50 (10:1 hexane:ethyl acetate).

^1H NMR (CDCl_3 , 400 MHz) δ 8.26-8.19 (m, 1H, $\text{N}=\text{CH}$), 7.31-7.21 (m, 2H, Ar- H), 6.97 (d, 1H, J = 8.5 Hz, Ar- H), 6.87-6.83 (m, 1H, Ar- H), 5.22-5.16 (m, 1H), 5.04 (dd, 1H, J = 22.2 Hz, 12.1 Hz, $\text{CH}(\text{CH}_3)-\text{CH}=\text{C}$), 3.73 (s, 1H, $\text{NH}-\text{CH}_2$), 3.57 (s, 1H, $\text{NH}-\text{CH}_2$), 2.71-2.81 (m, 1H, $\text{CH}_2-\text{CH}-\text{CH}(\text{CH}_3)_2$), 2.17-1.98 (m, 4H, C- CH_2-CH_2), 1.55-1.35 (m, 5H, $\text{CH}_2-\text{CH}_2-\text{CH}_2$), 1.01-0.84 (m, 6H, $\text{CH}-(\text{CH}_3)_2$).

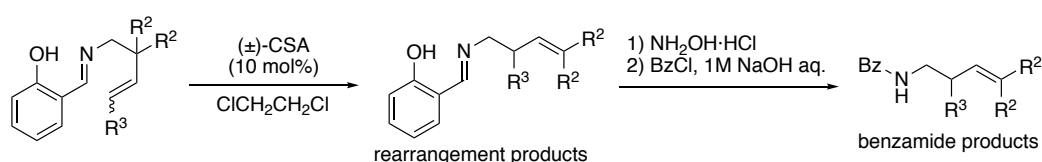


(*E*)-2-(((2-ethyl-4,4-diphenylbut-3-en-1-yl)imino)methyl)phenol

TLC $R_f = 0.55$ (10:1 hexane:ethyl acetate).

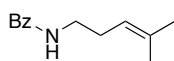
^1H NMR (CDCl_3 , 400 MHz) δ 8.23 (s, 1H, $\text{N}=\text{CH}$), 7.33-7.17 (m, 11H, Ar-*H*), 6.95 (d, 1H, $J = 8.0$ Hz, Ar-*H*), 6.83 (td, 1H, $J = 7.4, 1.0$ Hz, Ar-*H*), 5.89 (d, 1H, $J = 10.3$ Hz, $\text{CH}=\text{C}$), 3.63-3.50 (m, 2H, N- CH_2), 1.62-1.36 (m, 2H, $\text{CH}-\text{CH}_2-\text{CH}_3$), 1.12 (t, 3H, $J = 7.4$ Hz, CH_3).

2.4.4 Procedure and characterization of derivatives



Scheme 6. Reaction of new rearrangement and derivatization

Due to the stability of ene-imine rearrangement products, the characterization data are provided by ^1H NMR, ^{13}C NMR, and HRMS of derived benzamides. And because some of rearrangement products were low boiling point and instable, derivatization is performed. The rearrangement products are subjected into hydrolysis condition by the use of hydroxylamine hydrochloride ($\text{NH}_2\text{OH}\cdot\text{HCl}$) to cleave salicylaldehyde to afford amine products. And then the amine products are protected by benzoyl chloride in the basic condition providing benzamide products (Scheme 6). The characterization data are shown below.



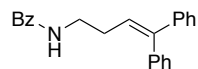
N-(4-methylpent-3-en-1-yl)benzamide

TLC $R_f = 0.21$ (3:1 hexane:ethyl acetate).

^1H NMR (CDCl_3 , 600 MHz) δ 7.76-7.71 (m, 2H, Ar-*H*), 7.51-7.46 (m, 1H, Ar-*H*), 7.44-7.40 (m, 2H, Ar-*H*), 6.26-6.17 (br, 1H, *NH*), 5.18-5.13 (m, 1H, $\text{CH}=\text{C}$), 3.55 (m, 2H, N- CH_2), 2.32 (td, 2H, $J = 6.9$ Hz, $J = 6.9$ Hz, N- CH_2-CH_2), 1.73 (s, 3H, CH_3), 1.65 (s, 3H, CH_3).

^{13}C NMR (CDCl_3 , 151 MHz) δ 167.5, 135.0, 134.9, 131.4, 128.6, 126.9, 120.8, 39.9, 28.2, 25.9, 18.0.

HRMS (ESI) Exact Mass Calcd. for C₁₃H₁₇NO ([M+Na]⁺): 226.1202. Found: 226.1202.



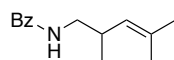
N-(4,4-diphenylbut-3-en-1-yl)benzamide

TLC R_f = 0.53 (4:1 hexane:ethyl acetate).

¹H NMR (CDCl₃, 400 MHz) δ 7.73-7.69 (m, 2H, Ar-*H*), 7.20-7.50 (m, 11H, Ar-*H*), 7.13-7.16 (m, 2H, Ar-*H*), 6.11 (t, *J* = 7.6 Hz, 2H, NH, CH=C), 3.56 (dd, 2H, *J* = 12.7, 6.8 Hz, NH-CH₂), 2.49-2.41 (m, 2H, CH₂-CH₂).

¹³C NMR (CDCl₃, 100 MHz) δ 168.0, 144.7, 142.3, 139.8, 134.8, 131.5, 129.9, 128.7, 128.5, 128.3, 127.4, 126.9, 125.8, 40.0, 30.1.

HRMS (FAB) Exact Mass Calcd. for C₂₃H₂₁NO ([M+H]⁺): 328.1696. Found: 328.1716.



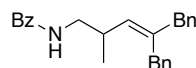
N-(2,4-dimethylpent-3-en-1-yl)benzamide

TLC R_f = 0.30 (3:1 hexane:ethyl acetate).

¹H NMR (CDCl₃, 600 MHz) δ 7.72-7.69 (m, 2H, Ar-*H*), 7.50-7.46 (m, 1H, Ar-*H*), 7.44-7.39 (m, 2H, Ar-*H*), 6.14-6.06 (br, 1H, NH), 4.97-4.92 (m, 1H, CH=C), 3.63-3.57 (m, 1H, N-CH₂), 3.03-2.97 (m, 1H, N-CH₂), 2.75-2.66 (m, 1H, N-CH₂-CH), 1.74 (d, 3H, *J* = 1.4 Hz, C=C-CH₃), 1.65 (d, 3H, *J* = 1.4 Hz, C=C-CH₃), 1.01 (d, 3H, *J* = 6.5 Hz, CH-CH₃).

¹³C NMR (CDCl₃, 151 MHz) δ 167.4, 135.1, 133.6, 131.3, 128.6, 128.0, 126.8, 45.9, 32.9, 25.9, 18.8, 18.3.

HRMS (ESI) Exact Mass Calcd. for C₁₄H₁₉NO ([M+Na]⁺): 240.1359. Found: 240.1359.



N-(4-benzyl-2-methyl-5-phenylpent-3-en-1-yl)benzamide

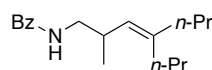
TLC R_f = 0.32 (3:1 hexane:ethyl acetate).

¹H NMR (CDCl₃, 600 MHz) δ 7.59-7.56 (m, 2H, Ar-*H*), 7.50-7.46 (m, 1H, Ar-*H*), 7.39-7.34 (m, 2H, Ar-*H*), 7.26-7.15 (m, 6H, Ar-*H*), 7.14-7.08 (m, 4H, Ar-*H*), 6.11-6.05 (br, 1H, NH), 5.30 (d, 1H, *J* = 10.0 Hz, CH=C), 3.74-3.68 (m, 1H, N-CH₂), 3.42 (d, 1H, *J* = 14.8 Hz, C-CH₂-Ph), 3.27 (d, 1H, *J* = 14.4 Hz, C-CH₂-Ph), 3.20 (d, 1H, *J* = 14.4 Hz, C-CH₂-Ph), 3.16 (d,

1H, $J = 14.8$ Hz, C-CH₂-Ph), 3.13-3.08 (m, 1H, N-CH₂), 2.96-2.88 (m, 1H, N-CH₂-CH), 1.13 (d, 3H, $J = 6.5$ Hz, N-CH₂-CH-CH₃).

¹³C NMR (CDCl₃, 151 MHz) δ 167.3, 140.1, 139.9, 139.4, 134.6, 131.8, 131.4, 129.0, 128.7, 128.6, 128.6, 128.5, 126.9, 126.3, 126.2, 45.9, 43.2, 35.9, 33.2, 19.0.

HRMS (ESI) Exact Mass Calcd. for C₂₆H₂₇NO ([M+Na]⁺): 392.1985. Found: 392.1984.



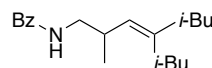
N-(2-methyl-4-propylhept-3-en-1-yl)benzamide

TLC R_f = 0.37 (3:1 hexane:ethyl acetate).

¹H NMR (CDCl₃, 600 MHz) δ 7.71-7.67 (m, 2H, Ar-*H*), 7.49-7.45 (m, 1H, Ar-*H*), 7.43-7.38 (m, 2H, Ar-*H*), 6.13-6.05 (br, 1H, NH), 4.94 (d, 1H, $J = 10.0$ Hz, CH=C), 3.66-3.60 (m, 1H, N-CH₂), 3.00-2.94 (m, 1H, N-CH₂), 2.77-2.68 (m, 1H, N-CH₂-CH), 2.10-1.90 (m, 4H), 1.48-1.32 (m, 4H), 1.02 (d, 3H, $J = 6.9$ Hz, N-CH₂-CH-CH₃), 0.88 (t, 3H, $J = 7.2$ Hz, C=C-CH₂-CH₂-CH₃), 0.86 (t, 3H, $J = 7.2$ Hz, C=C-CH₂-CH₂-CH₃).

¹³C NMR (CDCl₃, 151 MHz) δ 167.4, 141.6, 135.0, 131.3, 128.6, 128.3, 126.8, 45.9, 39.0, 32.5, 32.3, 21.9, 21.5, 19.1, 14.2, 13.9.

HRMS (ESI) Exact Mass Calcd. for C₁₈H₂₇NO ([M+Na]⁺): 296.1985. Found: 296.1984.



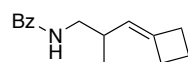
N-(4-isobutyl-2,6-dimethylhept-3-en-1-yl)benzamide

TLC R_f = 0.43 (3:1 hexane:ethyl acetate).

¹H NMR (CDCl₃, 400 MHz) δ 7.71-7.69 (m, 2H, Ar-*H*), 7.48-7.46 (m, 1H, Ar-*H*), 7.43-7.37 (m, 2H, Ar-*H*), 6.09 (br, 1H, NH), 4.98 (d, 1H, $J = 9.9$ Hz, CH=C), 3.67-3.60 (m, 1H, N-CH₂), 3.04-2.95 (m, 1H, N-CH₂), 2.82-2.69 (m, 1H, N-CH₂-CH), 2.00-1.64 (m, 6H), 1.01 (d, 3H, $J = 6.6$ Hz, N-CH₂-CH-CH₃), 0.92-0.76 (m, 12H).

¹³C NMR (CDCl₃, 100 MHz) δ 167.3, 139.6, 134.8, 131.3, 130.4, 128.5, 126.7, 77.3, 77.0, 76.7, 46.6, 45.9, 38.9, 32.4, 26.5, 26.1, 23.0, 22.6, 22.3, 22.2, 19.0.

HRMS (ESI) Exact Mass Calcd. for C₂₀H₃₁NO ([M+Na]⁺): 324.2298. Found: 324.2298.



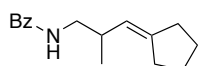
N-(3-cyclobutylidene-2-methylpropyl)benzamide

TLC R_f = 0.28 (3:1 hexane:ethyl acetate).

^1H NMR (CDCl_3 , 600 MHz) δ 7.76-7.73 (m, 2H, Ar-*H*), 7.52-7.48 (m, 1H, Ar-*H*), 7.46-7.42 (m, 2H, Ar-*H*), 6.24-6.10 (br, 1H, NH), 4.92-4.88 (m, 1H, CH=C), 3.63-3.58 (m, 1H, N- CH_2), 3.02-2.97 (m, 1H, N- CH_2), 2.72-2.57 (m, 4H), 2.47-2.39 (m, 1H, N- CH_2 -CH), 1.99-1.87 (m, 2H), 1.03 (d, 3H, J = 6.5 Hz, CH_3).

^{13}C NMR (CDCl_3 , 151 MHz) δ 167.4, 142.1, 135.1, 131.4, 128.7, 126.8, 123.3, 45.6, 33.4, 31.2, 29.8, 18.6, 17.2.

HRMS (ESI) Exact Mass Calcd. for $\text{C}_{15}\text{H}_{19}\text{NO}$ ($[\text{M}+\text{Na}]^+$): 252.1359. Found: 252.1359.



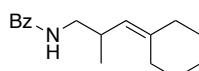
***N*-(3-cyclopentylidene-2-methylpropyl)benzamide**

TLC R_f = 0.32 (3:1 hexane:ethyl acetate).

^1H NMR (CDCl_3 , 600 MHz) δ 7.73-7.70 (m, 2H, Ar-*H*), 7.50-7.46 (m, 1H, Ar-*H*), 7.43-7.39 (m, 2H, Ar-*H*), 6.29-6.21 (br, 1H, NH), 5.09-5.05 (m, 1H, CH=C), 3.62-3.56 (m, 1H, N- CH_2), 3.05-2.99 (m, 1H, N- CH_2), 2.62-2.53 (m, 1H, N- CH_2 -CH), 2.31-2.14 (m, 4H), 1.75-1.52 (m, 4H), 1.01 (d, 3H, J = 6.5 Hz, CH- CH_3).

^{13}C NMR (CDCl_3 , 151 MHz) δ 167.4, 145.3, 135.1, 131.3, 128.6, 126.8, 123.2, 45.7, 34.8, 33.8, 29.0, 26.4, 26.3, 18.5.

HRMS (ESI) Exact Mass Calcd. for $\text{C}_{16}\text{H}_{21}\text{NO}$ ($[\text{M}+\text{Na}]^+$): 266.1515. Found: 266.1516.



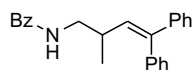
***N*-(3-cyclohexylidene-2-methylpropyl)benzamide**

TLC R_f = 0.31 (3:1 hexane:ethyl acetate).

^1H NMR (CDCl_3 , 600 MHz) δ 7.73-7.69 (m, 2H, Ar-*H*), 7.49-7.45 (m, 1H, Ar-*H*), 7.43-7.39 (m, 2H, Ar-*H*), 6.16-6.09 (br, 1H, NH), 4.88 (d, 1H, J = 9.6 Hz, CH=C), 3.61-3.56 (m, 1H, N- CH_2), 3.00-2.94 (m, 1H, N- CH_2), 2.77-2.69 (m, 1H, N- CH_2 -CH), 2.18-2.05 (m, 4H), 1.58-1.35 (m, 6H), 1.01 (d, 3H, J = 6.9 Hz, CH_3).

^{13}C NMR (CDCl_3 , 151 MHz) δ 167.4, 141.9, 135.0, 131.3, 128.6, 126.8, 124.7, 46.0, 37.4, 31.9, 29.3, 28.9, 28.2, 26.9, 19.2.

HRMS (ESI) Exact Mass Calcd. for $\text{C}_{17}\text{H}_{23}\text{NO}$ ($[\text{M}+\text{Na}]^+$): 280.1672. Found: 280.1671.



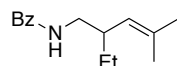
***N*-(2-methyl-4,4-diphenylbut-3-en-1-yl)benzamide**

TLC R_f = 0.22 (4:1 hexane:ethyl acetate).

^1H NMR (CDCl_3 , 400 MHz) δ 8.18-8.11 (m, 1H, Ar-*H*), 7.67-7.66 (m, 2H, Ar-*H*), 7.49-7.45 (m, 2H, Ar-*H*), 7.41-7.30 (m, 4H, Ar-*H*), 7.26-7.20 (m, 4H, Ar-*H*), 7.11-7.08 (m, 2H, Ar-*H*), 6.02 (br, 1H, NH), 5.92 (d, 1H, J = 10.3 Hz, CH=C), 3.51-3.45 (m, 1H, N-CH₂), 3.38-3.31 (m, 1H, N-CH₂), 2.72-2.60 (m, 1H, N-CH₂-CH), 1.14 (d, 3H, J = 6.9 Hz, CH₃).

^{13}C NMR (CDCl_3 , 100 MHz) δ 167.5, 143.0, 139.9, 133.6, 132.4, 131.3, 130.1, 129.6, 128.5, 128.4, 128.2, 127.3, 127.2, 126.8, 77.3, 77.0, 76.7, 45.8, 34.6, 18.7.

HRMS (ESI) Exact Mass Calcd. for $\text{C}_{24}\text{H}_{23}\text{NO}$ ($[\text{M}+\text{Na}]^+$): 364.1672. Found: 364.1672.



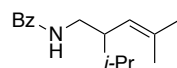
***N*-(2-ethyl-4-methylpent-3-en-1-yl)benzamide**

TLC R_f = 0.46 (3:1 hexane:ethyl acetate).

^1H NMR (CDCl_3 , 400 MHz) δ 7.71- 7.69 (m, 2H, Ar-*H*), 7.51-7.41 (m, 3H, Ar-*H*), 6.12 (br, 1H, NH), 4.88 (d, 1H, J = 9.8 Hz, CH=C), 3.75-3.67 (m, 1H, N-CH₂), 2.99-2.93 (m, 1H, N-CH₂), 2.48 (tt, 1H, J = 14.3 Hz, 4.8 Hz, N-CH₂-CH), 1.77 (s, 3H, C-CH₃), 1.65 (s, 3H, C-CH₃), 1.56-1.45 (m, 1H, CH-CH₂-CH₃), 1.30-1.19 (m, 1H, CH-CH₂-CH₃), 0.89 (t, 3H, J = 7.4 Hz, CH₂-CH₃).

^{13}C NMR (CDCl_3 , 100 MHz) δ 167.5, 135.1, 135.0, 131.4, 128.7, 126.9, 77.5, 77.2, 76.9, 44.5, 40.2, 26.5, 26.1, 18.6, 11.8.

HRMS (FAB) Exact Mass Calcd. for $\text{C}_{15}\text{H}_{21}\text{NO}$ ($[\text{M}+\text{H}]^+$): 232.1696. Found: 232.1708.



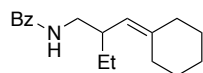
***N*-(2-isopropyl-4-methylpent-3-en-1-yl)benzamide**

TLC R_f = 0.37 (4:1 hexane:ethyl acetate).

^1H NMR (CDCl_3 , 400 MHz) δ 7.76-7.74 (m, 2H, Ar-*H*), 7.52-7.42 (m, 3H, Ar-*H*), 6.16 (br, 1H, NH), 5.24-5.13 (m, 2H, CH=C, CH-CH-(CH₃)₂), 3.43 (d, 2H, J = 6.0 Hz, N-CH₂), 2.88-2.77 (m, 1H, CH₂-CH-CH(CH₃)₂), 1.19 (s, 6H, CH=C(CH₃)₂), 0.96 (d, 6H, J = 6.4 Hz, CH-CH-(CH₃)₂).

^{13}C NMR (CDCl_3 , 100 MHz) δ 140.3, 135.0, 132.6, 131.5, 128.7, 126.9, 50.7, 37.7, 27.7, 27.5, 23.5.

HRMS (FAB) Exact Mass Calcd. for $\text{C}_{16}\text{H}_{23}\text{NO}$ ($[\text{M}+\text{H}]^+$): 246.1852. Found: 246.1854.



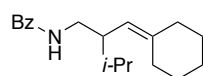
***N*-(2-(cyclohexylidenemethyl)butyl)benzamide**

TLC R_f = 0.34 (3:1 hexane:ethyl acetate).

^1H NMR (CDCl_3 , 600 MHz) δ 7.73-7.70 (m, 2H, Ar-*H*), 7.50-7.46 (m, 1H, Ar-*H*), 7.44-7.40 (m, 2H, Ar-*H*), 6.17-6.08 (br, 1H, NH), 4.81 (d, 1H, J = 10.0 Hz, CH=C), 3.73-3.67 (m, 1H, N- CH_2), 3.00-2.94 (m, 1H, N- CH_2), 2.55-2.48 (m, 1H, N- CH_2 -CH), 2.22-2.07 (m, 4H), 1.59-1.38 (m, 7H), 1.29-1.19 (m, 1H), 0.90 (t, 3H, J = 7.6 Hz, CH_2 - CH_3).

^{13}C NMR (CDCl_3 , 151 MHz) δ 167.4, 143.4, 135.1, 131.3, 128.6, 126.8, 123.4, 44.6, 39.1, 37.6, 29.5, 29.1, 28.2, 26.9, 26.4, 11.8.

HRMS (ESI) Exact Mass Calcd. for $\text{C}_{18}\text{H}_{25}\text{NO}$ ($[\text{M}+\text{Na}]^+$): 294.1828. Found: 294.1828.



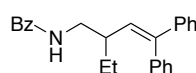
***N*-(2-(cyclohexylidenemethyl)-3-methylbutyl)benzamide**

TLC R_f = 0.33 (4:1 hexane:ethyl acetate).

^1H NMR (CDCl_3 , 400 MHz) δ 7.76-7.74 (m, 2H, Ar-*H*), 7.46-7.42 (m, 3H, Ar-*H*), 6.18 (br, 1H, NH), 5.36-5.30 (m, 1H, CH-CH(CH_3) $_2$), 5.09 (d, 1H, J = 12.1 Hz, CH=C), 3.54 (d, 2H, J = 6.0 Hz, N- CH_2), 2.82-2.79 (m, 1H, N- CH_2 -CH), 1.64-1.27 (m, 10H, C-(CH_2) $_5$), 0.96 (d, 6H, J = 6.6 Hz, CH-(CH_3) $_2$).

^{13}C NMR (CDCl_3 , 100 MHz) δ 167.7, 141.1, 135.2, 131.5, 131.0, 128.7, 126.9, 49.0, 41.2, 36.2, 28.2, 26.2, 23.2, 22.4.

HRMS (FAB) Exact Mass Calcd. for $\text{C}_{19}\text{H}_{27}\text{NO}$ ($[\text{M}+\text{H}]^+$): 268.2165. Found: 268.2167.



***N*-(2-ethyl-4,4-diphenylbut-3-en-1-yl)benzamide**

TLC R_f = 0.55 (3:1 hexane:ethyl acetate).

^1H NMR (CDCl_3 , 400 MHz) δ 7.67-7.65 (m, 2H, Ar-*H*), 7.41-7.39 (m, 1H, Ar-*H*), 7.39 (t, 2H, J = 7.4, Ar-*H*), 7.31-7.20 (m, 8, H, Ar-*H*), 7.09-7.06 (m, 2H, Ar-*H*), 6.01 (br, 3H, NH), 5.87

(d, 1H, $J = 10.5$, $CH=C$), 3.56-3.53 (m, 1H, N- CH_2), 3.34-3.28 (m, 1H, N- CH_2), 2.50-2.43 (m, 1H, N- CH_2-CH), 1.62-1.39 (m, 2H, CH_2-CH_3), 0.96 (t, 3H, $J = 7.6$ Hz, CH_3).

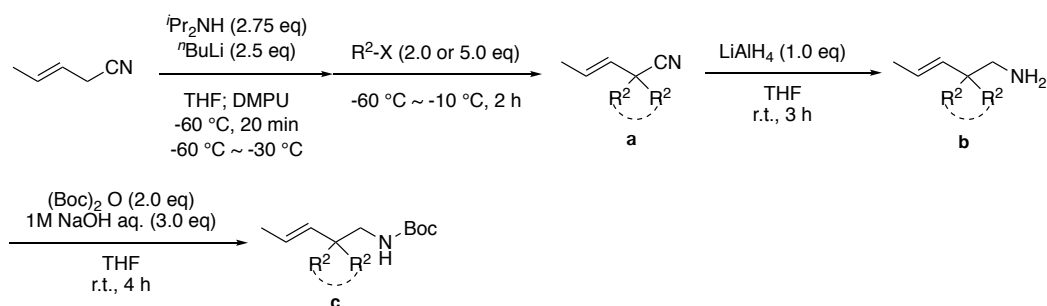
^{13}C NMR ($CDCl_3$, 100 MHz) δ 167.5, 135.1, 135.0, 131.4, 128.7, 126.9, 44.5, 40.2, 26.5, 26.1, 11.8.

HRMS (FAB) Exact Mass Calcd. for $C_{25}H_{26}NO$ ($[M+H]^+$): 356.2009. Found: 356.2019.

2.4.5 Synthesis and characterization of starting materials

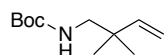
Synthesis of (E)-tert-butyl(2,2-alkyl or 2-cycloalkyl pent-3-en-1-yl)carbamate:

The (*E*)-olefin starting materials are synthesized from commercially available 3-pentenenitrile and alkyl halide (Scheme 7). The alkylation reaction of 3-pentenenitrile with alkyl halide in the presence of diisopropylamine and *n*-buthyl lithium bases provides (*E*)-2,2-dialkyl pent-3-enenitrile product (**S1**). After that the alkylation product is subjected into reduction condition to change nitrile moiety compound to be (*E*)-2,2-dialkyl or 2-cycloalkyl pent-3-en-1-amine (**S2**) as a single product. Finally, (*E*)-2,2-dialkyl or 2-cycloalkyl pent-3-en-1-amine is protected by di-*tert*-butyl decarbonate (Boc) to afford (*E*)-*tert*-butyl (2,2-alkyl or 2-cycloalkyl pent-3-en-1-yl)carbamate (**S3**) as stocked starting materials.⁹



Scheme 7. Synthesis of (*E*)-*tert*-butyl (2,2-alkyl or 2-cycloalkyl pent-3-en-1-yl)carbamate starting material

Characterization of (E)-tert-butyl (2,2-alkyl or 2-cycloalkyl pent-3-en-1-yl) carbamate:

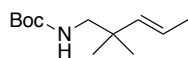


tert-butyl (2,2-dimethylbut-3-en-1-yl)carbamate

1H NMR ($CDCl_3$, 400 MHz) δ 5.73 (dd, 1H, $J = 7.2$ Hz, 10.8 Hz, $CH=CH_2$), 5.01 (dd, 2H, $J = 14.4$ Hz, 10.8 Hz, $CH=CH_2$), 4.51 (br, 1H, $NH-CH_2$), 3.01 (d, 2H, $J = 6.0$ Hz, $NH-CH_2$), 1.43 (s, 9H, $C-(CH_3)_3$) 1.00 (s, 6H, $(CH_3)_2$).

^{13}C NMR ($CDCl_3$, 100 MHz) δ 156.1, 145.6, 112.7, 79.0, 50.2, 37.9, 28.3, 24.3.

HRMS (FAB) Exact Mass Calcd. for $C_{11}H_{21}NO_2$ ($[M+H]^+$): 200.1645. Found: 200.1654.

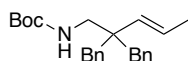


(E)-tert-butyl (2,2-dimethylpent-3-en-1-yl)carbamate

1H NMR ($CDCl_3$, 400 MHz) δ 5.45-5.30 (m, 2H, $CH=CH-CH_3$), 4.48 (br, 1H, NH), 4.51 (br, 1H, $NH-CH_2$), 2.96 (d, 2H, $J = 6.2$ Hz, $NH-CH_2$), 1.68-1.64 (m, 3H, $CH-CH_3$), 1.44 (s, 9H, $C-(CH_3)_3$) 0.97 (s, 6H, $C-(CH_3)_2$).

^{13}C NMR ($CDCl_3$, 100 MHz) δ 147.1, 138.7, 123.4, 85.5, 51.0, 28.7, 27.4, 25.3, 18.5.

HRMS (FAB) Exact Mass Calcd. for $C_{12}H_{23}NO_2$ ($[M+H]^+$): 214.1802. Found: 214.1815.

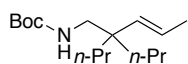


(E)-tert-butyl (2,2-dibenzylpent-3-en-1-yl)carbamate

1H NMR ($CDCl_3$, 600 MHz) δ 7.26 (t, 4H, $J = 7.2$ Hz, $Ar-H$), 7.21 (t, 2H, $J = 7.2$ Hz, $Ar-H$), 7.21 (d, 4H, $J = 7.2$ Hz, $Ar-H$), 5.37 (d, 1H, $J = 15.6$ Hz, $CH=C$), 5.30-5.26 (m, 1H, $CH_3-CH=C$), 4.46 (br, 1H, NH), 3.07 (d, 2H, $J = 4.8$ Hz, $N-CH_2$), 2.74 (d, 2H, $J = 13.2$ Hz, CH_2-Ph), 2.66 (d, 2H, $J = 13.2$ Hz, CH_2-Ph), 1.71 (dd, 3H, $J = 6.0$ Hz, 1.2 Hz, CH_3), 1.46 (s, 9H, $C-(CH_3)_3$).

^{13}C NMR ($CDCl_3$, 151 MHz) δ 155.9, 137.4, 134.9, 130.8, 127.8, 126.2, 124.9, 79.1, 44.5, 43.8, 43.3, 28.4, 18.3.

HRMS (FAB) Exact Mass Calcd. for $C_{24}H_{31}NO_2$ ($[M+H]^+$): 366.2428. Found: 366.2437.

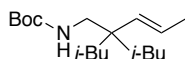


(E)-tert-butyl (2,2-dipropylpent-3-en-1-yl)carbamate

1H NMR ($CDCl_3$, 600 MHz) δ 5.38-5.34 (m, 1H, $CH_2-CH=C$), 5.21 (d, 1H, $J = 16.2$ Hz, $CH=C$), 4.39 (br, 1H, NH) 3.02 (d, 2H, $J = 6.0$ Hz, $N-CH_2$), 1.69 (d, 3H, $J = 6.0$ Hz, $CH_3-CH=C$), 1.44 (s, 9H, $C-(CH_3)_3$) 1.26-1.17 (8H), 0.87 (t, 6H, $J = 6.6$ Hz, CH_2-CH_3).

^{13}C NMR ($CDCl_3$, 151 MHz) δ 156.0, 137.4, 123.9, 78.9, 46.3, 42.4, 37.1, 28.4, 18.4, 16.5, 14.8.

HRMS (FAB) Exact Mass Calcd. for $C_{16}H_{31}NO_2$ ($[M+H]^+$): 270.2428. Found: 270.2423.

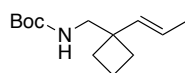


(E)-tert-butyl (2,2-diisobutylpent-3-en-1-yl)carbamate

^1H NMR (CDCl_3 , 400 MHz) δ 5.37-5.24 (m, 2H, $\text{CH}_3\text{-CH=CH}$), 5.28 (br, 1H, NH), 3.11 (d, 2H, $J = 5.7$ Hz, N- CH_2), 1.68 (d, 3H, $J = 5.3$ Hz, $\text{CH}_3\text{-CH=C}$), 1.43 (s, 9H, C-(CH_3) $_3$) 1.23 (ddd, 4H, $J = 25.6$ Hz, 14.2 Hz, 5.5 Hz, $\text{CH}_2\text{-CH-(CH}_3)_2$), 0.88 (q, 12H, $J = 12.00$ Hz, 3.20 Hz, $\text{CH}_2\text{-CH-(CH}_3)_2$).

^{13}C NMR (CDCl_3 , 100 MHz) δ 138.4, 122.6, 79.0, 45.7, 45.0, 42.9, 40.8, 28.4, 25.2, 23.6, 18.4.

HRMS (FAB) Exact Mass Calcd. for $\text{C}_{18}\text{H}_{35}\text{NO}_2$ ($[\text{M}]^+$): 297.2668. Found: 2297.2661.

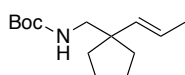


(E)-tert-butyl ((1-(prop-1-en-1-yl)cyclobutyl)methyl)carbamate

^1H NMR (CDCl_3 , 400 MHz) δ 5.49-5.38 (m, 2H, $\text{CH}_3\text{-CH=CH}$), 4.41 (br, 1H, NH) 3.21 (d, 2H, $J = 5.7$ Hz, N- CH_2), 1.95-1.91 (m, 2H, C- CH_2), 1.82-1.79 (m, 2H, C- CH_2), 1.71 (d, 2H, $J = 2.1$ Hz, CH- CH_3), 1.44 (s, 9H, C-(CH_3) $_3$).

^{13}C NMR (CDCl_3 , 100 MHz) δ 156.3, 136.5, 123.4, 78.9, 47.9, 44.0, 29.2, 28.3, 17.9, 15.3.

HRMS (FAB) Exact Mass Calcd. for $\text{C}_{13}\text{H}_{23}\text{NO}_2$ ($[\text{M}+\text{H}]^+$): 226.1802. Found: 226.1809.

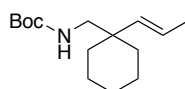


(E)-tert-butyl ((1-(prop-1-en-1-yl)cyclopentyl)methyl)carbamate

^1H NMR (CDCl_3 , 400 MHz) δ 5.44-5.36 (m, 2H, $\text{CH}_3\text{-CH=CH}$), 3.20 (d, 2H, $J = 15.8$ Hz, N- CH_2), 2.83 (d, 3H, $J = 16.9$ Hz, $\text{CH}_3\text{-CH=C}$), 1.68-1.66 (m, 2H, C- CH_2), 1.62-1.57 (m, 4H, $\text{CH}_2\text{-CH}_2$), 1.44 (s, 9H, C-(CH_3) $_3$).

^{13}C NMR (CDCl_3 , 100 MHz) δ 156.1, 146.6, 137.1, 123.1, 85.0, 77.3, 77.0, 76.7, 49.0, 48.0, 35.0, 28.3, 27.3, 23.8, 18.1.

HRMS (FAB) Exact Mass Calcd. for $\text{C}_{14}\text{H}_{25}\text{NO}_2$ ($[\text{M}]^+$): 225.1729. Found: 225.1727.



(E)-tert-butyl ((1-(prop-1-en-1-yl)cyclohexyl)methyl)carbamate

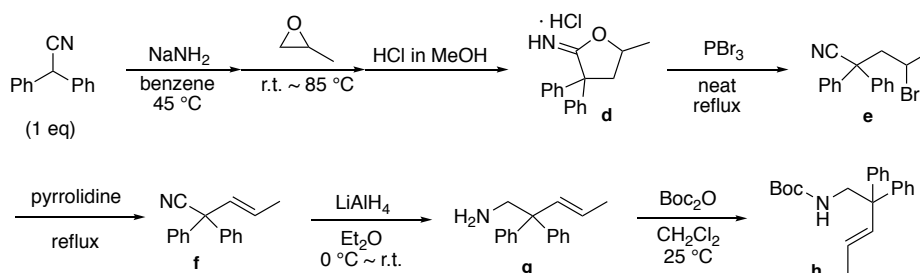
^1H NMR (CDCl_3 , 400 MHz) δ 5.45-5.41 (m, 1H, $\text{CH}_3\text{-CH=C}$), 5.19 (d, 1H, $J = 15.6$ Hz, CH=C), 4.45 (br, 1H, NH) 2.99 (d, 2H, $J = 6.0$ Hz, N-CH_2), 1.72 (d, 3H, $J = 5.4$ Hz, $\text{CH}_3\text{-CH=C}$), 1.43 (s, 9H, $\text{C-(CH}_3)_3$) 1.50-1.27 (10H).

^{13}C NMR (CDCl_3 , 100 MHz) δ 156.2, 137.0, 124.8, 78.8, 49.3, 40.0, 33.8, 28.4, 26.3, 21.9, 18.4.

HRMS (FAB) Exact Mass Calcd. for $\text{C}_{15}\text{H}_{27}\text{NO}_2$ ($[\text{M}]^+$): 253.2042. Found: 253.2045.

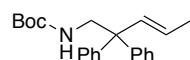
Synthesis of (E)-tert-Butyl (2,2-Phenyl Pent-3-en-1-yl)carbamate:

The (*E*)-*tert*-Butyl (2,2-Phenyl Pent-3-en-1-yl)carbamate (**S8**) was synthesized from aldol reaction of commercially available diphenyl acetonitrile with propylene oxide to give 5-methyl-3,3-diphenyldihydrofuran-2(3*H*)-imine hydrogen chloride salt (**S4**). And then the reaction of **S4** in the presence of phosphorous tribromide gave 4-bromo-2,2-diphenyl pentanenitrile (**S5**) before elimination to (*E*)-2,2-Diphenyl Pent-3-enenitrile (**S6**), and then reduction and protection with di-*tert*-butyl decarbonate (Boc) to afford *tert*-Butyl (*E*)-(2,2-Diphenylpent-3-en-1-yl)Carbamate (**S8**) in final step (Scheme 8).¹⁰⁻¹¹



Scheme 8. Synthesis of (*E*)-*tert*-butyl (2,2-phenyl pent-3-en-1-yl)carbamate starting material

Characterization of (E)-tert-Butyl (2,2-Phenyl Pent-3-en-1-yl)carbamate:



***tert*-butyl (*E*)-(2,2-diphenylpent-3-en-1-yl)carbamate**

TLC $R_f = 0.35$ (10:1 hexane:ethyl acetate).

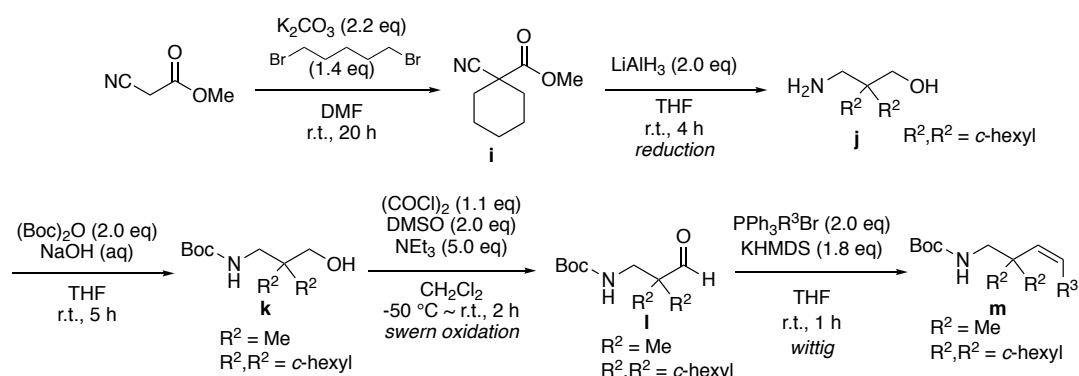
^1H NMR (CDCl_3 , 400 MHz) δ 7.31-7.18 (m, 10H, Ar-*H*), 5.98 (dd, 1H, $J = 15.6$, 1.4 Hz, C-CH=CH), 5.32-5.24 (m, 1H, C-CH=CH), 4.37 (br, 1H, NH), 3.97 (d, 2H, $J = 5.7$ Hz, NH-CH_2), 1.75 (dd, 3H, $J = 6.4$, 1.6 Hz, CH-CH_3), 1.38 (s, 9H, $\text{C-(CH}_3)_3$).

^{13}C NMR (CDCl_3 , 100 MHz) δ 155.8, 145.0, 135.5, 128.4, 128.2, 126.6, 126.4, 79.2, 53.7, 47.7, 31.6, 28.3, 18.4.

HRMS (FAB) Exact Mass Calcd. for $\text{C}_{22}\text{H}_{27}\text{NO}_2$ ($[\text{M}]^+$): 338.2115. Found: 338.2124.

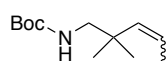
Synthesis of (Z)-tert-butyl-(2,2-dialkyl or 2-cycloalkyl alk-3-en-1-yl) carbamate:

The (Z)-olefin starting materials are synthesized from alkylation of commercially available methyl-2-cyanoethanoate with 1,5-dibromopentane in the presence of potassium carbonate to give **S9** product. And then subjected **S9** into reduction condition by the use of LiAlH₄ in THF solution followed by protection of free amine (**S10**) with di-*tert*-butyl decarbonate (Boc) to afford *N*-Boc amino alcohol (**S11**). The Swern oxidation of *N*-Boc amino alcohol gave *N*-Boc-amino-2-alkyl alkanal product (**S12**) before Wittig reaction in the final step to provide (*Z*)-*tert*-butyl-(2,2-dialkyl or 2-cycloalkyl alk-3-en-1-yl)carbamate (**S13**) as stocked starting materials (Scheme 9).¹²⁻¹³



Scheme 9. Synthesis of (*Z*)-*tert*-butyl-(2,2-dialkyl or 2-cycloalkyl alk-3-en-1-yl)carbamate

Characterization of (Z)-tert-butyl-(2,2-dialkyl or 2-cycloalkyl alk-3-en-1-yl)carbamate starting material:

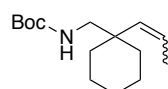


(Z)-tert-butyl (2,2-dimethylpent-3-en-1-yl)carbamate

¹H NMR (CDCl₃, 400 MHz) δ 5.48-5.42 (m, 1H, CH₃-CH=C), 5.20 (d, 1H, *J* = 12 Hz, CH=C), 4.58 (br, 1H, NH) 3.09 (d, 2H, *J* = 6.0 Hz, N-CH₂), 1.74 (dd, 3H, *J* = 7.2 Hz, 1.8 Hz, CH₃-CH=C), 1.44 (s, 9H, C-(CH₃)₃), 1.11 (s, 6H).

¹³C NMR (CDCl₃, 100 MHz) δ 156.3, 136.7, 125.3, 79.0, 51.1, 37.6, 28.4, 26.5, 14.3.

HRMS (FAB) Exact Mass Calcd. for C₁₂H₂₃NO₂ ([M]⁺): 213.1729. Found: 213.1724.

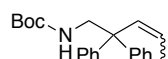


(Z)-tert-butyl ((1-(prop-1-en-1-yl)cyclohexyl)methyl)carbamate

^1H NMR (CDCl_3 , 400 MHz) δ 5.57-5.54 (m, 1H, $\text{CH}_3\text{-CH=C}$), 5.10 (d, 1H, $J = 12$ Hz, CH=C), 4.57 (br, 1H, *NH*) 3.14 (d, 2H, $J = 6.6$ Hz, N-CH_2), 1.73 (dd, 3H, $J = 7.2$ Hz, 1.8 Hz, $\text{CH}_3\text{-CH=C}$), 1.43 (s, 9H, $\text{C-(CH}_3)_3$), 1.56-1.22 (10H).

^{13}C NMR (CDCl_3 , 100 MHz) δ 156.2, 135.0, 126.3, 78.8, 49.4, 41.7, 35.3, 28.4, 26.1, 22.2, 14.4.

HRMS (FAB) Exact Mass Calcd. for $\text{C}_{15}\text{H}_{27}\text{NO}_2$ ($[\text{M}+\text{H}]^+$): 254.2115. Found: 254.2130.

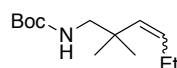


(*Z*)-tert-butyl (2,2-diphenylpent-3-en-1-yl)carbamate

^1H NMR (CDCl_3 , 400 MHz) δ 7.31-7.27(m, 4H, *Ar-H*), 7.23-7.14 (m, 6H, *Ar-H*), 5.98 (d, 1H, $J = 15.5$ Hz, $\text{CH}_3\text{-CH=CH}$), 5.33-5.18 (m, 1H, $\text{CH}_3\text{-CH=CH}$), 4.37 (br, 1H, *NH*) 3.95 (d, 2H, $J = 6.5$ Hz, N-CH_2), 1.75 (dd, 3H, $J = 6.5$ Hz, 1.4 Hz, $\text{CH}_3\text{-CH}$), 1.38 (s, 9H, $\text{C-(CH}_3)_3$).

^{13}C NMR (CDCl_3 , 100 MHz) δ 156.0, 144.5, 134.3, 128.7, 128.4, 128.3, 128.2, 126.4, 79.3, 77.3, 77.0, 76.7, 53.6, 49.6, 28.3, 18.4, 15.0.

HRMS (FAB) Exact Mass Calcd. for $\text{C}_{22}\text{H}_{27}\text{NO}_2$ ($[\text{M}+\text{H}]^+$): 338.2115. Found:338.2126.

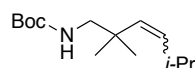


(*Z*)-tert-butyl (2,2-dimethylhex-3-en-1-yl)carbamate

^1H NMR (CDCl_3 , 400 MHz) δ 5.33-5.29 (m, 1H, $\text{CH}_3\text{-CH=C}$), 5.15 (d, 1H, $J = 12$ Hz, CH=C), 4.58 (br, 1H, *NH*) 3.07 (d, 2H, $J = 6.0$ Hz, N-CH_2), 1.74 (quin, 2H, $J = 7.2$ Hz, $\text{CH}_3\text{-CH}_2\text{-CH=C}$), 1.44 (s, 9H, $\text{C-(CH}_3)_3$), 1.1 (s, 6H), 0.98 (t, 3H, $J = 7.8$ Hz, $\text{CH}_2\text{-CH}_3$).

^{13}C NMR (CDCl_3 , 100 MHz) δ 156.1, 144.8, 136.6, 132.8, 128.5, 128.4, 128.3, 126.5, 79.4, 53.9, 49.8, 28.4, 22.6, 13.3.

HRMS (FAB) Exact Mass Calcd. for $\text{C}_{13}\text{H}_{25}\text{NO}_2$ ($[\text{M}+\text{H}]^+$): 228.1958. Found: 228.1966.

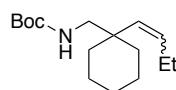


(*Z*)-tert-butyl (2,2,5-trimethylhex-3-en-1-yl)carbamate

^1H NMR (CDCl_3 , 400 MHz) δ 5.12 (dd, 1H, $\text{CH(CH}_3)_2\text{-CH=C}$), 5.05 (d, 1H, $J = 12$ Hz, $\text{CH(CH}_3)_2\text{-CH=CH}$), 4.58 (br, 1H, *NH*) 3.06 (d, 2H, $J = 6.6$ Hz, N-CH_2), 2.80-2.76 (m, 1H, $\text{CH(CH}_3)_2\text{-CH=C}$), 1.44 (s, 9H, $\text{C-(CH}_3)_3$), 1.1 (s, 6H), 0.953 (d, 3H, $J = 6.6$ Hz, CH_3), 0.950 (d, 3H, $J = 6.6$ Hz, CH_3).

^{13}C NMR (CDCl_3 , 100 MHz) δ 156.6, 139.9, 132.0, 79.3, 51.7, 37.9, 28.7, 27.9, 27.3, 23.7.

HRMS (FAB) Exact Mass Calcd. for $\text{C}_{14}\text{H}_{27}\text{NO}_2$ ($[\text{M}+\text{H}]^+$): 242.2115. Found: 242.2115.

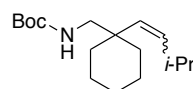


(Z)-tert-butyl ((1-(but-1-en-1-yl)cyclohexyl)methyl)carbamate

^1H NMR (CDCl_3 , 400 MHz) δ 5.42-5.39 (m, 1H, $\text{CH}_2\text{-CH}=\text{C}$), 5.03 (d, 1H, $J = 12.6$ Hz, $\text{CH}=\text{C}$), 4.55 (br, 1H, NH) 3.12 (d, 2H, $J = 6.0$ Hz, N-CH_2), 2.16 (quin, 2H, $J = 7.8$ Hz, $\text{CH}_3\text{-CH}_2\text{-CH}=\text{C}$), 1.70 (2H) 1.54 (s, 9H, $\text{C-(CH}_3)_3$), 1.53-1.22 (8H) 0.98 (t, 3H, $J = 7.2$ Hz, $\text{CH}_3\text{-CH}_2$).

^{13}C NMR (CDCl_3 , 100 MHz) δ 156.2, 134.5, 133.3, 78.8, 49.6, 41.7, 35.5, 28.4, 26.2, 22.3, 22.0, 14.4.

HRMS (FAB) Exact Mass Calcd. for $\text{C}_{16}\text{H}_{29}\text{NO}_2$ ($[\text{M}+\text{H}]^+$): 268.2271. Found: 268.2280.

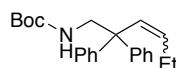


(Z)-tert-butyl ((1-(3-methylbut-1-en-1-yl)cyclohexyl)methyl)carbamate

^1H NMR (CDCl_3 , 400 MHz) δ 5.25-5.15 (m, 1H, $\text{CH-CH}=\text{C}$), 4.93 (d, 1H, $J = 12.1$ Hz, $\text{CH}=\text{C}$), 4.55 (br, 1H, NH) 3.11 (d, 2H, $J = 6.4$ Hz, N-CH_2), 2.77-2.65 (m, 1H, $\text{CH}_3\text{-CH-CH}_3$), 1.67 (2H) 1.42 (s, 9H, $\text{C-(CH}_3)_3$), 1.53-1.18 (8H) 0.93 (d, 6H, $J = 6.4$ Hz, $\text{CH}_3\text{-CH}$).

^{13}C NMR (CDCl_3 , 100 MHz) δ 156.6, 140.8, 131.3, 79.0, 50.3, 41.8, 36.1, 28.8, 28.2, 26.5, 23.4, 22.7.

HRMS (FAB) Exact Mass Calcd. for $\text{C}_{17}\text{H}_{31}\text{NO}_2$ ($[\text{M}+\text{H}]^+$): 282.2428. Found: 282.2441.



(Z)-tert-butyl (2,2-diphenylhex-3-en-1-yl)carbamate

^1H NMR (CDCl_3 , 400 MHz) δ 7.30-7.19 (m, 10H, Ar-H), 5.92 (d, 1H, $J = 11.7$ Hz, $(\text{Ph})_2\text{C-CH}=\text{CH}$), 5.57-5.64 (m, 1H, $\text{CH}=\text{CH-CH}_2$), 4.38 (s, 1H, NH), 3.93 (d, 2H, $J = 6.0$ Hz, NH-CH_2), 0.66 (t, 3H, $J = 7.4$ Hz, $\text{CH}_2\text{-CH}_3$).

^{13}C NMR (CDCl_3 , 100 MHz) δ 144.6, 137.1, 133.3, 128.8, 128.6, 126.7, 54.3, 49.8, 28.7, 23.2, 13.3.

HRMS (FAB) Exact Mass Calcd. for $\text{C}_{23}\text{H}_{29}\text{NO}_2$ ($[\text{M}+\text{H}]^+$): 352.2271. Found: 352.2286.

2.5 References

1. Agami, C.; Couty, F.; Poursoulis, M. *Synlett*. **1992**, 847–848.
2. Sugiura, M.; Mori, C.; Kobayashi, S. *J. Am. Chem. Soc.* **2006**, *128*, 11038–11039.
3. Bosque, I.; Foubelo, F.; Gomez J. C. *Org. Biomol. Chem.* **2013**, *11*, 7505–7515.
4. Sugiura, M.; Mori, C.; Kobayashi, S. *J. Am. Chem. Soc.* **2006**, *128*, 11038–11039.
5. Bosque, I.; Foubelo, F.; Gonzalez-Gomez, J. *Org. Biomol. Chem.* **2013**, *11*, 7507–7515.
6. Schlummer, B.; Hartwig, J. F. *Org. Lett.* **2002**, *4*, 1471–1474.
7. Haskins, C. M.; David W.; Knight, D. W. *Chem. Commun.* **2002**, 2724–2725.
8. Bower, J. F.; Williams, J. M. *Synlett* **1996**, 685–686.
9. Boechman, R. K. Jr.; Breining, S. R.; Arvanitis, A. *Tetrahedron* **1997**, 8941–8962.
10. Easton, N. R.; Gardner, J. H.; Stevens, J. R. *J. Am. Chem. Soc.* **1947**, *69*, 2941–2942.
11. Liu, F.; Worthy, K. M.; Bindu, L.; Giubellino, A.; Bottaro, D. P.; Fisher, R. J.; Burke, T. R. Jr. *Org. Biomol. Chem.* **2007**, *5*, 367–372.
12. Reuyl, D. I.; Basak, A.; Silverman, L. S. *J. Nat. Pro.* **1993**, *56*, 1373–1396.
13. Coldham, I.; Fernandez, J. C.; Snowden, D. J. *J. Org. Chem.* **2000**, *65*, 3788–3795.

CHAPTER 3

MECHANISTIC STUDIES ON BRØNSTED ACID-INITIATED REARRANGEMENT REACTION OF ENE-ALDIMINES

3.1 Introduction

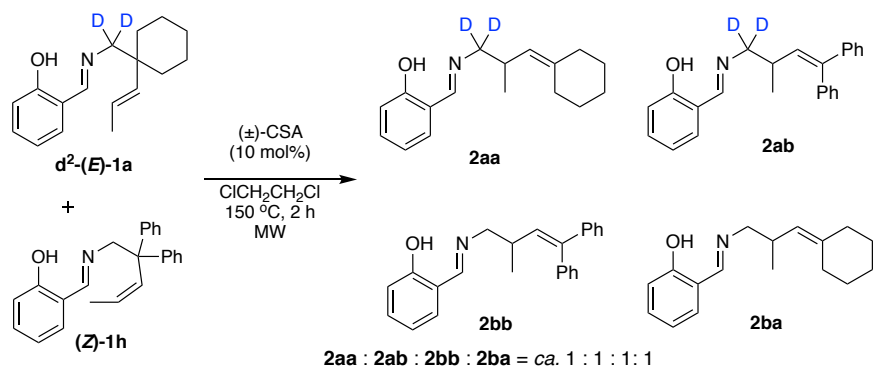
According to the previous reports, the reaction of ene-imines typically proceeds through [3,3]-rearrangement, which is called 2-azonia-[3,3]-Cope rearrangement as mentioned earlier. On the other hand, as described in chapter 2, Brønsted acid-initiated formal [1,3]-rearrangement reaction of ene-aldimines was discovered and developed, which bond formation is in contrast to previous reports. The reaction mechanism of this formal [1,3]-rearrangement is totally unclear. Therefore, detailed mechanistic studies were conducted and the results are summarized in this chapter.

3.2 Crossover experiment studies

Crossover experiments were initially examined to gain insight into reaction pathways either intermolecular- or intramolecular ones.

3.2.1 Crossover experiment study of substrates

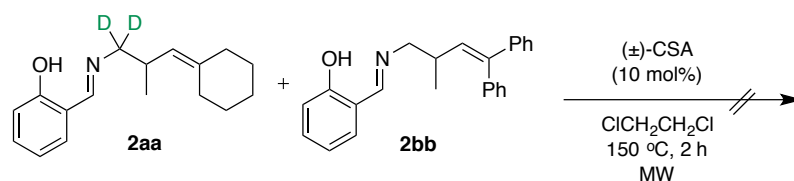
An isotopic labelled ene-alimine substrate was used to clearly evaluate the stage of C(α)–C(β) bond cleavage without considering the imine exchange. Furthermore, in the point of similar reactivities, cyclohexyl- and diphenyl groups were selected as substituents at the β -position.¹ Therefore, the deuterium-labeled substrate d²-(*E*)-**1a** was synthesized according to the developed procedure by the use of deuterated lithium aluminum hydride.² Then, a 1:1 mixture of deuterium-labeled substrate d²-(*E*)-**1a** and normal substrate (*Z*)-**1h** were subjected into optimized rearrangement reaction condition. It was found that two normal rearrangement products (**2aa** and **2bb**) and crossover rearrangement products (**2ab** and **2ba**) were observed in a ratio of *ca.* 1:1:1:1 (Scheme 1).



Scheme 1. Crossover experiment of substrates

3.2.2 Crossover experiment study of products

In order to demonstrate that cleavage of C(α)-C(β) bond occurs during the rearrangement process or not, the crossover experiment of products was carried out. When a 1:1 mixture of deuterated product **2aa** and normal product **2bb** was treated with 10 mol% of (\pm)-CSA under rearrangement condition, no crossover products **2ab** and **2ba** were generated, and **2aa** and **2bb** were recovered (Scheme 2). These results suggested that reaction involves C(α)-C(β) cleavage during the rearrangement process, and this reaction is irreversible.



Scheme 2. Crossover experiment of products

3.3 Speculation of reaction mechanism

The results of crossover experiments indicated that this rearrangement proceeded through intermolecular pathway. According to deep considerations based on the results of crossover experiments, 2-azaallenium³-mediated chain reaction⁴ mechanism was speculated (Figure 1). To propose details of reaction mechanism, DFT calculations were carried out by Dr. Honda in HPC SYSTEMS and Dr. Suzuki in IMS as collaborative studies.

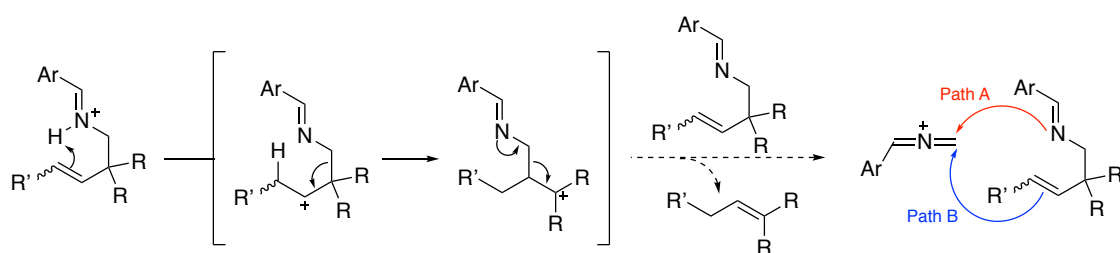


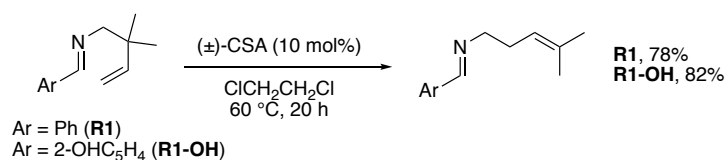
Figure 1. Intermolecular reaction *via* generation of 2-azaallenium cation

3.4 Experimental and computational study for generation of 2-azaallenium cation

2-Azaallenium cation was initially considered as a chain carrier in proposed chain reaction mechanism. To simplify the reaction system, experimental studies were conducted by use of ene-aldimine substrates possessing no methyl group at the terminal olefin. Furthermore, to support the proposed reaction mechanism based on the experimental results, the computational results were partially summarized.⁵

3.4.1 Experimental study on the effect of the 2-OH of aryl group on benzylidene

On the basis of results in chapter 2,⁶ the 2-OH of aryl group on benzylidene seemed not to significantly affect the reaction progress. To confirm about this point, benzaldehyde and salicylaldehyde-derived ene-aldimines **R1** and **R1-OH** were prepared and subjected to reaction at 60 °C in dichloroethane. It was revealed that reaction of both **R1** and **R1-OH** smoothly proceeded to formal [1,3]-rearrangement products in high yields without any events, and salicylaldehyde-derived ene-aldimines (**R1-OH**) gave desired product in slightly higher yield. It was hypothesized that 2-hydroxy group may have little electronic effect to stabilize 2-azaallenium intermediate. However, 2-hydroxy group on ene-aldimine substrate did not influence the reaction yield according to these results.



Scheme 3. Formal [1,3]-rearrangement reaction of ene-aldimine possessing no methyl group at the terminal olefin

3.4.2 Computational study for the structure of 2-azaallenium cation

To demonstrate the conformational stability of 2-azaallenium cation, *o*-quinonoid as the resonance structure of 2-azaallenium cation was selected and considered (Figure 2). DFT calculations indicated that the Gibbs free energy of 2-azaallenium was lower than another one. The *o*-quinonoid lose aromaticity resulting in higher Gibbs free energy and instability. Therefore, 2-azaallenium is a key intermediate for mediating the reaction.

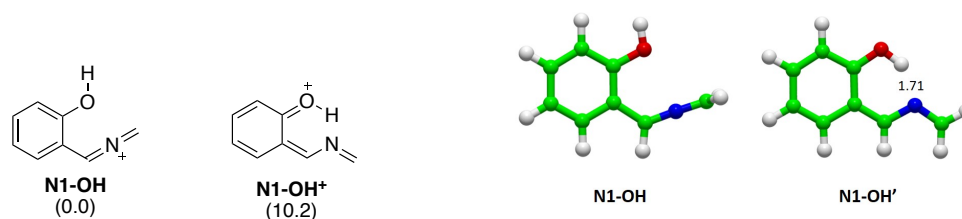


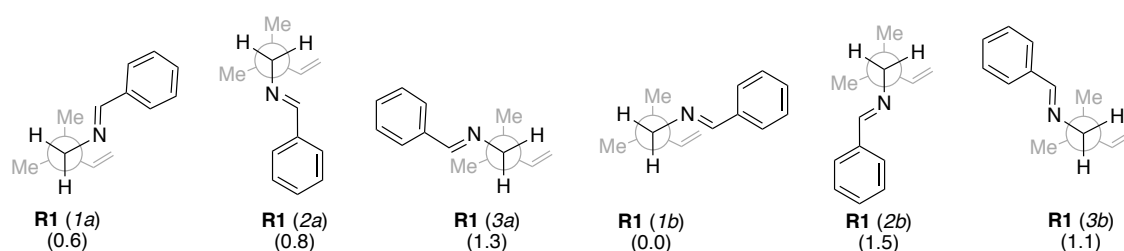
Figure 2. Conformational stability of 2-azaallenium and *o*-quinonoid. Optimized geometries and the Gibbs free energies in parentheses (ΔG , in kcal/mol) were calculated at the SMD(DCE)/M06-2X-D3/6-311+G(d,p) level at 333 K.

3.4.3 Conformation and stability of ene-aldimine substrate

As described in section 3.4.1 and 3.4.2, the 2-OH of aryl group on benzylidene does not significantly affect the reaction progress. Therefore, benzaldehyde-derived ene-aldimine with dimethyl group **R1** (Ar = Ph; R,R = Me,Me; R' = H) was used as a model substrate for DFT calculation.

Six conformers of substrate **R1** were considered, and their conformational stability were investigated (Figure 3(a)). The DFT calculations revealed that the conformation *1b*, *1a* and *2a* were more energetically stabilized than the other three conformations *3a*, *2b*, and *3b*. The energy differences between *1b*, *1a* and *2a* were within 1 kcal/mol, and conformation *1b* is the most stable among these three conformers. This result suggests that these three conformations (*1b*, *1a*, and *2a*) are favorable to involve protonation in the chain reaction. In contrast, once ene-aldimines were protonated to become ene-aldiminiums, the Gibbs free energies of *1a* and *1b* were approximately 1 kcal/mol, and conformation *1a* is energetically more stable than conformer *1b* (Figure 3b). It is speculated that the differences in the energetically stable conformers under protonation affect the conformation of the rearrangement products, and protonated conformation *1a* plays a key role to facilitate the newly discovered formal [1,3]-rearrangement at the state of initiation.

(a) Conformation of **R1**



(b) Conformation of **R1-H⁺**

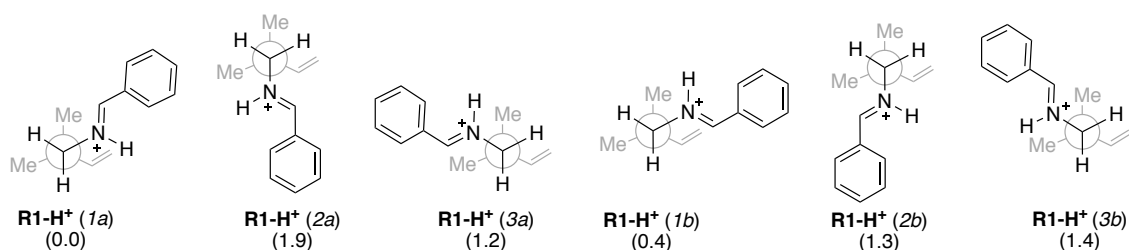


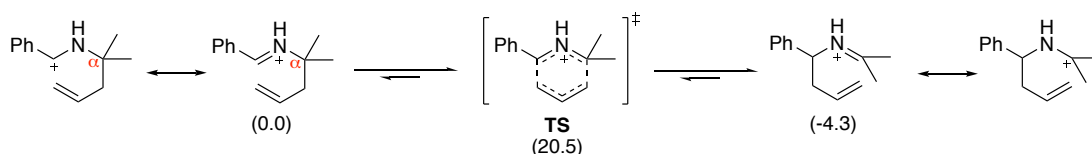
Figure 3. DFT calculations for conformational stabilities of (a) ene-aldimine substrate (**R1**), (b) protonated ene-aldimine substrate (**R1-H⁺**). Optimized geometries and the Gibbs free energies in parentheses (ΔG , in kcal/mol) were calculated at the SMD(DCE)/M06-2X-D3/6-311+G(d,p) level at 333 K.

3.4.4 DFT calculation of 2-azonia-[3,3]-sigmatropic rearrangement

The energetical differences between conformation *1a* and *1b* are less than 1 kcal/mol, and conformation *1b* is favorable conformation for 2-azonia-[3,3]-sigmatropic rearrangement.⁷ Therefore, to further support formal [1,3]-rearrangement reaction of β -substituted ene-aldimines, DFT calculations of 2-azonia-[3,3]-sigmatropic rearrangement of *1b* were conducted in the cases for both α - and β -substituted ene-aldimines.

In the case of the α -substituted ene-aldimine substrate, DFT calculation indicated exothermic reaction ($\Delta G = -4.3$ kcal/mol) (Figure 4(a)); 2-azonia-[3,3]-Sigmatropic rearrangement easily undergoes to give [3,3]-rearrangement product. This is because the resonance form of [3,3]-rearrangement product of α -substituted ene-aldimine is tertiary carbocation, which is expected to be energetically more favorable than the benzylic carbocation of substrate. In contrast, DFT calculation shows positive Gibbs free energy ($\Delta G = 5.2$ kcal/mol) in the case of β -substituted ene-aldimine substrate (Figure 4(b)). This result supports that 2-azonia-[3,3]-sigmatropic rearrangement of β -substituted ene-aldimine is an endothermic reaction and does not proceed. This reason is understood from the resonance form of [3,3]-rearrangement product: which is primary carbocation and energetically less stabilized than the benzylic carbocation of substrate.

(a) 2-azonia-[3,3]-sigmatropic rearrangement of α -substituted ene-imine



(b) 2-azonia-[3,3]-sigmatropic rearrangement of β -substituted **R1**

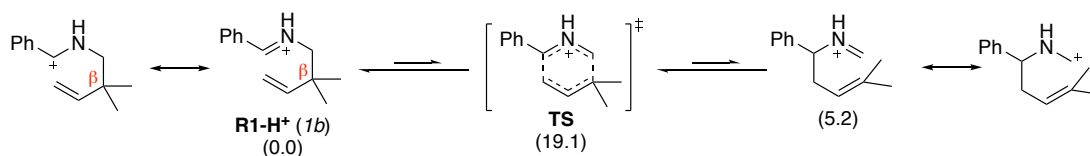


Figure 4. Concerted chair transition state in 2-azonia-[3,3]-sigmatropic rearrangement under protonation, (a) α -substituted ene-imine, (b) β -substituted ene-aldimine (**R1**). Optimized geometries and the Gibbs free energies in parentheses (ΔG , in kcal/mol) were calculated at the SMD(DCE)/M06-2X-D3/6-311+G(d,p) level at 333 K.

3.5 Proposed chain reaction mechanism

3.5.1 Proposed mechanism in initiation step

Referring to the results in section 3.4, initiation step in chain reaction mechanism is proposed as follows: The proton on imine nitrogen of **R1-H**⁺ transfers to allylic carbon to yield secondary carbocation **C1**, then a 1,2-shift of **C1** leads to give the tertiary carbocation **C2** as an intermediate. The C–C bond cleavage takes place to form a 2-azaallenium cation **N1** which further reacts with **R1** in the propagation step (Figure 5).

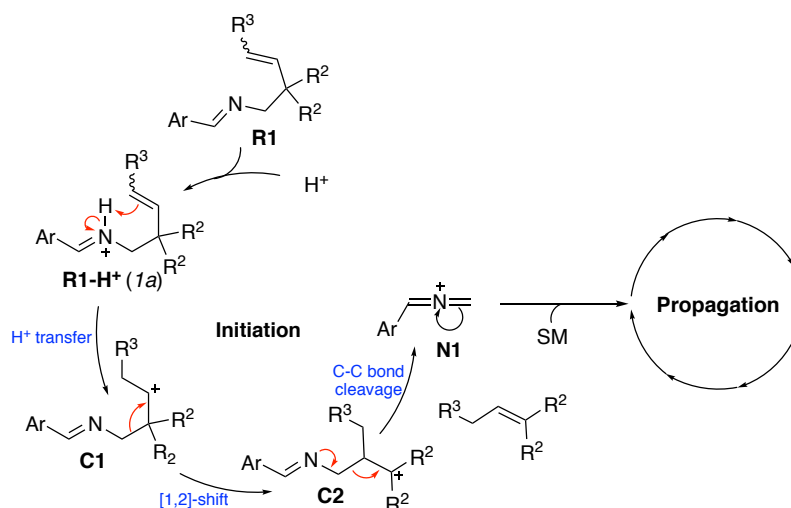


Figure 5. Proposed mechanism in initiation step in chain reaction mechanism

3.5.2 Proposed mechanism in propagation step

In propagation step, two possible pathways (**Path A** and **Path B**) were proposed due to different nucleophilic sites on **R1**. Path A (left half in Figure 6), Imino nitrogen nucleophile of **R1** makes C-N bond formation with **N1** to afford an iminium cation **N2**. The

ring closure leads to the formation of a 1,3-diazetidinium cation **N3**.^{8,9} The C–N bond cleavage of **N3** is taken place to yield an iminium cation **N4**, and then **N4** undergoes 2-azonia-[3,3]-sigmatropic rearrangement to afford an iminium cation **N5**.¹⁰ A formal [1,3]-imine shift of **N5** to **N7** takes place through a 1,3-diazetidinium intermediate **N6**. The C–N bond cleavage of **N7** provides the product **P1** in the final step, and the newly generated **N1** reacts again with **R1** for the next propagation step.

In **Path B** (right half in Figure 6), DFT calculations indicate the electrophilic allylic rearrangement, which is a stepwise electrophilic substitution rather than a concerted S_E2' process.^{11,12} First, allyl moiety nucleophile of **R1** attacks **N1** to form a secondary carbocation **C3**. Then, the 1,2-shift provides tertiary carbocation **C4** as an intermediate. Finally, the C–C bond cleavage of **C4** occurs to afford **P1**, and the regenerated **N1** reacts again with **R1** for the next propagation step.

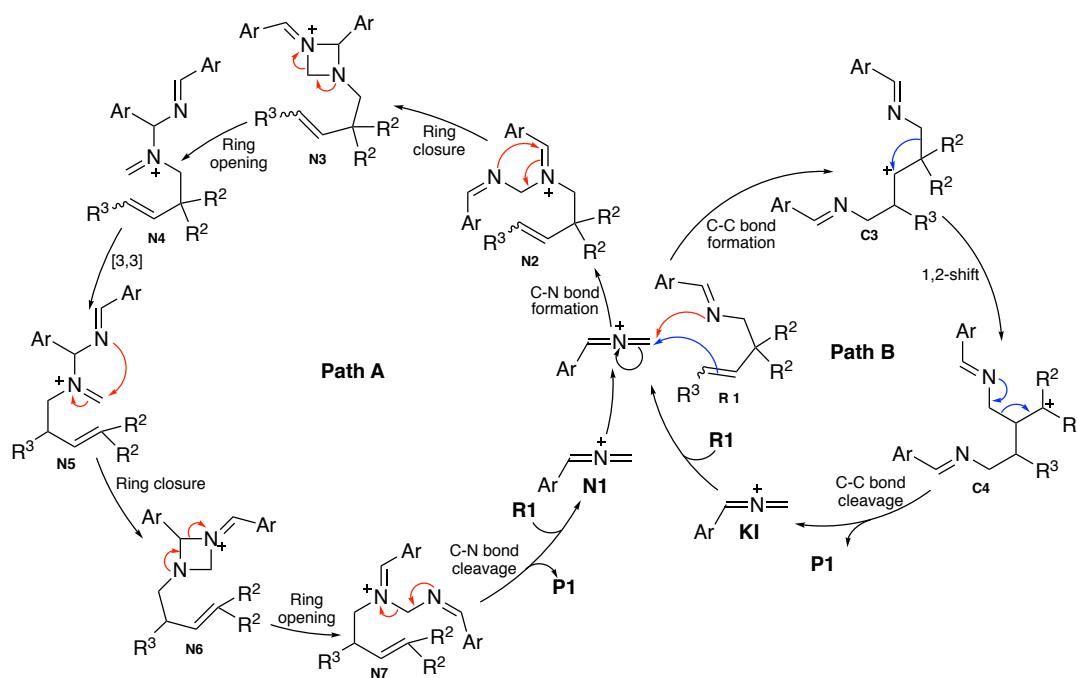


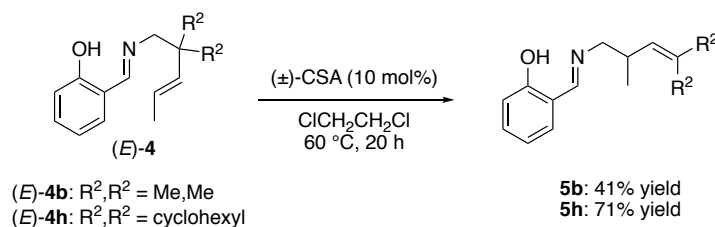
Figure 6. Proposed mechanism in propagation step

3.5.3 Experimental study using model ene-aldimine substrate

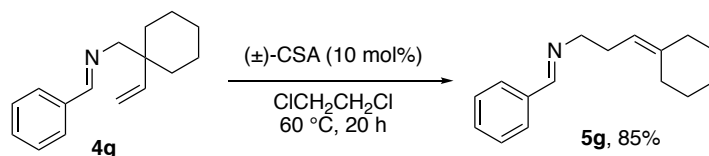
To decide the model substrate for DFT calculations, formal [1,3]-rearrangement reaction was examined under normal heating conditions (60 °C, 20 h). It is found that salicylaldehyde-derived ene-aldimine (*E*)-**4h** having cyclohexyl group at the β -position gave better reactivity than dimethyl substituent on β -position ((*E*)-**4b**) (Scheme 4(a)). According to these results, benzaldehyde-derived β -cyclohexyl ene-aldimine **4g** was prepared and applied to the rearrangement reaction at the same conditions (Scheme 4(b)). It is revealed that the

reaction proceeded smoothly to give the formal [1,3]-rearrangement in 85% yield. Therefore, ene-aldimine **4g** was decided to use as model substrate for further computational studies.

(a)



(b)



Scheme 4. Experimental studies on β -substituents of ene-aldimine substrate under normal heating condition. (a) Comparison of cyclohexyl with methyl group, (b) examination of benzaldehyde-derived β -cyclohexyl ene-aldimine

3.5.4 Computation and discussion for initiation step

Free energy diagram for initiation step is summarized (Figure 7), and the structure of intermediates and transition states are described (Figure 8). The initiation step starts with **R1-H⁺** (*1a*) (Figure 8(a)) with the shortest NH–C6 distance among all conformers (2.79 Å in Figure 8(b)). The proton transfer firstly takes place from N to C6 in the transition state **TS1** with $\Delta G^\ddagger = 32.8$ kcal/mol in Figure 7 (H–C6: 1.18 Å in Figure 8(b)). The distance between C3–C4 is extended in **TS1** (1.60 Å in Figure 8(b)), and then the 1,2-shift occurs to give tertiary carbocation **C2** as an intermediate. The C3–C6 bond cleavage takes place in **TS2** ($\Delta G^\ddagger = 15.8$ kcal/mol in Figure 7; C3–C5: 2.28 Å in Figure 8(b)) to form a complex of 2-azaallenium (**N1**) and **E1** (**N1**···**E1**: C3–C5, 3.03 Å in Figure 8(b)). Then, **N1** separates from **E1** and further reacts with **R1** in the propagation step. Even though the formation of 2-azaallenium is highly endothermic (**N1**: $\Delta G = 27.4$ kcal/mol in Figure 7), the exothermic rearrangement in the propagation step provides thermodynamic driving force to the chain reaction.

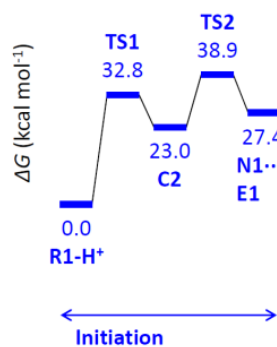
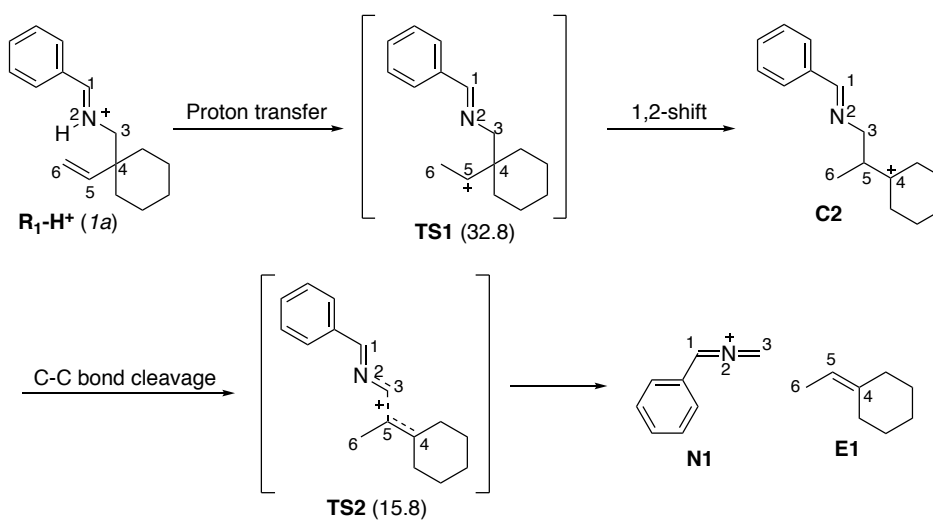


Figure 7. Free energy diagram for the initiation steps. The Gibbs free energies (ΔG in kcal/mol) were calculated at the SMD(DCE)/M06-2X-D3/6-311+G(d,p) level at 333 K.

(a)



(b)

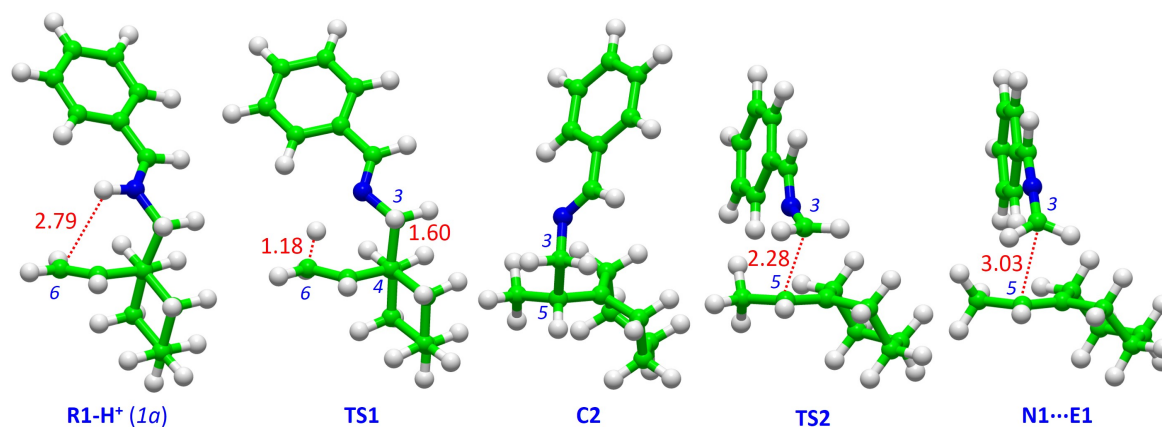


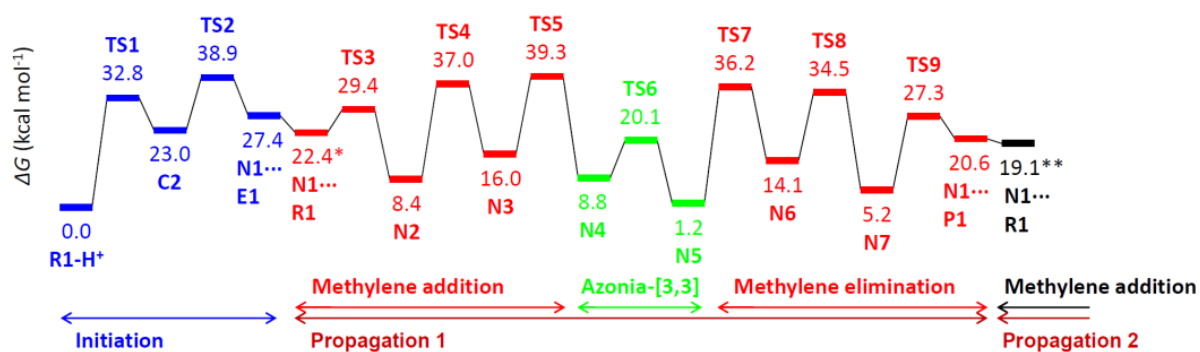
Figure 8. DFT Calculation of reaction pathway of initiation step. (a) Initiation step, (b) optimized geometries for the initiation step; the Gibbs free energies of activation in

parentheses (ΔG^\ddagger in kcal/mol) were calculated at the SMD(DCE)/M06-2X-D3/6-311+G(d,p) level at 333 K. The atomic distances are given in Å.

3.5.5 Computation and discussion for propagation step

The β -cyclohexyl substituted ene-aldimine gave better reactivity than β -dimethyl substituted ene-aldimine in experimental results. Therefore, **R1** (β -cyclohexyl substituted ene-aldimine) was used as representative substrate in computational calculation for mechanistic studies in both **Path A** and **B** referring to the speculated mechanism in 3.5.2. DFT calculations were conducted at the SMD(dichloroethane)/M06-2X-D3/6-311+G(d,p) level at 333 degrees kelvin. The Gibbs free energy diagrams (Figure 9), the structure of intermediates, and transition states are summarized in each pathway (Figures 10, 11, and 12).

(a)



(b)

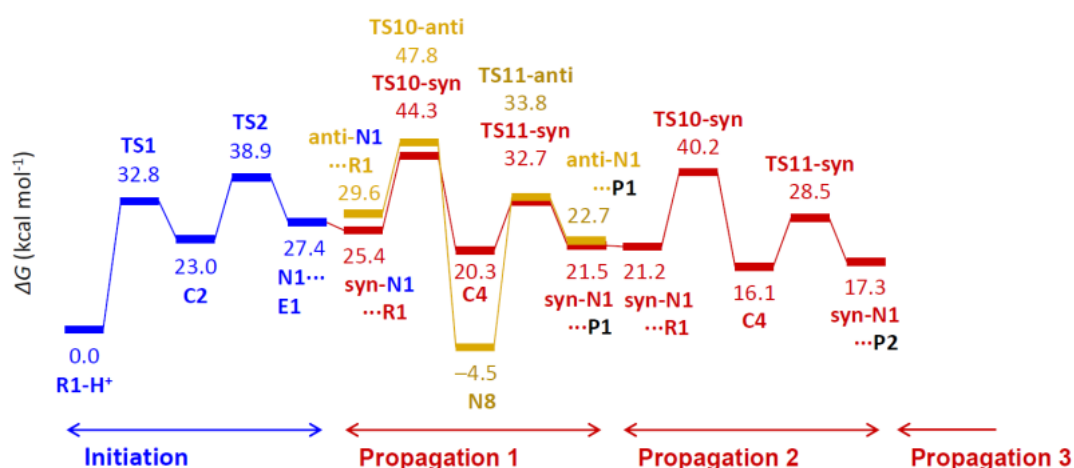
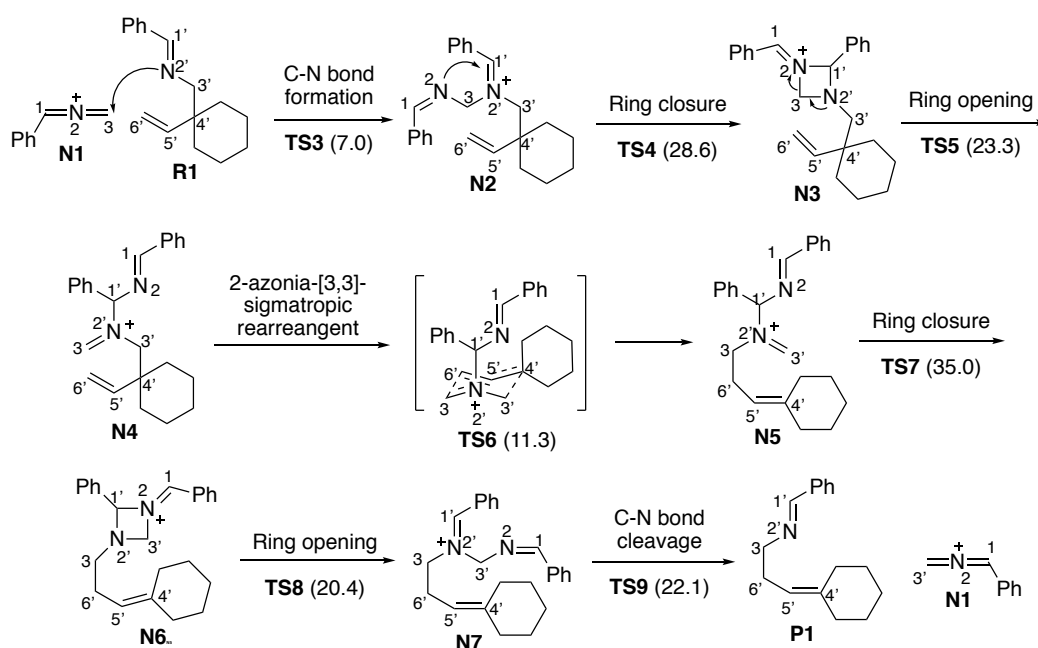


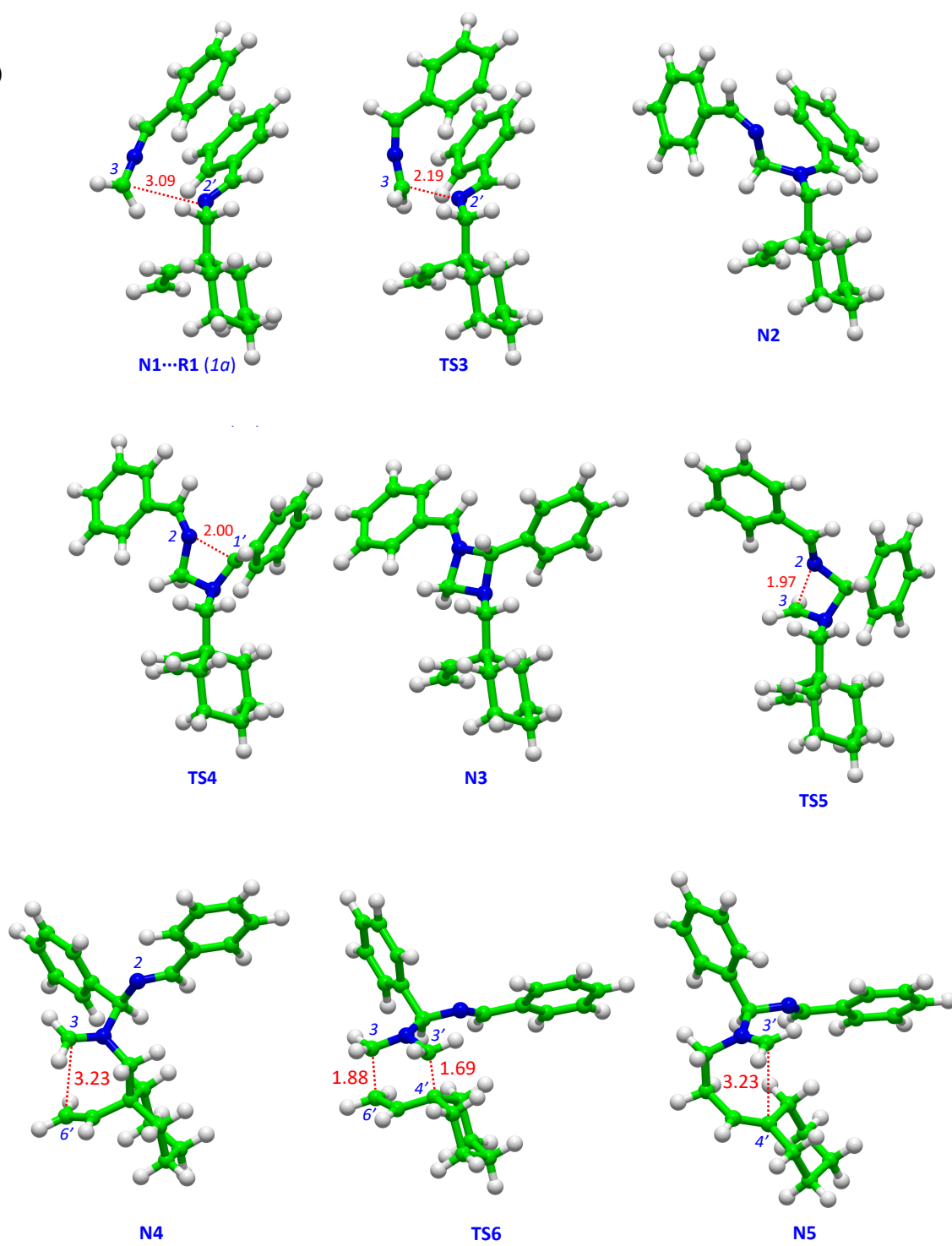
Figure 9. Free energy diagram for the initiation and propagation steps. (a) **Path A**; (b) **Path B**. The Gibbs free energies (ΔG in kcal/mol) were calculated at the SMD(DCE)/M06-2X-D3/6-311+G(d,p) level at 333 K.

Propagation **Path A**: **N1** generated from the initiation step forms a complex of **N1**···**R1** (*Ia*) and then imino nucleophile of **R1** attacks 2-azaallenium in **TS3** ($\Delta G^\ddagger = 7.0$ kcal/mol in Figure 10a) to form an iminium cation **N2**. The ring closure of **N2** takes place in **TS4** ($\Delta G^\ddagger = 28.6$ kcal/mol in Figure 10a; N2–C1': 2.00 Å in Figure 10b) to give a 1,3-diazetidinium cation **N3** after that an iminium cation **N4** is formed by ring opening of 1,3-diazetidinium cation **N3** in **TS5** ($\Delta G^\ddagger = 23.3$ kcal/mol in Figure 10a; N2–C3: 1.97 Å in Figure 10b). **N4** undergoes 2-azonia-[3,3]-sigmatropic rearrangement *via* a concerted chair transition state **TS6** ($\Delta G^\ddagger = 7.4$ kcal/mol in Figure 10a; C3–C6': 1.88 Å, C3'–C4': 1.69 Å in Figure 10b) leading to afford a more stable iminium cation **N5**. The formation of formal [1,3]-rearrangement product proceeds through ring closure in **TS7** ($\Delta G^\ddagger = 35.0$ kcal/mol in Figure 10a; C3–C6': 1.95 Å in Figure 10b), ring opening in **TS8** ($\Delta G^\ddagger = 20.4$ kcal/mol in Figure 10a; C3–C6': 2.02 Å in Figure 10b), and followed by C-N bond cleavage in the final step (**TS9**) ($\Delta G^\ddagger = 22.1$ kcal/mol in Figure 10a; C3–C6': 2.21 Å in Figure 10b) to afford the complex of desired product **P1** and new generation of 2-azaallenium (**N1**···**P1** (*Ia*)). **N1** separates from **P1** (*Ia*) and reacts again with **R1** (*Ia*) in the next cycle of propagation. The Gibbs free energy of starting point for the second propagation cycle is 19.1 kcal/mol, which is 3.3 kcal/mol lower than the first cycle of propagation ($\Delta G = 22.4$) corresponding to the exothermic conversion from **R1** to **P1** (Figure 9).

(a)



(b)



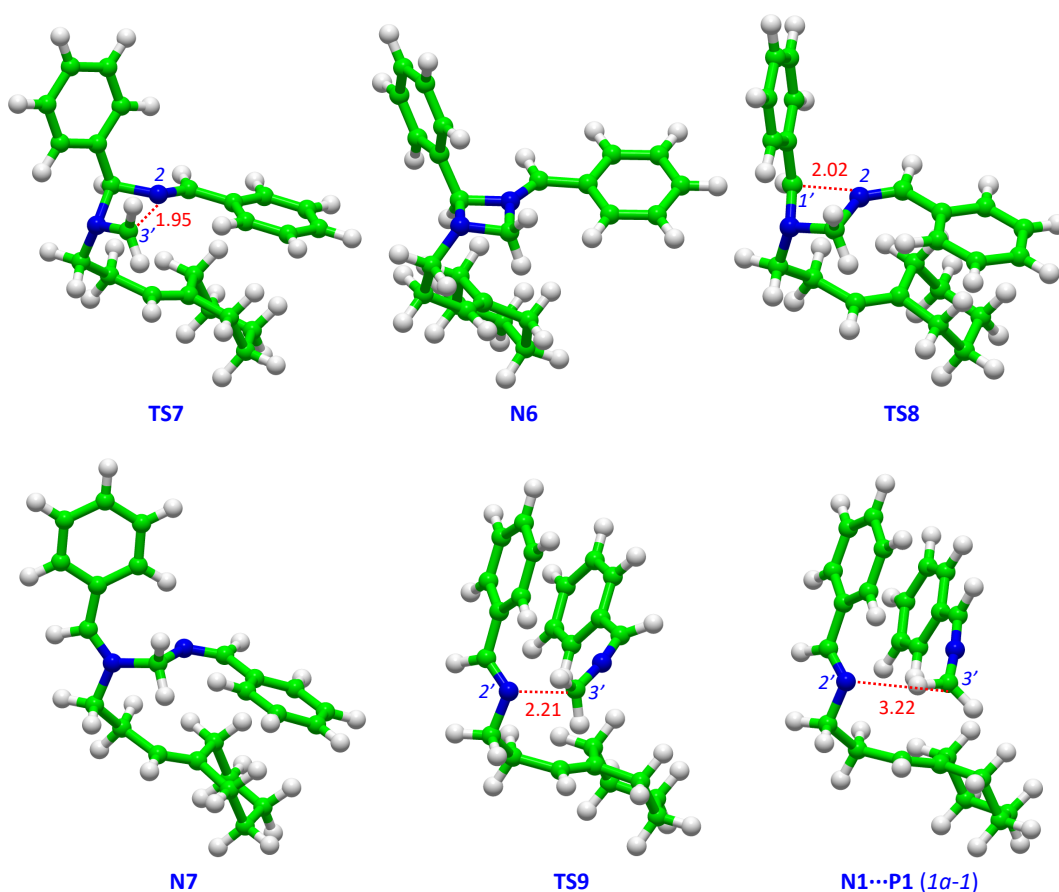
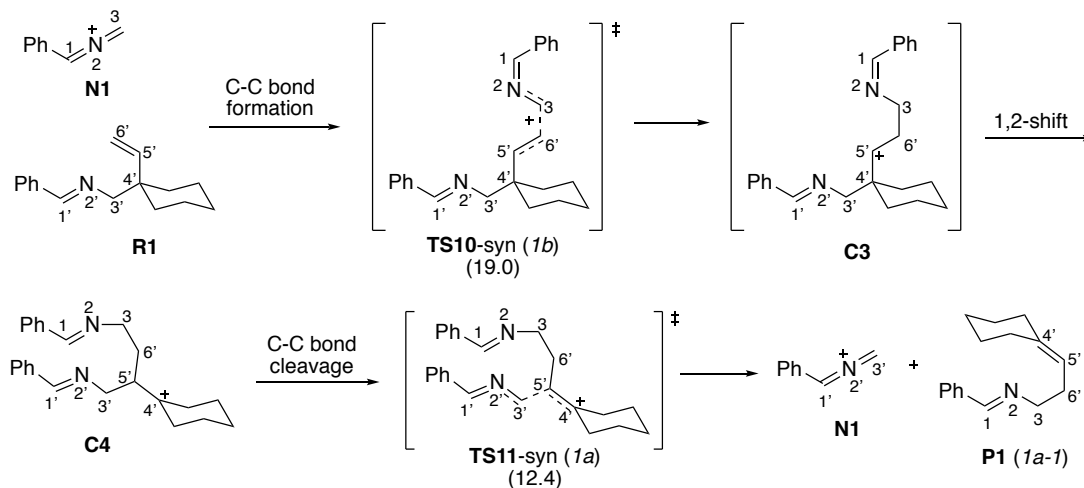


Figure 10. DFT calculation of reaction pathway for propagation step in **Path A**. (a) Propagation step; (b) optimized geometries; the Gibbs free energies of activation in parentheses (ΔG^\ddagger in kcal/mol) were calculated at the SMD(DCE)/M06-2X-D3/6-311+G(d,p) level at 333 K. The atomic distances are given in Å

Propagation **Path B**: the DFT calculation suggests that the electrophilic allylic rearrangement is a stepwise electrophilic substitution rather than a concerted S_E2' process. In the first step, 2-azaallenium **N1** is attacked by allyl nucleophile which is two possible directions; *syn* and *anti*. Therefore, the propagation B is further studied in both *syn*- and *anti*-additions. The *syn*-propagation path B (Figure 11), the lowest Gibbs free energies are observed when **R1** (*1b*) attacks **N1**; thus, **R1** (*1b*) is a representative structure to propose this pathway. Firstly, **N1** forms a *syn*-complex with **R1** (*1b*) (**syn-N1**⋯**R1**, (*1b*)) (C3–C6': 3.04 Å in Figure 11b). And then, allyl nucleophile of **R1** attacks **N1** by *syn*-direction in **TS10-syn** ($\Delta G^\ddagger = 19.0$ kcal/mol in Figure 11a; C3–C6': 2.12 Å in Figure 11b) to give a secondary carbocation **C3**. Next, the 1,2-shift leads to form tertiary carbocation **C4** before undergoing to afford a complex of desired product **P1** and new generated **N1** (**syn-N1**⋯**P1**) (C3'–C5': 3.15 Å in Figure 11b) via C-C bond cleavage in **TS11-syn** ($\Delta G^\ddagger = 12.4$ kcal/mol in Figure

11a; C3'–C5': 2.29 Å in Figure 11b). **N1** finally separates from **P1** and reacts again with **R1** (*1b*) in the next propagations.

(a)



(b)

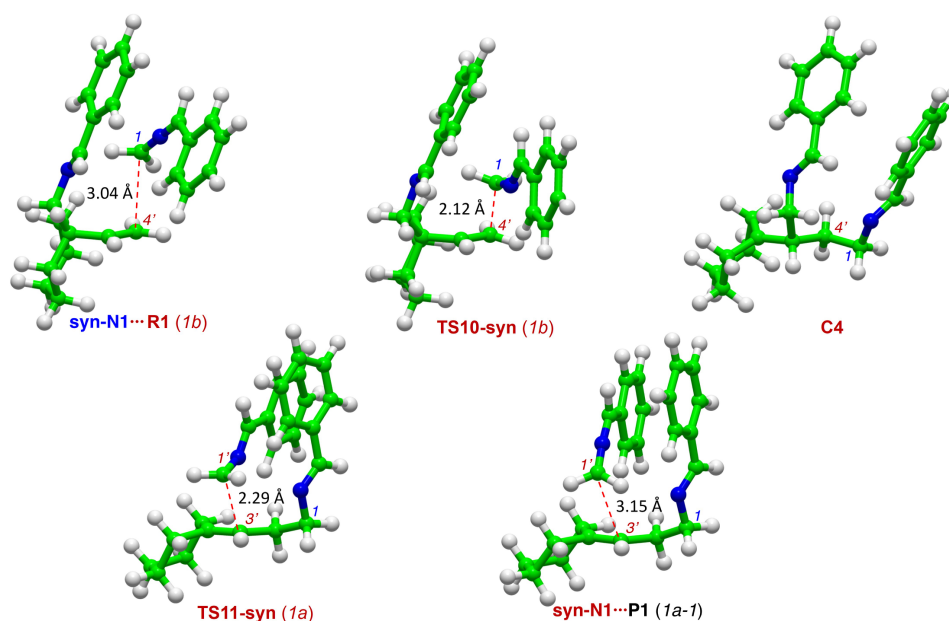
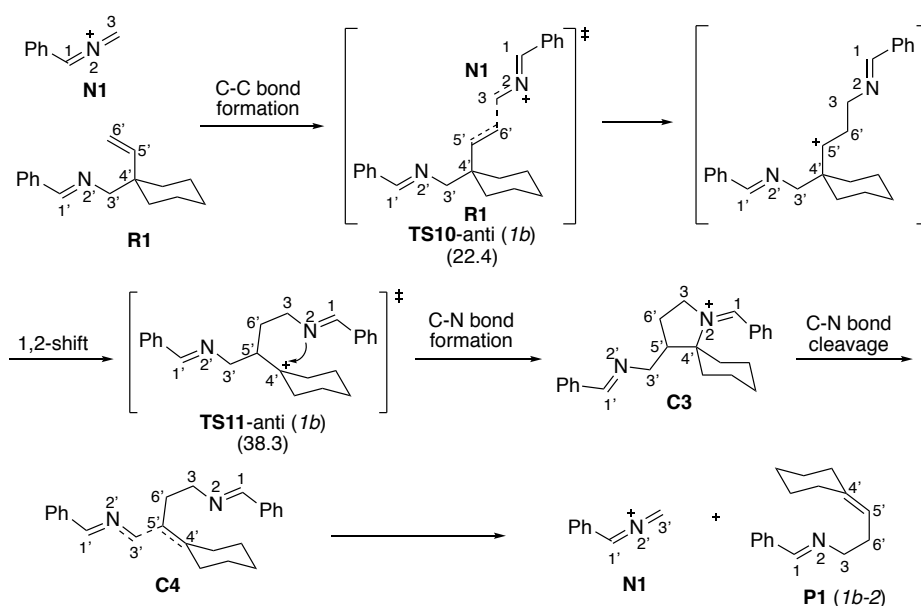


Figure 11. DFT calculation of the *syn*-pathway in **Path B**. (a) The *syn*-pathway of the propagation step from **R1** (*1b*); (b) optimized geometries for the propagation steps of the *syn*-pathway; the Gibbs free energies of activation in parentheses (ΔG^\ddagger in kcal/mol) were calculated at the SMD(DCE)/M06-2X-D3/6-311+G(d,p) level at 333 K.

The *anti*-propagation **Path B** (Figure 12), the reaction mechanism is similar to *syn*-propagation at beginning step. The coordination between **N1** and **R1** gives the lowest Gibbs free energy when **N1** approaches **R1** (*1a*), thus, the coordination between **N1** and **R1** (*1a*)

occurs (**anti-N1**···**R1**, C3–C6': 3.14 Å in Figure 11b), and then **N1** is attacked by allyl nucleophile **R1** (*1a*) by *anti*-direction in **TS10-anti** ($\Delta G^\ddagger = 22.4$ kcal/mol in Figure 12a; C3–C6': 2.12 Å in Figure 12b), which is less stable compared to **TS10-syn** (Figures 11 and 9b). Similar to *syn*-propagation path B, 1,2-shift takes place after the C-C bond formation to give tertiary carbocation followed by C-N bond formation in the next step leading to spiro **N8** intermediate that is more stable than **C4** intermediate in *syn*-propagation **B**. Due to high stability of **N8**, C-C bond cleavage occurs in higher barrier **TS11-anti** (*1b*) ($\Delta G^\ddagger = 38.3$ kcal/mol in Figure 12a; C3'–C5': 2.23 Å in Figure 12b) after pyrrolidine ring of **N8** opens to afford **anti-N1**···**P1** (*1b-2*) (C1'–C3': 3.04 Å in Figure 11b). Because **TS10-anti** is higher Gibbs free energy than **TS10-syn**, the *syn*-propagation **B** is predicted to provide 99% *syn*-stereoselectivity (Figure 9).

(a)



(b)

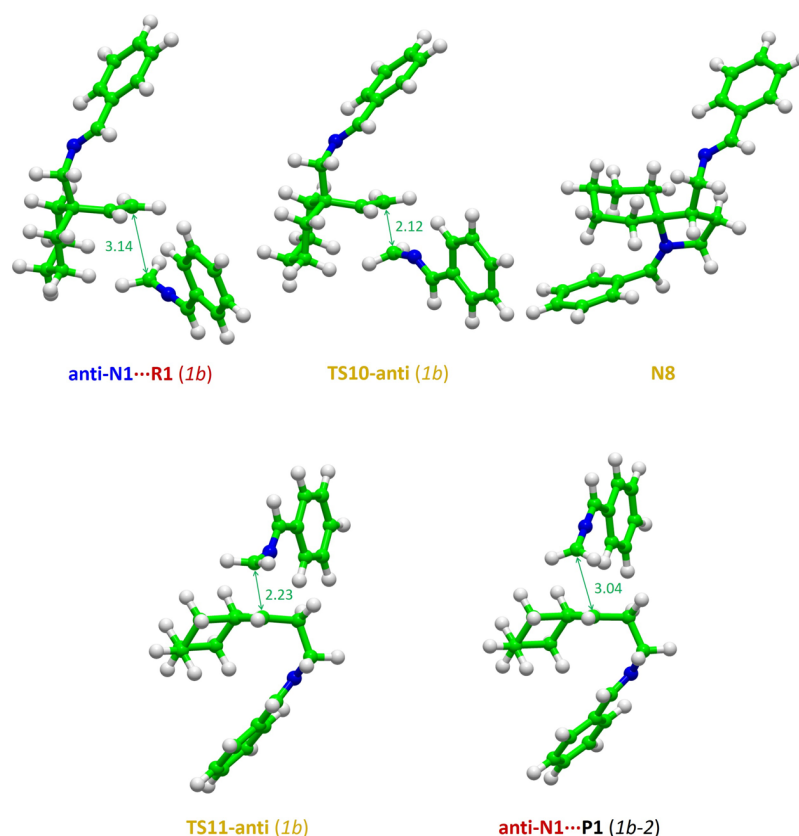


Figure 12. DFT calculation of the *anti*-pathway in **Path B**. (a) The *anti*-pathway of the propagation step from **R1** (*1b*); (b) optimized geometries for the *anti*-pathway of the propagation step; the C–C distances are given in Å; the Gibbs free energies of activation in parentheses (ΔG^\ddagger in kcal/mol) were calculated at the SMD(DCE)/M06-2X-D3/6-311+G(d,p) level at 333 K.

3.6 Conclusion

We have studied mechanism of this newly discovered rearrangement of ene-aldimines. The reaction proceeded through intermolecular pathway and irreversible process. The 2-azaallenium cation was generated in initiation step and played an important role as a chain carrier in propagation steps. Detailed reaction mechanism was proposed based on experimental and computational studies, where high level of DFT calculations was conducted.

3.7 Experimental Sections

3.7.1 General method

All reactions for mechanistic studies were performed in a Biotage Initiator Microwave system under an atmosphere magnetic stirring. 1,2-dichloroethane solvent was purchased

from commercial supplier as anhydrous solvents, and 2-hydroxybenzaldehyde was distilled before use. Other reagents were purchased from commercial suppliers and used without further purification. Purification of reaction products was carried out by flash column chromatography on silica gel 60 (spherical, neutral, 100-210 μm ; Merck). Analytical thin layer chromatography (TLC) was performed on E. Merck precoated (0.25 mm) silica gel 60-F254 plates. Visualization was accomplished with UV light, potassium permanganate solution in water, and phosphomolybdic acid solution in ethanol by heating. ^1H NMR spectra were recorded on a JEOL ECA-400 (100 MHz), spectrometer at ambient temperature. CDCl_3 NMR solvents were purchased from CIL, and it was dried over activated MS 4 \AA before used. Data are reported as follows: chemical shifts are reported in ppm from tetramethylsilane on the δ scale, with solvent resonance employed as internal standard (CDCl_3 7.26 ppm, DMSO-d_6 2.49 ppm), multiplicity (b = broad, s = singlet, d = doublet, dd = doublet of doublet, t = triplet, q = quartet, and m = multiplet), integration, coupling constant (Hz) and assignment. ^{13}C NMR spectra were recorded on a JEOL ECA-400 (100 MHz), spectrometer at ambient temperature. Chemical shifts are reported in ppm from tetramethylsilane on the δ scale, with solvent resonance employed as internal standard (CDCl_3 77.0 ppm). Mass spectra were obtained on Applied Biosystem Voyager DE-STR in Instrument center of IMS.

3.7.2 Procedure and characterization of crossover experiments

Procedure of crossover experiments:

A test tube for microwave reaction apparatus was used. To a (\pm)-10-camphorsulfonic acid (10 mol%) was added the solution of ene-imine in 1,2-dichloroethane (0.5 M) at room temperature, and then the resulting solution was stirred at an indicated temperature in a microwave reactor for an indicated time. The reaction was quenched with NEt_3 . After stirred for 15 min, the resulting mixture was extracted with CH_2Cl_2 (5 mL x 3). The organic layer was washed with brine (10 mL x 3), and aqueous layer was extracted with CH_2Cl_2 (20 mL x 3). The combined organic extracts were dried over Na_2SO_4 and concentrated under reduced pressure after filtration to give the ene-imine as product.

Characterization of crossover experiments:

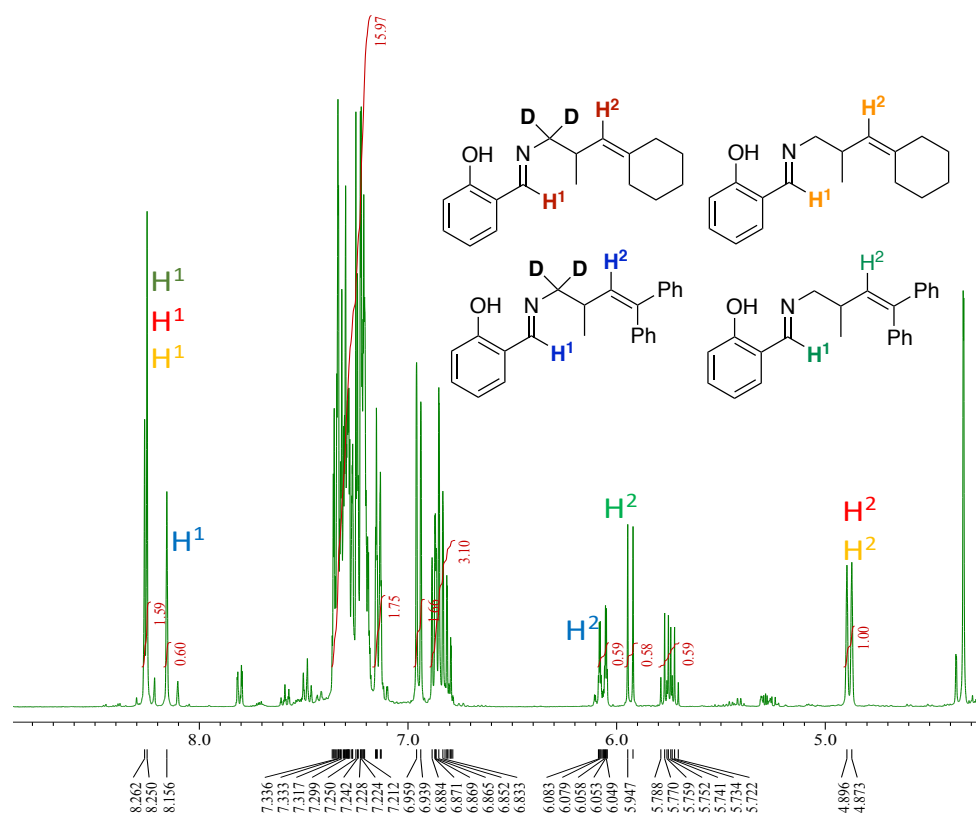


Figure 13. ^1H NMR chart of crossover experiment of substrates from 8.50 ppm to 4.50 ppm

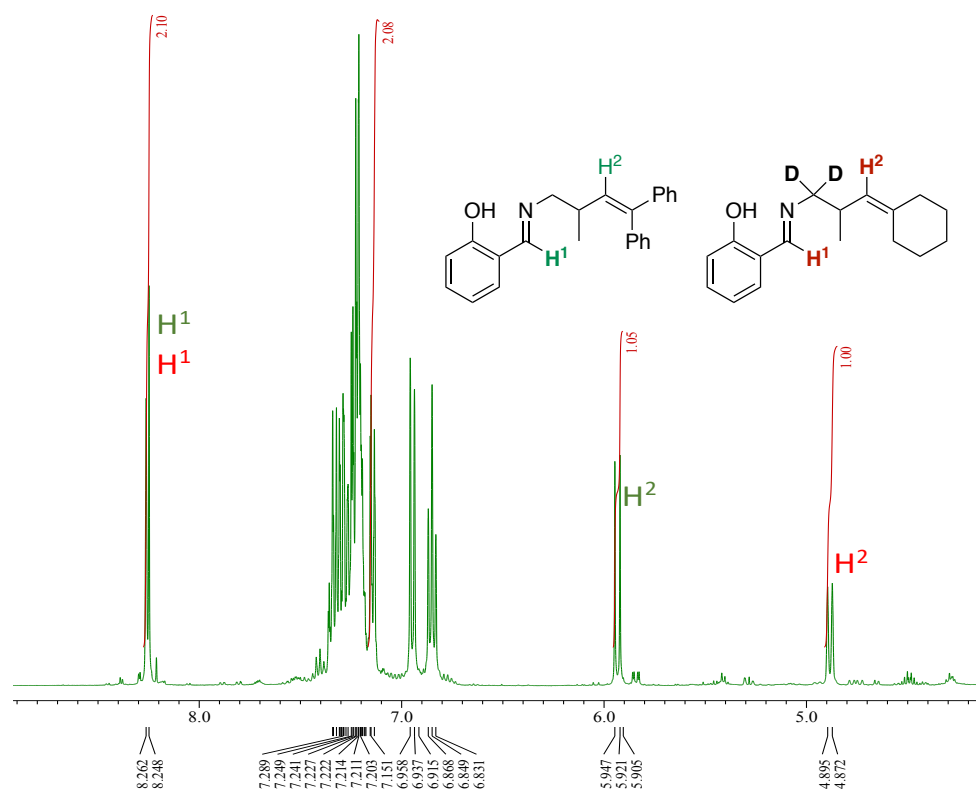
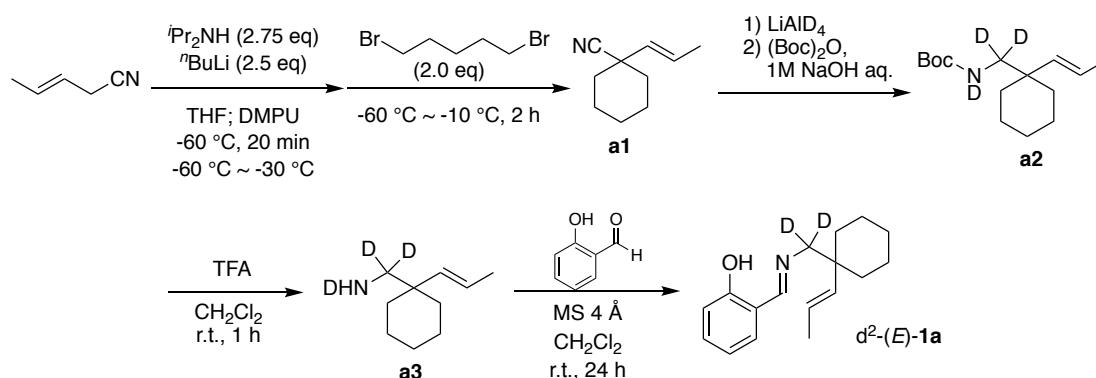


Figure 14. ^1H NMR chart of crossover experiment of products from 8.50 ppm to 4.50 ppm

3.7.3 Procedure and characterization of starting materials

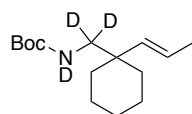
Synthesis of Deuterated Substrates d^2 -(*E*)-**1a**:

The (*E*)-olefin starting materials are synthesized from alkylation reaction of commercially available of 3-pentenenitrile with 1,5-dibromopentane in the presence of diisopropylamine and *n*-butyl lithium bases provides (*E*)-2-cyclohexyl pent-3-enenitrile product (**a1**). After that the alkylation product is subjected into reduction condition to change nitrile moiety to be deuterated 2-cyclohexyl pent-3-en-1-amine as a single product. Finally, deuterated 2-cyclohexyl pent-3-en-1-amine is protected by di-*tert*-butyl decarbonate (Boc) to afford (*E*)-*tert*-butyl (2-cyclohexyl pent-3-en-1-yl) carbamate (**a2**) as stocked starting materials (Scheme 5). Boc deprotection of **a2** gave **a3** product before condensation with salicylaldehyde to provide d^2 -(*E*)-**1a** substrate.



Scheme 5. Synthesis of deuterated substrates d^2 -(*E*)-**1a**

Characterization of deuterated substrates d^2 -(*E*)-**1a**:



$^1\text{H NMR}$ (CDCl_3 , 400 MHz) δ 5.43 (dt, 1H, $J = 22.1, 6.2$ Hz, $\text{CH}=\text{CH}-\text{CH}_3$), 5.19 (d, 1H, $J = 15.8$ Hz, $\text{CH}=\text{CH}-\text{CH}_3$), 1.71 (d, 3H, $J = 6.2$ Hz, $\text{CH}-\text{CH}_3$), 1.53-1.57 (m, 8H), 1.40-1.47 (m, 9H, $\text{O}-\text{C}-(\text{CH}_3)_3$), 1.28 (t, 2H, $J = 8.7$ Hz, $\text{C}-\text{CH}_2-\text{CH}_2$).

$^{13}\text{C NMR}$ (CDCl_3 , 100 MHz) δ 156.07, 146.65, 136.87, 124.61, 84.90, 78.60, 39.85, 33.63, 28.30, 27.27, 26.30, 21.76, 18.32.

HRMS (FAB) Exact Mass Calcd. for $\text{C}_{15}\text{H}_{24}\text{D}_3\text{NO}_2$ ($[\text{M}]^+$): 256.2230. Found: 256.2242.

3.7.4 Density functional theory calculations¹³

To elucidate the favored conformation of substrates, intermediates, and mechanism of this new rearrangement reaction, we investigated the reaction pathways by DFT calculations at the M06-2X/6-31+G(d,p) level using the Gaussian 16 program.¹² All ground-state and transition-state geometries were reoptimised at the M06-2X-D3/6-311+G(d,p) level with the SMD solvation model (dichloroethane) at 333 K. The 2-OH of aryl group does not affect the reaction mechanism, since essentially the same transition states and intermediates were obtained.

Table 1. N1-OH and its isomer

structure	<i>E</i>	<i>H</i>	<i>G</i>	ΔG
N1-OH	-439.3749246	-439.218757	-439.269524	0.00
N1-OH'	-439.3589656	-439.203072	-439.253279	10.19

Table 2. R1 and P1

structure	<i>E</i>	<i>H</i>	<i>G</i>	ΔG
R1 (<i>1b</i>)	-676.9673460	-676.611224	-676.683192	0.00
R1 (<i>3b</i>)	-676.9663795	-676.610300	-676.682570	0.39
R1 (<i>1a</i>)	-676.9669579	-676.610862	-676.682418	0.49
R1 (<i>3a</i>)	-676.9663040	-676.610197	-676.682251	0.59
R1 (<i>2a</i>)	-676.9666553	-676.610392	-676.682134	0.66
R1 (<i>2b</i>)	-676.9665543	-676.610357	-676.682079	0.70

Table 3. Initiation step

structure	<i>E</i>	<i>H</i>	<i>G</i>	ΔG
R1-H ⁺ (<i>1a</i>)	-677.4196133	-677.049593	-677.118410	0.00
TS1	-677.3595871	-676.995418	-677.066188	32.77
C2	-677.3770705	-677.008216	-677.081684	23.05
TS2	-677.3507194	-676.983989	-677.056469	38.87
N1...E1	-677.3641817	-676.996864	-677.074733	27.41
N1	-364.1447692	-363.994593	-364.042760	
E1	-313.2104430	-312.995858	-313.044695	

Table 4. Propagation step in **Path A**

structure	<i>E</i>	<i>H</i>	<i>G</i>	ΔG
N1...R1 (<i>1a</i>)	-1041.1289527	-1040.620848	-1040.720414	22.41
TS3	-1041.1235566	-1040.615382	-1040.709266	29.41
N2	-1041.1627329	-1041.162733	-1040.742705	8.43
TS4	-1041.1134997	-1040.603451	-1040.697110	37.04

N3	-1041.1500265	-1040.637953	-1040.730711	15.95
TS5	-1041.1113126	-1040.601618	-1040.693561	39.26
N4	-1041.1608707	-1040.648793	-1040.742186	8.75
TS6	-1041.1455382	-1040.634234	-1040.724118	20.09
N5	-1041.1728169	-1040.659752	-1040.754286	1.16
TS7	-1041.1191300	-1040.608313	-1040.698497	36.17
N6	-1041.1526057	-1040.639327	-1040.733684	14.09
TS8	-1041.1221039	-1040.610994	-1040.701200	34.47
N7	-1041.1694207	-1040.655575	-1040.747806	5.23
TS9	-1041.1277233	-1040.618842	-1040.712610	27.31
N1...P1 (<i>Ia-I</i>)	-1041.1356501	-1040.626297	-1040.723366	20.56

Table 5. TS10 in the propagation step in Path B

structure	<i>E</i>	<i>H</i>	<i>G</i>	ΔG
TS10-syn (<i>Ib</i>)	-1041.1014063	-1040.593080	-1040.686261	0.00
TS10-syn (<i>Ia</i>)	-1041.0972041	-1040.589096	-1040.685290	0.61
TS10-syn (<i>2b</i>)	-1041.0987694	-1040.590767	-1040.684768	0.94
TS10-syn (<i>2a</i>)	-1041.1002444	-1040.592134	-1040.684528	1.09
TS10-syn (<i>3b</i>)	-1041.0900095	-1040.581857	-1040.680013	3.92
TS10-syn (<i>3a</i>)	-1041.0906229	-1040.582303	-1040.679612	4.17
TS10-anti (<i>Ia</i>)	-1041.0925254	-1040.584363	-1040.681591	2.93
TS10-anti (<i>Ib</i>)	-1041.0921836	-1040.583859	-1040.680789	3.43
TS10-anti (<i>2a</i>)	-1041.0917652	-1040.583626	-1040.680751	3.46
TS10-anti (<i>2b</i>)	-1041.0922419	-1040.583793	-1040.679742	4.09
TS10-anti (<i>3a</i>)	-1041.0898917	-1040.581642	-1040.678509	4.86
TS10-anti (<i>3b</i>)	-1041.0899267	-1040.581446	-1040.678196	5.06

Table 6. TS11 in the propagation step in Path B

structure	<i>E</i>	<i>H</i>	<i>G</i>	ΔG
TS11-syn (<i>Ia</i>)	-1041.1198546	-1040.610929	-1040.704823	0.00
TS11-anti (<i>Ib</i>)	-1041.1153291	-1040.606420	-1040.702998	1.15

Table 7. Syn-pathway of the propagation step in Path B

structure	<i>E</i>	<i>H</i>	<i>G</i>	ΔG
syn-N1...R1 (<i>Ib</i>)	-1041.1285916	-1040.619497	-1040.716502	25.35
TS10-syn (<i>Ib</i>)	-1041.1014063	-1040.593080	-1040.686261	44.33
C4	-1041.1420082	-1040.630842	-1040.724636	20.25
TS11-syn (<i>Ia</i>)	-1041.1198546	-1040.610929	-1040.704823	32.68
syn-N1...P1 (<i>Ia-I</i>)	-1041.1347443	-1040.625139	-1040.722645	21.50

Table 8. Anti-pathway of the propagation step in Path B

structure	<i>E</i>	<i>H</i>	<i>G</i>	ΔG
anti-N1...R1 (<i>Ib</i>)	-1041.1187619	-1040.609496	-1040.709745	29.59

TS10-anti (<i>Ib</i>)	-1041.0921836	-1040.583859	-1040.680789	47.76
N8	-1041.1877913	-1040.673512	-1040.764015	-4.46
TS11-anti (<i>Ib</i>)	-1041.1153291	-1040.606420	-1040.702998	33.83
anti-N1...P1 (<i>Ib-2</i>)	-1041.1289592	-1040.619129	-1040.720743	22.69

Table 9. H1–N and C1–N distances (Å) between N1 and R1 in TS10-syn.

Short contacts less than the sum of van der Waals radii (H–N, 2.75 Å; C–N, 3.25 Å) are shown in entries *Ib*, *Ia*, and *2b*. These distances correlate well with ΔG s (kcal/mol)

TS10-syn	H1–N	C1–N	ΔG
<i>Ib</i>	2.26	3.12	0.00
<i>Ia</i>	2.18	3.13	0.61
<i>2b</i>	2.47	3.20	0.94
<i>2a</i>	2.88	3.45	1.09
<i>3b</i>	4.05	4.93	3.92
<i>3a</i>	4.00	4.87	4.17

3.8 References

1. See, page 20, section 2.2.3.
2. See, page 60, section 3.7.3.
3. Bottger, G. M.; Frohlich, R.; Wurthwein, E. U. *Eur. J. Org. Chem.* **2000**, 1589-1593.
4. Hoshino, Y.; Shimbo, Y.; Ohtsuka, N.; Honda, K. *Tetrahedron Lett.* **2015**, 56,710-712.
5. See, page 61, section 3.7.4 (Table 3).
6. See, page 14, section 2.2.1 (Table 1).
7. See, page 46, section 3.4.4.
8. Al-Talib, M.; Jibril, I.; Jochims, J. C.; Huttner, G. *Tetrahedron* **1985**, 41, 527.
9. See, page 61, section 3.7.4 (Table 4).
10. Jabbari, A.; Houk, K. N. *Org. Lett.* **2006**, 8, 5975-5978.
11. Galabov, B.; Nalbantova, D.; Schleyer, P. V.; Schaefer, H. F. *Acc. Chem. Res.* **2016**, 49, 1191-1199.
12. See, page 62, section 3.7.4 (Table 5).
13. Gaussian 16, Revision A.03, Frisch, M. J.; Trucks, G. W.; Schlegel, H. B.; Scuseria, G. E.; Robb, M. A.; Cheeseman, J. R.; Scalmani, G.; Barone, V.; Petersson, G. A.; Nakatsuji, H.; Li, X.; Caricato, M.; Marenich, A. V.; Bloino, J.; Janesko, B. G.; Gomperts, R.; Mennucci, B.; Hratchian, H. P.; Ortiz, J. V.; Izmaylov, A. F.; Sonnenberg, J. L.; Williams-Young, D.; Ding, F.; Lipparini, F.; Egidi, F.; Goings, J.; Peng, B.; Petrone, A.; Henderson, T.; Ranasinghe, D.; Zakrzewski, V. G.; Gao, J.; Rega, N.; Zheng, G.; Liang, W.; Hada, M.; Ehara, M.; Toyota, K.; Fukuda, R.; Hasegawa, J.; Ishida, M.; Nakajima, T.; Honda, Y.; Kitao,

O.; Nakai, H.; Vreven, T.; Throssell, K.; Montgomery, J. A.; Jr., Peralta, J. E.; Ogliaro, F.; Bearpark, M. J.; Heyd, J. J.; Brothers, E. N.; Kudin, K. N.; Staroverov, V. N.; Keith, T. A.; Kobayashi, R.; Normand, J.; Raghavachari, K.; Rendell, A. P.; Burant, J. C.; Iyengar, S. S.; Tomasi, J.; Cossi, M.; Millam, J. M.; Klene, M.; Adamo, C.; Cammi, R.; Ochterski, J. W.; Martin, R. L.; Morokuma, K.; Farkas, O.; Foresman, J. B.; Fox, D. J. Gaussian; Inc., Wallingford CT, 2016.

CHAPTER 4

BRØNSTED ACID-INITIATED ASYMMETRIC REARRANGEMENT REACTION OF CHIRAL-ENE ALDIMINES

4.1 Introduction

Asymmetric rearrangement reactions are one of the ideal methods to serve enantiomerically enriched products.¹ In addition, chirality transfer experiments using chiral ene-aldimines give the useful information to think about the reaction mechanisms.

As described in the chapter 3, chain reaction mechanism *via* generation of 2-azaallenium cation has been proposed, and DFT calculation supports two possible pathways in propagation step.² Further mechanistic studies would be helpful to discuss details of reaction mechanism. Therefore, chiral ene-aldimines is designed and synthesized, and asymmetric reaction of chiral ene-aldimines is studied. These results are summarized in this chapter.

4.2 Design and synthesis of chiral substrates

As summarized in chapter 2,³ ene-aldimine substrates with cyclohexyl ((*E*)- and (*Z*)-**2d**) and diphenyl ((*E*)- and (*Z*)-**2h**) substituents gave excellent yields, and similar reactivities were observed. On the basis of these results, these two substituents were combined and 1,2,3,4-tetrahydronaphthyl group was selected as the β -substituent to design chiral substrate (Figure 1).

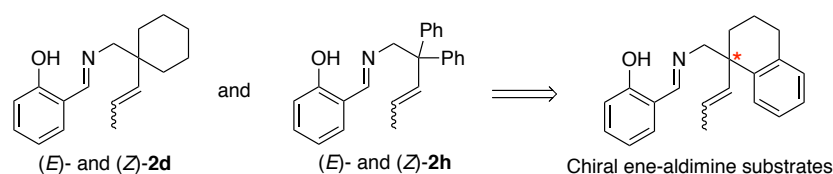
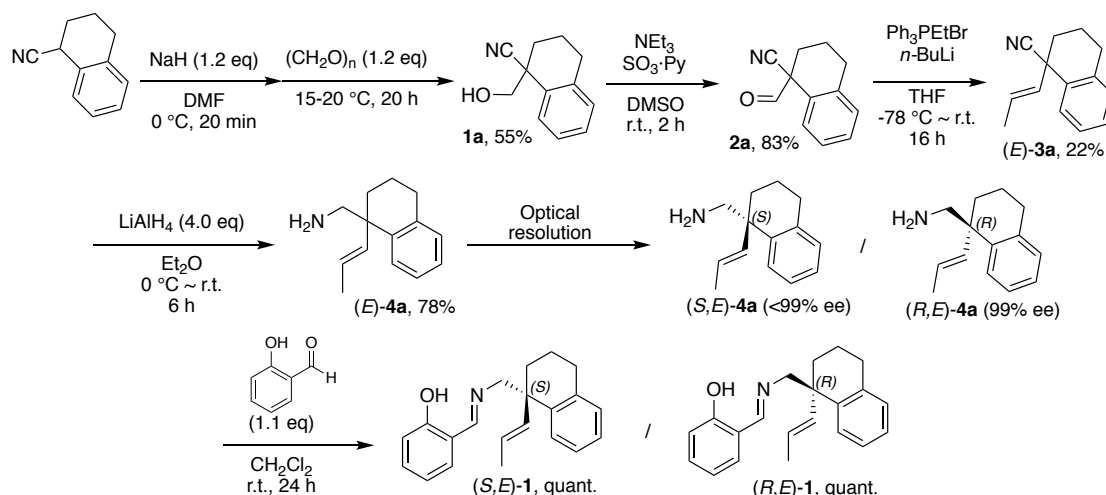


Figure 1. Design of chiral substrates

4.2.1 *E*-Olefin substrate

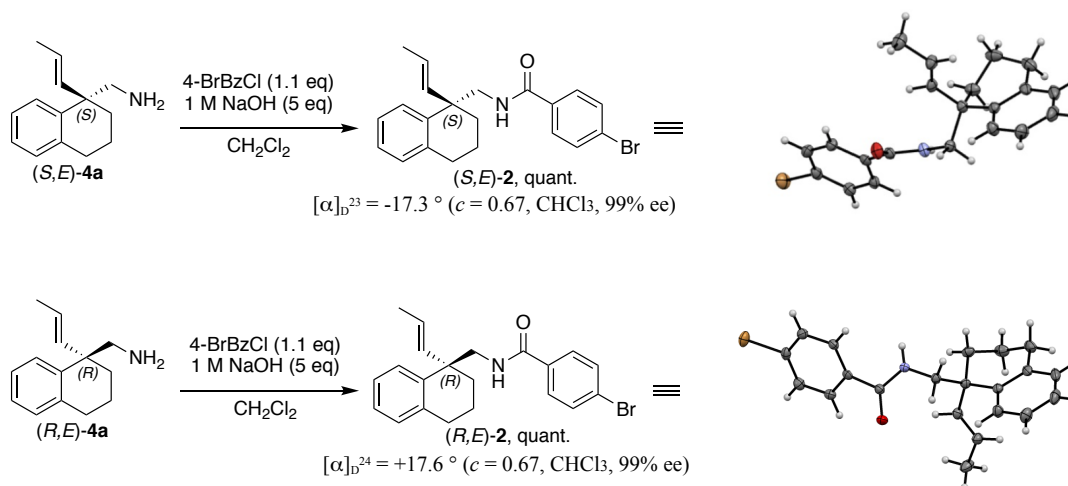
Chiral substrates with *E*-olefin ((*S,E*)-**1** and (*R,E*)-**1**) were synthesized from commercially available 1,2,3,4-tetrahydronaphthalene-1-carbonitrile. The aldol reaction of 1,2,3,4-tetrahydronaphthalene-1-carbonitrile gave **1a** in 55% yield, and then alcohol group on compound **1a** was oxidized to **2a** in the presence of $\text{SO}_3 \cdot \text{Py}$ as an oxidizing agent using triethylamine (NEt_3) as a base.^{4,5} Aldehyde functional group on **2a** was converted to *E*-olefin

3a by Wittig reagents at $-78\text{ }^{\circ}\text{C}$.⁶ Moreover, nitrile group was reduced to free amine (*E*)-**4a** by the use of LiAlH_4 as a reducing agent. In the optical resolution step, semi-preparative HPLC was used to separate each enantiomer ((*S,E*)-**4a** and (*R,E*)-**4a**) (CHIRALCEL OD-H (10 mm ϕ \times 250 mm L), 98/2 hexane/*i*-PrOH, 5 mL/min, 254 nm, 40 $^{\circ}\text{C}$, t_r = 8.0 min and 11.6 min). Finally, condensation of ((*S,E*)-**4a** and (*R,E*)-**5**) with salicylaldehyde were performed to give (*S,E*)-**1** and (*R,E*)-**1** in excellent yields (Scheme 1).



Scheme 1. Synthesis of (*S,E*)- and (*R,E*)-**1** chiral substrates

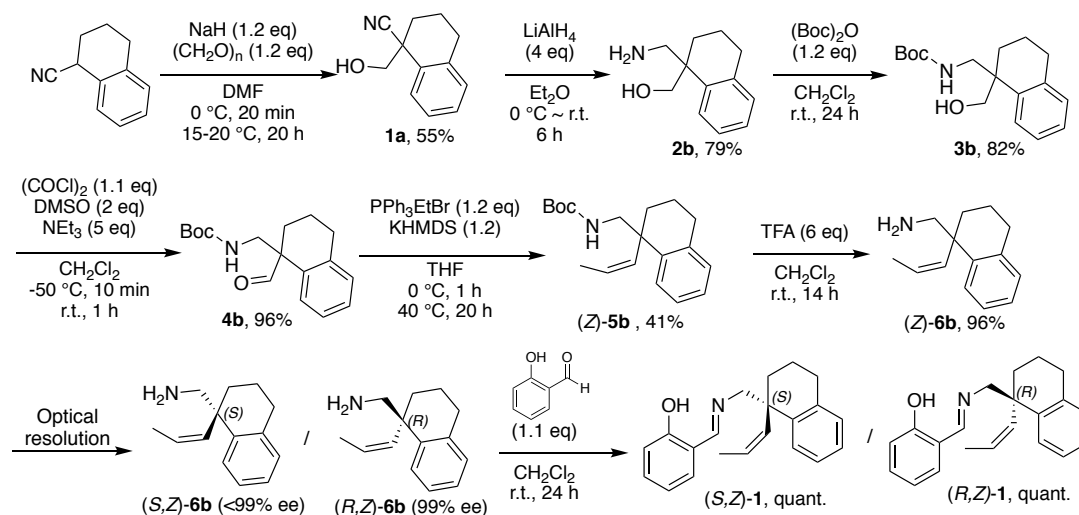
Absolute configuration and *E/Z* geometry of **2** were determined using the amines derivatives. Optically pure amides (*E*)-**2** were synthesized from the treatment of optically pure (*E*)-**4a** with 4-bromobenzoyl chloride and 1M NaOH. The obtained amide derivatives (*E*)-**2** were recrystallized under dichloromethane (CH_2Cl_2) as inner solvent and hexane as outer solvent. As expected, X-ray diffraction analysis clearly showed *E*-olefin of the derivatives **2**. In addition, the first HPLC peak of the derivatives **2** is (*S*)-configuration and the second one is (*R*)-configuration (Scheme 2).⁷



Scheme 2. Protection of (*E*)-**4** and determination of absolute configurations

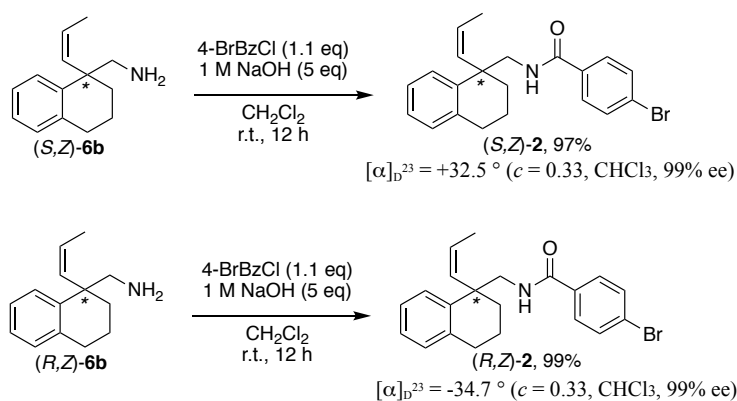
4.2.2 *Z*-Olefin substrate

Chiral substrates with *Z*-olefin (*(S,Z)*-**1** and *(R,Z)*-**1**) were synthesized from commercially available 1,2,3,4-tetrahydronaphthalene-1-carbonitrile. The first step was as same as (*E*)-chiral substrates (*(S,E)*-**1** and *(R,E)*-**1**). After aldol reaction in the first step, reduction of **1a** by LiAlH₄ gave free amine **2b** in good yield; additionally, free amine **2b** was protected by *tert*-butyl carbamate ((Boc)₂O) to provide Boc protected amine **3b** in 82% yield. The Swern oxidation of **3b** followed by the Wittig reaction of **4b** gave (*Z*)-**5b** as stocked starting material in moderated yield. After deprotection of (*Z*)-**5b** by trifluoroacetic acid (TFA), the optical resolution of starting material (*Z*)-**6b** was performed by semi-preparative HPLC (CHIRALCEL OD-H (10 mm ϕ \times 250 mm L), 98/2 hexane/*i*-PrOH, 5 mL/min, 254 nm, 40 °C, t_{r} = 8.0 min and 11.6 min). In the final step, condensation reaction of optically pure (*Z*)-**6b** with salicylaldehyde were performed to afford optically pure *(S,Z)*-**1** and *(R,Z)*-**1** in excellent yields (Scheme 3).



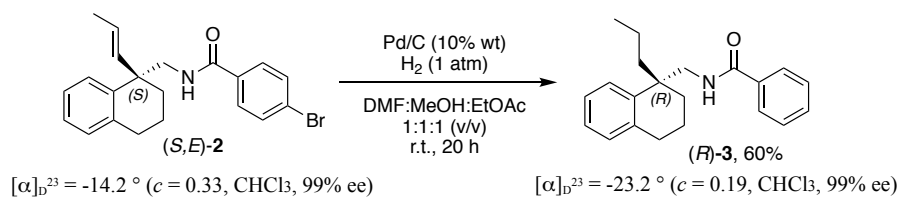
Scheme 3. Synthesis of (*S,Z*)- and (*R,Z*)-1 chiral substrates

To determine the absolute configuration, the optically pure amines (*Z*)-6b were also derivatized to optically pure amides (*Z*)-2; unfortunately, optically pure amides (*Z*)-2 were oil, and could not be recrystallized. In addition, the optical rotation of (*S,Z*)-2 (first peak of HPLC) and (*R,Z*)-2 (second peak of HPLC) were in the opposite values (Scheme 4). Therefore, derivatization and crystal sponge method⁸ were used to determine absolute configuration of these compounds (Figure 6).



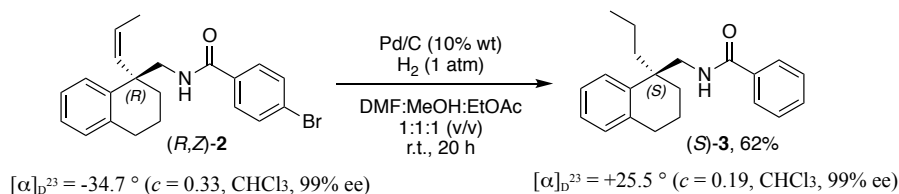
Scheme 4. Synthesis of optically pure derivatives (*Z*)-2

Hydrogenation reaction was selected to synthesize reference compounds, and the known configuration (*R*)-3 was used as a reference to compare absolute configuration of (*R,Z*)-2. The (*R*)-3 was synthesized from hydrogenation of (*S,E*)-2 with Pd catalyst in mixed solvents of DMF, MeOH, and EtOAc. During the course of hydrogenation, 4-bromo of benzoyl group eliminated to give (*R*)-3. The optical rotation of hydrogenated (*R*)-3 was observed at -23.2° in CHCl_3 solvent (Scheme 5).



Scheme 5. Hydrogenation reaction of (*S,E*)-**2** to hydrogenated (*R*)-**3**

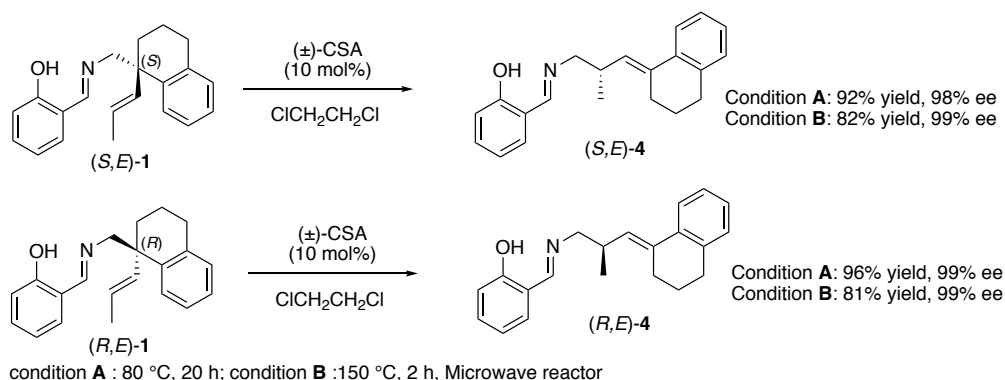
With reference compound (*R*)-**3** in hand, derivatization of optically pure (*Z*)-**2**, which was second peak of HPLC was conducted. Hydrogenation of (*R,Z*)-**2** afforded hydrogenated (*S*)-**3** in appropriated yield, and optical rotation showed in the opposite value of (*R*)-**3**; $+23.2^\circ$ under the same conditions (Scheme 6). As a result, the absolute configuration of (*Z*)-**2**, second peak compound of HPLC, was determined as (*R,Z*)-**2**.



Scheme 6. Hydrogenation reaction of protected (*R,Z*)-**2** to give hydrogenated product (*S*)-**3**

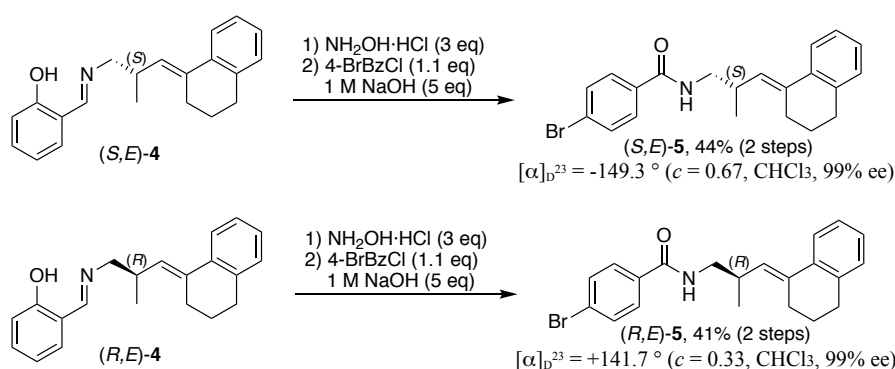
4.3 Chirality transfer studies

After preparation, characterization, and determination of absolute configurations of (*E*)- and (*Z*)-chiral substrates, the chirality transfer experiments were performed under both normal and microwave conditions. At first, asymmetric [1,3]-rearrangement of (*E*)-substrates was examined, and the reaction gave high to excellent yields in both reaction conditions. Importantly, chirality transfer ratios were also excellent (Scheme 7).



Scheme 7. Asymmetric formal [1,3]-rearrangements of (*E*)-chiral ene-aldimines.

For the determination of absolute configuration and geometrical isomerism of the product (*S,E*)- and (*R,E*)-**4**, these chirality transfer products were subjected into the hydrolysis condition by the use of hydroxylamine hydrochloride to afford chiral homoallylic amines, followed by protection of free amines by 4-bromobenzoyl chloride to give protected homoallylic amines (*S,E*)- and (*R,E*)-**5** in good yields (Scheme 8). (*S,E*)- and (*R,E*)-**5** were recrystallized to determine absolute configuration by the use of single crystal X-ray diffraction analysis (Figure 2). The results showed that (*S*)-substrate gave (*S*)-product while (*R*)-substrate gave (*R*)-product. The optical rotation of (*S,E*)- and (*R,E*)-**11** in CHCl₃ at 24°C were correlated; (*S,E*)-**5** showed -149.3° and (*R,E*)-**5** showed at $+141.7^\circ$ (Scheme 8).



Scheme 8. Derivatization of chirality transfer products (*S,E*)-**4** and (*R,E*)-**4**

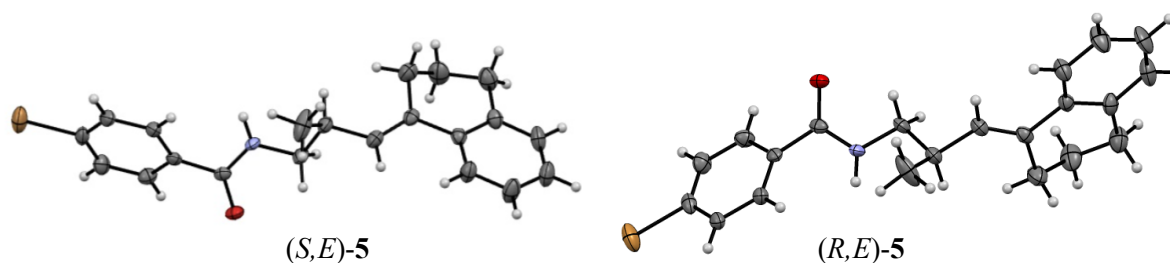
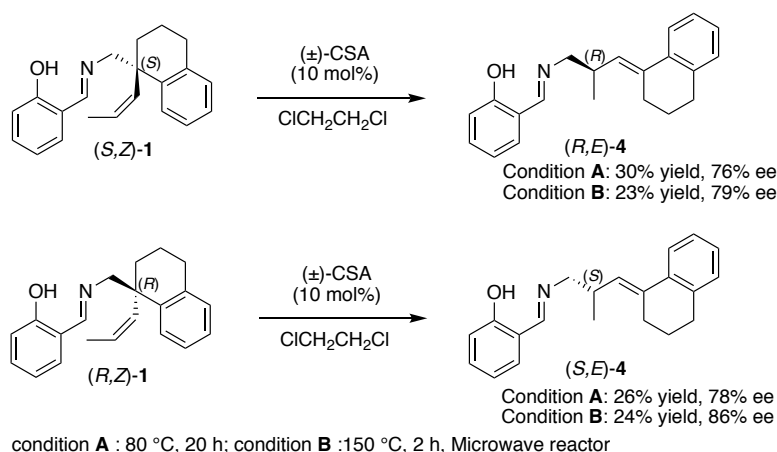


Figure 2. ORTEP diagram of derivatized rearrangement products

Next, chirality transfer of (*Z*)-chiral substrates was carried out under both normal and microwave conditions. The results were in contrast to chirality transfer of (*E*)-olefin substrates. The reactions yielded rearrangement products in low yields (23-30%) with remaining of starting material. Importantly, chirality transfer ratios of the products (*R,E*)- and (*S,E*)-**4** were lower than those of (*E*)-chiral substrate, and inversion configuration of products were observed (Scheme 9). On the other hand, optical purities of remaining starting materials (*S,Z*)-**4** and (*R,Z*)-**4** were 99% in both cases.



Scheme 9. Asymmetric formal [1,3]-rearrangements of (*Z*)-chiral ene-aldimines

4.4 Proposed mechanism

As described in chapter 3,⁹ two mechanisms, **Path A** and **Path B**, were proposed. It was speculated that azonia-[3,3]-rearrangement step affects chirality transfer from the substrates to the products. Of two proposed mechanisms; **Path A** and **Path B**, DFT calculation indicated high enantioselectivities in **Path A**. In contrast, **Path B** was not optimized to give enantioselectivities, indicating that **Path B** yields a racemate. Based on these suggestions by DFT calculations, the possible pathway was proposed to explain for these observed chirality transfer ratios and absolute stereochemistries (Figures 3 and 4).

For the (*R,E*)-**R*1**, the methylene transfer from 2-azaallenium to (*R,E*)-**1** affords two conformations, **E-N*4trans** and **E-N*4cis**, which were in equilibrium. **E-N*4trans** underwent azonia-[3,3]-sigmatropic rearrangement to give **E-N*5trans** via chair-like transition state **E-TS*IVtrans**. Although transition state **E-N*4cis** was also expected to provide **E-N*5cis** via **E-TS*IVcis**, Gibbs free energy at **E-TS*IVcis** demonstrated that this transition state was disfavored due to 1,3-diaxial interaction. Therefore, this prediction anticipate 99% ee of products (*R,E*)-**P*1** (Figure 3) related to experimental result of (*R,E*)-**1** substrate in Scheme 7.

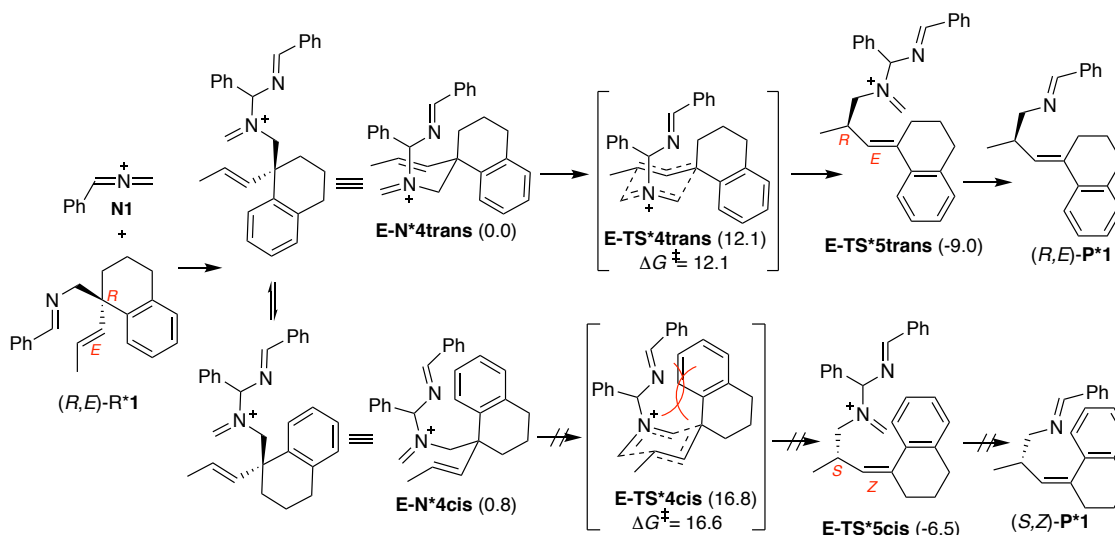


Figure 3. DFT calculation for azonia-[3,3]-sigmatropic rearrangement step in asymmetric formal [1,3]-rearrangement of (R,E) -1 substrate. The Gibbs free energies in parenthesis (ΔG , in kcal/mol) were calculated at the SMD(DCE)/M06-2X-D3/6-311+G(d,p) level at 333K.

For (R,Z) -R*1, the enantiomeric excess of the rearrangement product was reasonably explained based on chair-like transition state $Z-TS^*IVtrans$; similar to $E-TS^*IVtrans$. DFT calculation found that both $Z-N^*4trans$ and $Z-N^*4cis$ were energetically unstable (6.1 and 7.9 kcal/mol), probably because of large steric bulkiness of 1,3-diaxial interactions.

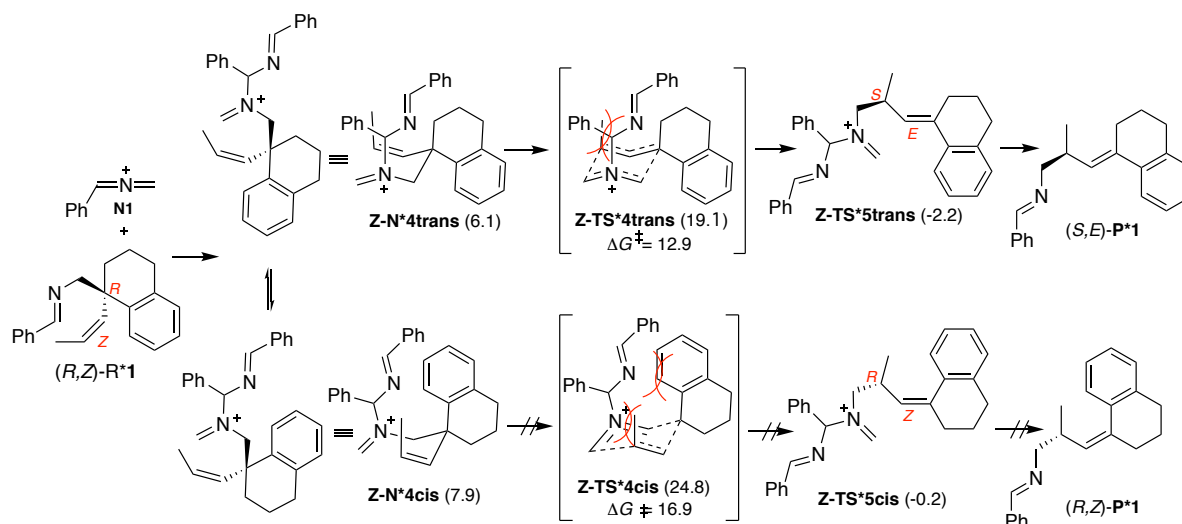


Figure 4. DFT calculation for azonia-[3,3]-sigmatropic rearrangement step in asymmetric formal [1,3]-rearrangement of (R,Z) -1 substrate. The Gibbs free energies in parentheses (ΔG , in kcal/mol) were calculated at the SMD(DCE)/M06-2X-D3/6-311+G(d,p) level at 333K.

According to experimental results and computational calculations, the reaction of (*R,E*)-**1** was preferable to **Path A** to give enantiopure (*R,E*)-**4** in excellent yield; on the other hand, the reaction of (*R,Z*)-**1** was speculated to both **Path A** and **Path B**. The reaction may preferably proceed through **Path A** to give completely chirality transfer product, but 1,3-diaxial interaction may also interfere azonia-[3,3]-rearrangement step in propagation. Therefore, **Path B** may competitively involve giving a racemate at low conversions. Consequently, chirality transfer ratio of (*R,Z*)-**1** was lower than (*R,E*)-**1**, whereas DFT calculations for Gibbs free energy of activation indicates an excellent chirality transfer ratio even in the case of (*R,Z*)-**1** (Figure 4).

According to all experimental and computational results, plausible mechanisms were proposed *via* two pathways (Figure 5). In **Path A**, nitrogen nucleophile on **R1** makes C-N bond formation to **N2** and then intramolecular ring closure occurs between nitrogen nucleophile and electrophile to 1,3-diazetidinium cation **N3**. Ring opening of **N3** takes place due to ring strain to give iminium cation **N4**. Then, **N4** undergoes azonia-[3,3]-rearrangement to **N5** before shifting to **N7** by ring closure and ring opening. The C-N bond cleavage of **N7** takes place to afford formal [1,3]-rearrangement product with regeneration of 2-azaallenium intermediate (**N1**) in final step (**Path A**). Similarly, **Path B** begins with C-C bond formation of 2-azaallenium (**N1**) and reactant (**R1**) to give secondary carbocation **C3**. The 1,2-shift rearrangement of **C3** occurs to afford more stable tertiary carbocation **C4**, after that C-C bond cleavage occurs in the final step to give formal [1,3]-rearrangement product with generation of new 2-azaallenium (**N1**) as reaction medium for the next propagation cycles (**Path B**).

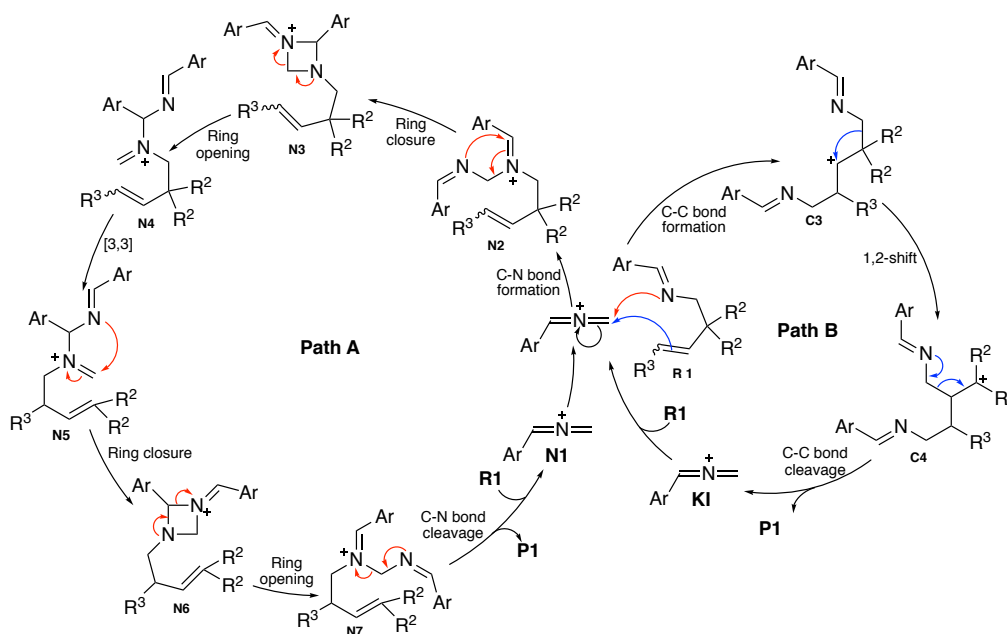


Figure 5. Plausible mechanisms of ene-aldimine rearrangement reaction

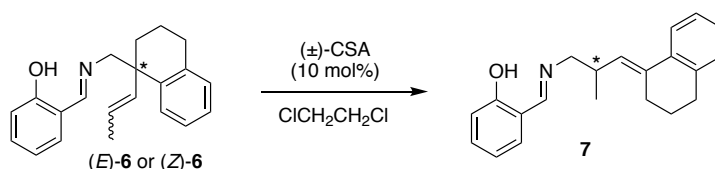
4.5 Conclusion

The chiral ene-aldimine substrates were successfully synthesized and characterized. The absolute configuration of chiral substrates was determined by single X-ray diffraction analysis, derivatization, and crystal sponge method. The previously undeveloped asymmetric formal [1,3]-rearrangement reaction of ene-aldimines has been studied. It is suggested that the reaction preferably proceeded through **Path A** in the case of (*E*)-chiral ene-aldimines giving completely chirality transfer products; in the alternative (*Z*)-chiral ene-aldimine substrates, the reaction involved two pathways, **Path A** and **Path B**, giving lower yields and lower chirality transfer ratio than that in case of (*E*)-chiral ene-aldimines.

4.6 Experimental Section

4.6.1 Procedure and characterization of chirality transfer

Chirality Transfer Experiments:

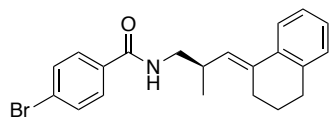


Normal heating condition: To a (±)-10-camphorsulfonic acid (10 mol%) was added the solution of ene-aldimines in 1,2-dichloroethane (0.1 M) at room temperature. Then, the reaction was stirred at an indicated temperature for 20 hours. After cooled to room

temperature, the reaction was quenched with NEt_3 . After stirred at room temperature for 15 min, the resulting mixture was extracted with CH_2Cl_2 (5 mL x 3). The organic layer was washed with brine (10 mL x 3), and aqueous layer was extracted with CH_2Cl_2 (20 mL x 3). The combined organic extracts were dried over Na_2SO_4 and concentrated under pressure after filtration to give the ene-aldimine as product.

Microwave condition: A test tube for microwave reaction apparatus should be used. To a (\pm)-10-camphorsulfonic acid (10 mol%) was added the solution of ene-aldimine in 1,2-dichloroethane (0.5 M) at room temperature with sealed reaction vessel, and then the resulting solution was stirred at an indicated temperature in a microwave reactor 600 rpm (75-400 W.) for an indicated time. The reaction was quenched with NEt_3 . After stirred for 15 min, the resulting mixture was extracted with CH_2Cl_2 (5 mL x 3). The organic layer was washed with brine (10 mL x 3), and aqueous layer was extracted with CH_2Cl_2 (20 mL x 3). The combined organic extracts were dried over Na_2SO_4 and concentrated under pressure after filtration to give the ene-aldimine as product.

Characterization of products:



(*R,E*)-4-bromo-*N*-(3-(3,4-dihydronaphthalen-1(2*H*)-ylidene)-2-methylpropyl)benzamide

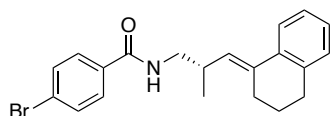
TLC R_f = 0.34 (5:1 hexane:ethyl acetate).

^1H NMR (CDCl_3 , 400 MHz) δ 7.61-7.50 (m, 5H Ar-*H*), 7.16 (dt, 2H, J = 9.5, 3.7 Hz, Ar-*H*), 7.11-7.08 (m, 1H, Ar-*H*), 6.18 (s, 1H, NH), 5.78 (d, 1H, J = 9.6 Hz, CH-CH=C), 3.72-3.66 (m, 1H, NH- CH_2), 3.15-3.08 (m, 1H, NH- CH_2), 3.02-2.93 (m, 1H, CH_2 -CH- CH_3), 2.81-2.69 (m, 2H, C- CH_2 - CH_2), 2.54-2.49 (m, 2H, CH_2 - CH_2 -C), 1.83-1.69 (m, 2H, CH_2 - CH_2 - CH_2), 1.12 (d, 3H, J = 6.6 Hz, CH- CH_3).

^{13}C NMR (CDCl_3 , 100 MHz) δ 166.5, 137.4, 136.1, 135.6, 133.5, 131.8, 129.0, 128.4, 127.1, 126.9, 126.0, 123.7, 45.9, 32.8, 30.3, 26.8, 23.4, 18.6.

HRMS (FAB) Exact Mass Calcd. For $\text{C}_{21}\text{H}_{22}\text{NOBr}$ ($[\text{M}+\text{H}]^+$): 384.0958. Found: 384.0953.

Enantiomeric excess was determined by HPLC with a CHIRALCEL OD-3 (95/5 hexane/*i*-PrOH, 1.0 mL/min, 254 nm, 40 °C), minor enantiomer t_r = 21.5 min, major enantiomer t_r = 35.9 min.



(*S,E*)-4-bromo-*N*-(3-(3,4-dihydronaphthalen-1(2*H*)-ylidene)-2-methylpropyl)benzamide

TLC $R_f = 0.34$ (5:1 hexane:ethyl acetate).

^1H NMR (CDCl_3 , 400 MHz) δ 7.61-7.50 (m, 5H Ar-H), 7.16 (dt, 2H, $J = 9.5, 3.7$ Hz, Ar-H), 7.11-7.08 (m, 1H, Ar-H), 6.18 (s, 1H, NH), 5.78 (d, 1H, $J = 9.6$ Hz, CH-CH=C), 3.72-3.66 (m, 1H, NH- CH_2), 3.15-3.08 (m, 1H, NH- CH_2), 3.02-2.93 (m, 1H, CH_2 -CH- CH_3), 2.81-2.69 (m, 2H, C- CH_2 - CH_2), 2.54-2.49 (m, 2H, CH_2 - CH_2 -C), 1.83-1.69 (m, 2H, CH_2 - CH_2 - CH_2), 1.12 (d, 3H, $J = 6.6$ Hz, CH- CH_3).

^{13}C NMR (CDCl_3 , 100 MHz) δ 166.5, 137.4, 136.1, 135.6, 133.5, 131.8, 129.0, 128.4, 127.1, 126.9, 126.0, 123.7, 45.9, 32.8, 30.3, 26.8, 23.4, 18.6.

HRMS (FAB) Exact Mass Calcd. For $\text{C}_{21}\text{H}_{22}\text{NOBr}$ ($[\text{M}+\text{H}]^+$): 384.0958. Found: 384.0953.

Enantiomeric excess was determined by HPLC with a CHIRALCEL OD-3 (95/5 hexane/*i*-PrOH, 1.0 mL/min, 254 nm, 40 °C), minor enantiomer $t_r = 35.9$ min, major enantiomer $t_r = 21.5$ min.

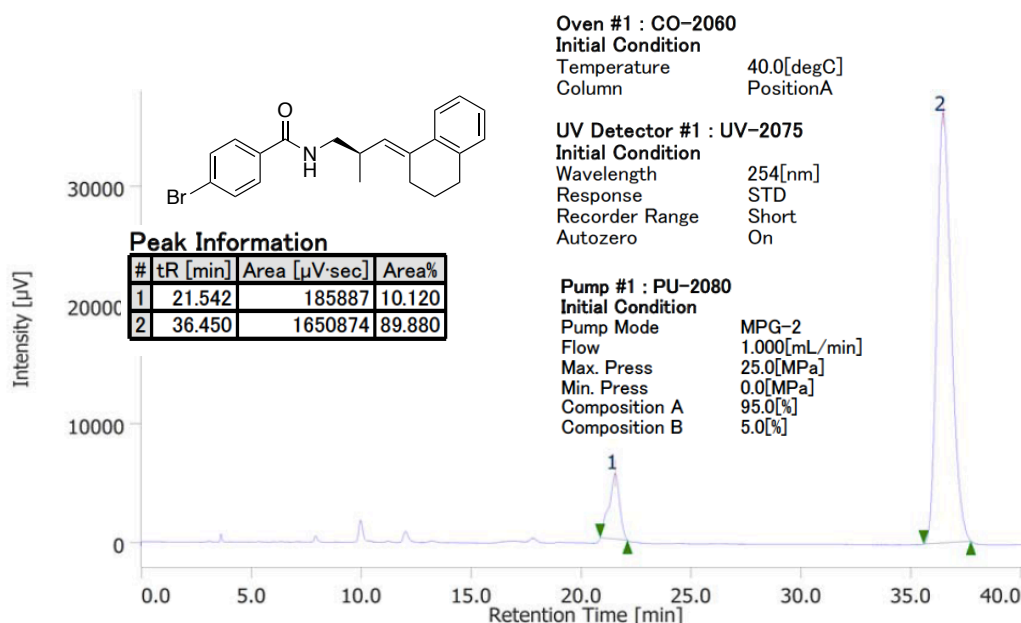


Chart 1. HPLC chart for (*R*)-10 compound. Enantiomeric excess was determined by analytical HPLC with a CHIRALCEL OD-3 (95/5 hexane/*i*-PrOH, 1.0 mL/min, 254 nm, 40 °C), major enantiomer $t_r = 36.55$ min, minor $t_r = 21.5$ min.

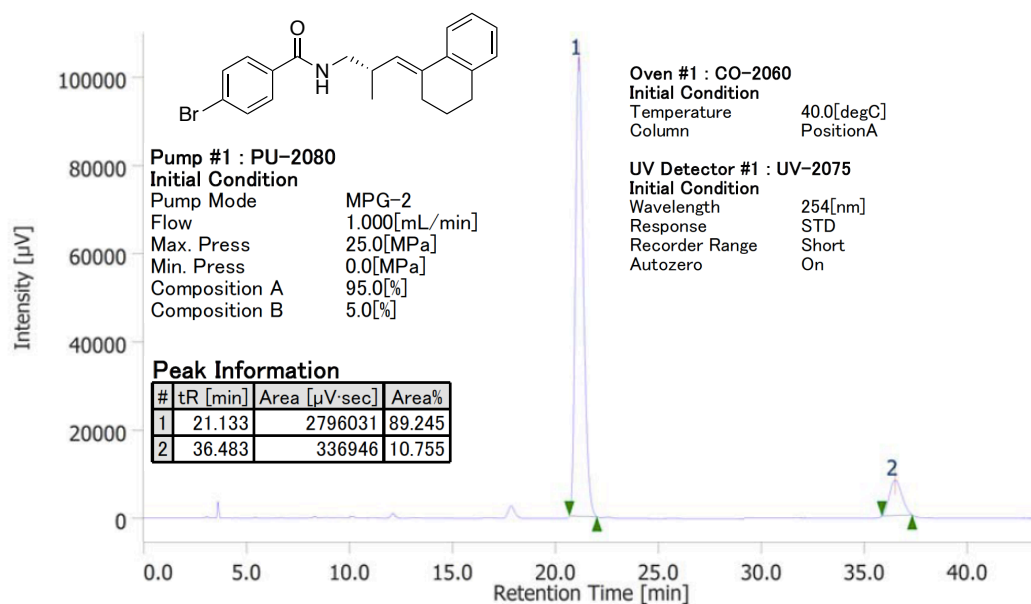
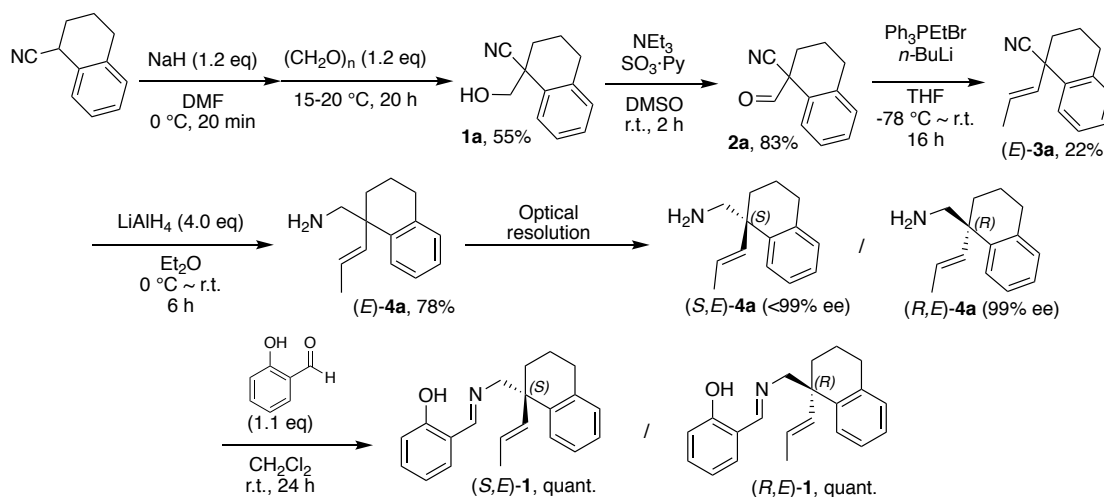


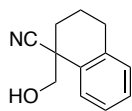
Chart 2. HPLC chart for (*S*)-10 compound. Enantiomeric excess was determined by analytical HPLC with a CHIRALCEL OD-3 (95/5 hexane/*i*-PrOH, 1.0 mL/min, 254 nm, 40 °C), major enantiomer $t_r = 21.1$ min, minor $t_r = 36.5$ min.

4.6.2 Procedure and characterization of starting material

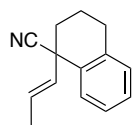
Synthesis of (E)-chiral starting substrates:



Scheme 10. Synthesis of (*E*)-chiral substrates



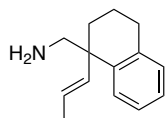
The NaH (60% dispersion in oil, 0.64 g, 9.5 mmol, 1.2 equiv.) was washed with anhydrous pentane (50 mL) in two-neck round-bottom flask. After pentane was removed, DMF (6.4 mL) was added. To suspension of NaH in DMF was added dropwise a solution of 1-cyanonitraline (2.1 g, 13.4 mmol, 1.0 equiv.) at 0 °C. After stirred at this temperature for 30 min, formaldehyde was added. The resulting reaction mixture was stirred at 0 °C for 20 min, then the reaction was allowed to warm up slowly to room temperature. After stirred for 20 h, the reaction was quenched by saturated NH₄Cl aq, and extracted with diethyl ether, and washed with sat. NaHCO₃ aq and brine, respectively. The combined organic extracts were dried over MgSO₄, filtrated, concentrated, and purified by flash column chromatography on silica gel to afford desired 1-(hydroxymethyl)-1,2,3,4-tetrahydronaphthalene-1-carbonitrile in 50% yield (1.25 g, 6.7 mmol).¹



To a solution of 1-(hydroxymethyl)-1,2,3,4-tetrahydronaphthalene-1-carbonitrile (1.3 g, 6.7 mmol, 1.0 equiv.) in DMSO (54.2 mL) and NEt₃ (5.6 mL) was added sulfur trioxide pyridine complex (3.2 g, 20 mmol, 3.0 equiv.) at 0 °C, and then the resulting solution was allowed to warm up to room temperature for 2 h. After cooling at 0 °C, the reaction was quenched with 1 M HCl aq. The resulting mixture was filtrated, and the crude mixture was extracted with ethyl acetate (20 mL x 4). The combined organic layer was washed with water and brine respectively, then dried over K₂CO₃, and evaporated after filtration to afford brown oil residue. The oil residue was purified by short-plug column chromatography to provide desired 1-formyl-1,2,3,4-tetrahydronaphthalene-1-carbonitrile in 95% yield (1.18 g, 6.4 mmol).²

To a solution of triphenylphosphonium ethyl bromide (1.9 g, 10.0 mmol, 1.2 equiv.) in THF (47.2 mL) was slowly added *n*-BuLi (1.6 M in hexane, 7.6 mL, 7.6 mmol, 1.2 equiv.) at -60 °C, and stirred at this temperature for 10 minutes. To the resulting mixture was added *n*-BuLi (1.6 M in hexane, 3.5 mL, 5.1 mmol, 0.8 equiv.) and a solution of 1-formyl-1,2,3,4-tetrahydronaphthalene-1-carbonitrile (11.2 g, 6.4 mmol, 1.0 equiv.) in THF (30 mL), and mixed solution was stirred at this temperature to room temperature for 16 hours. The reaction

was quenched by iced water and extracted with diethyl ether (20 mL x 3), then the combined organic layer was washed with water and brine, respectively. The combined organic extracts were dried over Na₂SO₄ and concentrated under vacuum after filtration. The residual crude product was purified by flash column chromatography on silica gel to afford desired (*E*)-1-(prop-1-en-1-yl)-1,2,3,4-tetrahydronaphthalene-1-carbonitrile in 22% yield (0.43 g, 2.2 mmol).³



To a suspension of LiAlH₄ (195.6 mg, 4.9 mmol, 4.0 equiv.) in Et₂O (6 mL) was added dropwise (*E*)-1-(prop-1-en-1-yl)-1,2,3,4-tetrahydronaphthalene-1-carbonitrile in (242.5 mg, 5 mmol, 1.0 equiv.) in Et₂O (6 mL) at 0 °C, and the resulting mixture was stirred at room temperature for 6 h. After cooling at 0 °C, the reaction was carefully quenched with H₂O (2 mL) and 1M NaOH aq (1 mL). To the resulting mixture was further carefully added H₂O at 0 °C and stirred at 0 °C to room temperature for a few hours. The resulting mixture was filtrated and extracted with diethyl ether (20 mL x 3). The combined extracts were dried over K₂CO₃ and evaporated after filtration to give (*E*)-(1-(prop-1-en-1-yl)-1,2,3,4-tetrahydronaphthalen-1-yl)methanamine as a crude product.

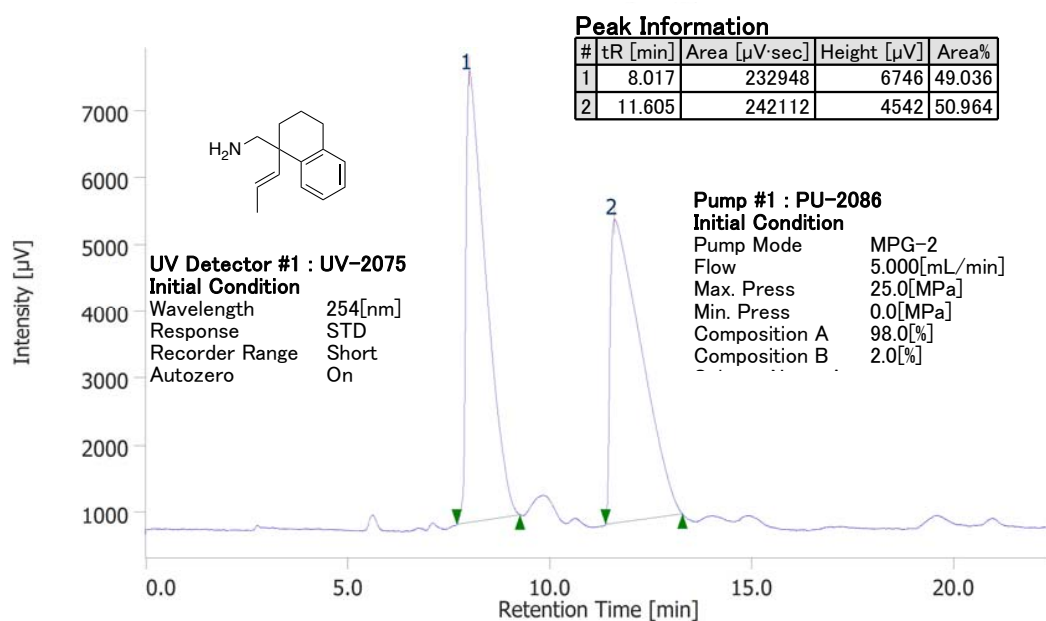


Chart 3. HPLC chart for racemic (*E*)-(1-(prop-1-en-1-yl)-1,2,3,4-tetrahydronaphthalen-1-yl)methanamine. Semi-preparative HPLC was used to separate each enantiomer (CHIRALCEL

OD-H (10 mm ϕ \times 250 mm L), 98/2 hexane/*i*-PrOH, 5 mL/min, 254 nm, 40 °C, t_r = 8.0 min and 11.6 min).

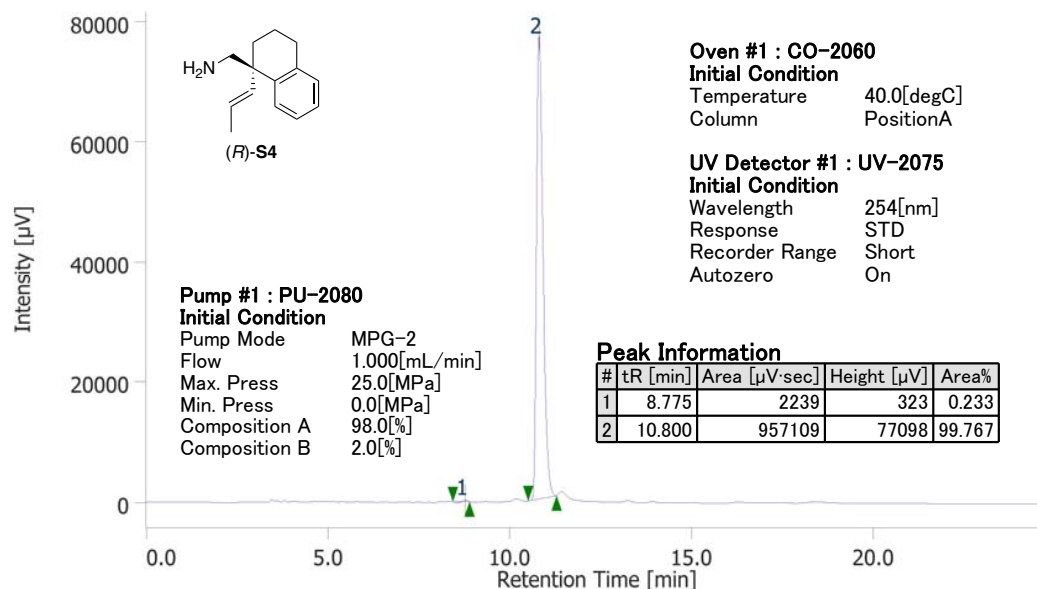


Chart 4. HPLC chart for (*R,E*)-(1-(prop-1-en-1-yl)-1,2,3,4-tetrahydronaphthalen-1-yl) methanamine. Enantiomeric excess was determined by analytical HPLC with a CHIRALCEL OD-3 (98/2 hexane/*i*-PrOH, 1.0 mL/min, 254 nm, 40 °C), minor enantiomer t_r = 8.8 min, major enantiomer t_r = 10.8 min.

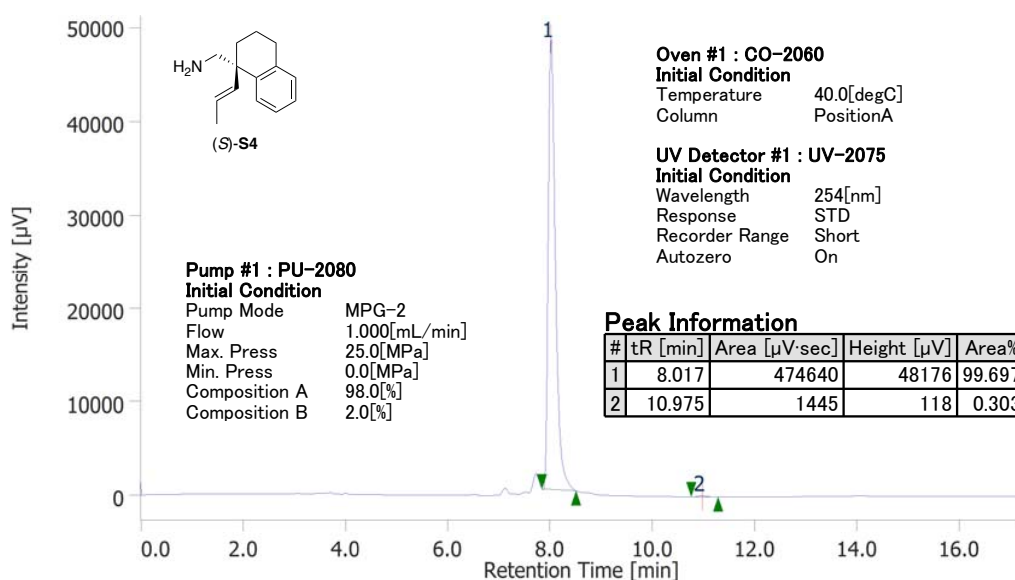
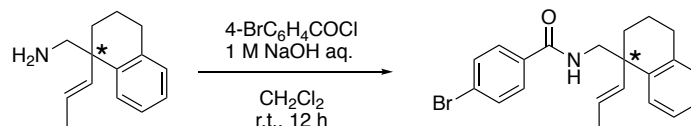


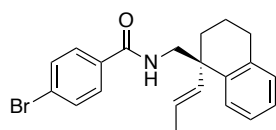
Chart 5. HPLC chart for (*S,E*)-(1-(prop-1-en-1-yl)-1,2,3,4-tetrahydronaphthalen-1-yl) methanamine. Enantiomeric excess was determined by analytical HPLC with a CHIRALCEL

OD-3 (98/2 hexane/*i*-PrOH, 1.0 mL/min, 254 nm, 40 °C), major enantiomer $t_r = 8.0$ min, minor enantiomer $t_r = 11.0$ min.

Characterization of (*E*)-chiral starting substrates:



To a mixture of (*R*) or (*S*)-(*E*)-2-tetrahydronaphthyl pent-3-en-1-amine (11.3 mg, 0.06 mmol, 1.0 equiv.) in CH₂Cl₂ (1.5 mL) and 1M NaOH aq (0.33 mL, 0.28 mmol, 5 equiv.) was added dropwise 4-bromo benzoyl chloride (13.6 mg, 0.062 mmol, 1.1 equiv.) at room temperature, and the resulting solution was stirred at this temperature for 6 h. The reaction solution was poured into H₂O and extracted with dichloromethane (10 mL x 3). The combined organic extracts were dried over Na₂SO₄ and concentrated under reduced pressure after filtration. The residual product was purified by flash column chromatography on silica gel to give 4-bromobenzoyl protected (*R*)- or (*S*)-(*E*)-4-bromo-*N*-((1-(prop-1-en-1-yl)-1,2,3,4-tetrahydronaphthalen-1-yl)methyl)benzamide quantitatively (25.8 mg, 0.07 mmol).



(*R*)-(*E*)-4-bromo-*N*-((1-(prop-1-en-1-yl)-1,2,3,4-tetrahydronaphthalen-1-yl)methyl)benzamide

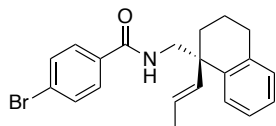
$[\alpha]_D^{24} = +17.6^\circ$ ($c = 0.67$, CHCl₃, 99% ee).

TLC $R_f = 0.58$ (5:1 hexane:ethyl acetate).

¹H NMR (CDCl₃, 400 MHz) δ 7.55-7.53 (m, 2H, Ar-*H*), 7.47-7.44 (m, 2H, Ar-*H*), 7.31-7.30 (m, 1H, Ar-*H*), 7.25-7.16 (m, 3H, Ar-*H*) 5.84 (s, 1H, NH), 5.62 (dd, 1H, $J = 15.6, 1.6$ Hz, C-CH=CH), 5.30-5.21 (m, 1H, C-CH=CH), 3.91 (dd, 1H, $J = 13.6, 7.4$ Hz, NH-CH₂-C), 3.73 (dd, 1H, $J = 13.7, 4.6$ Hz, NH-CH₂-C), 2.80-2.77 (m, 2H, C-CH₂-CH₂), 1.86-1.82 (m, 4H, CH₂-CH₂-CH₂), 1.72 (dd, 3H, $J = 1.6$ Hz, CH=CH-CH₃).

¹³C NMR (CDCl₃, 100 MHz) δ 166.5, 138.4, 137.8, 131.8, 129.7, 128.3, 127.7, 126.4, 126.1, 126.0, 47.8, 44.8, 32.6, 30.2, 18.8, 18.2.

HRMS (FAB) Exact Mass Calcd. for C₂₁H₂₂NOBr ([M+H]⁺) 384.0958. Found: 384.0975.



(*R*)-(*E*)-4-bromo-*N*-((1-(prop-1-en-1-yl)-1,2,3,4-tetrahydronaphthalen-1-yl)methyl)benzamide

$[\alpha]_D^{24} = -17.3^\circ$ ($c = 0.67$, CHCl_3 , 99% ee).

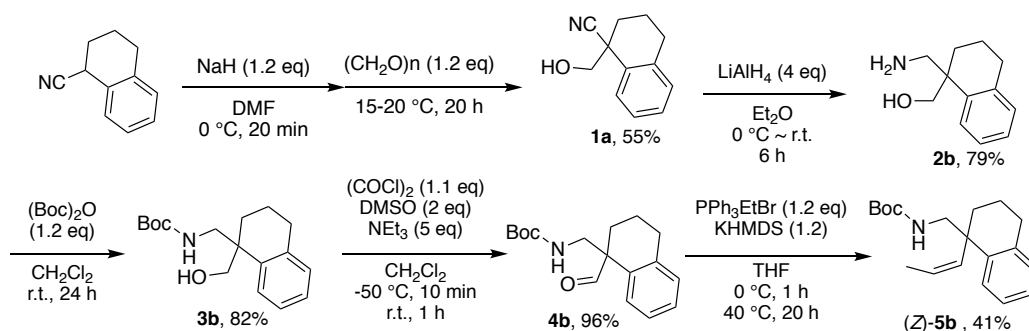
TLC $R_f = 0.58$ (5:1 hexane:ethyl acetate).

$^1\text{H NMR}$ (CDCl_3 , 400 MHz) δ 7.55-7.53 (m, 2H, Ar-*H*), 7.47-7.44 (m, 2H, Ar-*H*), 7.31-7.30 (m, 1H, Ar-*H*), 7.25-7.16 (m, 3H, Ar-*H*) 5.84 (s, 1H, NH), 5.62 (dd, 1H, $J = 15.6, 1.6$ Hz, C-CH=CH), 5.30-5.21 (m, 1H, C-CH=CH), 3.91 (dd, 1H, $J = 13.6, 7.4$ Hz, NH-CH₂-C), 3.73 (dd, 1H, $J = 13.7, 4.6$ Hz, NH-CH₂-C), 2.80-2.77 (m, 2H, C-CH₂-CH₂), 1.86-1.82 (m, 4H, CH₂-CH₂-CH₂), 1.72 (dd, 3H, $J = 1.6$ Hz, CH=CH-CH₃).

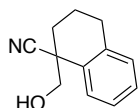
$^{13}\text{C NMR}$ (CDCl_3 , 100 MHz) δ 166.5, 138.4, 137.8, 131.8, 129.7, 128.3, 127.7, 126.4, 126.1, 126.0, 47.8, 44.8, 32.6, 30.2, 18.8, 18.2.

HRMS (FAB) Exact Mass Calcd. for $\text{C}_{21}\text{H}_{22}\text{NOBr}$ ($[\text{M}+\text{H}]^+$) 384.0958. Found: 384.0975.

Synthesis of (Z)-chiral starting substrates:

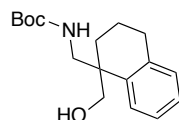


Scheme 11. Synthesis of (*Z*)-chiral substrates



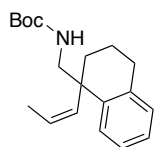
The NaH (60% dispersion in oil, 0.38 g, 9.46 mmol, 1.2 equiv.) was washed with anhydrous pentane in 50 mL two-neck round-bottom flask and added DMF. To suspension of NaH in DMF was added dropwise a solution of 1-cyanonitraline (1.24 g, 7.9 mmol, 1 equiv.) at 0 °C, and the resulting mixture was stirred at this temperature for 30 min, then formaldehyde was added into resulting mixture. The mixed reaction was stirred at 0 °C for 20

min after that the reaction was allowed to slowly warm up to room temperature. After 20 hours, the reaction was quenched by NH_4Cl aq, extracted with diethyl ether, and washed with sat. NaHCO_3 aq and brine, respectively. The combined organic extracts were dried over MgSO_4 , filtrated, concentrated, and purified by flash column chromatography on silica gel to afford desired 1-(hydroxymethyl)-1,2,3,4-tetrahydronaphthalene-1-carbonitrile (**1a**) in 55% yield (813.6 mg, 4.3 mmol).¹



To a suspension of LiAlH_4 (391 mg, 9.82 mmol, 4 equiv.) in Et_2O (11.4 mL) was added dropwise 1-(hydroxymethyl)-1,2,3,4-tetrahydronaphthalene-1-carbonitrile (5 mmol, 1 equiv.) in Et_2O (11.4 mL) at 0 °C, and the resulting mixture was stirred at room temperature for 6 h. After cooling to 0 °C, the reaction was carefully quenched with H_2O (2 mL) and 1M NaOH aq. (2 mL). To the resulting mixture was further added H_2O carefully at 0 °C, and stirred at 0 °C to room temperature for several hours. The resulting mixture was filtrated and extracted with diethylether (20 mL x 3). The combined extracts were dried over K_2CO_3 , and evaporated after filtration to give 3-hydroxyl-2-tetrahydronaphthyl propylamine as a crude product in 79% yield (370.1 mg, 1.94 mmol).

To a solution of 3-hydroxyl-2-tetrahydronaphthyl propylamine (370 mg, 1.93 mmol, 1.0 equiv.) in CH_2Cl_2 (30 mL) was slowly added di-*tert*-butyl dicarbonate (530 μL , 2.32 mmol, 1.2 equiv.) at room temperature, and stirred at this temperature for 24 h. The reaction was poured into water and extracted with CH_2Cl_2 (20 mLx3), and then combined CH_2Cl_2 extracts were dried over Na_2SO_4 and concentrated under vacuum after filtration. The residual reaction was purified by flash column on silica gel to afford desired 3-hydroxyl-*tert*-butyl-2-(1,2,3,4-tetrahydronaphthyl)carbamate in 82% yield (460 mg, 1.57 mmol).

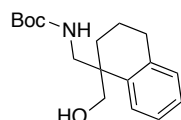


To a solution of $(\text{COCl})_2$ (117 μL , 1.38 mmol, 2.0 equiv.) in CH_2Cl_2 (30 mL) was slowly added DMSO (178 μL , 2.5 mmol, 2.0 equiv.) at -50 °C, and stirred at this temperature for 5 min. To the resulting mixture was added solution of 3-hydroxyl-*tert*-butyl-2-(1,2,3,4-tetrahydronaphthyl)carbamate (365.8 mg, 1.25 mmol, 1.0 equiv.) in CH_2Cl_2 (3.4 mL) then

mixed solution was stirred at this temperature to room temperature for 20 min. The resulting mixture was slowly add NEt_3 (870 μL , 6.28 mmol, 5.0 equiv.) after that resulting solution was warmed to temperature for 1.5 h after stirring at $-50\text{ }^\circ\text{C}$ for 10 min. The reaction was diluted by water and extracted with CH_2Cl_2 (x3), and then combined CH_2Cl_2 extracts were dried over MgSO_4 and concentrated under vacuum after filtration. The residual reaction was purified by flash silica gel to afford desired 1-formyl-*tert*-butyl-(1,2,3,4-tetrahydronaphthyl)carbamate quantitatively (362 mg, 1.25 mmol).

To a solution of triphenylphosphonium ethyl bromide (620 mg, 1.66 mmol, 1.2 equiv.) in THF (3.5 mL) was added KHMDS (3.4 mL, 1.66 mmol, 1.2 equiv.) at $0\text{ }^\circ\text{C}$, and stirred at this temperature for 1 h. To the resulting mixture was slowly added a solution of 1-formyl-*tert*-butyl-(1,2,3,4-tetrahydronaphthyl)carbamate (400 g, 1.38 mmol, 1.0 equiv.) in THF (3.5 mL), and mixed solution was stirred at this temperature for 30 min and at room temperature for 30 min and then the reaction was warmed to $40\text{ }^\circ\text{C}$ for 20 h. The reaction mixture was poured into sat. NH_4Cl aq and extracted with diethyl ether (x3). The combined organic extracts were dried over Na_2SO_4 and concentrated under vacuum after filtration. The residual reaction was purified by flash silica gel to afford (*Z*)-*tert*-butyl (1,2,3,4-tetrahydronaphthyl)carbamate in 43% yield (179.2 mg, 0.6 mmol).

Characterization of (Z)-chiral starting substrates:

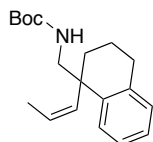


TLC $R_f = 0.21$ (5:1 hexane:ethyl acetate).

^1H NMR (CDCl_3 , 400 MHz) δ 7.51-7.49 (m, 1H, Ar-*H*), 7.19-7.10 (m, 3H, Ar-*H*), 4.82 (t, 1H, $J = 6.3$ Hz, NH), 3.76-3.67 (m, 2H, NH- CH_2), 3.52-3.42 (m, 2H, HO- CH_2), 3.27 (dd, 1H, $J = 14.4, 6.6$ Hz, OH), 2.77 (t, 2H, $J = 6.1$ Hz, C- CH_2), 1.81-1.68 (m, 4H, - CH_2 -), 1.47 (s, 9H, C-(CH_3)₃).

^{13}C NMR (CDCl_3 , 100 MHz), δ 157.49, 138.97, 137.81, 129.48, 127.46, 126.29, 125.89, 80.18, 67.84, 46.59, 42.52, 30.63, 29.58, 28.38, 18.95.

HRMS (FAB) Exact Mass Calcd. for $\text{C}_{17}\text{H}_{23}\text{NO}_3$ ($[\text{M}+\text{H}]^+$) 292.1907. Found: 292.1908.

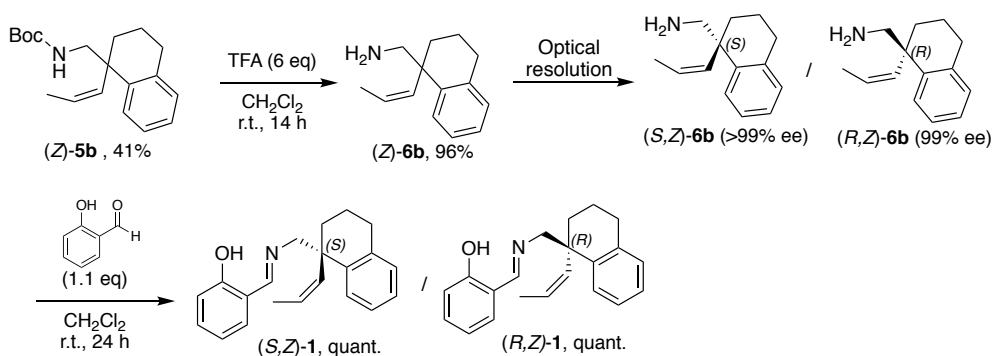


TLC $R_f = 0.49$ (5:1 hexane:ethyl acetate).

^1H NMR (CDCl_3 , 400 MHz), δ 7.25-7.19 (m, 1H, Ar-*H*), 7.12-7.06 (m, 3H, Ar-*H*), 5.59 (dd, 1H, $J = 11.7, 1.6$ Hz, $\text{CH}_3\text{-CH=CH}$), 5.50-5.42 (m, 1H, $\text{CH}_3\text{-CH=CH}$), 4.49 (s, 1H, *NH*), 3.51-3.44 (m, 1H, *NH-CH}_2*), 3.37 (m, 1H, *NH-CH}_2*), 2.80 (t, 2H, $J = 6.2$ Hz, C-CH_2 -), 1.94-1.74 (m, 4H, $-\text{CH}_2$ -), 1.42 (s, 9H, $-\text{C}(\text{CH}_3)_3$), 1.07 (dd, 3H, $J = 7.1, 1.6$ Hz, CH=CH-CH_3).

^{13}C NMR (CDCl_3 , 100 MHz), δ 156.22, 140.59, 137.52, 136.98, 129.20, 128.34, 126.08, 125.90, 79.16, 77.31, 77.00, 76.69, 50.21, 44.07, 32.86, 30.15, 28.36, 19.36, 14.09.

HRMS (FAB) Exact Mass Calcd. for $\text{C}_{17}\text{H}_{23}\text{NO}_3$ ($[\text{M}+\text{H}]^+$) 302.2115. Found: 302.2056.



Scheme 12. Synthesis of (*R,Z*)-**6** and (*S,Z*)-**6** substrates

To a solution of (*Z*)-*tert*-butyl (1,2,3,4-tetrahydronaphthyl)carbamate (143.0 mg, 0.47 mmol, 1 equiv.) in CH_2Cl_2 (5 mL) was added dropwise trifluoroacetic acid (TFA, 212 μL , 2.84 mmol, 6.0 equiv.) at room temperature. After stirred at room temperature for 4 h, the reaction mixture was treated with 1M NaOH aq (5 mL), cooled with iced water, and extracted with CH_2Cl_2 (20 mL x 3). The combined organic layer was dried over Na_2SO_4 . After filtration and evaporation. The 2-tetrahydronaphthyl pent-3-en-1-amine was obtained in 96% yield (91.3 mg, 0.45 mmol) which was separated between (*R*)- or (*S*)-enantiomer by the use of semi-preparative chiral HPLC (CHIRALCEL OD-H (10 mm ϕ \times 250 mm L), 98/2 hexane/*i*-PrOH, 5 mL/min, 254 nm, 40 $^\circ\text{C}$, $t_r = 7.4$ and 11.2 min).

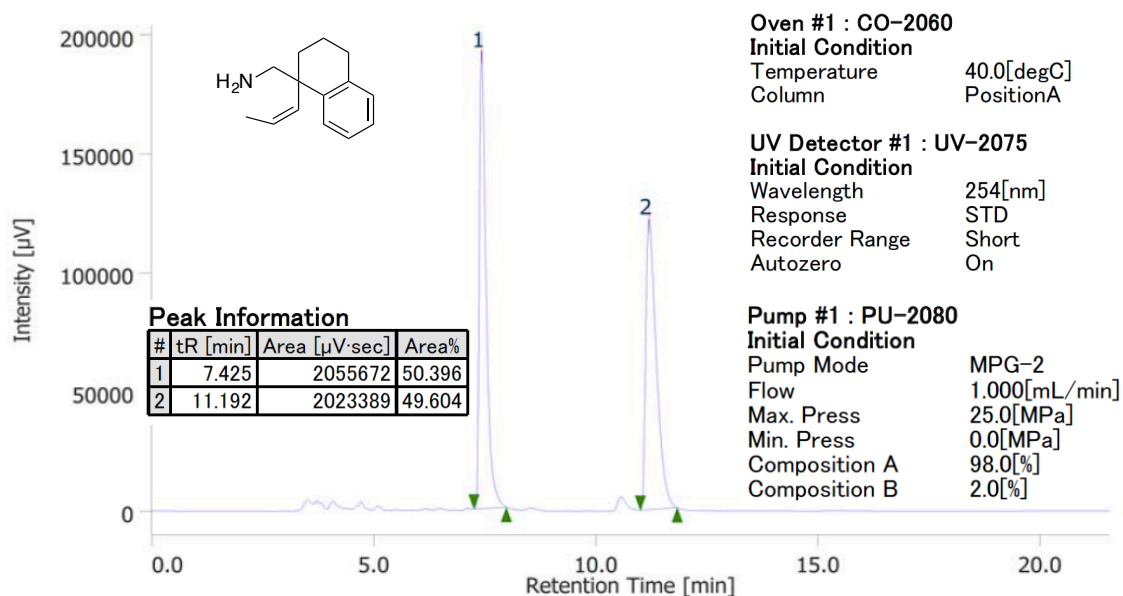


Chart 6. HPLC chart for racemic racemic-(Z)-2-tetrahydronaphthyl pent-3-en-1-amine compound. Semi-preparative HPLC was used to separate each enantiomer (CHIRALCEL OD-H (10 mm ϕ \times 250 mm L), 98/2 hexane/*i*-PrOH, 5 mL/min, 254 nm, 40 °C, t_r = 7.4 and 11.2 min). Retention times were determined by analytical HPLC with a CHIRALCEL OD-3 (98/2 hexane/*i*-PrOH, 1.0 mL/min, 254 nm, 40 °C), t_r = 7.4 and 11.2 min.

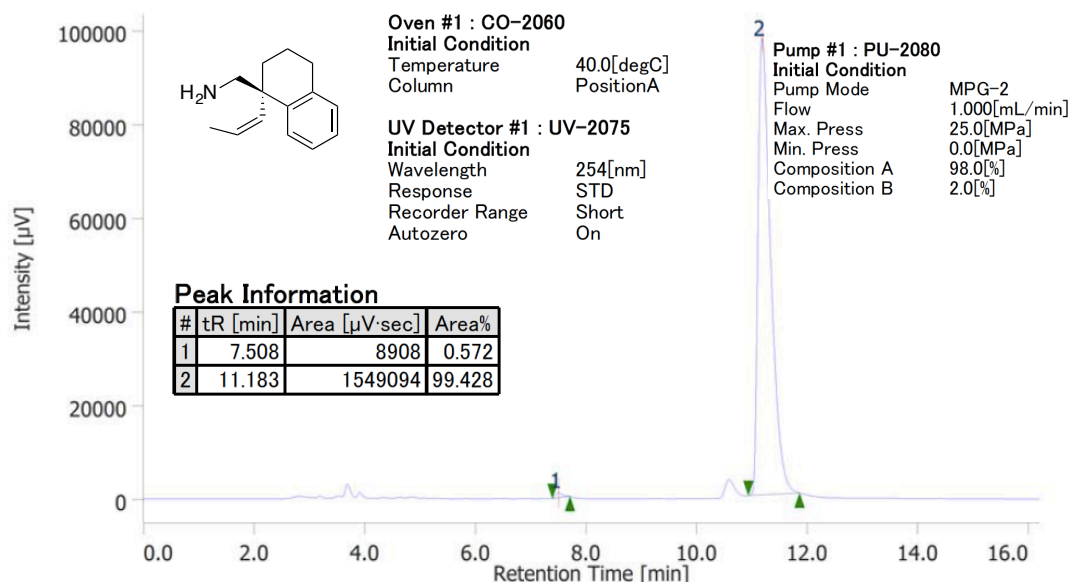


Chart 7. HPLC chart for (*R,Z*)-2-tetrahydronaphthyl pent-3-en-1-amine compound. Enantiomeric excess was determined by analytical HPLC with a CHIRALCEL OD-3 (98/2 hexane/*i*-PrOH, 1.0 mL/min, 254 nm, 40 °C), major enantiomer t_r = 11.2 min, minor t_r = 7.5 min.

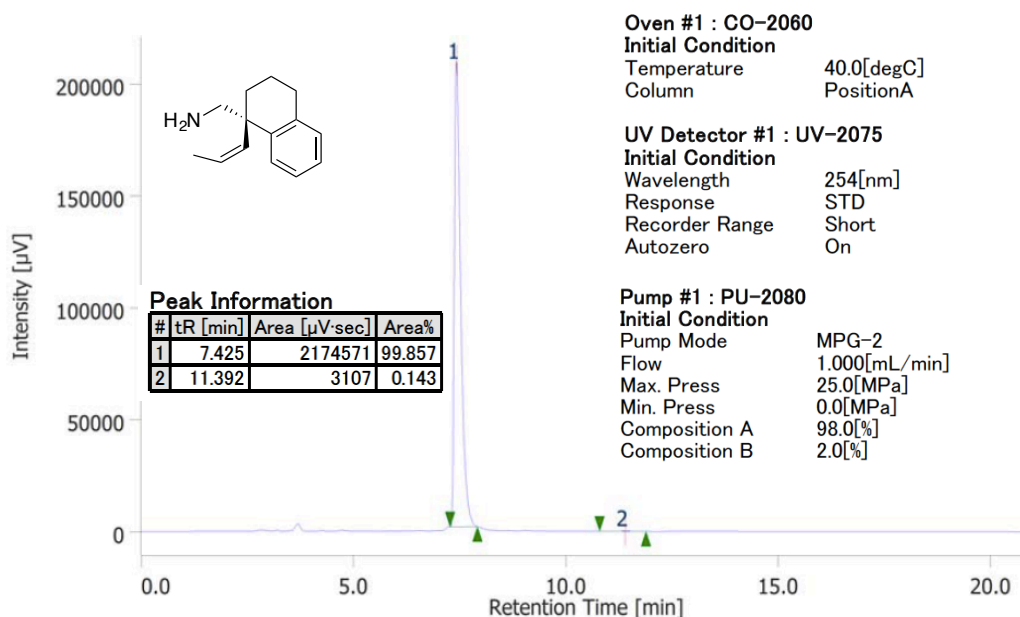
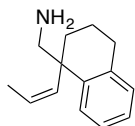


Chart 8. HPLC chart for (*S,Z*)-2-tetrahydronaphthyl pent-3-en-1-amine compound. Enantiomeric excess was determined by analytical HPLC with a CHIRALCEL OD-3 (98/2 hexane/*i*-PrOH, 1.0 mL/min, 254 nm, 40 °C), major enantiomer $t_r = 11.4$ min, minor $t_r = 7.4$ min.

To a mixture of (*S*) or (*R*)-(*Z*)-2-tetrahydronaphthyl pent-3-en-1-amine (60.4 mg, 0.3 mmol, 1.0 equiv.) and MS 4Å (150 mg, 50 mg/0.1 mmol) in CH₂Cl₂ (1 mL) was added 2-hydroxy benzaldehyde (32 µL, 0.33 mmol, 1.1 equiv.) at room temperature, and the resulting mixture was stirred at this temperature for 24 h. After filtration, the resulting solution was concentrated in *vacuo* to give 2-((*E*)-((*Z*)-(*S*) or (*R*)-2-tetrahydronaphthyl pent-3-en-1-yl)imino)methyl)phenol quantitatively.

Characterization of (*Z*)-chiral starting substrates:

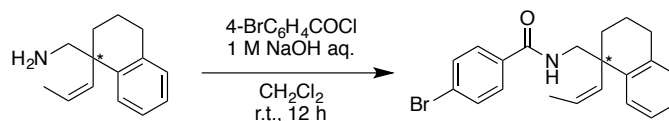


TLC $R_f = 0.41$ (7:1 CHCl₃:MeOH).

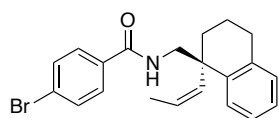
¹H NMR (CDCl₃, 400 MHz), δ 7.22 (dd, 1H, $J = 6.1, 2.6$ Hz, Ar-*H*), 7.14-7.07 (m, 3H, Ar-*H*), 5.61 (dq, 1H, $J = 11.7, 1.7$ Hz, C-CH=CH), 5.51-5.42 (m, 1H, CH=CH-CH₃), 2.99 (d, 1H, $J = 13.3$ Hz, NH₂-CH₂), 2.83-2.76 (m, 3H, NH₂-CH₂), 1.98-1.93 (m, 1H, -CH₂-), 1.84-1.74 (m, 3H, -CH₂-), 1.21 (d, 2H, $J = 6.0$ Hz, -CH₂-), 1.09 (dd, 3H, $J = 7.1, 1.8$ Hz, CH-CH₃).

¹³C NMR (CDCl₃, 100 MHz), δ 141.3, 137.6, 137.4, 129.1, 128.4, 125.9, 125.6, 52.8, 45.0, 32.5, 30.2, 25.4, 19.4, 14.2.

Characterization of Substrates:



To a mixture of (*R*) or (*S*)-(*Z*)-2-tetrahydronaphthyl pent-3-en-1-amine (90 mg, 0.4 mmol, 1.0 equiv.) in CH₂Cl₂ (2 mL) and 1M NaOH aq (2.2 mL, 2.0 mmol, 5 equiv.) was added 4-bromo benzoyl chloride (96 mg, 0.44 mmol, 1.1 equiv.) at room temperature, and the resulting solution was stirred at this temperature for 6 h. The reaction solution was poured into H₂O and extracted with dichloromethane (10 mL x 3). The combined organic extracts were dried over Na₂SO₄ and concentrated under reduced pressure after filtration. The residual product was purified by flash column chromatography on silica gel to give 4-bromobenzoyl protected (*R*)- or (*S*)-(*Z*)-4-bromo-*N*-((1-(prop-1-en-1-yl)-1,2,3,4-tetrahydronaphthalen-1-yl)methyl)benzamide in 81% yield (124.8 mg, 0.32 mmol).



(*R*)-(*Z*)-4-bromo-*N*-((1-(prop-1-en-1-yl)-1,2,3,4-tetrahydronaphthalen-1-yl)methyl)benzamide ((*R*)-S12)

$[\alpha]_D^{24} = -34.7^\circ$ ($c = 0.33$, CHCl₃, 99% ee).

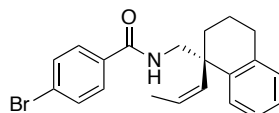
TLC R_f = 0.53 (5:1 hexane:ethyl acetate).

¹H NMR (CDCl₃, 400 MHz), δ 7.50 (ddt, 4H, $J = 18.5, 8.5, 1.9$ Hz, Ar-*H*), 7.31-7.29 (m, 1H, Ar-*H*), 7.19-7.11 (m, 3H, Ar-*H*), 6.00 (s, 1H, NH), 5.67 (dq, 1H, $J = 11.6, 1.6$ Hz, CH₃CH=CH), 5.55-5.47 (m, 1H, CH₃CH=CH), 3.80 (q, 1H, $J = 6.9$ Hz, NH-CH₂), 3.69 (dd, 1H, $J = 13.5, 5.3$ Hz, NH-CH₂), 2.84-2.81 (m, 2H, C-CH₂-), 1.95-1.78 (m, 4H, -CH₂-), 1.12 (dd, 3H, $J = 7.2, 1.7$ Hz, CH=CH-CH₃).

¹³C NMR (CDCl₃, 100 MHz), δ 166.6, 140.1, 137.6, 136.6, 133.5, 131.8, 129.5, 128.35, 128.2, 126.6, 126.3, 126.0, 49.4, 44.2, 33.5, 30.0, 19.4, 14.2.

HRMS (FAB) Exact Mass Calcd. for C₂₁H₂₂NOBr ([M+H]⁺) 384.0958. Found: 384.0964.

Enantiomeric excess was determined by analytical HPLC with a CHIRALCEL OD-3 (95/5 hexane/*i*-PrOH, 1.0 mL/min, 254 nm, 40 °C), minor enantiomer t_r = 15.6 min, major enantiomer t_r = 22.3 min.



(S)-(Z)-4-bromo-N-((1-(prop-1-en-1-yl)-1,2,3,4-tetrahydronaphthalen-1-yl)methyl)benzamide

$[\alpha]_D^{24} = +32.5^\circ$ ($c = 0.33$, CHCl_3 , 99% ee).

TLC $R_f = 0.53$ (5:1 hexane:ethyl acetate).

$^1\text{H NMR}$ (CDCl_3 , 400 MHz), δ 7.50 (ddt, 4H, $J = 18.5, 8.5, 1.9$ Hz, Ar- H), 7.31-7.29 (m, 1H, Ar- H), 7.19-7.11 (m, 3H, Ar- H), 6.00 (s, 1H, NH), 5.67 (dq, 1H, $J = 11.6, 1.6$ Hz, $\text{CH}_3\text{CH}=\text{CH}$), 5.55-5.47 (m, 1H, $\text{CH}_3\text{CH}=\text{CH}$), 3.80 (q, 1H, $J = 6.9$ Hz, NH- CH_2), 3.69 (dd, 1H, $J = 13.5, 5.3$ Hz, NH- CH_2), 2.84-2.81 (m, 2H, C- CH_2 -), 1.95-1.78 (m, 4H, - CH_2 -), 1.12 (dd, 3H, $J = 7.2, 1.7$ Hz, $\text{CH}=\text{CH}-\text{CH}_3$).

$^{13}\text{C NMR}$ (CDCl_3 , 400 MHz), δ 166.6, 140.1, 137.6, 136.6, 133.5, 131.8, 129.5, 128.35, 128.2, 126.6, 126.3, 126.0, 49.4, 44.2, 33.5, 30.0, 19.4, 14.2.

HRMS (FAB) Exact Mass Calcd. for $\text{C}_{21}\text{H}_{22}\text{NOBr}$ ($[\text{M}+\text{H}]^+$) 384.0958. Found: 384.0964.

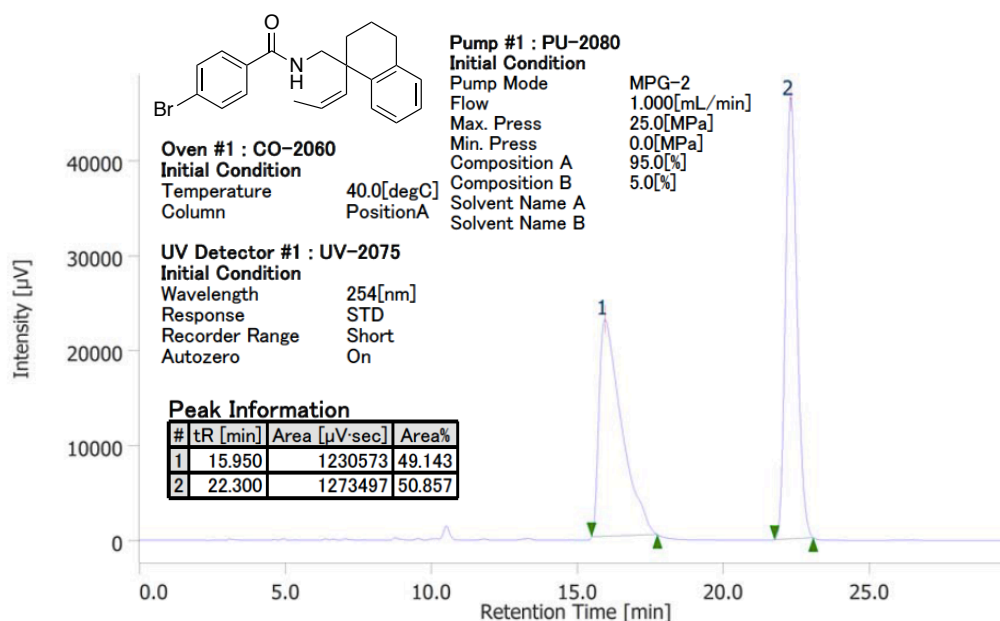


Chart 9. HPLC chart for racemic (Z)-4-bromo-N-((1-(prop-1-en-1-yl)-1,2,3,4-tetrahydronaphthalen-1-yl)methyl)benzamide. Retention times were determined by analytical HPLC with a CHIRALCEL OD-3 (95/5 hexane/*i*-PrOH, 1.0 mL/min, 254 nm, 40 °C), $t_r = 16.0$ and 22.3 min.

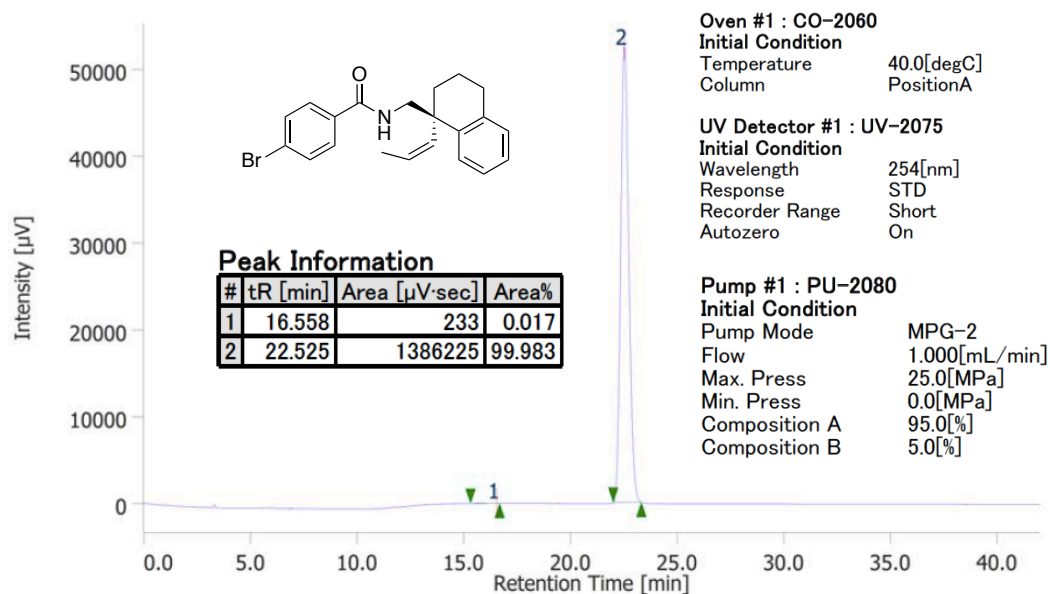


Chart 10. HPLC chart for (*R,Z*)-4-bromo-*N*-((1-(prop-1-en-1-yl)-1,2,3,4-tetrahydronaphthalen-1-yl)methyl)benzamide. Enantiomeric excess was determined by analytical HPLC with a CHIRALCEL OD-3 (95/5 hexane/*i*-PrOH, 1.0 mL/min, 254 nm, 40 °C), major enantiomer $t_r = 22.53$ min, minor $t_r = 16.56$ min.

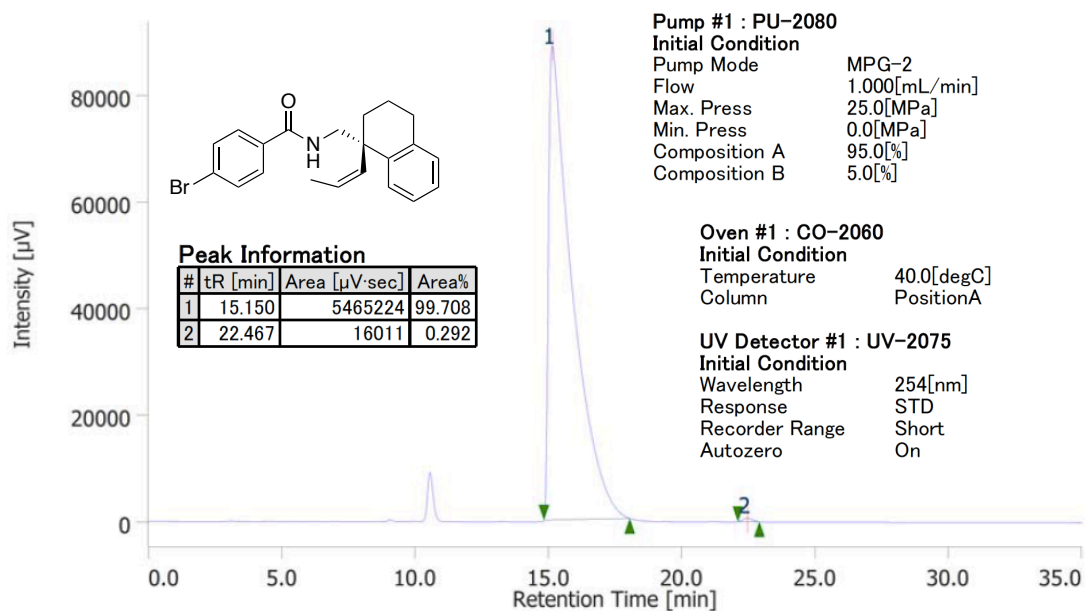


Chart 11. HPLC chart for (*S,Z*)-4-bromo-*N*-((1-(prop-1-en-1-yl)-1,2,3,4-tetrahydronaphthalen-1-yl)methyl)benzamide. Enantiomeric excess was determined by analytical HPLC with a CHIRALCEL OD-3 (95/5 hexane/*i*-PrOH, 1.0 mL/min, 254 nm, 40 °C), major enantiomer $t_r = 15.2$ min, minor $t_r = 22.5$ min.

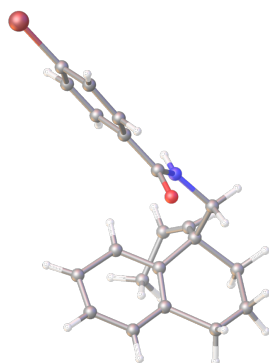
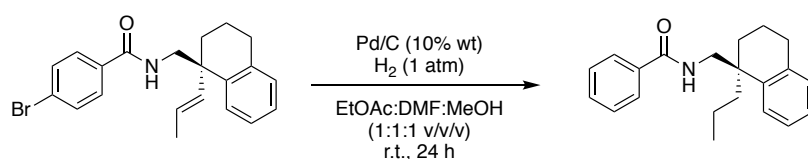
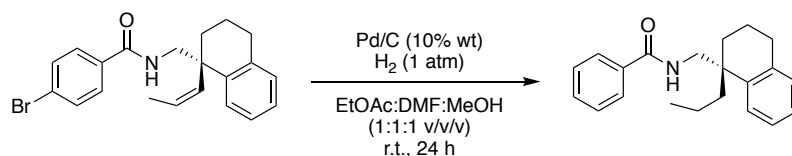


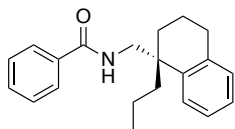
Figure 6. ORTEP diagram of (*R,Z*)-**2** substrate by Sponge X-ray analysis



To a mixture of (*S*)-(*E*)-4-bromo-*N*-((1-(prop-1-en-1-yl)-1,2,3,4-tetrahydronaphthalen-1-yl)methyl)benzamide (8.3 mg, 0.02 mmol, 1.0 equiv.) in EtOAc:DMF:MeOH (1:1:1 v/v/v) (1.2 mL) was added Pd/C (0.8 mg, 10% wt) at room temperature, and the resulting solution was stirred under H₂ gas (1 atm) at room temperature for 24 h. The reaction solution was filtrated by celite by the use of EtOAc for washing. The EtOAc solution was concentrated in vacuum to give (*S*)-*N*-((1-(propyl)-1,2,3,4-tetrahydronaphthalen-1-yl)methyl)benzamide in 60% yield (4.6 mg, 0.01 mmol).



To a mixture of (*R*)-(*Z*)-4-bromo-*N*-((1-(prop-1-en-1-yl)-1,2,3,4-tetrahydronaphthalen-1-yl)methyl)benzamide (24 mg, 0.06 mmol, 1.0 equiv.) in EtOAc:DMF:MeOH (1:1:1 v/v/v) (1.5 mL) was added Pd/C (2.4 mg, 10% wt) at room temperature, and the resulting solution was stirred under H₂ gas (1 atm) at room temperature for 24 h. The reaction solution was filtrated by Celite by the use of EtOAc for washing. The EtOAc solution was concentrated in vacuum to give (*R*)-*N*-((1-(propyl)-1,2,3,4-tetrahydronaphthalen-1-yl)methyl)benzamide in 62% yield (14.8 mg, 0.03 mmol).



(R)-N-((1-(propyl)-1,2,3,4-tetrahydronaphthalen-1-yl)methyl)benzamide

$[\alpha]_D^{23} = -23.2^\circ$ ($c = 0.19$, CHCl_3 , 99% ee).

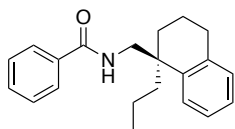
TLC $R_f = 0.31$ (5:1 hexane:ethyl acetate).

^1H NMR (CDCl_3 , 400 MHz), δ 7.58-7.55 (m, 2H, Ar-H), 7.47-7.43 (m, 1H, Ar-H), 7.39-7.35 (m, 2H, Ar-H), 7.31 (d, 1H, $J = 7.6$ Hz, Ar-H), 7.23-7.13 (m, 2H, Ar-H), 3.82 (dd, 1H, $J = 13.5, 7.8$ Hz, NH- CH_2), 3.58 (dd, 1H, $J = 13.5, 4.6$ Hz, NH- CH_2), 2.76-2.74 (m, 2H, - CH_2 -), 1.91-1.73 (m, 5H, - CH_2 -), 1.64-1.55 (m, 1H, CH= CH_2 -), 1.40-1.25 (m, 1H, CH= CH_2 -), 1.23-1.10 (m, 1H), 0.87 (t, 3H, $J = 7.2$ Hz, CH_3).

^{13}C NMR (CDCl_3 , 100 MHz), δ 167.5, 140.4, 138.6, 134.8, 131.3, 129.6, 128.5, 126.68, 126.5, 126.3, 126.1, 49.3, 43.1, 41.4, 31.0, 30.5, 19.7, 17.4, 14.9.

HRMS (ESI) Exact Mass Calcd. for $\text{C}_{21}\text{H}_{22}\text{NO}$ ($[\text{M}+\text{Na}]^+$) 330.1828. Found: 330.1830.

Enantiomeric excess was determined by HPLC with a CHIRALCEL OD-3 (95/5 hexane/*i*-PrOH, 1.0 mL/min, 254 nm, 40 °C), minor enantiomer $t_r = 10.1$ min, major enantiomer $t_r = 11.3$ min.



(S)-N-((1-(propyl)-1,2,3,4-tetrahydronaphthalen-1-yl)methyl)benzamide

$[\alpha]_D^{23} = +23.5^\circ$ ($c = 0.19$, CHCl_3 , 99% ee)

TLC $R_f = 0.26$ (5:1 hexane:ethyl acetate).

^1H NMR (CDCl_3 , 400 MHz), δ 7.58-7.55 (m, 2H, Ar-H), 7.47-7.43 (m, 1H, Ar-H), 7.39-7.35 (m, 2H, Ar-H), 7.31 (d, 1H, $J = 7.6$ Hz, Ar-H), 7.23-7.13 (m, 2H, Ar-H), 3.82 (dd, 1H, $J = 13.5, 7.8$ Hz, NH- CH_2), 3.58 (dd, 1H, $J = 13.5, 4.6$ Hz, NH- CH_2), 2.76-2.74 (m, 2H, - CH_2 -), 1.91-1.73 (m, 5H, - CH_2 -), 1.64-1.55 (m, 1H, CH= CH_2 -), 1.40-1.25 (m, 1H, CH= CH_2 -), 1.23-1.10 (m, 1H), 0.87 (t, 3H, $J = 7.2$ Hz, CH_3).

^{13}C NMR (CDCl_3 , 100 MHz), δ 167.5, 140.4, 138.6, 134.8, 131.3, 129.6, 128.5, 126.68, 126.5, 126.3, 126.1, 49.3, 43.1, 41.4, 31.0, 30.5, 19.7, 17.4, 14.9.

HRMS (ESI) Exact Mass Calcd. for $\text{C}_{21}\text{H}_{22}\text{NO}$ ($[\text{M}+\text{Na}]^+$) 330.1828. Found: 330.1830.

Enantiomeric excess was determined by HPLC with a CHIRALCEL OD-3 (95/5 hexane/*i*-PrOH, 1.0 mL/min, 254 nm, 40 °C), minor enantiomer $t_r = 11.3$ min, major enantiomer $t_r = 10.1$ min.

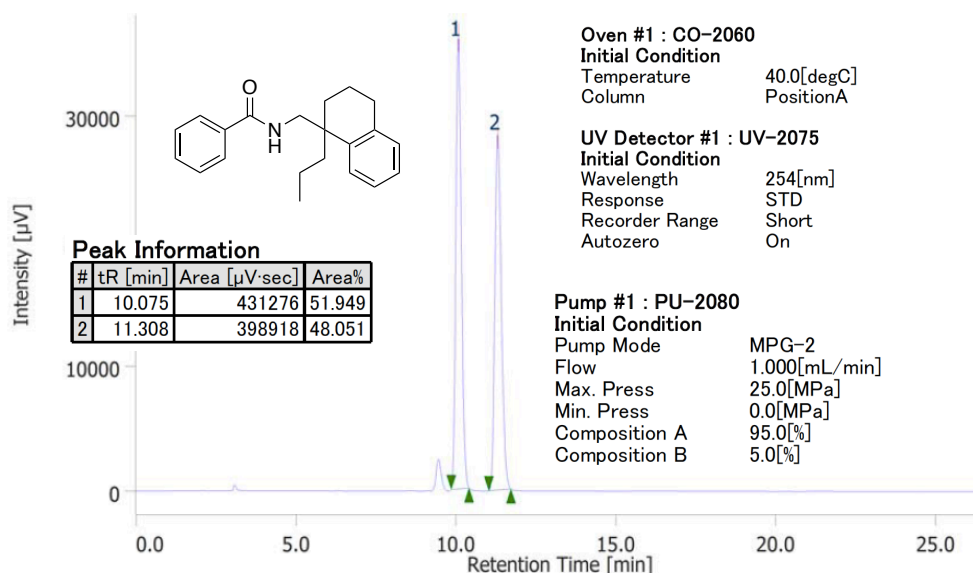


Chart 11. HPLC chart for racemic-*N*-((1-(propyl)-1,2,3,4-tetrahydro naphthalene-1-yl)methyl)benzamide. Enantiomeric excess was determined by analytical HPLC with a CHIRALCEL OD-3 (95/5 hexane/*i*-PrOH, 1.0 mL/min, 254 nm, 40 °C), major enantiomer $t_r = 11.4$ min, minor $t_r = 10.2$ min.

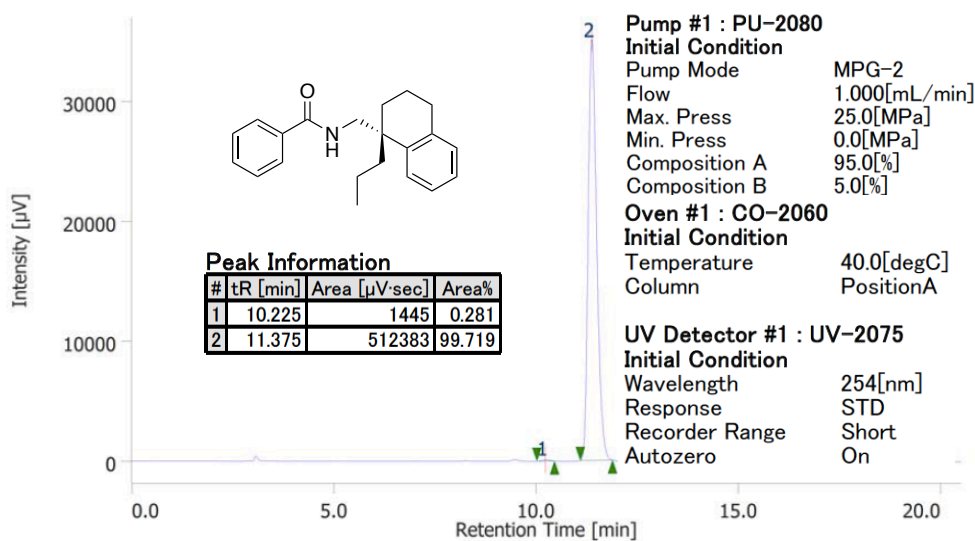


Chart 12. HPLC chart for (*R*)-*N*-((1-(propyl)-1,2,3,4-tetrahydro naphthalene-1-yl)methyl)benzamide. Enantiomeric excess was determined by analytical HPLC with a CHIRALCEL

OD-3 (95/5 hexane/*i*-PrOH, 1.0 mL/min, 254 nm, 40 °C), major enantiomer $t_r = 11.4$ min, minor $t_r = 10.2$ min.

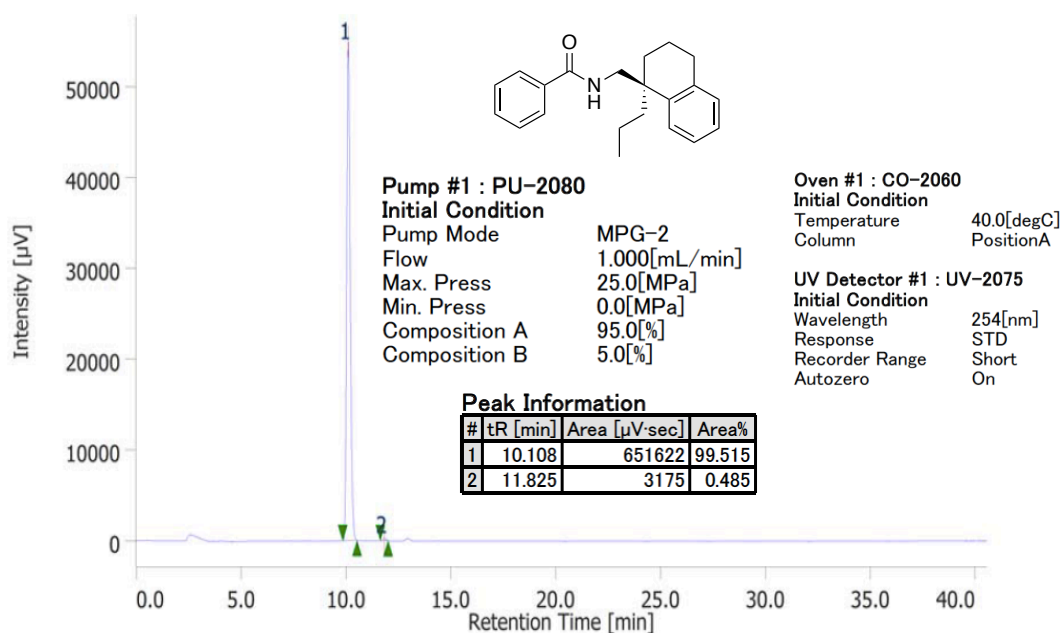


Chart 13. HPLC chart for (*S*)-*N*-((1-(propyl)-1,2,3,4-tetrahydro naphthalene-1-yl)methyl) benzamide. Enantiomeric excess was determined by analytical HPLC with a CHIRALCEL OD-3 (95/5 hexane/*i*-PrOH, 1.0 mL/min, 254 nm, 40 °C), major enantiomer $t_r = 11.4$ min, minor $t_r = 10.2$ min.

4.7 References

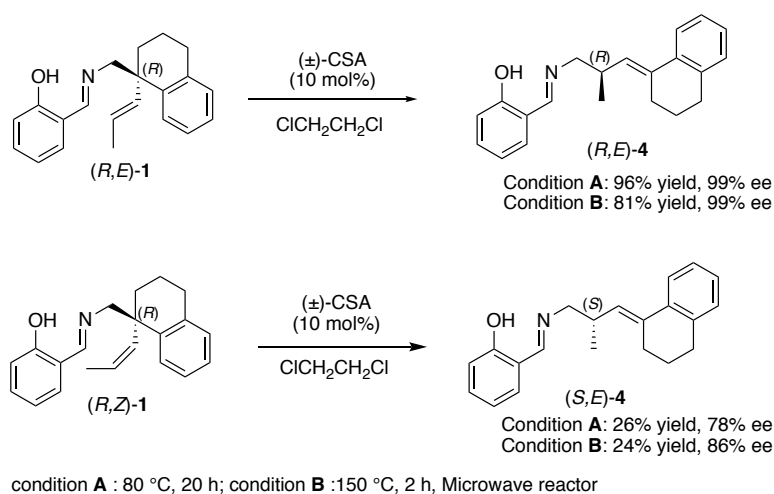
- Hill, R. K. In *Comprehensive Organic Synthesis*; Trost, B. M., Fleming, Eds.; Pergamon: Oxford, 1991; Vol. 5, Chapter 7.1.
- See, page 51, section 3.5.5.
- See, page 20, section 2.2.3.
- Im, D. S.; Cheong, Ch. S.; Lee, S. H. *J. Mol. Catal B-Enzym.* **2003**, *26*, 131-143.
- Parikh, J. R. *J. Am. Chem. Soc.* **1967**, *89*, 5505-5507.
- Corey, E. J.; Yamamoto, H. *J. Am. Chem. Soc.* **1970**, *92*, 226-228.
- See, page 77, section 4.6.2.
- See, page 91, section 4.6.2.
- See, page 51, section 3.5.5.

CHAPTER 5

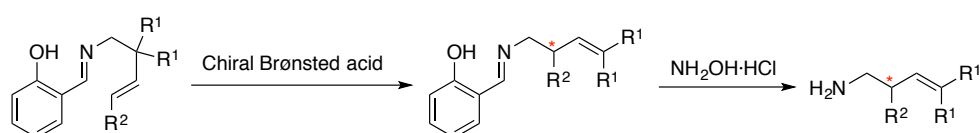
CATALYTIC ASYMMETRIC FORMAL [1,3]-REARRANGEMENT OF ENE-ALDIMINE INITIATED BY CHIRAL BRØNSTED ACID

5.1 Introduction

Since this formal [1,3]-rearrangement reaction has been discovered, the reaction condition, substrate scope, and mechanism have been studied and described in previous chapters. 2-Azaallenium has been found to be a chain carrier; in addition, studies summarized in chapter 4 indicated that 2-azonia-[3,3]-sigmatropic rearrangement of ene-aldiminium intermediate proceeds with excellent chirality transfer ratios in the case of *E*-Olefin (Scheme 1). Although catalytic asymmetric formal [1,3]-rearrangement of ene-aldimine has not been reported and chiral catalyst-controlled asymmetric chemical chain reaction is very challenging, development of catalytic asymmetric version of this reaction will expand the utility of this reaction in homoallylic amine synthesis (Scheme 2).



Scheme 1. Asymmetric formal [1,3]-rearrangement of chiral substrates



Scheme 2. Enantioselective synthesis of homoallylic amines promoted by chiral Brønsted acid

On the basis of our proposed mechanism in chapter 4, it was hypothesized that controlling of stereochemistry of the desired product is possible by chiral Brønsted acid. There are two possibilities in transition state to provide enantioenriched product. First possibility is that the chiral counteranion of chiral Brønsted acid may give an enantioenriched diazetidinium intermediate N*3 from a racemic iminium intermediate N2 in propagation step (Figure 1), and then, this chiral carbon center of N*3 works as a part of chiral auxiliary of chiral ene-aldiminium intermediates for 2-azonia-[3,3]-sigmatropic rearrangement step. It was speculated that chiral ene-aldiminium intermediate N*4 undergoes asymmetric 2-azonia [3,3]-sigmatropic rearrangement to give enantioenriched ene-aldiminium N5*. Ene-aldiminium N5* will finally be transformed to the product P1. Second possibility is that chiral counteranion of chiral Brønsted acid may directly give the asymmetric induction for N*5 regardless of the enantioselectivity of N*4 from N*3, in which hydrogen bonding interaction between catalyst and ene-aldiminium N*4 will contribute to increase enantioselectivity of N*5 by proximity effect and provide enantioselective product P1.

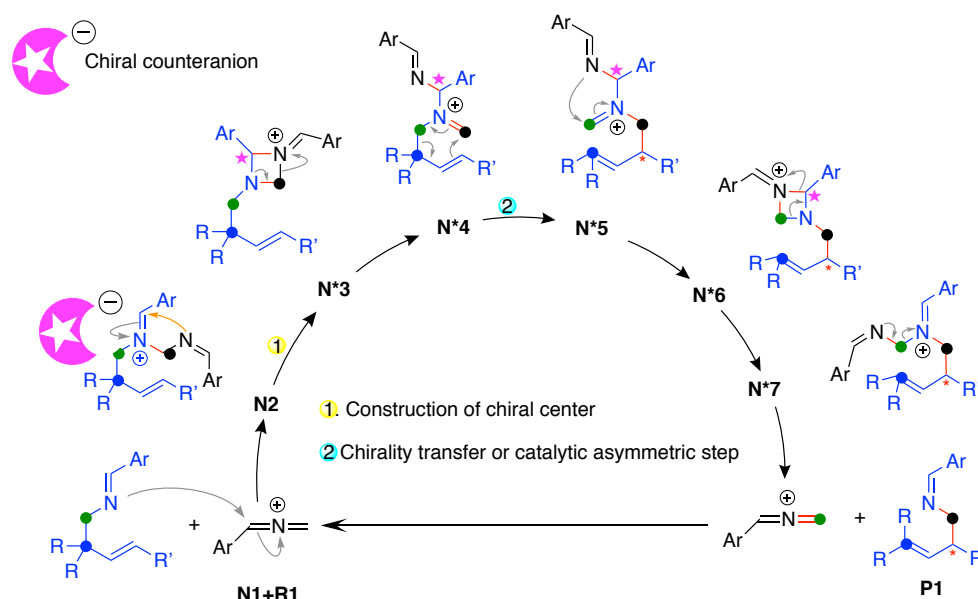


Figure 1. Working hypothesis of catalytic asymmetric formal [1,3]-rearrangement by chiral counteranion

5.2 Catalytic asymmetric formal [1,3]-rearrangement initiated by (1*S*)-(+)-10-champhorsulfonic acid

In chapter 2, 3, and 4, racemic-10-champhorsulfonic acid ((±)-CSA) has been used as an initiator in formal [1,3]-rearrangement reaction. Therefore, (1*S*)-(+)-CSA was initially

selected to develop catalytic asymmetric version of this rearrangement. Moreover, diphenyl substituted ene-aldimine (*E*)-**1a** was chosen as a representative substrate for asymmetric synthesis due to good reactivity and handling.¹ On the basis of reaction optimization in the presence of racemic CSA, acetonitrile and 1,2-dichloroethane were used as solvents.² As the results, the reaction was conducted at 50 °C for 20 h, the rearrangement product was obtained in moderate to good yields; however, no enantioselectivities were observed in both cases (Table 1, entries 1 and 2).

Table 1. Catalytic asymmetric formal [1,3]-rearrangement initiated by (+)-CSA

Entry	Solvent	Catalyst loading (mol%)	Yield (%) ^a	ee (%) ^b
1	MeCN	10	52	<1
2	ClCH ₂ CH ₂ Cl	30	70	<1

^aDetermined by ¹H NMR using dibromomethane as an internal standard.

^bEnantiomeric excess was determined by chiral HPLC after derivatization of **2a**.

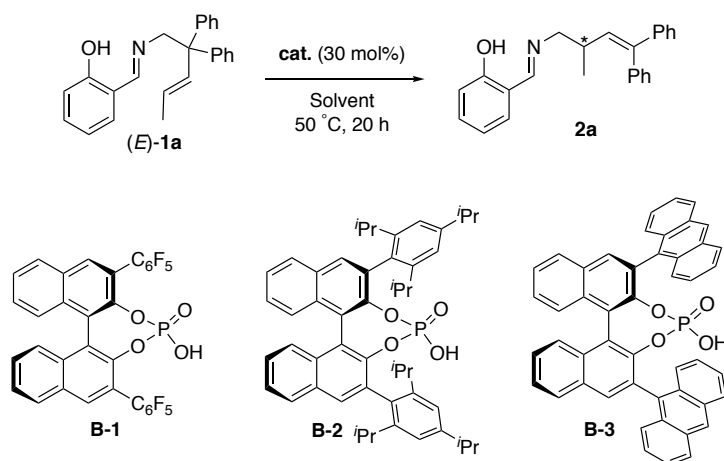
5.3 Catalytic asymmetric formal [1,3]-rearrangement initiated by (*R*)-BINOL-derived phosphoric acid

The Binaphthol (BINOL)-derived Brønsted acids have been known as chiral Brønsted acid catalyst and widely used to yield enantiomeric enriched products in many enantioselective transformations.³ Thus, chiral Brønsted acid may be able to give asymmetric induction for diazetidinium intermediate in propagation step of this formal [1,3]-rearrangement reaction, and give enantiomeric enriched homoallylic amine product after hydrolysis. Among a variety of chiral Brønsted acids developed to date, 3,3'-substituted BINOL-derived phosphoric acids⁴⁻⁶ were selected as chiral Brønsted acid catalyst because phosphoric acid moiety has been known as a donor and acceptor for hydrogen bonding interaction, and chiral phosphoric acids have recently become one of the most useful catalysts in catalytic asymmetric synthesis. Furthermore, recent theoretical study demonstrated that the substituents at the 3 and 3'-positions are able to create sophisticated asymmetric reaction space to realize high enantioselectivities.⁷⁻¹¹

5.3.1 Substituent effect at the 3,3'-position of chiral phosphoric acid

For initial studies, the (*R*)-BINOL-derived phosphoric acids with different substituents at the 3,3'-position: pentafluorophenyl **B-1**, 2,4,6-triisopropylphenyl **B-2**, and anthryl **B-3** were explored (Table 2). As mentioned earlier in section 5.2, MeCN and ClCH₂CH₂Cl solvents were applicable, thus, these solvents were selected in this study. The reactions were conducted at 50 °C under 30 mol% catalyst loading. It was found that (*R*)-BINOL-phosphoric acid **B-1** gave desired product **2a** in good yields but was not able to give enantioselectivity (Table 2, entries 1 and 2). The (*R*)-BINOL-phosphoric acid **B-2** with 2,4,6-triisopropylphenyl at the 3,3'-positions showed low yields, but slightly higher enantioselectivity than that by **B-1** (Table 2, entries 3 and 4). Consequently, (*R*)-BINOL-phosphoric acid **B-3** having anthryl at the 3,3'-positions was tested, and it was found that the highest enantioselectivity was obtained in ClCH₂CH₂Cl solvent (21% ee, Table 2, entry 6).

Table 2. Substituent effect of chiral phosphoric acid



Entry	Solvent	(<i>R</i>)-BINOL-phosphoric acid	Yield (%) ^a	ee (%) ^b
1	MeCN	B-1	77	2
2	ClCH ₂ CH ₂ Cl	B-1	75	7
3	MeCN	B-2	51	5
4	ClCH ₂ CH ₂ Cl	B-2	21	13
5	MeCN	B-3	65	11
6	ClCH ₂ CH ₂ Cl	B-3	72	21

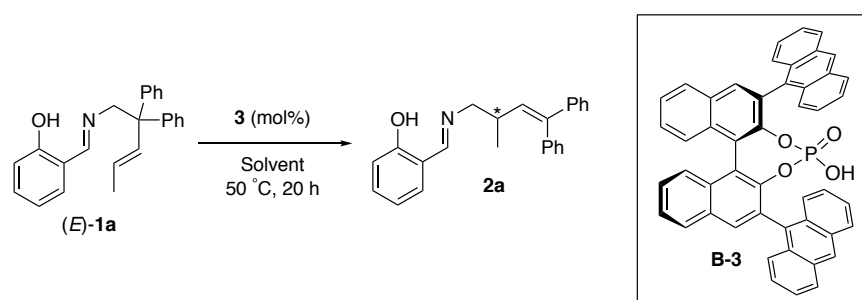
^aDetermined by ¹H NMR using dibromomethane as an internal standard.

^bEnantiomeric excess was determined by chiral HPLC after derivatization of **2a**.

5.3.2 Reaction optimization in the presence of chiral phosphoric acid

Since (*R*)-3,3'-anthryl-BINOL-phosphoric acid **B-3** gave the highest enantioselectivity, the optimized reaction condition of the formal [1,3]-rearrangement reaction was carried out in the presence of **B-3**. Before exploration of solvents, catalyst loading of **B-3** was reduced to 20 mol% at 50 °C and 40 °C. It was found that although yields significantly dropped at 40 °C and 50 °C, 20 mol% of catalyst loading of **B-3** did not affect the enantioselectivity of the product (Table 3, entries 1-3). Thus, the studies of solvents were carried out at 50 °C under 20 mol% catalyst loading. In screening solvents, chloroform (CHCl₃), chlorobenzene, tetrahydrofuran (THF), ethyl acetate (EtOAc), and toluene were used. Among these solvents, toluene gave superior results in the term of enantiomeric excess (52% ee) (Table 3, entry 8). Although the enantioselectivity was the highest at 50 °C in toluene solvent, the chemical yield was only 24%. Therefore, the reaction was conducted at 80 °C to improve chemical yield. As a result, although chemical yield was improved to 76%, enantioselectivity dropped to 41% ee, (Table 3, entry 9).

Table 3. Reaction optimization in the presence of (*R*)-BINOL-derived phosphoric acid **B-3**



Entry	Solvent	Temp (°C)	Phosphoric acid B-3 (mol%)	Yield (%) ^a	ee (%) ^b
1	ClCH ₂ CH ₂ Cl	50	30	72	21
2	ClCH ₂ CH ₂ Cl	50	20	47	21
3	ClCH ₂ CH ₂ Cl	40	20	29	20
4	CHCl ₃	50	20	46	25
5	Chlorobenzene	50	20	23	23
6	THF	50	20	51	16
7	EtOAc	50	20	13	25
8	Toluene	50	20	24	52
9	Toluene	80	20	76	41

^aDetermined by ¹H NMR using dibromomethane as an internal standard.

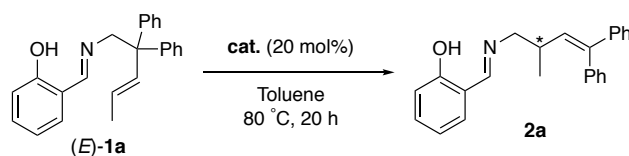
^bEnantiomeric excess was determined by chiral HPLC after derivatization of **2a**.

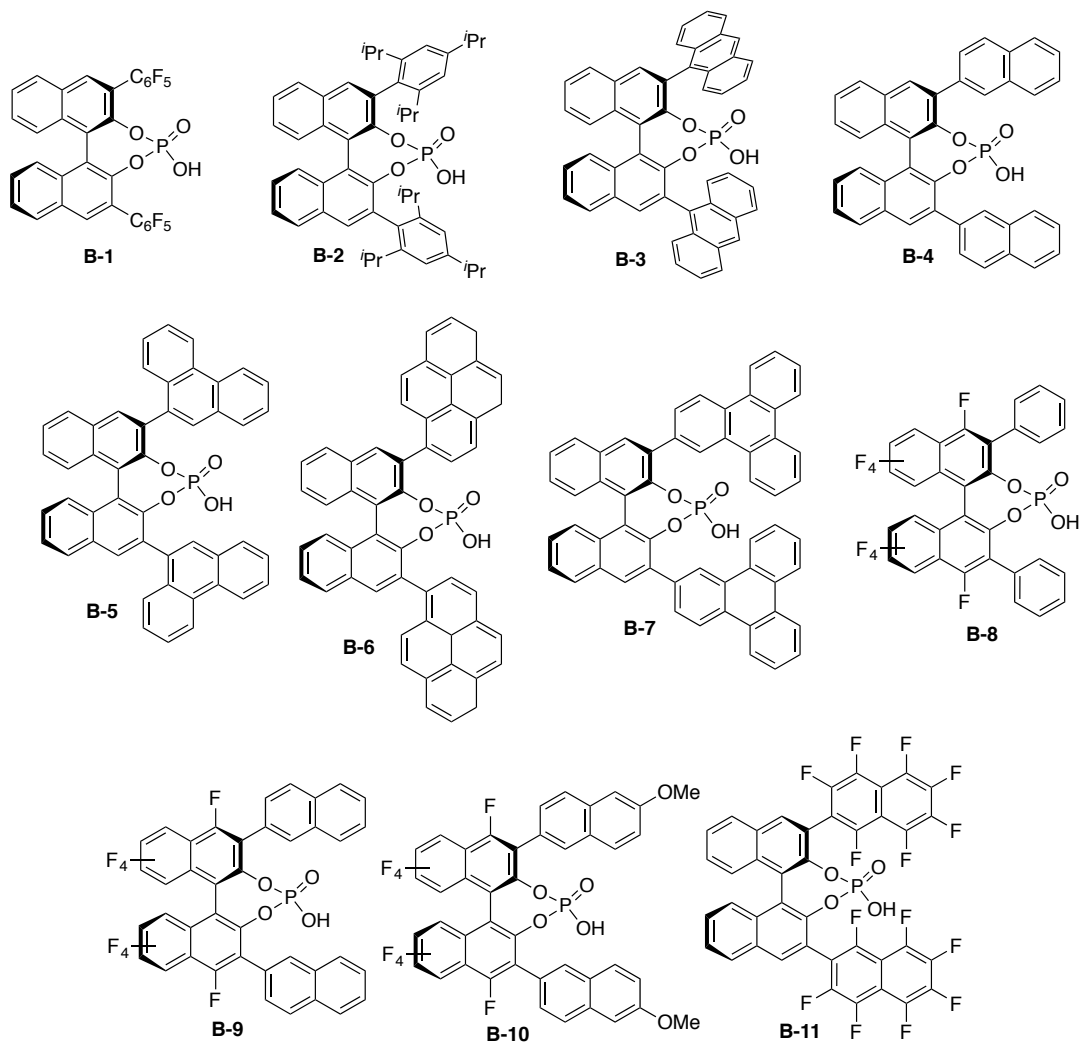
5.3.3 Screening of (*R*)-BINOL-derived phosphoric acids

It has been known that the substituents at the 3,3'-positions would be important to create suitable reaction space and increase enantioselectivity. Based on the initial studies in the section of 5.3.1 and 5.3.2, the reaction was conducted at 80 °C in toluene to optimize substituents of chiral phosphoric acid catalysts (Table 4).

The chiral phosphoric acids **B-1**, **B-2**, and **B-3** were examined again under the new reaction condition to compare with the results in Table 2. It was revealed that higher yields and enantioselectivities were obtained than those in Table 2 (Table 2 vs. Table 4, entries 1-3). Among chiral phosphoric acids **B-1**, **B-2**, and **B-3**, anthryl-substituted **B-3** was still the best enantioselectivity. Therefore, other π -conjugated substituents such as 2-naphthyl, phenanthryl, pyrenyl, and 2-triphenylenyl groups were next introduced at the 3,3'-position of the chiral phosphoric acid and examined in the reaction. It was found that the chiral phosphoric acids **B-4** to **B-7** with 2-naphthyl, phenanthryl, pyrenyl, and 2-triphenylenyl groups yielded the formal [1,3]-rearrangement product **2a** in similar yields with those by chiral phosphoric acids **B-1**, **B-2**, and **B-3** (Table 4, entries, 4-7). Importantly, the phosphoric acid **B-5** with phenanthryl group gave the highest enantioselectivity (Table 4, entry 5). Furthermore, (*R*)-F₁₀BINOL phosphoric acids **B-8** to **B-10** and perfluorinated naphthalene-introduced **B-11** were attempted to evaluate the effect of acidity of the chiral phosphoric acids. Excellent yields were obtained in all cases of **B-8** to **B-11**, unfortunately enantioselectivities were less than 10 % (Table 4, entries 8-11).

Table 4. Electronic effect of BINOL Brønsted acids





Entry	Catalyst	Yield (%) ^a	ee (%) ^b
1	B-1	95	9
2	B-2	76	33
3	B-3	81	39
4	B-4	73	20
5	B-5	90	65-74 ^c (70) ^d
6	B-6	93	39
7	B-7	85	11
8	B-8	95	9
9	B-9	91	2
10	B-10	90	4
11	B-11	93	<1

^aDetermined by ¹H NMR using dibromomethane as an internal standard.

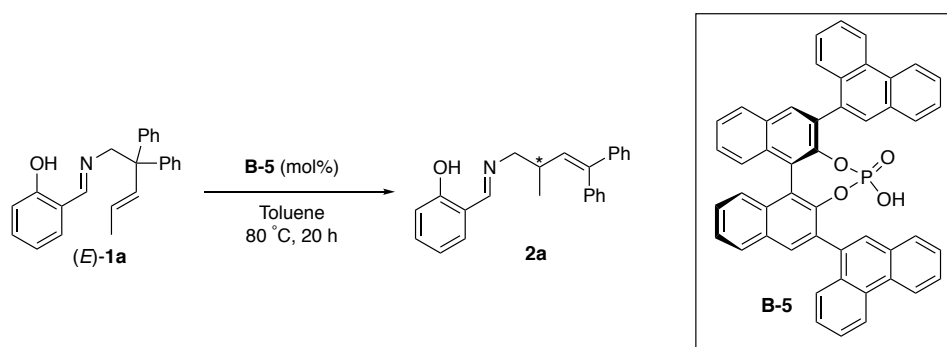
^bEnantiomeric excess was examined by chiral HPLC after derivatization of **2a**.

^cRanges of enantioselectivities. ^dAverage of enantioselectivities.

5.3.4 Catalyst loading of (*R*)-BINOL phosphoric acid

To further optimize the reaction conditions, the catalyst loading amount was studied by use of chiral phosphoric acid **B-5** (Table 5). The results showed that the enantioselectivities were significantly decreased when 5 mol% of **B-5** was used. These results indicated that once 2-azaallenium was generated, propagation step would smoothly proceed, therefore both enantioselective and racemic reaction pathway of propagation steps competed to give the products.

Table 5. Catalyst loading studies



Entry	Phosphoric acid B-5 (mol%)	Yield (%) ^a	ee (%) ^b
1	20	90	65-74 ^c (70) ^d
2	15	75	69
3	10	71	65
4	5	60	46

^aDetermined by ¹H NMR using dibromomethane as an internal standard.

^bEnantiomeric excess was examined by chiral HPLC after derivatization of **2a**.

^cRanges of enantioselectivities. ^dAverage of enantioselectivities.

5.4 Mechanistic consideration in interaction mode

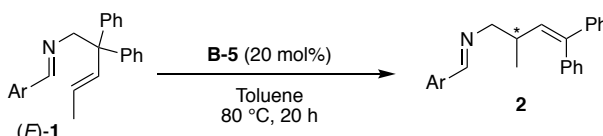
According to the results of enantioselectivities in catalytic asymmetric formal [1,3]-rearrangement reaction, the interaction among chiral phosphoric acid catalyst, 2-azaallenium cation, and ene-alimine (*E*)-**1** was very important point to propose the transition state. Therefore, substituents on benzyldiene unit further studied, and absolute configuration of the

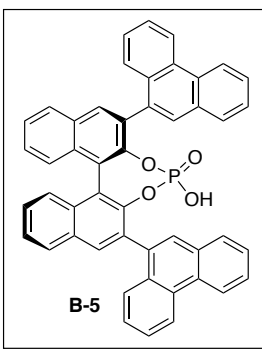
product was determined. Finally, transition state of the [3,3]-rearrangement stage in propagation step would be proposed.

5.4.1 Substituents effect of benzylidene unit

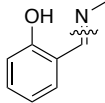
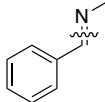
The hydroxy group of benzylidene unit was expected to be important as hydrogen bonding donor to phosphoryl oxygen of chiral phosphoric acid catalyst. Therefore, benzaldehyde derived-ene-aldimine (**1b**) was initially evaluated. As expected, enantioselectivity in the reaction of **1b** significantly dropped (Table 6, entry 1 vs. 2). Based on this result, salicylaldehyde derived ene-aldimine (*E*)-**1c** to (*E*)-**1f** were further examined to study on electronic and steric effects of benzylidene unit (Table 6, entries 3-5). These substrates (*E*)-**1a** to (*E*)-**1e** yielded formal [1,3]-rearrangement products in high yields while (*E*)-**1f** only gave desired product in moderate yield. Importantly, the results of these enantioselectivities suggested that hydroxy group is effective as a directing group to yield enantiomeric enriched products (Table 6, entries 1 and 2). The substituent at the 5-position on benzylidene unit gave no affect to enantioselectivity (Table 6, entry 3). In contrast, enantioselectivities were gradually decreased by increasing steric bulkiness of substituent on 4-position of benzylidene moiety (Table 7, entries 4-6).

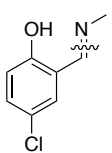
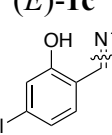
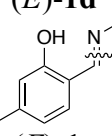
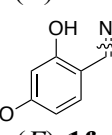
Table 6. Electronic and steric effects on benzylidene unit





B-5

Entry	Ar	Yield (%) ^a	ee (%) ^b
1	 (E)-1a	77	65 ^c
2	 (E)-1b	79	26

3	 (E)-1c	80	65
4	 (E)-1d	81	49
5	 (E)-1e	77	45
6	 (E)-1f	49	30

^aDetermined by ¹H NMR using dibromomethane as an internal standard.

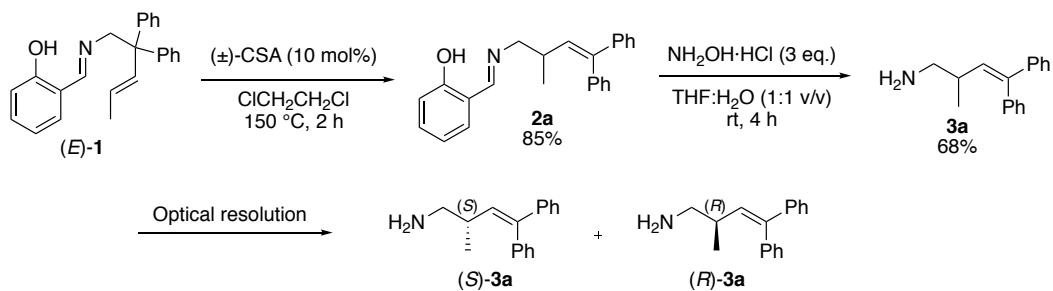
^bEnantiomeric excess was examined by chiral HPLC after derivatization of **2a**.

^cEnantioselectivity given by **B-5** which was used in entries 2-6.

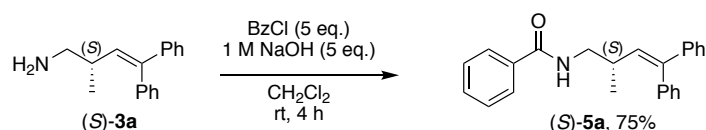
5.4.2 Absolute configuration of the ene-aldimine product

The absolute configuration of the product was important to propose the transition state in the stage of [3,3]-rearrangement. X-ray diffraction analysis of optically pure products **2a** derivative was used.

To get the optically pure product **2a**, formal [1,3]-rearrangement reaction of (*E*)-**1** substrate was conducted in the presence of (±)-CSA, and then the obtained rearrangement product **2a** was subjected to hydrolysis conditions to provide free amine **3a** (top of Scheme 3). In the optical resolution step, semi-preparative HPLC was used to separate each enantiomer (*S*)-**3a** and (*R*)-**3a** (bottom of Scheme 3, CHIRALCEL OD-H (10 mm φ × 250 mm L), 98/2 hexane/*i*-PrOH, 5 mL/min, 254 nm, 40 °C, *t_r* = 11.1 min and 13.4 min). Optically pure amides (*S*)-**5a** was synthesized from the treatment of optically pure (*S*)-**3a** with benzoyl chloride and 1M NaOH (Scheme 4). The enantioselectivity of obtained amide derivative (*S*)-**5a** was determined by analytical HPLC with a CHIRALCEL OD-3 (95/5 hexane/*i*-PrOH, 1.0 mL/min, 254 nm, 40 °C, the major *t_r* = 19.7 min and minor *t_r* = 16.7 min). It was confirmed that optical purity of (*S*)-**5a** was 99%.

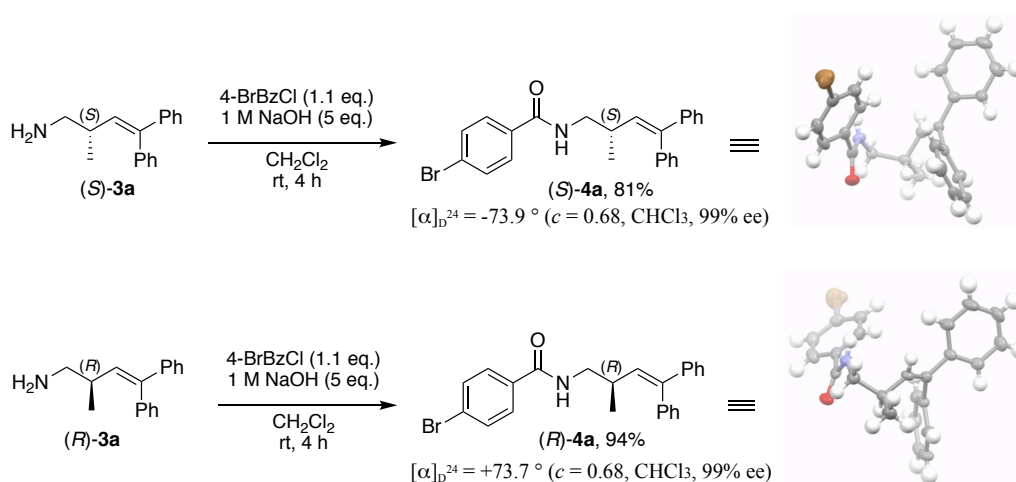


Scheme 3. Hydrolysis and optical resolution of rearrangement product **2a**



Scheme 4. Protection of **(S)-3a** for determination of retention time

Finally, the absolute configuration of **2a** was determined by the use of 4-bromobenzoyl derivatives **4a**. Thus, the optically pure amides **(S)-4a** and **(R)-4a** were synthesized from the treatment of optically pure **(S)-3a** and **(R)-3a** with 4-bromobenzoyl chloride and 1M NaOH (Scheme 5). The obtained amide derivatives **(S)-4a** and **(R)-4a** were recrystallized under dichloromethane (CH_2Cl_2) as inner solvent and hexane as outer solvent. X-ray diffraction analysis clearly showed that **(S)-4a** is **(S)**-configuration (first peak in HPLC), on the other hand, **(R)-4a** is **(R)**-configuration (second peak in HPLC) (Scheme 5). On the basis of the results by X-ray diffraction and HPLC analyses, **(R)-B-5** gave **(S)-2a** as major product.



Scheme 5. Protection of **(S)-** and **(R)-3a** and determination of absolute configurations

5.4.3 Proposed transition state

As shown in Figure 1, the enantioselectivity of the product would be determined in the stage of [3,3]-azonia rearrangement step in formal [1,3]-rearrangement.¹² On the basis of results in Table 6, it was suggested that the hydroxy group of benzylidene unit is important to give enantioselectivities. Therefore, hydrogen bonding interaction between counteranion of the chiral Brønsted acid and intermediate was considered.

Two possibilities were proposed, i) the counteranion of **B-5** would give enantioselective intermediate **N*4** via hydrogen bonding between OH groups of substrate and phosphoryl oxygen of **B-5**, then chirality of **N*4** would be transferred to yield (*S*)-**N*5** in the stage of [3,3]-azonia rearrangement step, ii) the counteranion of **B-5** would determine enantioselectivity of (*R*)-**N*5** directly via hydrogen bonding between OH groups of substrate and phosphoryl oxygen of **B-5** regardless of the enantioselectivity for the intermediate **N*4**.

Experimental results could not exclude either these two possibilities; therefore, one of possibilities for hydrogen bonding interaction was proposed in the transition state for the stage of [3,3]-azonia rearrangement step (Figure 2). According to the absolute configuration of the product, chiral counteranion of **B-5** would exist the side of *Re* face and allylic carbon attack to iminium carbon from the side of *Si* face (Figure 2 a)) because of steric hindrance between diphenyl group of intermediate **N*4** and anthryl groups of **B-5** (Figure 2 b)). As a result, (*S*)-**N*5** would be yielded to give (*S*)-**2a**.

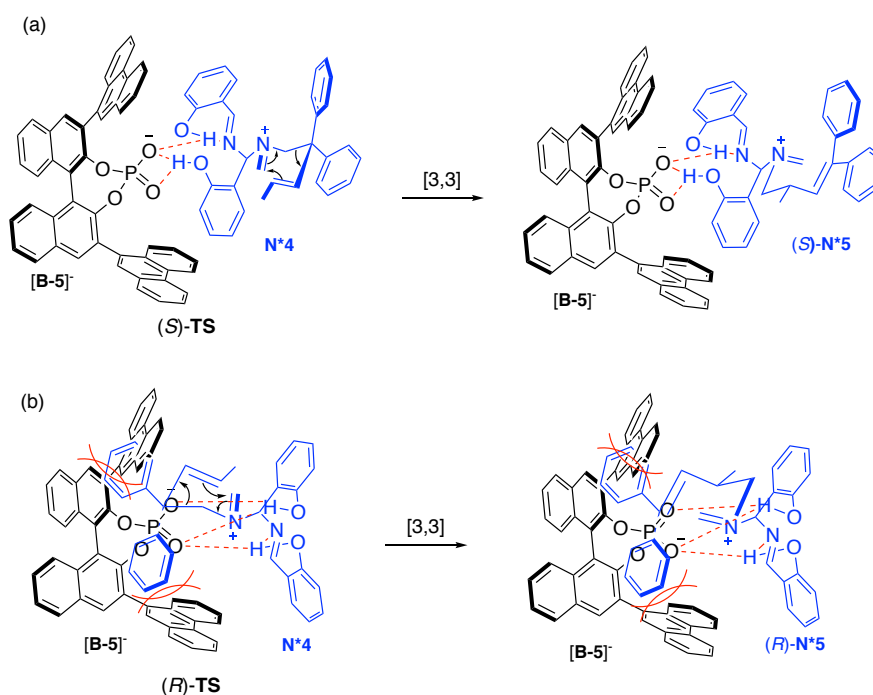


Figure 2. Proposed interaction in transition state for (a) (*S*)-product and (b) (*R*)-product

As mentioned in Table 6 (entries 4-6), the enantioselectivities were affected by the size of substituent at the 4-position, but not affected by the substituent at the 5-position; therefore (*S*)-**TS4** and (*S*)-**TS5** were proposed (Figure 3). Substituents at 4-position of the substrate interfered with phenanthryl groups at the 3,3'-position of **B-5**; hydrogen bonding interactions between counteranion of **B-5** and **N*4** would lead to poor in the transition state (Figure 3, (*S*)-**TS4**); in contrast, the substituent at the 5-position of the substrate was far away from phenanthryl group and not affected to hydrogen bonding networks (Figure 3, (*S*)-**TS5**).

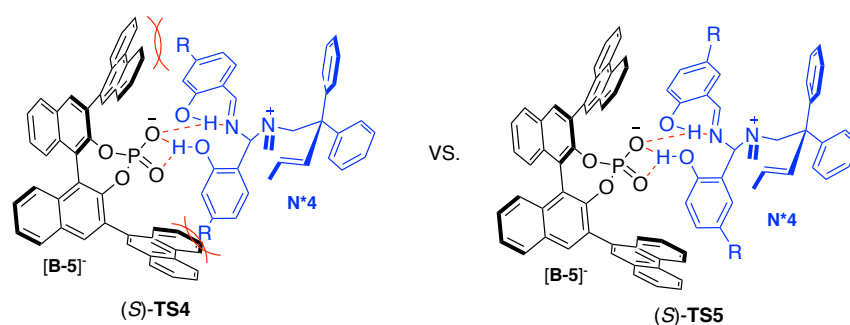


Figure 3. Proposed transition state of substituent at the 4- and 5-position on benzylidene unit

5.5 Conclusion

Catalytic asymmetric reaction for formal [1,3]-rearrangement reaction was studied. (*R*)-BINOL-derived phosphoric acid with phenanthryl group at the 3 and 3'-position gave the highest enantioselectivities in toluene as solvent. The hydrogen bonding between counteranion of the chiral phosphoric acid and hydroxy group of the substrate plays an important role to get high enantioselectivities.

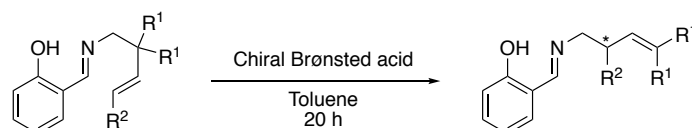
5.6 Experimental section

5.6.1 General method

All reactions were carried out under an atmosphere of standard grade nitrogen gas (oxygen <10 ppm) in flame-dried glassware with magnetic stirring. Toluene and tetrahydrofuran were used as anhydrous in solvent line system from KANTO. 1,2-dichloroethane was purchased from commercial supplier as anhydrous solvents. 2-hydroxybenzaldehyde was distilled before use. Other reagents were purchased from commercial suppliers and used without further purification. Purification of reaction products was carried out by flash column chromatography on silica gel 60 (spherical, neutral, 100-210 μm ; Merck). Analytical thin layer chromatography (TLC) was performed on E. Merck precoated (0.25 mm) silica gel 60-F254 plates. Visualization was accomplished with UV

light and phosphomolybdic acid solution in ethanol by heating. ^1H NMR spectra were recorded on a JEOL ECA-400 (400 MHz) spectrometer at ambient temperature. CDCl_3 NMR solvents were purchased from CIL, and it was dried over activated MS 4Å before used. Data are reported as follows: chemical shifts are reported in ppm from tetramethylsilane on the δ scale, with solvent resonance employed as internal standard (CDCl_3 7.26 ppm, DMSO-d_6 2.49 ppm), multiplicity (b = broad, s = singlet, d = doublet, dd = doublet of doublet, t = triplet, q = quartet, and m = multiplet), integration, coupling constant (Hz) and assignment. ^{13}C NMR spectra were recorded on a JEOL ECA-400 (100 MHz) spectrometer at ambient temperature. Chemical shifts are reported in ppm from tetramethylsilane on the δ scale, with solvent resonance employed as internal standard (CDCl_3 77.0 ppm).

5.6.2 Procedure for catalytic asymmetric rearrangement reaction of ene-aldimines

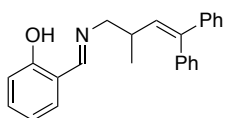


Scheme 6. Reaction of catalytic asymmetric formal [1,3]-rearrangement of ene-aldimine

To a chiral Brønsted acid (5-30 mol%) was added the solution of ene-aldimine in toluene (0.1 M) at room temperature. Then, the reaction was stirred at an indicated temperature for an indicated time. After cooled to room temperature, the reaction was quenched by NEt_3 . After stirred at room temperature for 15 min, the resulting mixture was extracted with CH_2Cl_2 (5 mL x 3). The organic layer was washed with brine (10 mL x 3), and aqueous layer was extracted with CH_2Cl_2 (20 mL x 3). The combined organic extracts were dried over Na_2SO_4 and concentrated under pressure after filtration to give the ene-aldimine as product.

5.6.3 Characterization of rearrangement products

Because of stability of rearrangement products, the characterization data are only provided by ^1H NMR.

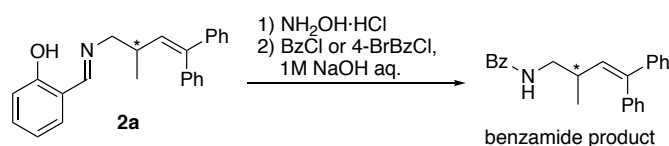


(*E*)-2-(((2-methyl-4,4-diphenylbut-3-en-1-yl)imino)methyl)phenol

TLC R_f = 0.18 (10:1 hexane:ethyl acetate).

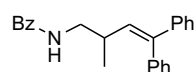
^1H NMR (CDCl_3 , 400 MHz) δ 8.26 (s, 1H, N=CH), 7.30-7.10 (m, 12H, Ar-H), 6.97-6.93 (m, 1H, Ar-H), 6.88-6.84 (m, 1H, Ar-H), 5.93 (d, 1H, $J = 10.3$ Hz, CH=C), 3.57-3.54 (m, 2H, N-CH₂), 2.76-2.67 (m, 1H, N-CH₂-CH), 1.12 (d, 3H, $J = 6.9$ Hz, CH₃).

5.6.4 Procedure and characterization of derivatives



Scheme 7. Derivatization of formal [1,3]-rearrangement product

Due to the stability of ene-aldimine rearrangement products, the characterization data are provided by ^1H NMR, ^{13}C NMR, and HRMS of derived benzamides. The rearrangement products were subjected into hydrolysis condition by the use of hydroxylamine hydrochloride ($\text{NH}_2\text{OH}\cdot\text{HCl}$) to cleave salicylaldehyde to afford amine products. And then, the amine products were protected by benzoyl chloride or 4-bromobenzoyl chloride in the basic condition providing benzamide or 4-bromo benzamine products (Scheme 7). The characterization data are shown below.



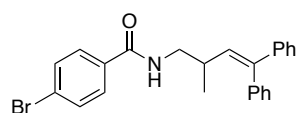
***N*-(2-methyl-4,4-diphenylbut-3-en-1-yl)benzamide**

TLC $R_f = 0.22$ (4:1 hexane:ethyl acetate).

^1H NMR (CDCl_3 , 400 MHz) δ 8.18-8.11 (m, 1H, Ar-H), 7.67-7.66 (m, 2H, Ar-H), 7.49-7.45 (m, 2H, Ar-H), 7.41-7.30 (m, 4H, Ar-H), 7.26-7.20 (m, 4H, Ar-H), 7.11-7.08 (m, 2H, Ar-H), 6.02 (br, 1H, NH), 5.92 (d, 1H, $J = 10.3$ Hz, CH=C), 3.51-3.45 (m, 1H, N-CH₂), 3.38-3.31 (m, 1H, N-CH₂), 2.72-2.60 (m, 1H, N-CH₂-CH), 1.14 (d, 3H, $J = 6.9$ Hz, CH₃).

^{13}C NMR (CDCl_3 , 150 MHz) δ 167.5, 143.0, 139.9, 133.6, 132.4, 131.3, 130.1, 129.6, 128.5, 128.4, 128.2, 127.3, 127.2, 126.8, 77.3, 77.0, 76.7, 45.8, 34.6, 18.7.

HRMS (ESI) Exact Mass Calcd. for $\text{C}_{24}\text{H}_{23}\text{NO}$ ($[\text{M}+\text{Na}]^+$): 364.1672. Found: 364.1672.



4-bromo-*N*-(2-methyl-4,4-diphenylbut-3-en-1-yl)benzamide.

TLC $R_f = 0.21$ (3:1 hexane:ethyl acetate).

^1H NMR (CDCl_3 , 400 MHz) δ 7.52 (s, 4H, Ar-*H*), 7.36-7.30 (m, 3H, Ar-*H*), 7.19-7.28 (m, 5H, Ar-*H*), 7.09-7.05 (m, 2H, Ar-*H*), 5.97 (s, 1H, NH), 5.89 (d, 1H, $J = 10.5$ Hz, CH=C), 3.44 (dt, 1H, $J = 13.2, 5.7$ Hz, N- CH_2), 3.36-3.29 (m, 1H, N- CH_2), 2.71-2.60 (m, 1H, N- CH_2 -CH), 1.13 (d, 3H, $J = 6.6$ Hz, - CH_3).

^{13}C NMR (CDCl_3 , 150 MHz) δ 166.4, 143.1, 141.9, 139.8, 133.5, 132.2, 131.7, 129.6, 128.5, 128.4, 128.2, 127.3, 127.2, 125.9, 45.8, 34.6, 18.7.

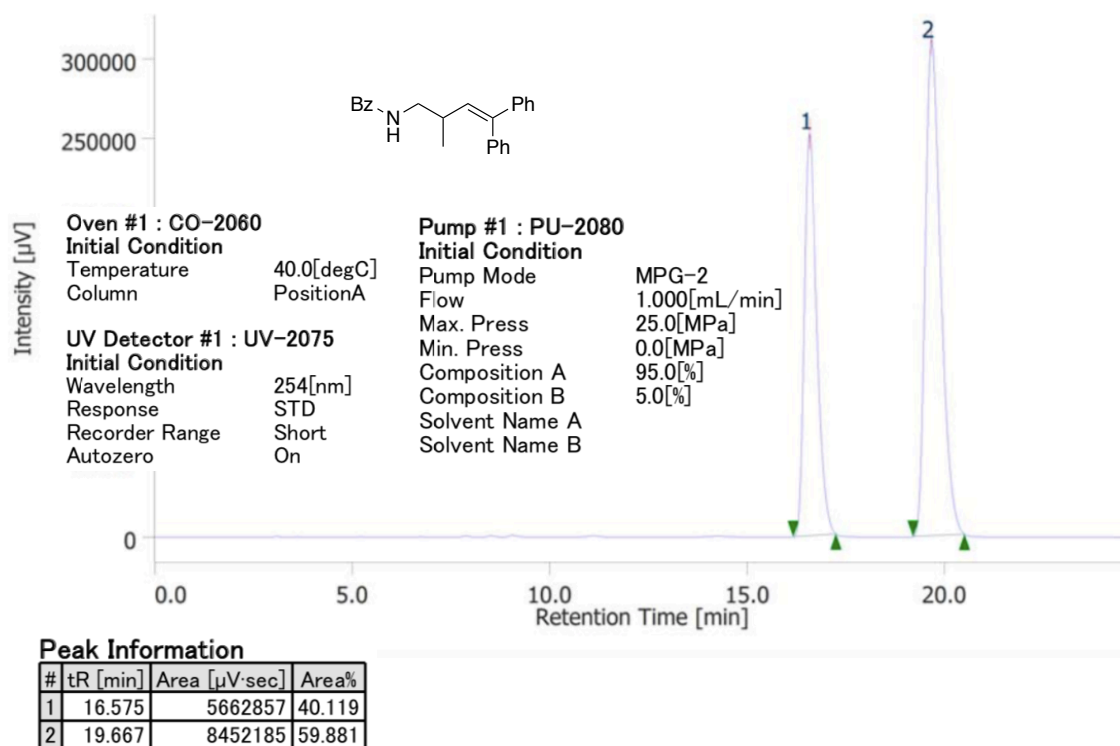


Chart 1. HPLC chart for benzamide compound. Enantiomeric excess was determined by analytical HPLC with a CHIRALCEL OD-3 (95/5 hexane/*i*-PrOH, 1.0 mL/min, 254 nm, 40 °C), the retention times $t_r = 16.6$ and 19.7 min.

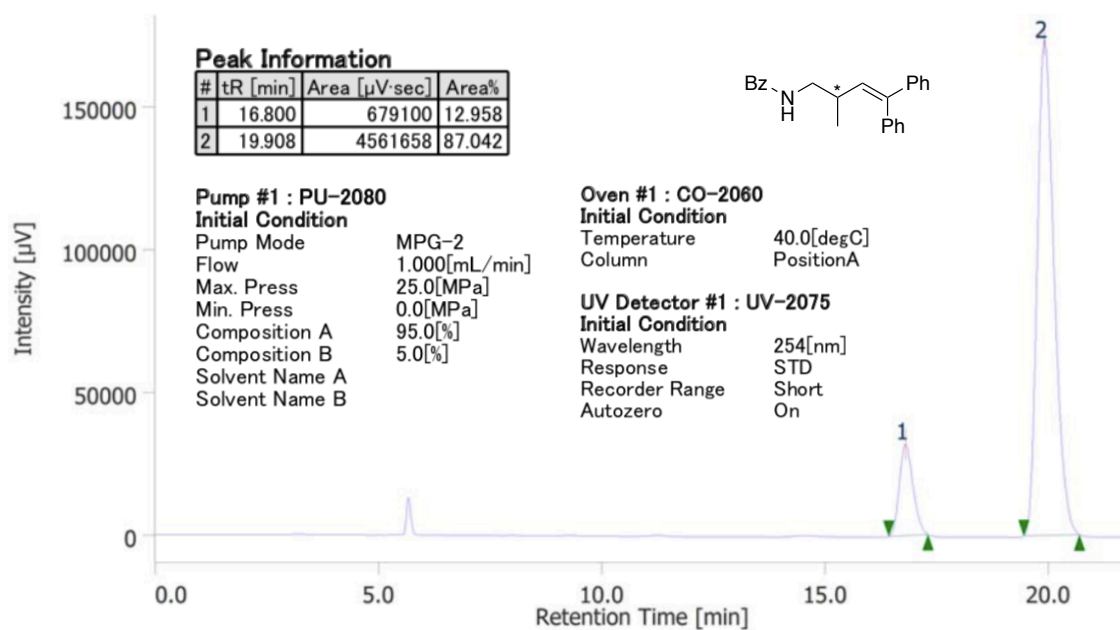


Chart 2. HPLC chart for benzamide compound. Enantiomeric excess was determined by analytical HPLC with a CHIRALCEL OD-3 (95/5 hexane/*i*-PrOH, 1.0 mL/min, 254 nm, 40 °C), major enantiomer 19.9 min, minor enantiomer $t_r = 16.8$ min.

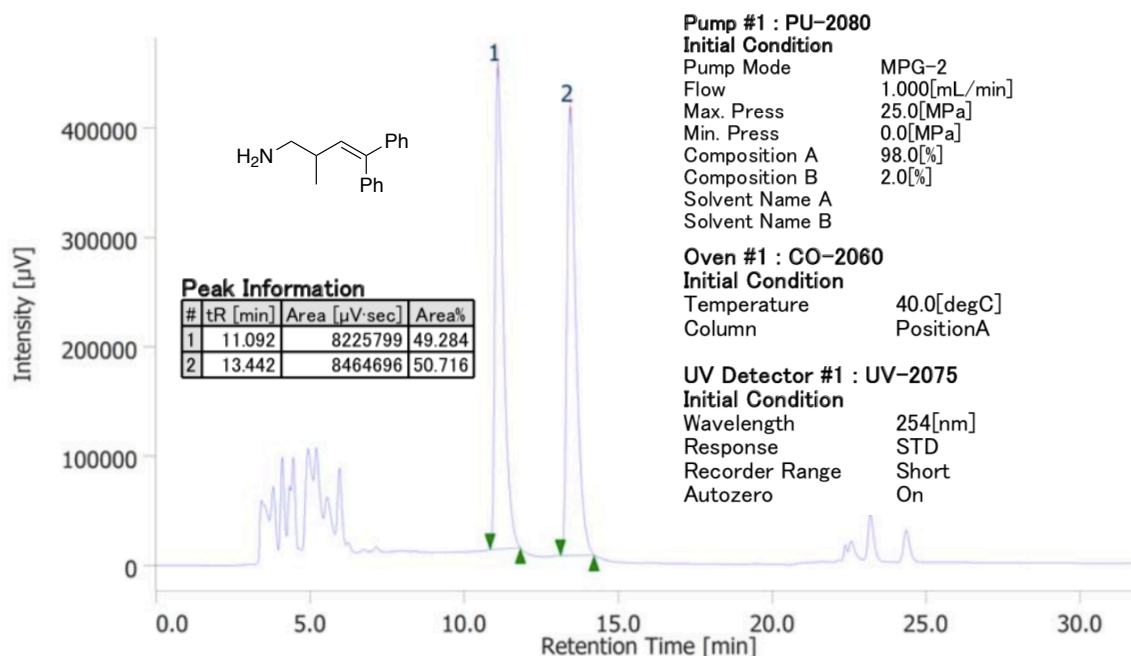


Chart 3. HPLC chart for racemic homoallylic amine compound. Enantiomeric excess was determined by analytical HPLC with a CHIRALCEL OD-3 (98/2 hexane/*i*-PrOH, 1.0 mL/min, 254 nm, 40 °C), $t_r = 11.1$ min and 13.4 min.

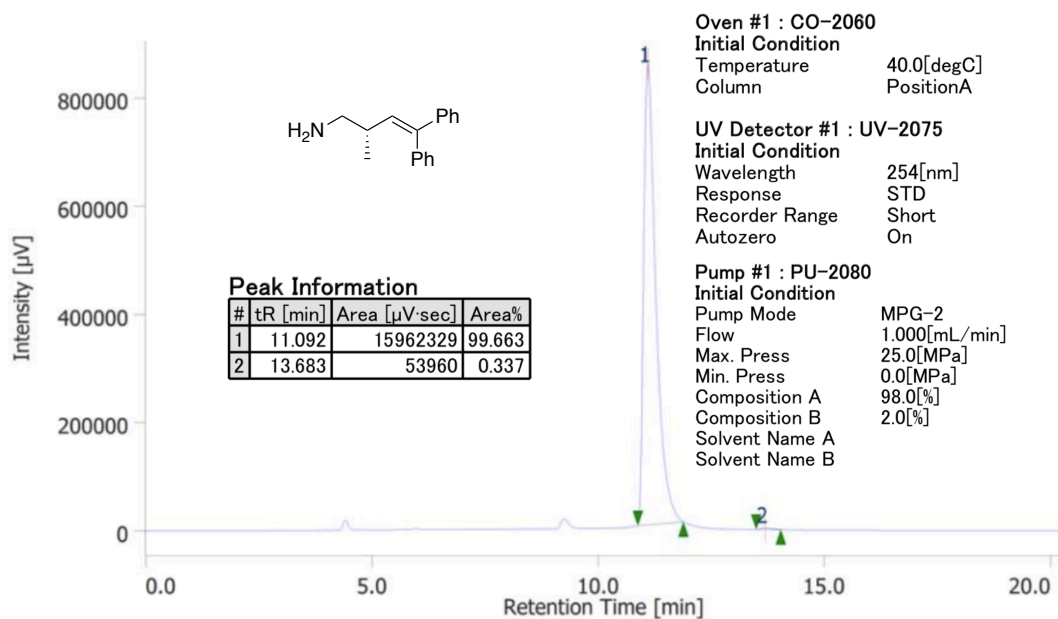


Chart 4. HPLC chart for (*S*)-homoallylic amine compound. Enantiomeric excess was determined by analytical HPLC with a CHIRALCEL OD-3 (98/2 hexane/*i*-PrOH, 1.0 mL/min, 254 nm, 40 °C), major enantiomer 11.1 min, minor enantiomer $t_r = 13.7$ min.

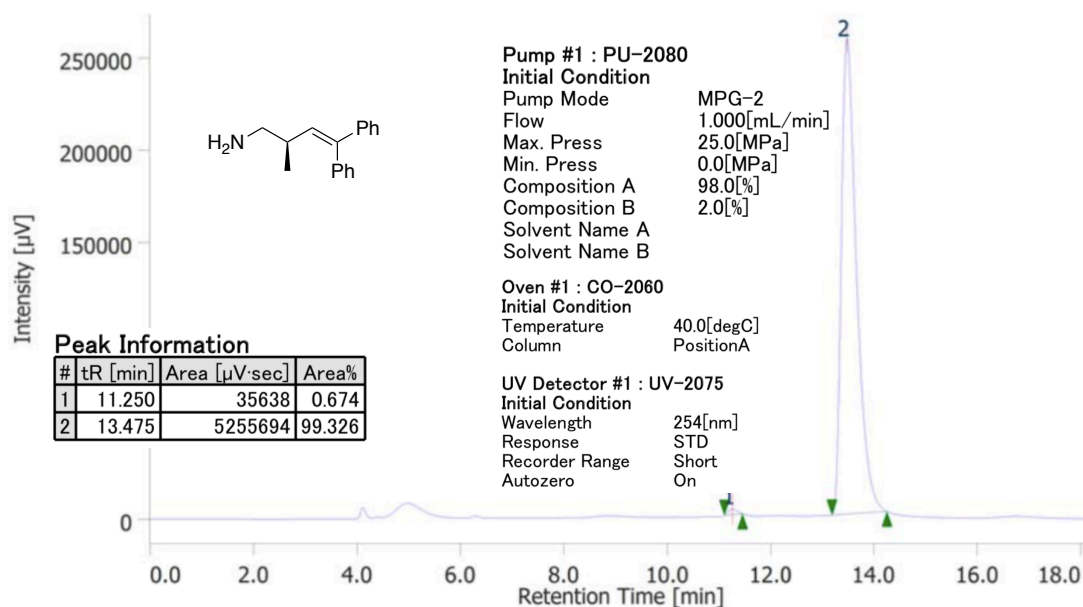


Chart 5. HPLC chart for (*R*)-homoallylic amine compound. Enantiomeric excess was determined by analytical HPLC with a CHIRALCEL OD-3 (98/2 hexane/*i*-PrOH, 1.0 mL/min, 254 nm, 40 °C), major enantiomer 13.5 min, minor enantiomer $t_r = 11.3$ min.

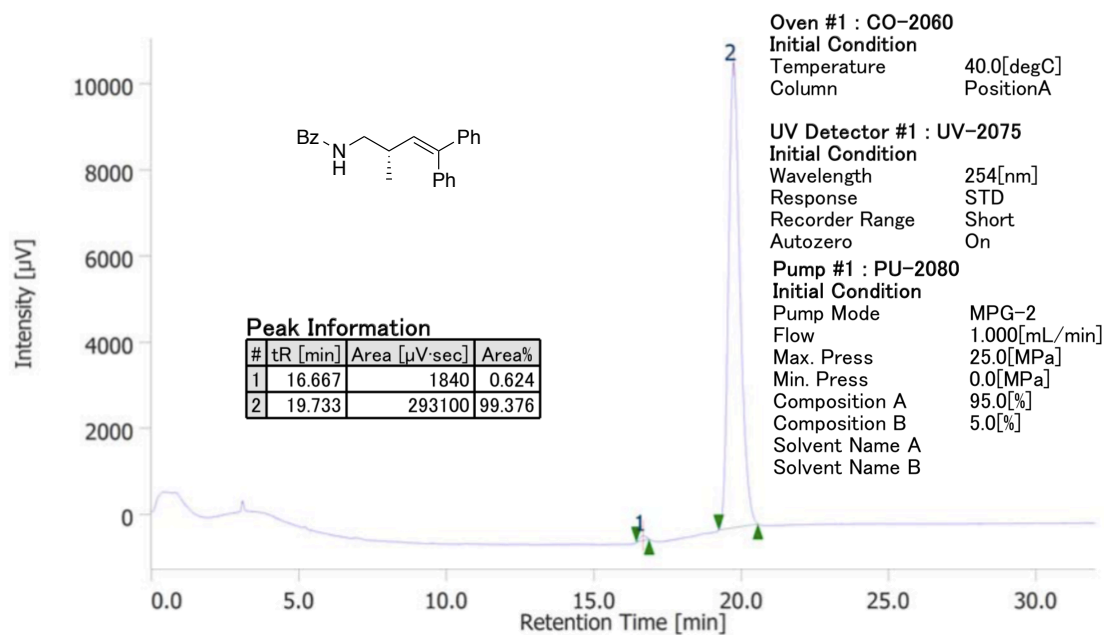


Chart 6. HPLC chart for (*S*)-benzamide compound. Enantiomeric excess was determined by analytical HPLC with a CHIRALCEL OD-3 (95/5 hexane/*i*-PrOH, 1.0 mL/min, 254 nm, 40 °C), major enantiomer 19.7 min, minor enantiomer $t_r = 16.7$ min.

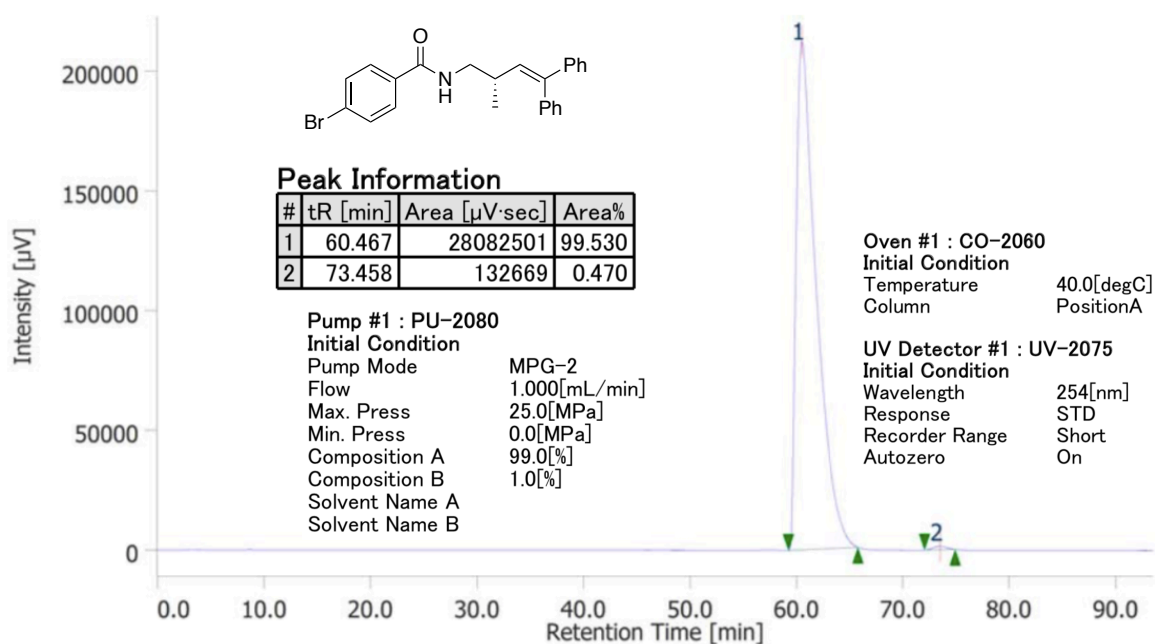


Chart 7. HPLC chart for (*S*)-4-bromo benzamide compound. Enantiomeric excess was determined by analytical HPLC with a CHIRALCEL OD-3 (99/1 hexane/*i*-PrOH, 1.0 mL/min, 254 nm, 40 °C), major enantiomer 60.5 min, minor enantiomer $t_r = 73.5$ min.

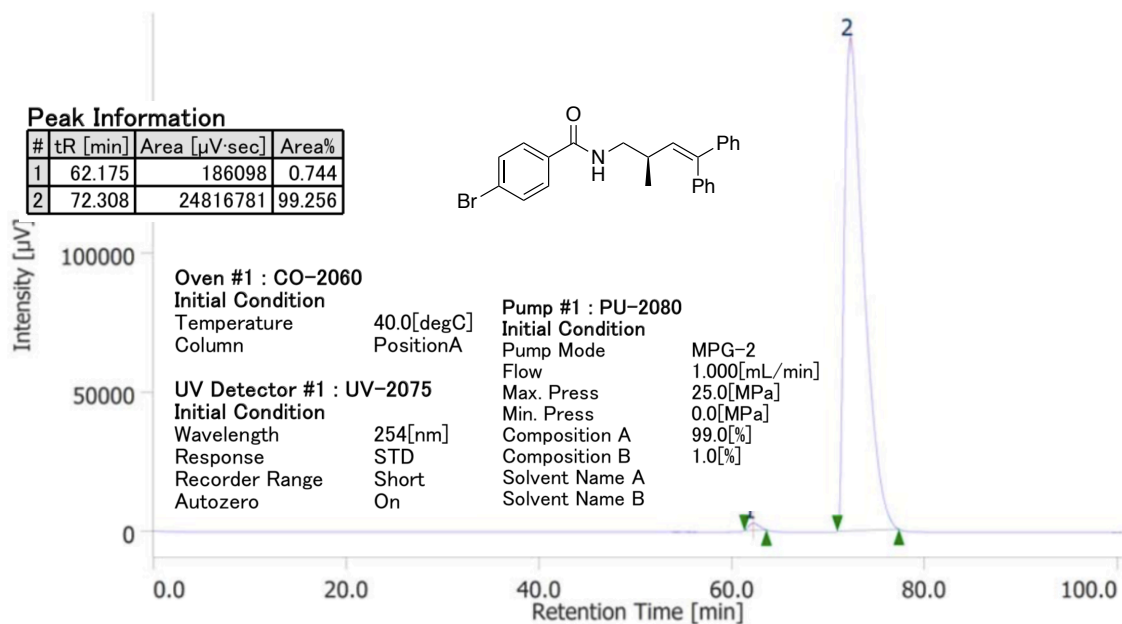


Chart 8. HPLC chart for (*R*)-4-bromo benzamide compound. Enantiomeric excess was determined by analytical HPLC with a CHIRALCEL OD-3 (99/1 hexane/*i*-PrOH, 1.0 mL/min, 254 nm, 40 °C), major enantiomer 72.3 min, minor enantiomer t_r = 62.2 min.

5.7 References

1. See, page 20, section 2.2.3.
2. See, page 14, section 2.2.1.
3. Akiyama, T.; Mori, K. *Chem. Rev.* **2015**, *115*, 9277–9306.
4. Terada, M. *Synthesis* **2010**, *2*, 1929-1982.
5. Akiyama, T. In *Asymmetric Synthesis II*, Christmann, M., Brase, S. Eds.; Wiley-VCH: Weinheim, 2012, pp 261-266.
6. Parmar, D.; Sugiono, E.; Raja, S.; Rueping, M. *Chem. Rev.* **2014**, *114*, 9047–9153.
7. Simon, L.; Goodman, J. M. *J. Am. Chem. Soc.* **2008**, *130*, 8741–8747.
8. Simon, L.; Goodman, J. M. *J. Am. Chem. Soc.* **2009**, *131*, 4070–4077.
9. Simon, L.; Goodman, J. M. *J. Org. Chem.* **2011**, *76*, 1775–1788.
10. Shibata, Y.; Yamanaka, M. *J. Org. Chem.* **2013**, *78*, 3731–3736.
11. Reid, J. P.; Goodman, J. M. *J. Am. Chem. Soc.* **2016**, *138*, 7910–7917.
12. See, page 71, section 4.4.

CHAPTER 6

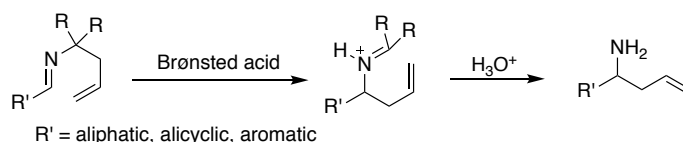
SUMMARY AND PERSPECTIVES

6.1 Summary

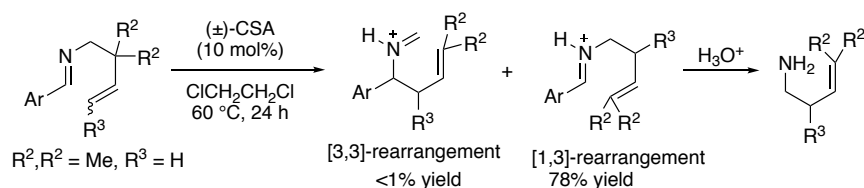
The Brønsted acid-initiated formal [1,3]-rearrangement of β -substituted ene-aldimines was developed to synthesize 2,4,4-substituted homoallylic amines. Details of experimental studies and computational insights by collaborations were summarized in this thesis.

In Chapter 1, importance and synthetic methodology of homoallylic amines, our discovery for formal [1,3]-rearrangement of ene-imines, and scope of this thesis were summarized as general introduction. In particular, design concept of β -substituted ene-aldimine substrates was demonstrated to yield linear-type homoallylic amines. Next, the initial discovery of the formal [1,3]-rearrangement was clearly summarized. Importantly, only [1,3]-rearrangement products were obtained (Scheme 1). These initial results were in contrast to previous reports by Couty; therefore, study of my thesis was focused on the development of formal [1,3]-rearrangement using β -substituted ene-aldimines and application to 2,4,4-homoallylic amine synthesis by introducing the substituent at the terminal olefin.

a) Reported rearrangement reaction of ene-imines



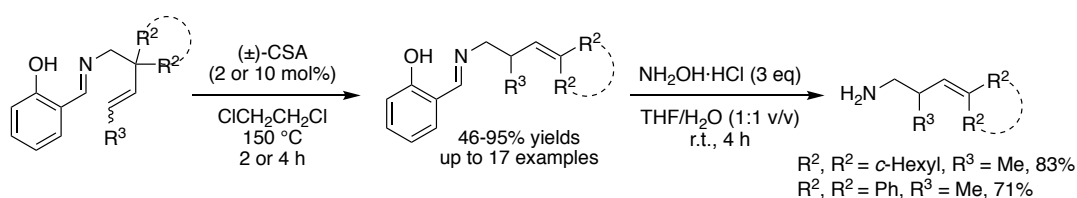
b) New design of substrate and discovery of formal [1,3]-rearrangement reaction



Scheme 1. Rearrangement reaction of ene-imines. (a) General design in previous reports; (b) our design of β -substituted ene-aldimine substrate and our discovery of formal [1,3]-rearrangement

In chapter 2, experimental results for reaction developments were summarized (Scheme 2). The investigation of electronic effects on aryl group, solvent effects, Brønsted

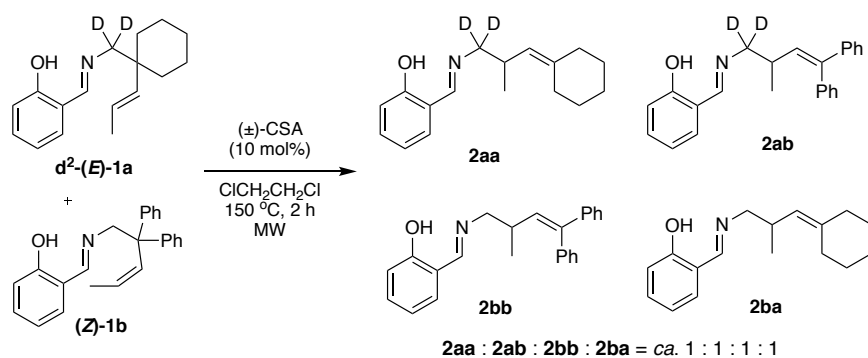
acid, and reaction temperature found that Brønsted acids, such as trifluoro acetic acid (TFA), phosphoric acid diphenyl ester, and (\pm)-10-camphorsulfonic acid (CSA) efficiently promoted the formal [1,3]-rearrangement in acetonitrile (MeCN) and 1,2-dichloroethane (DCE) as solvents under normal or microwave heating method. Importantly, the formal [1,3]-rearrangement proceeded smoothly under 1 mol% catalyst loading when microwave heating method was used. After optimizing the formal [1,3]-rearrangement reaction, a variety of substituents on ene-aldimine substrates were tolerated and gave corresponding rearrangement products in good to excellent yields. Furthermore, 2,4,4-substituted homoallylic amines were easily obtained under hydrolysis condition. And, the obtained 2,4,4-homoallylic amines were used for the synthesis of a spiro compound and a β -amino acid precursor.



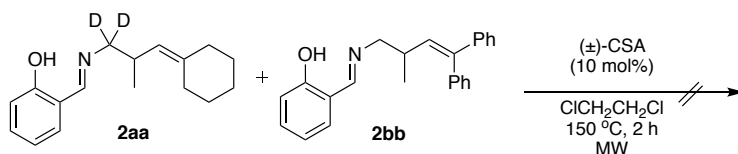
Scheme 2. Development of formal [1,3]-rearrangement of β -substituted ene-aldimines to synthesize 2,4,4-substituted homoallylic amines

In chapter 3, crossover experiments for the mechanistic studies revealed that two normal- and two crossover rearrangement products were observed in a ratio of *ca.* 1:1:1:1 (Scheme 3). When the two normal rearrangement products were subjected in the presence of (\pm)-CSA under the heating condition, the reaction did not give the crossover products. Therefore, intermolecular pathway was proposed for this formal [1,3]-rearrangement reaction. Furthermore, collaborative study for DFT calculations by Dr. Honda in HPC SYSTEMS and Dr. Suzuki in IMS suggested chain reaction mechanism of 2-azaallenium cation as a chain carrier.

a) Crossover experiment of substrates

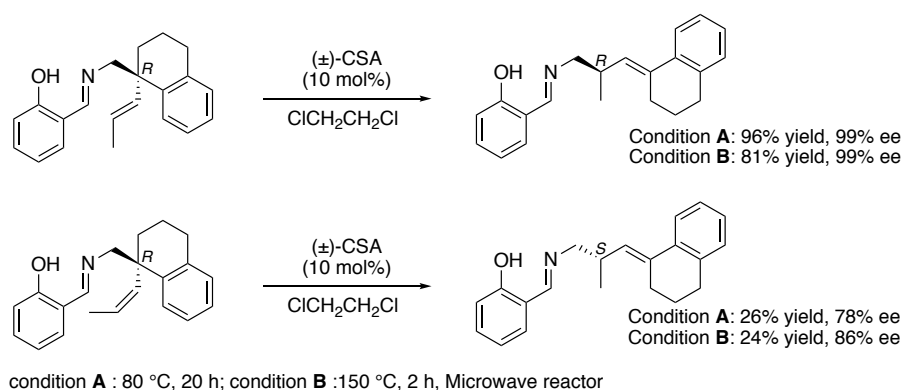


b) Crossover experiment of products



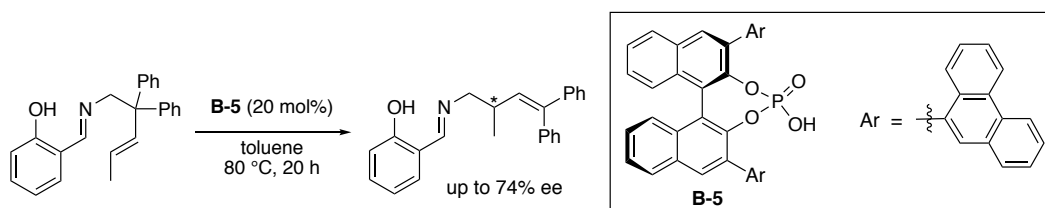
Scheme 3. Crossover experiments of (a) substrates, and (b) products

In chapter 4, asymmetric formal [1,3]-rearrangement of chiral ene-aldimine substrates was developed. On the basis of the results in chapter 2, tetrahydronaphthalene was chosen as substituent on chiral substrate, and this chiral substrate was synthesized from commercially available 1-cyano-1,2,3,4-tetrahydronaphthalene. The chirality transfer experiments clearly showed that asymmetric rearrangement of chiral substrate proceeded smoothly to give good to excellent enantioselective products in the cases of both *E*- and *Z*-olefin substrates (Scheme 4). Absolute configurations of the ene-aldimine substrates and products were determined by single crystal X-ray diffraction analysis, derivatization, and crystal sponge method. These results supported the reaction pathway that begins with C–N bond formation in the propagation step. Moreover, DFT calculation by Dr. Suzuki showed good agreement with the experimental results of stereochemistries.



Scheme 4. Asymmetric formal [1,3]-rearrangement of chiral ene-aldimines with tetrahydronaphthalene unit at the β -position

In chapter 5, the development of catalytic asymmetric formal [1,3]-rearrangement were summarized. It was found that although (+)-CSA did not give any asymmetric induction at all, chiral phosphoric acid with phenanthryl substituents at the 3,3'-position provided good enantioselectivities of the ene-aldimine products in toluene (Scheme 5).



Scheme 5. Enantioselective formal [1,3]-rearrangement of ene-aldimine promoted by chiral Brønsted acid

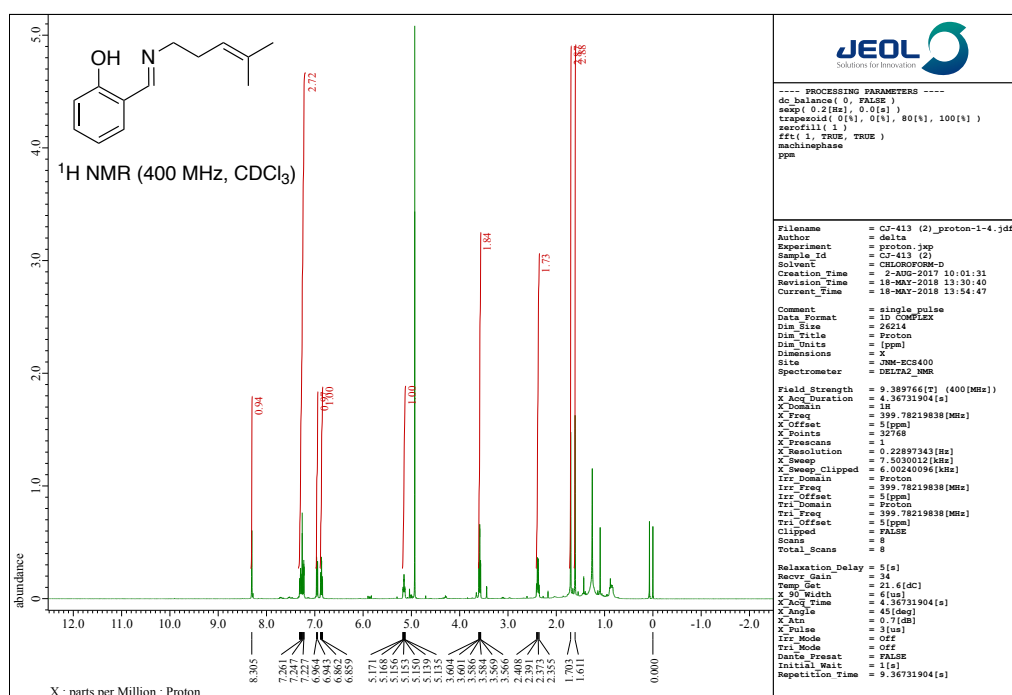
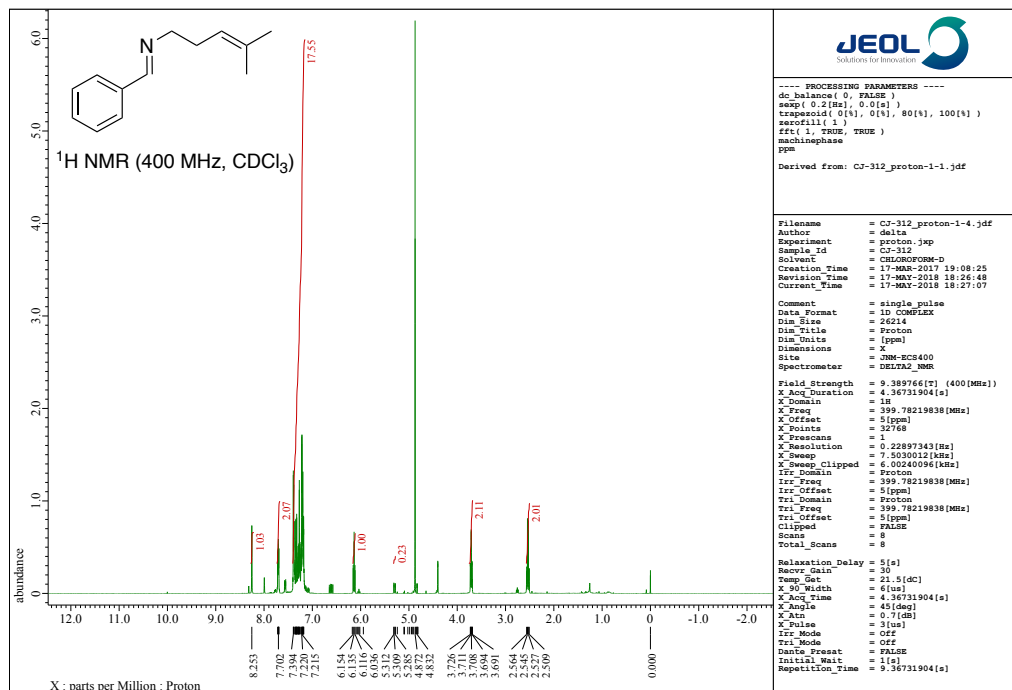
6.2 Perspectives

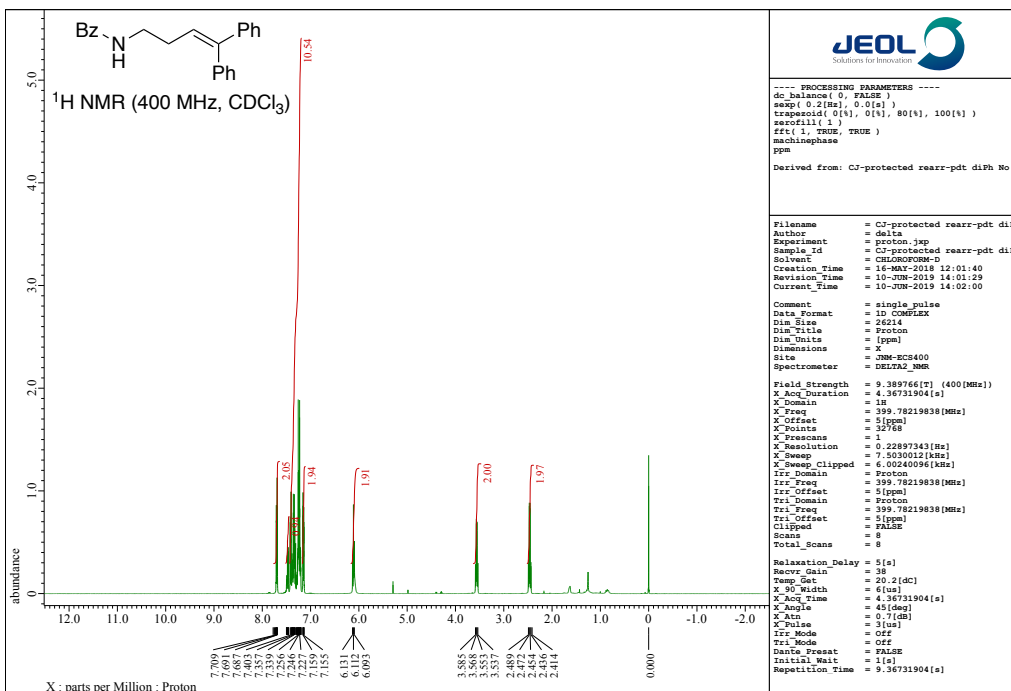
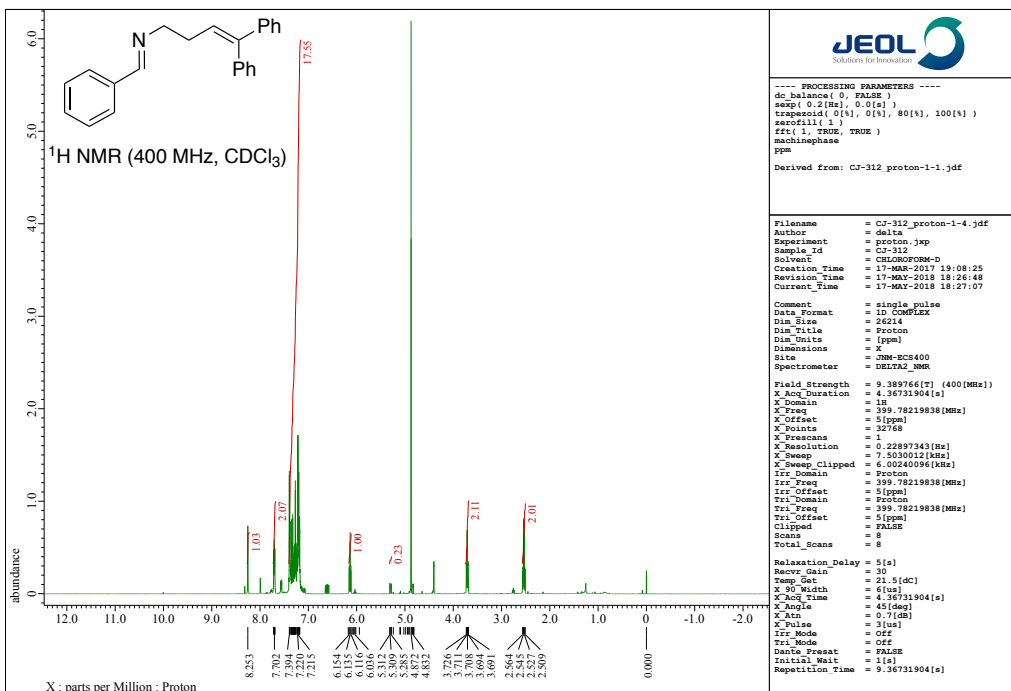
Our seminal advances in development of the new reaction for synthesis of homoallylic amines expand the synthetic strategy for small organic molecules containing a nitrogen atom. The experimental and computational studies open the new strategy to develop previously unknown rearrangement reactions. The chiral counteranion-directed catalytic asymmetric reactions provide a new approach to synthesize enantiomerically enriched molecules. I believe that this thesis contributes to the development of rearrangement process, in particularly [1,3]-rearrangement.

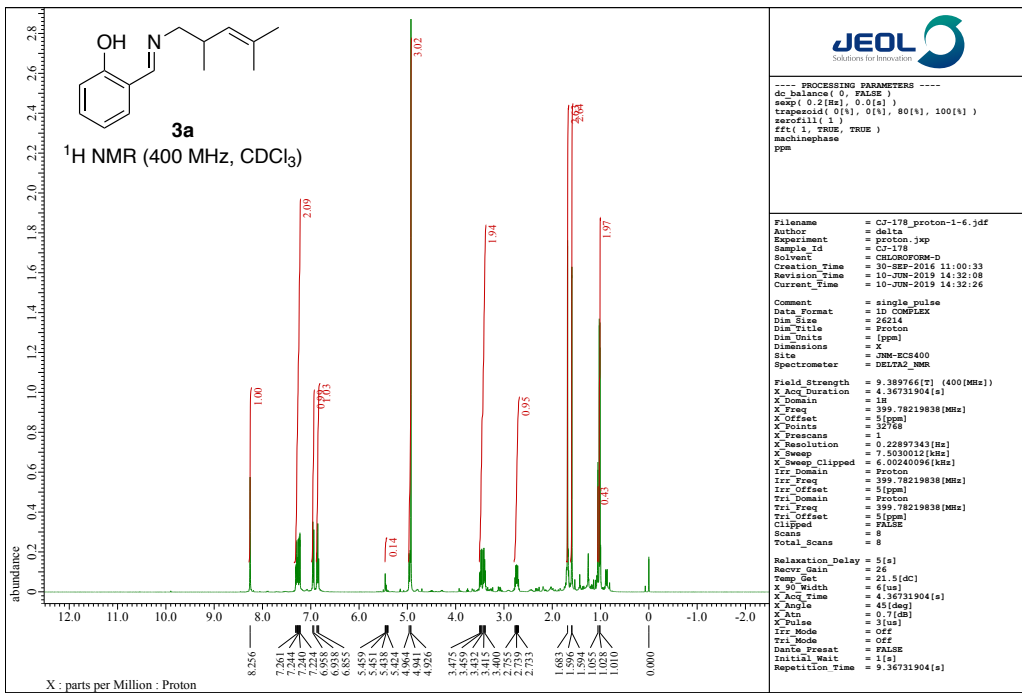
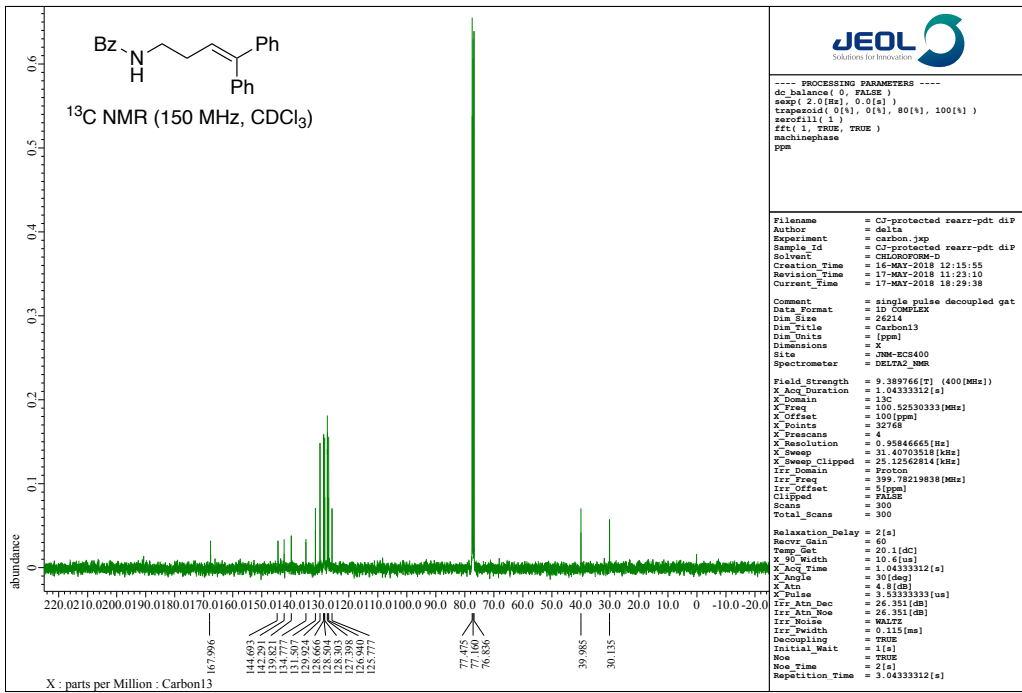
APPENDIX

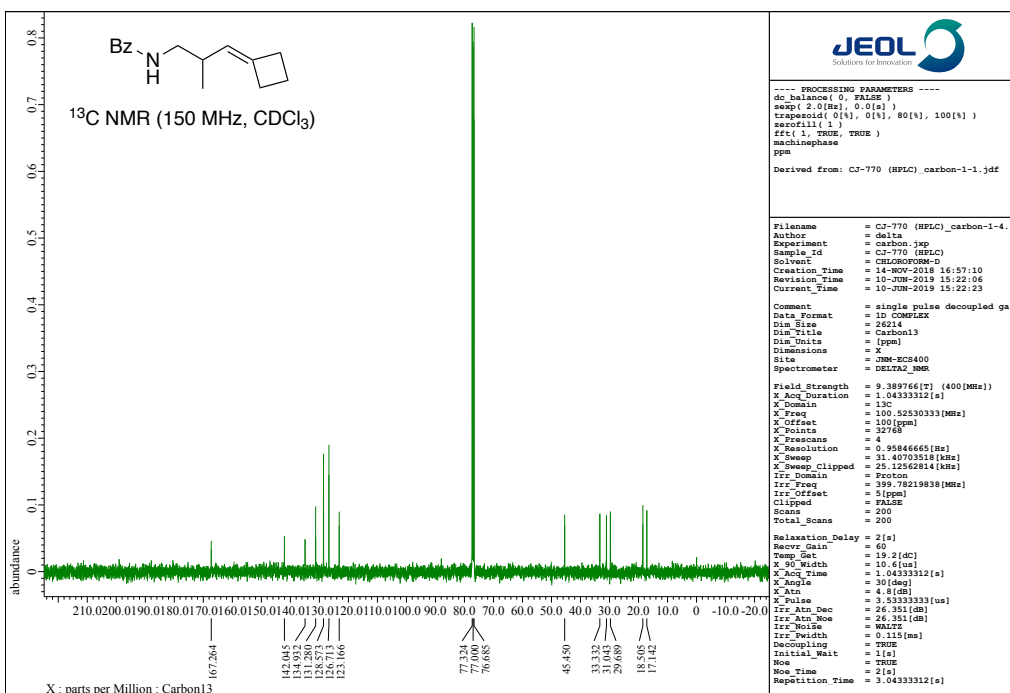
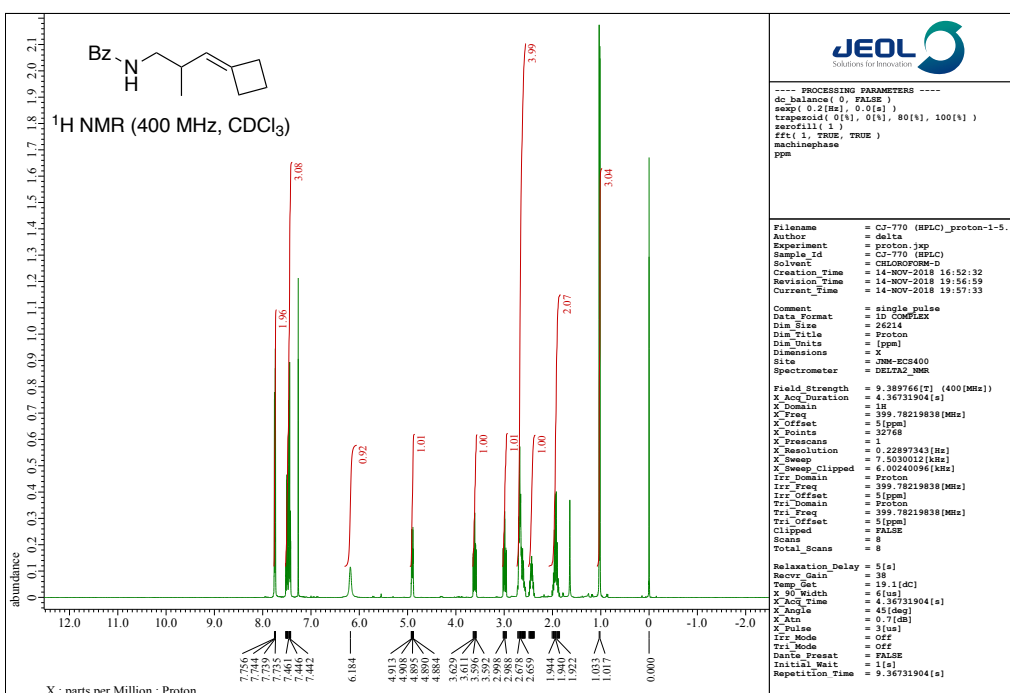
A. NMR CHARTS

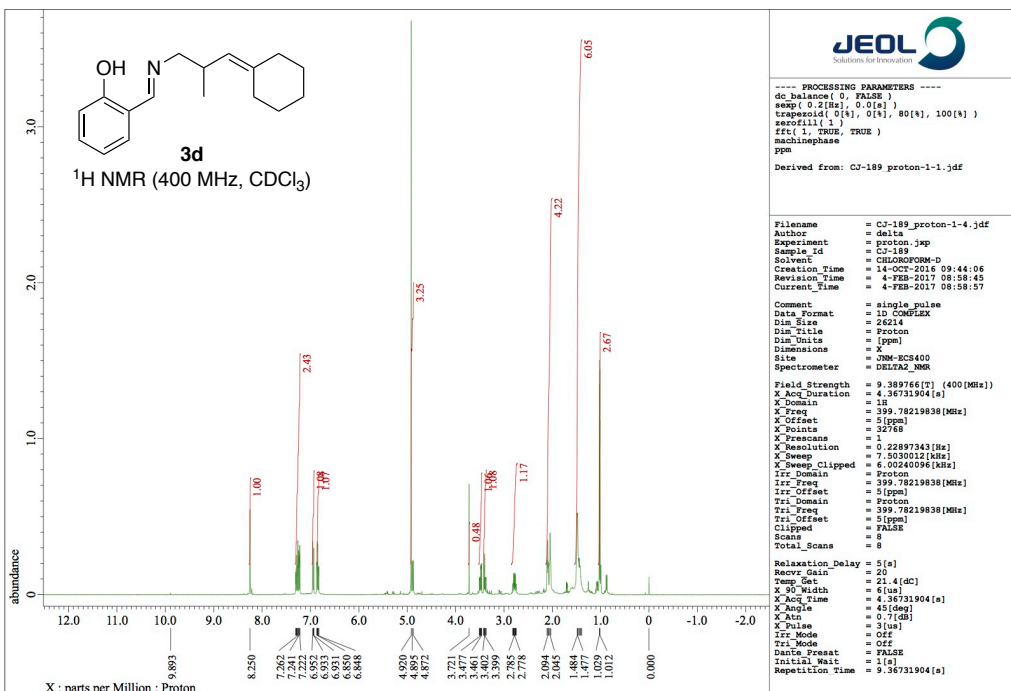
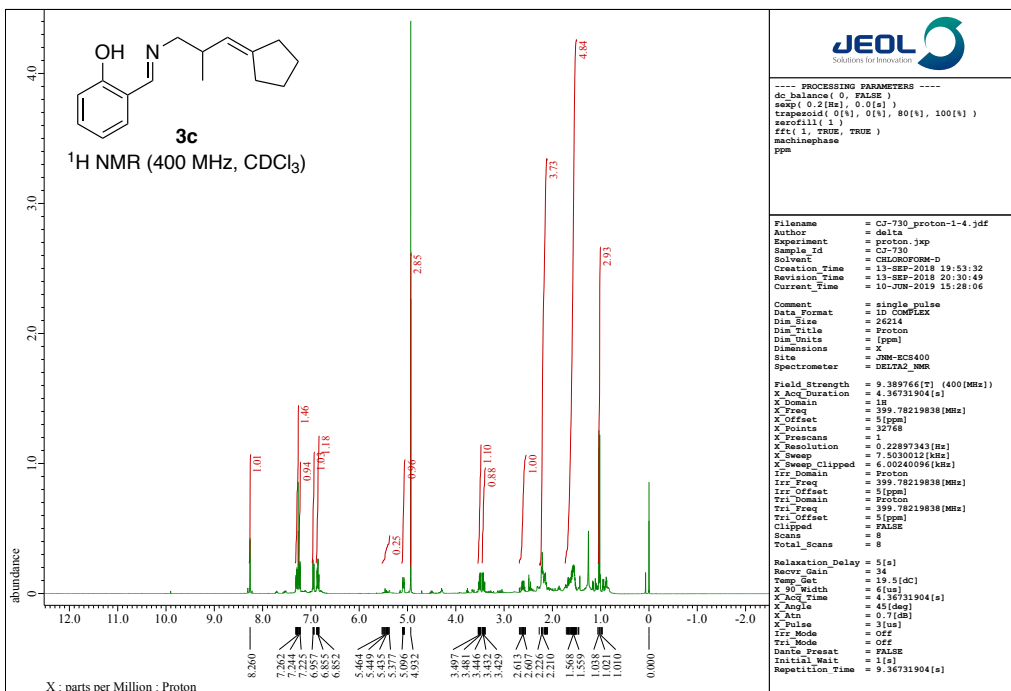
Chapter 2

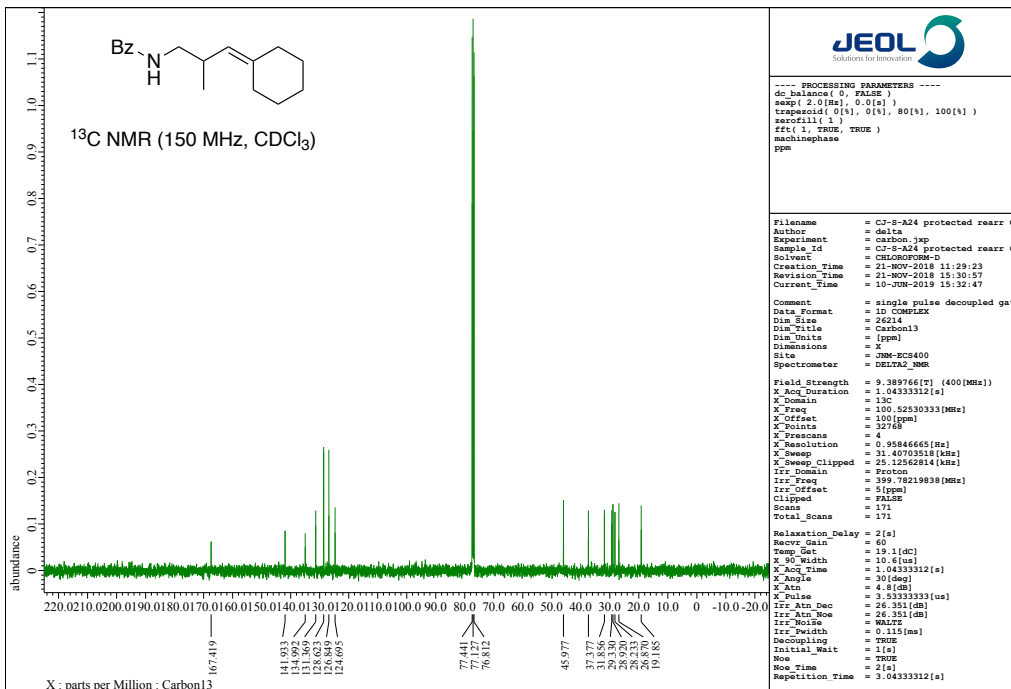
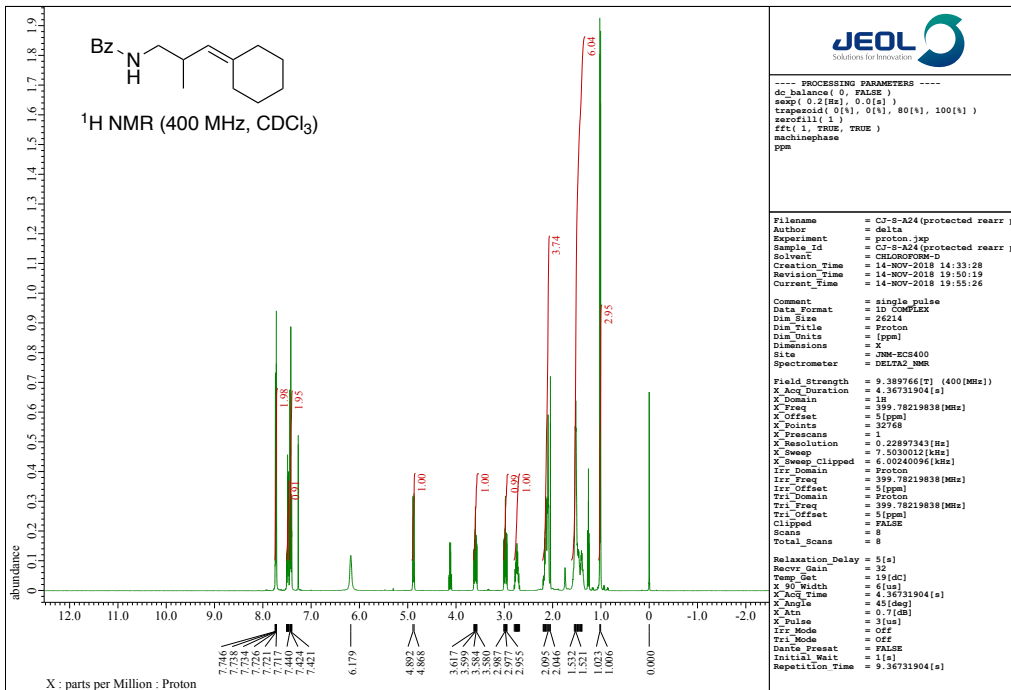


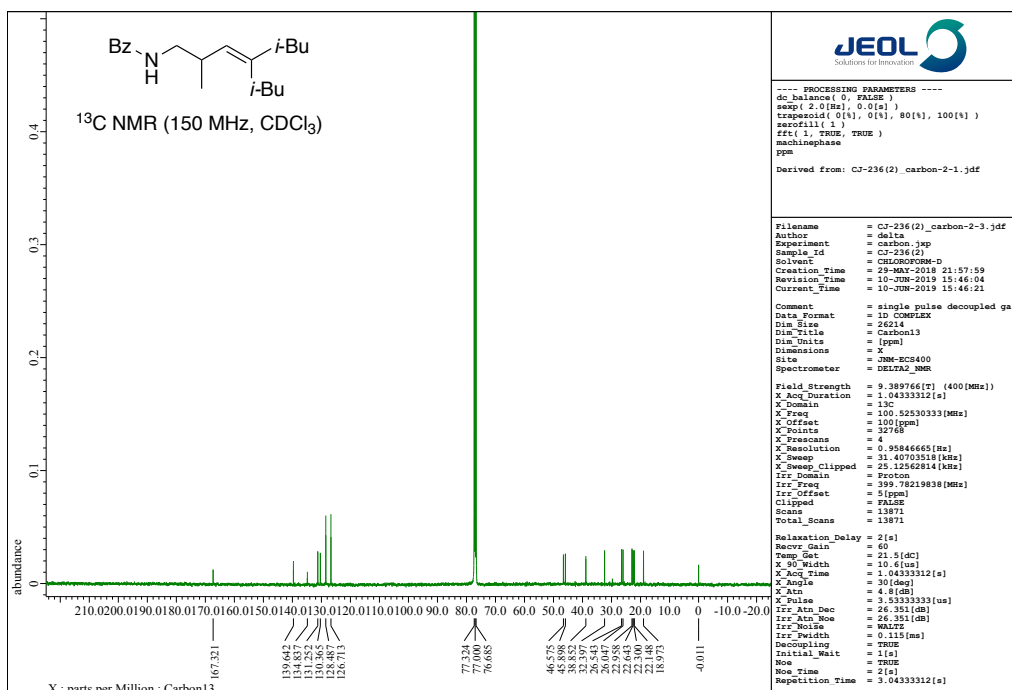
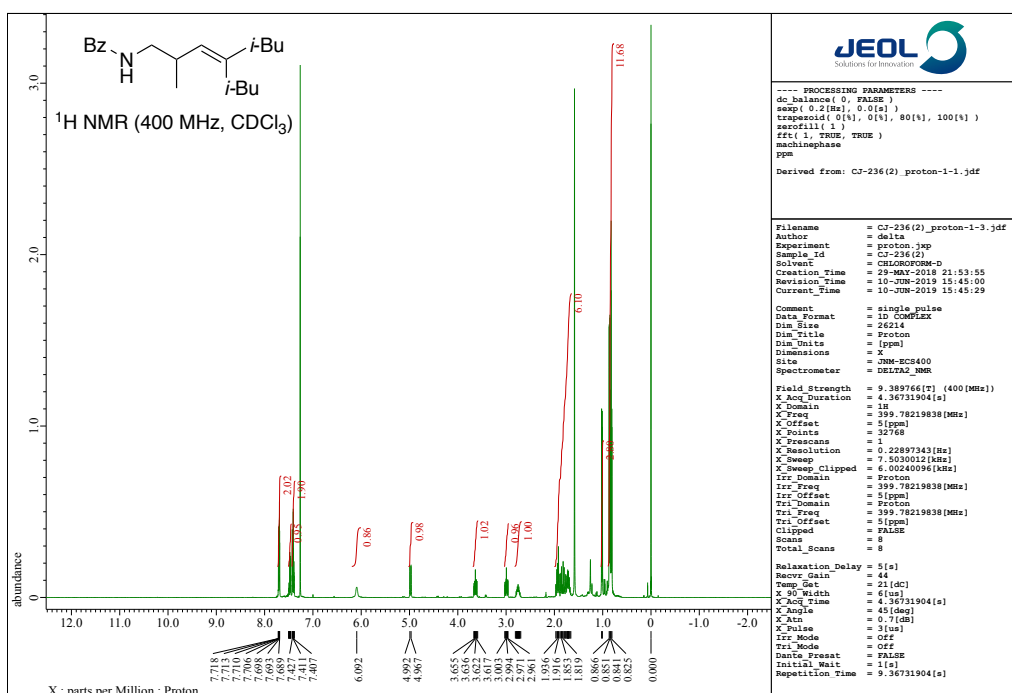


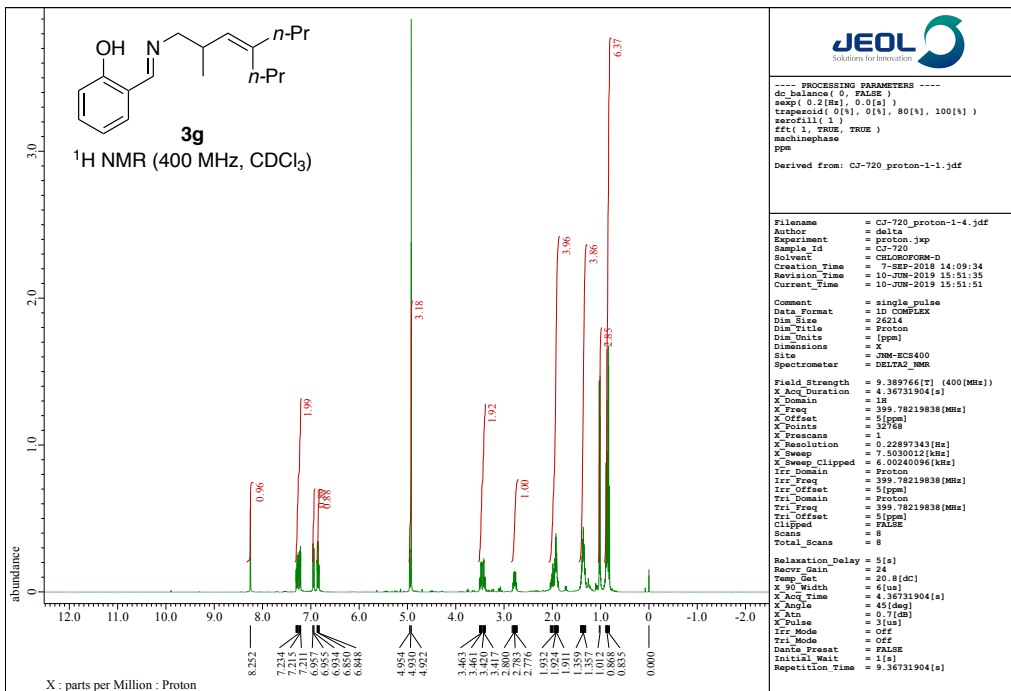
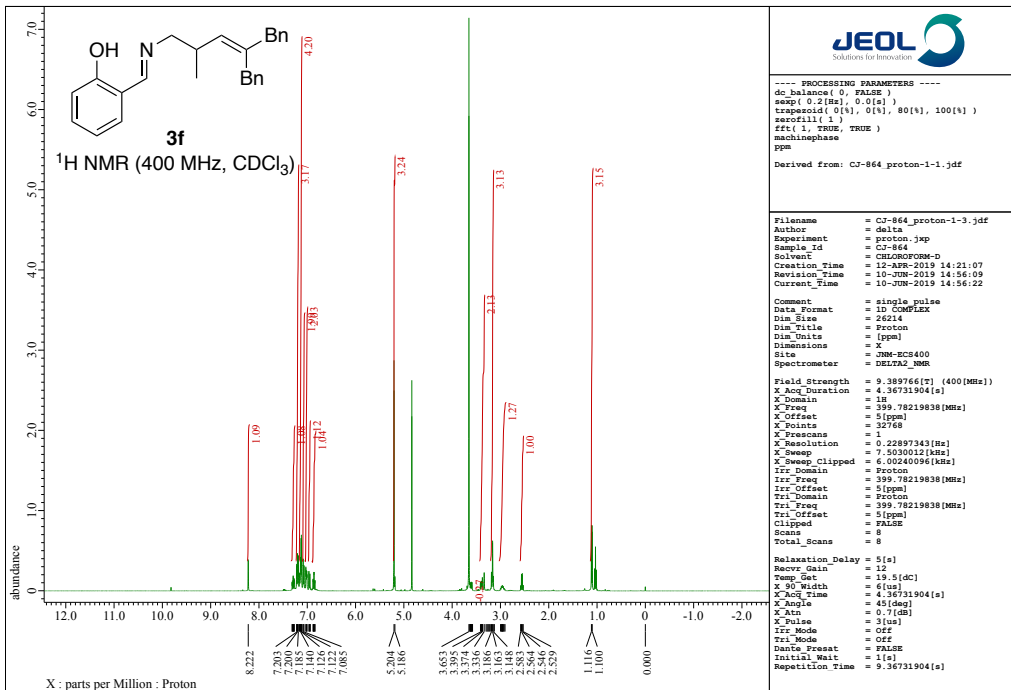


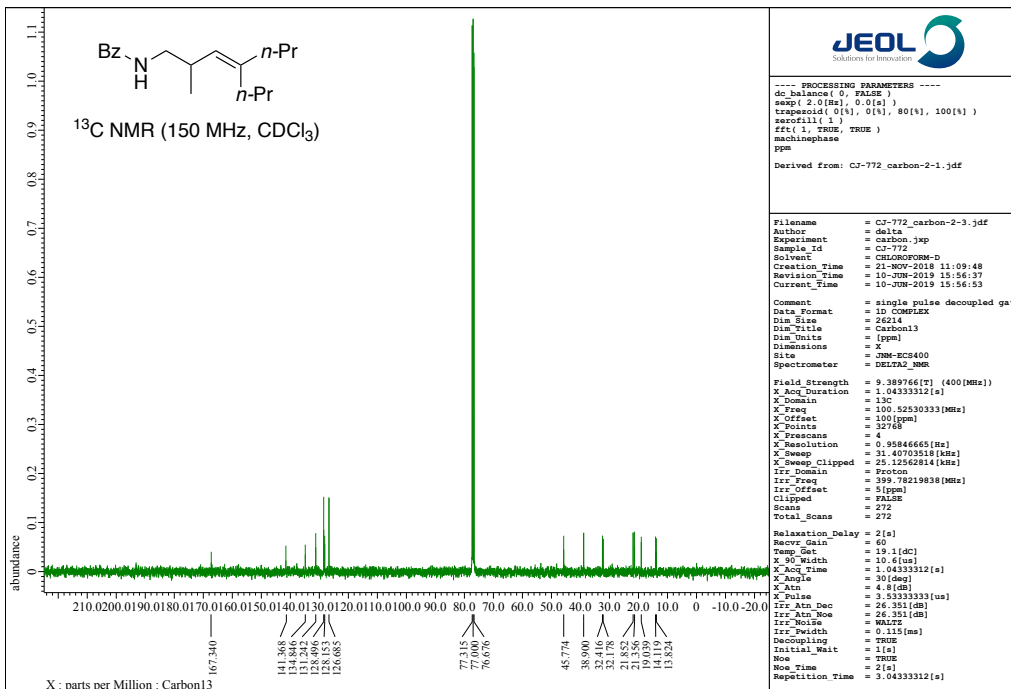
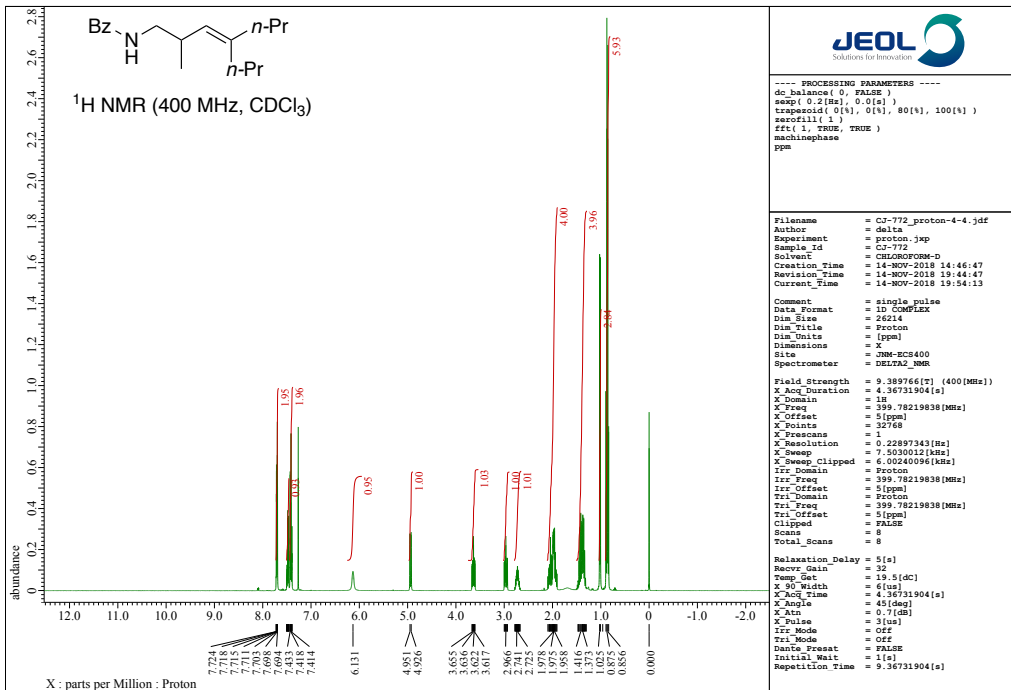


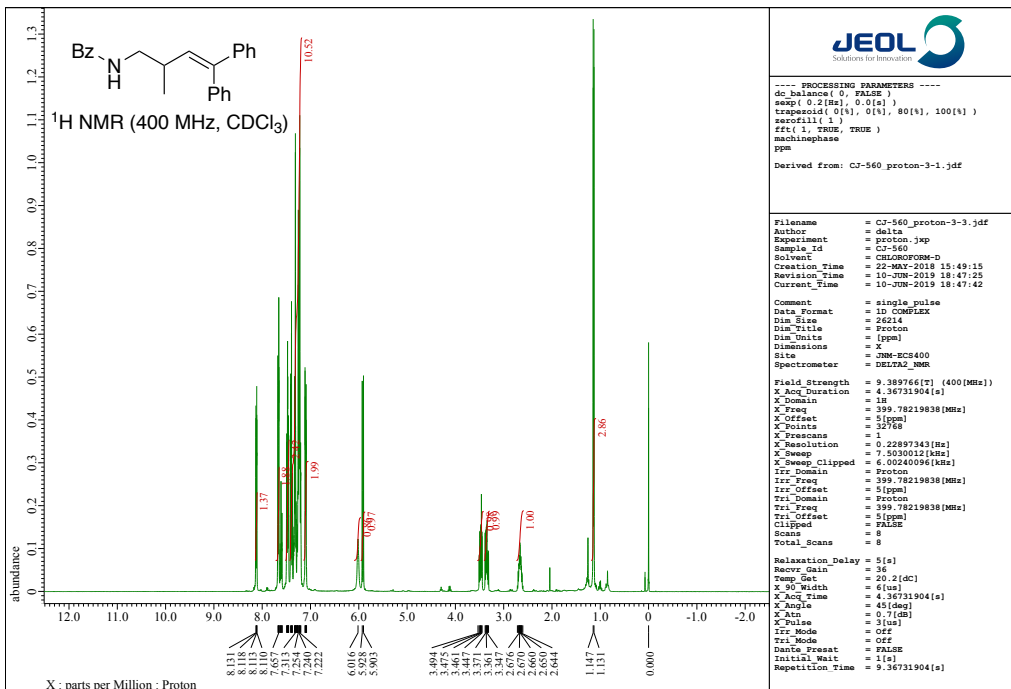
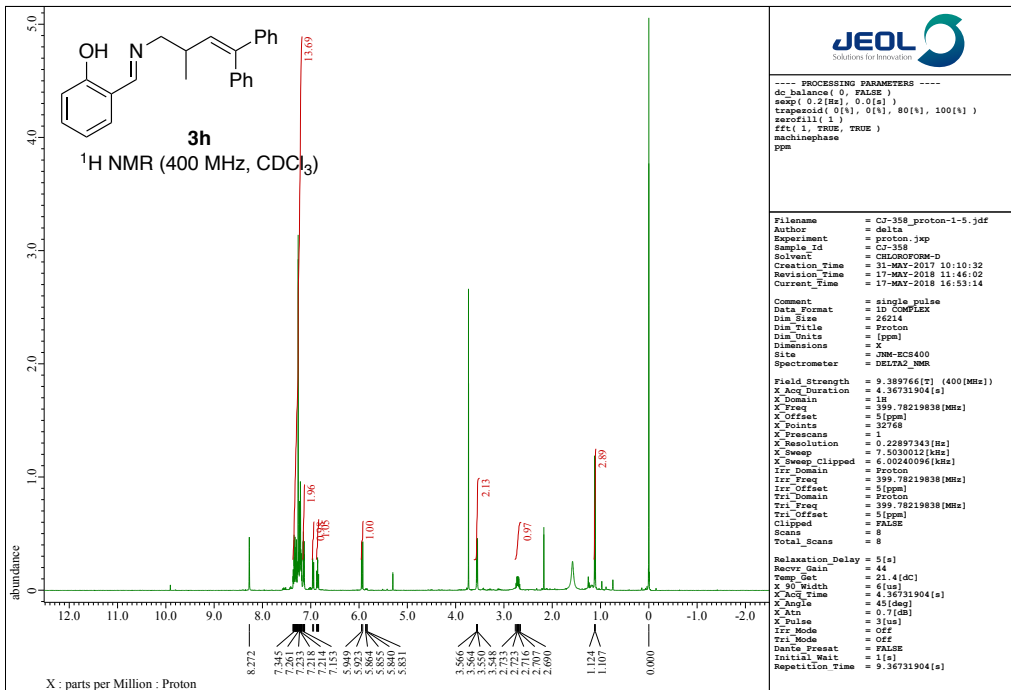


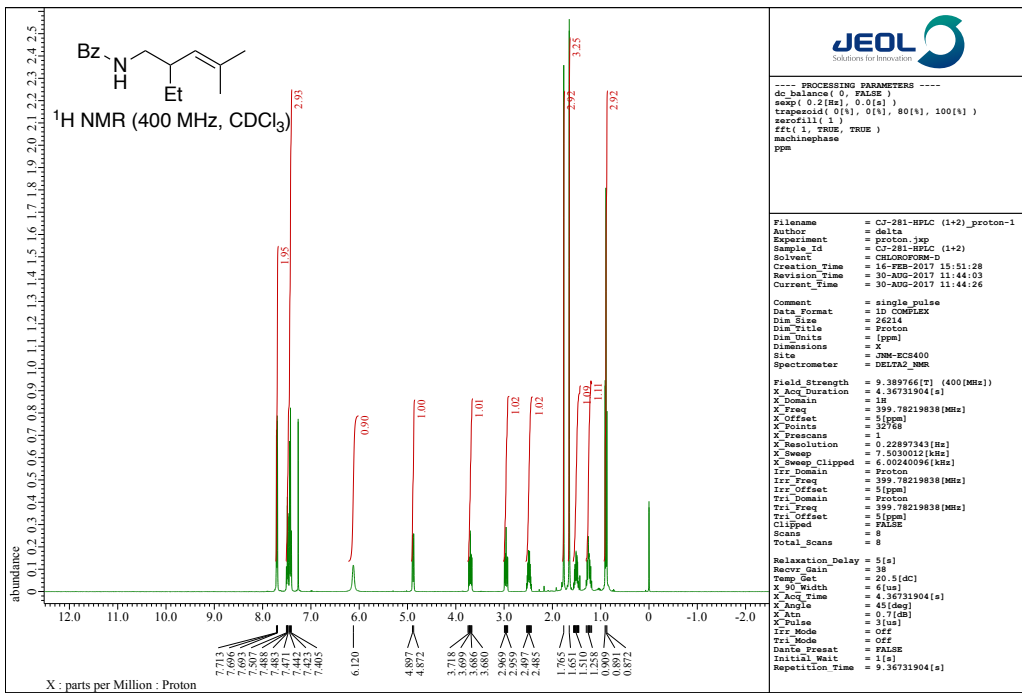
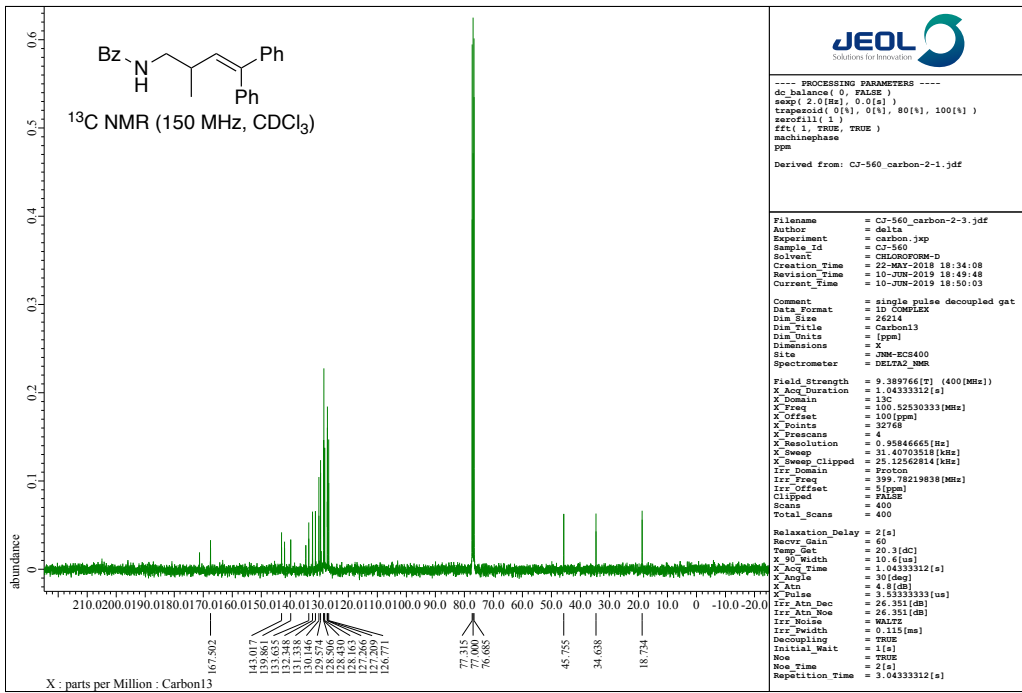


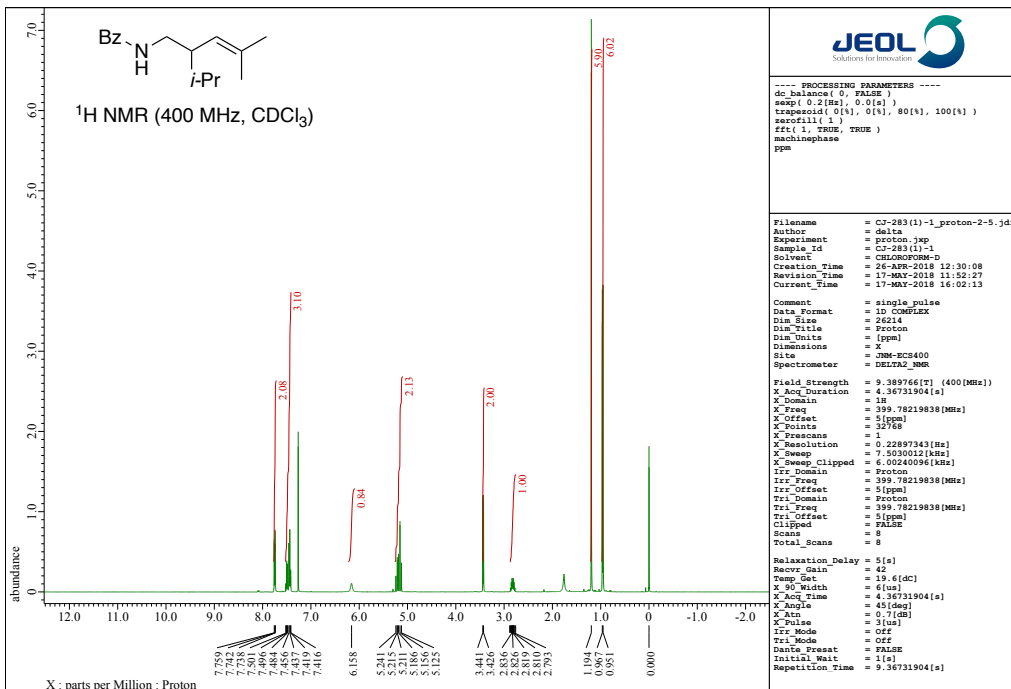
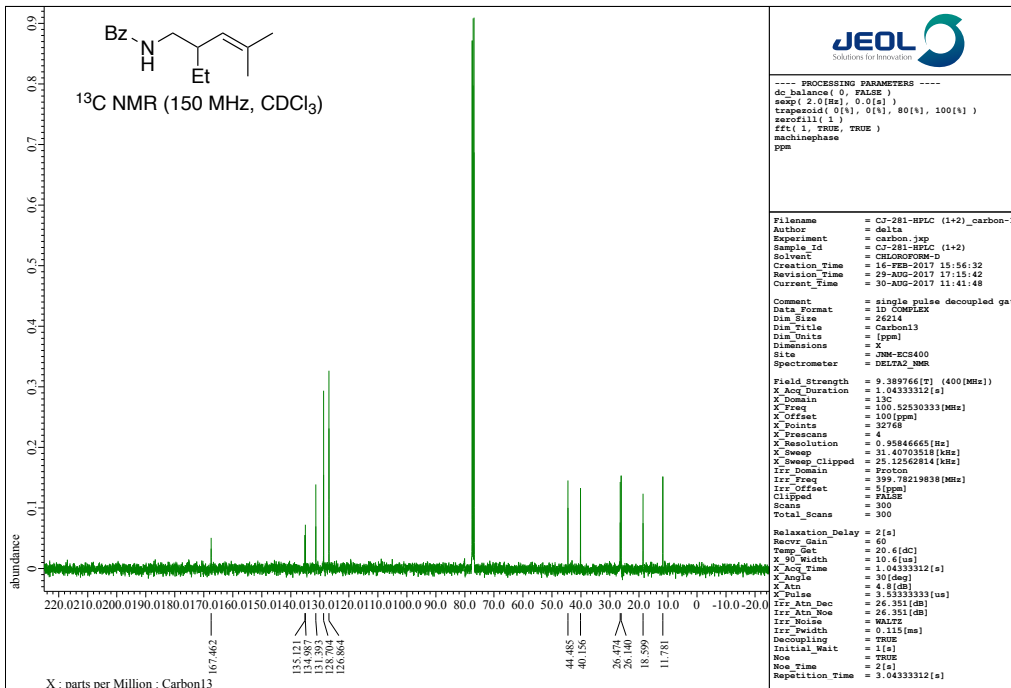


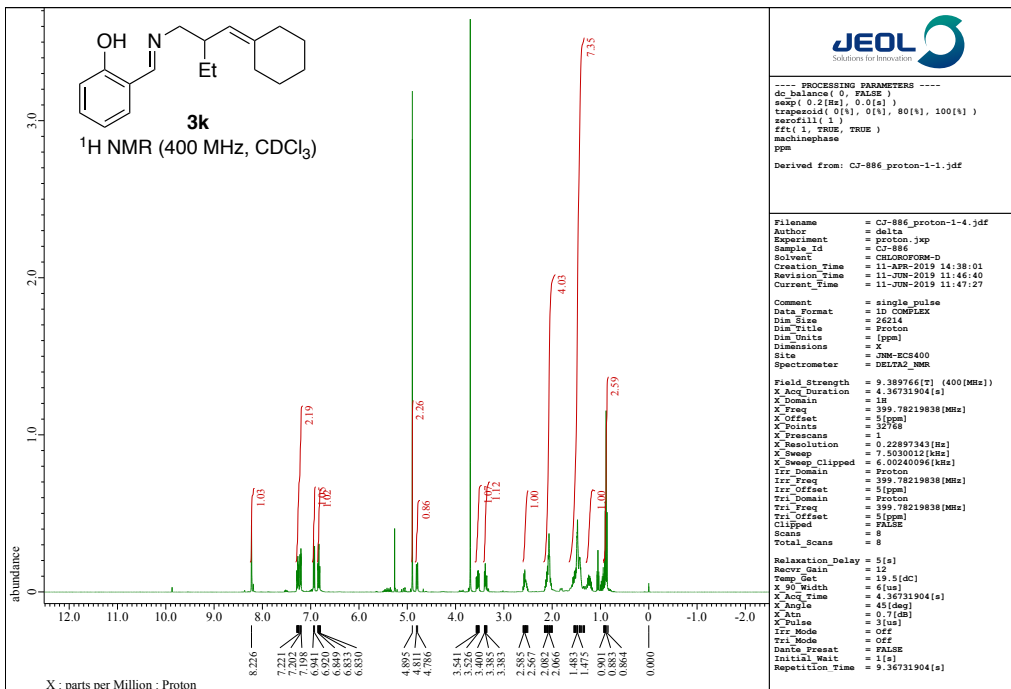
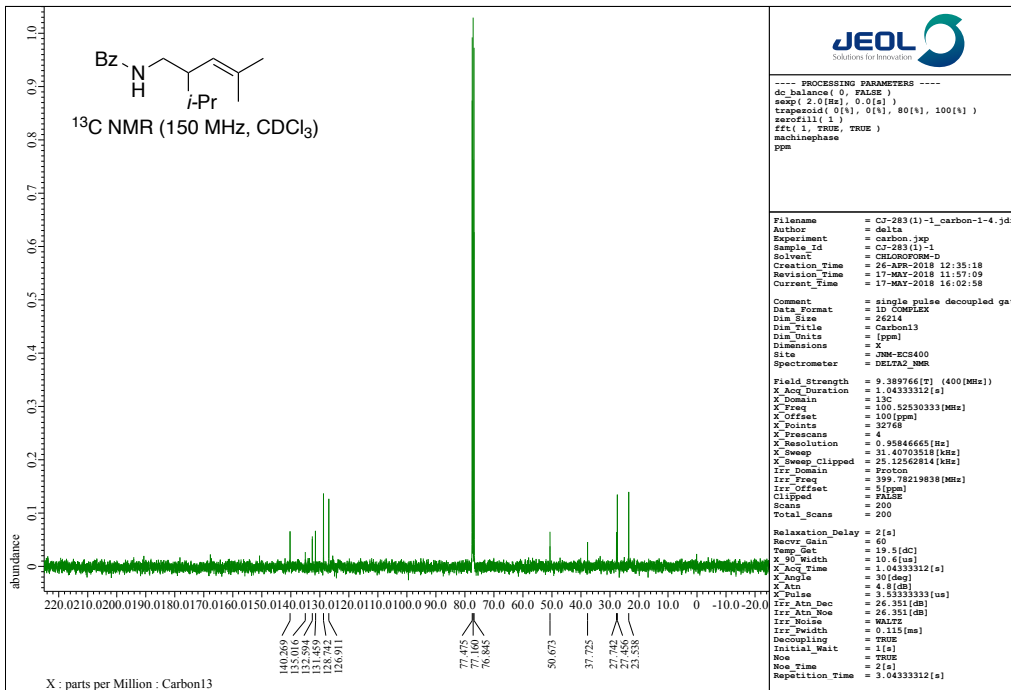


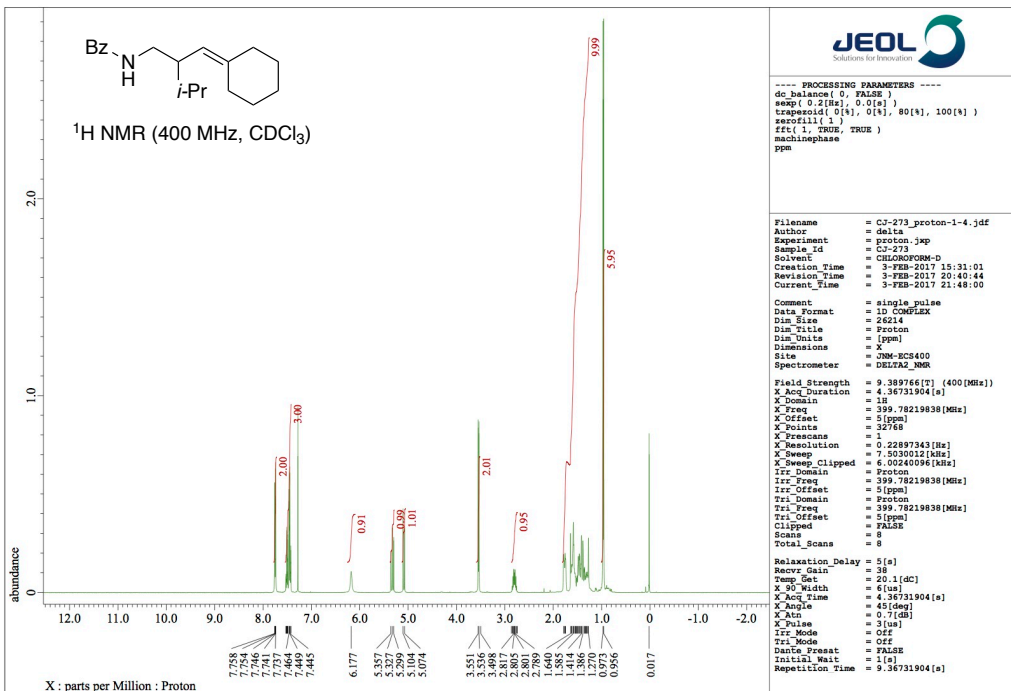
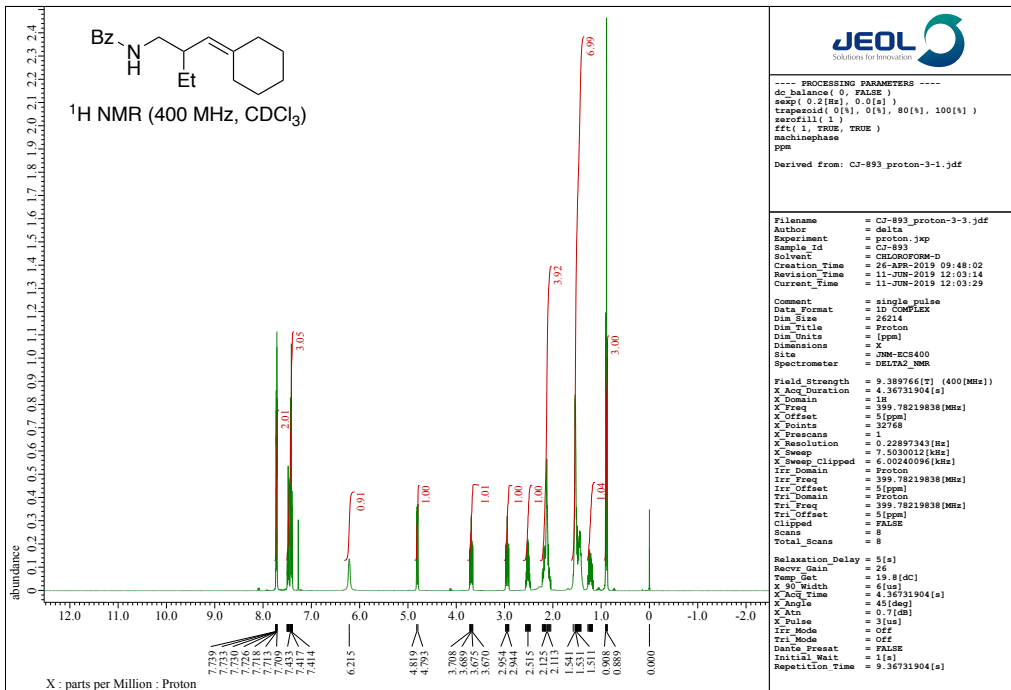


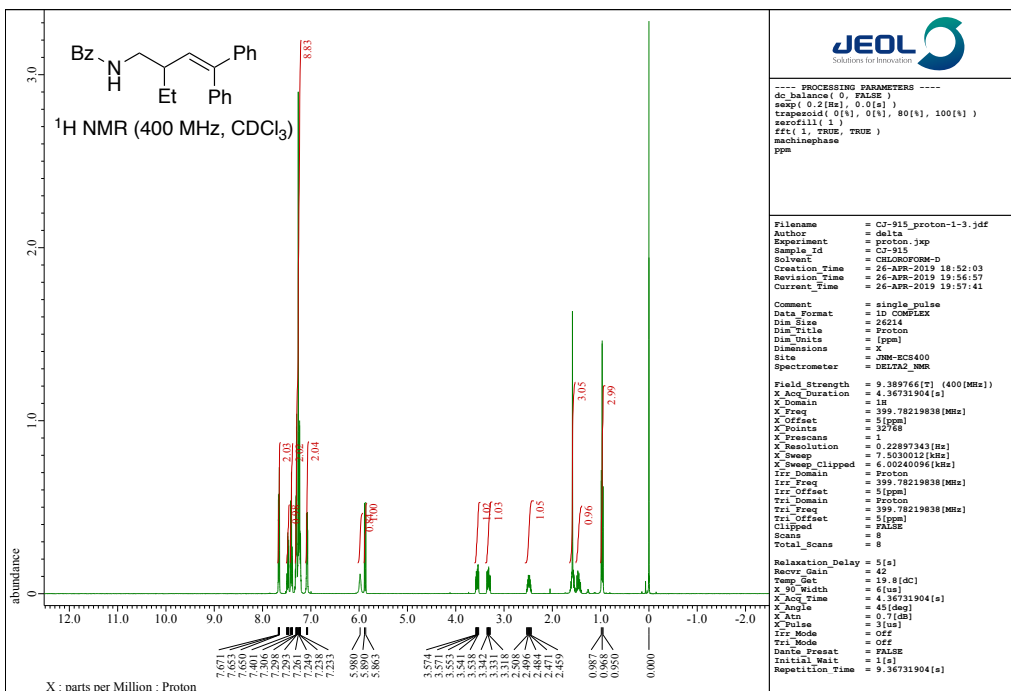
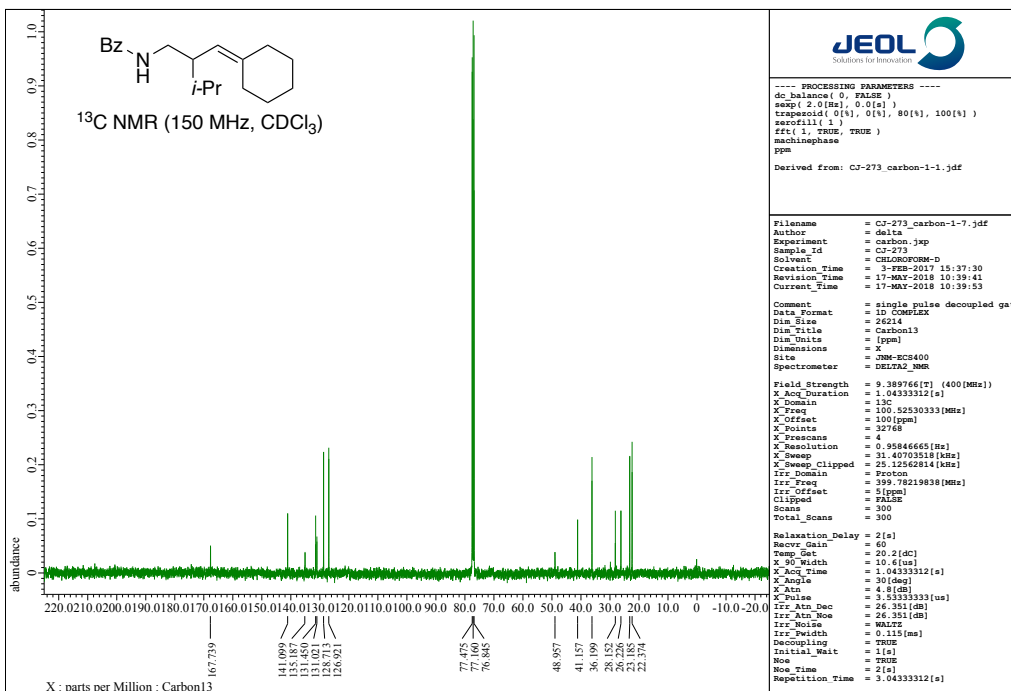


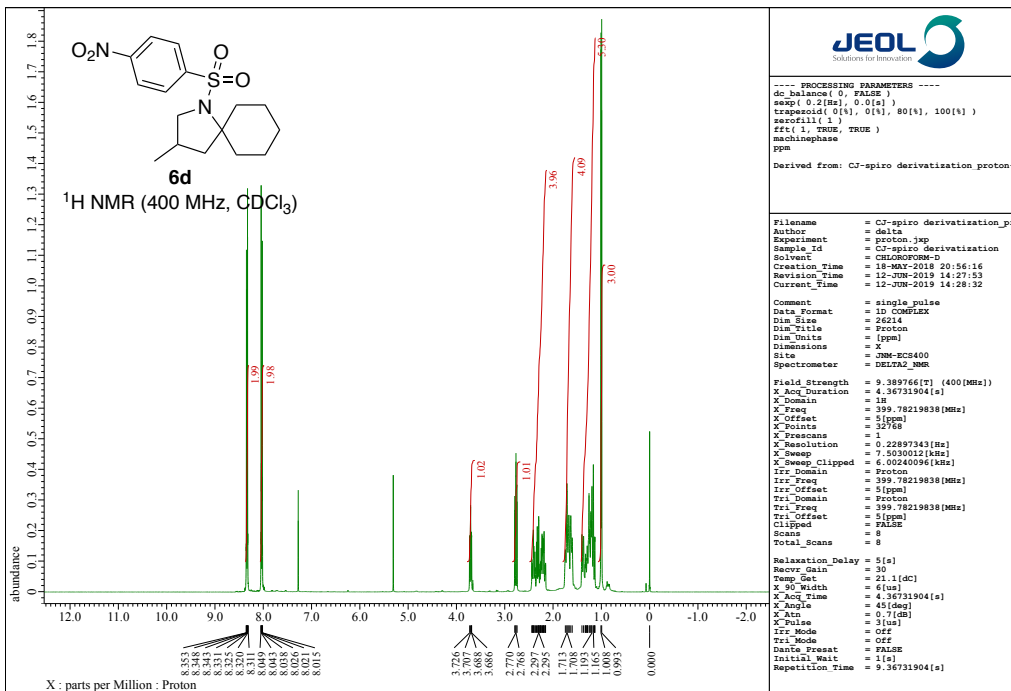
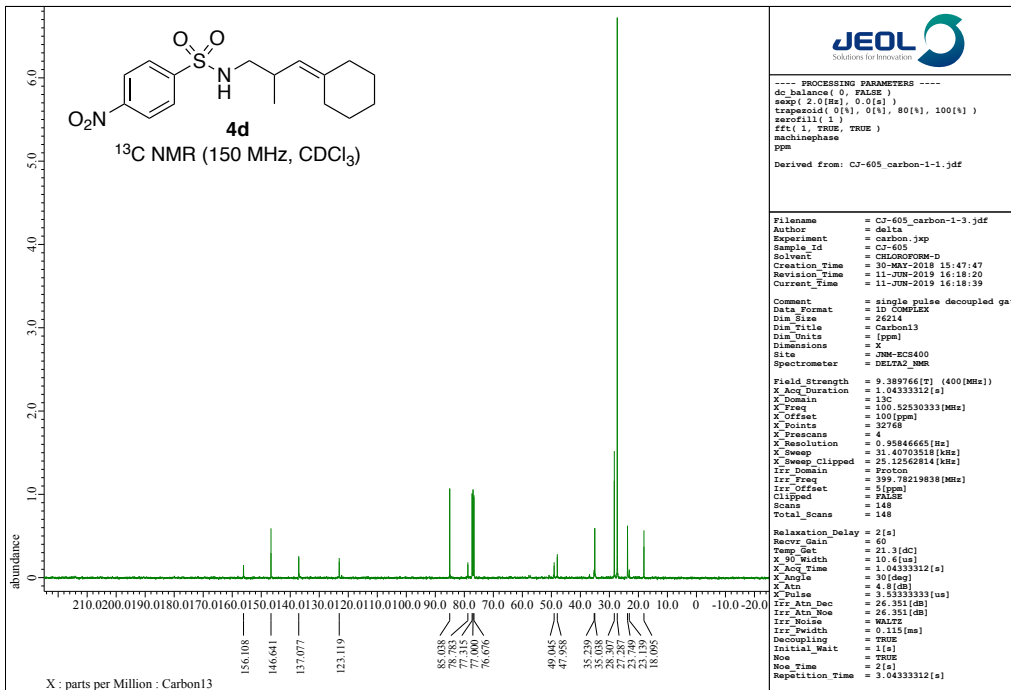


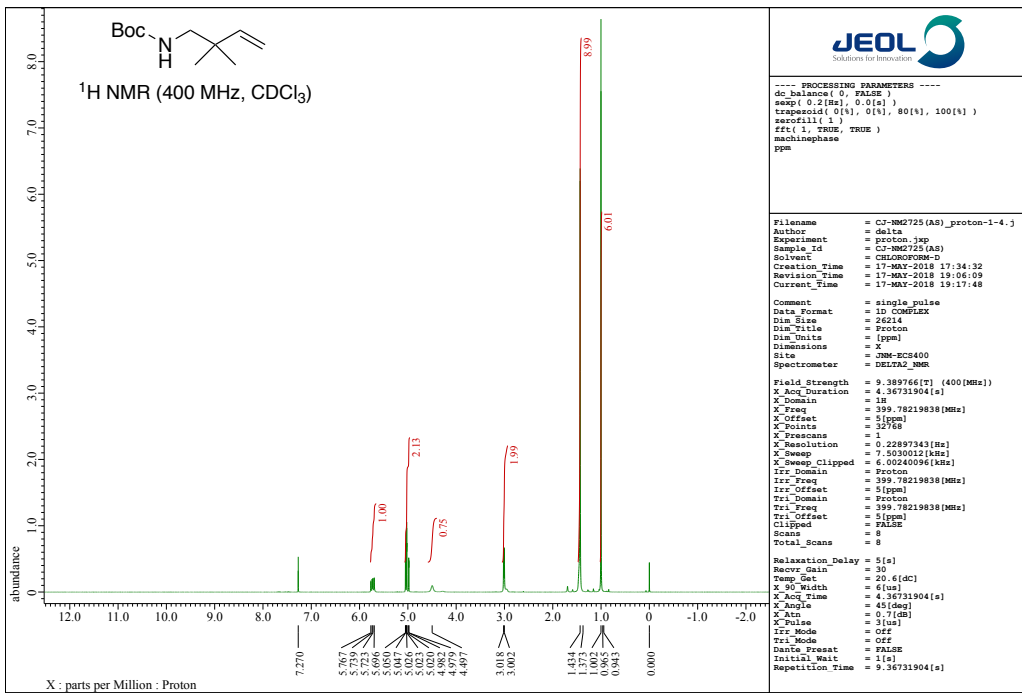
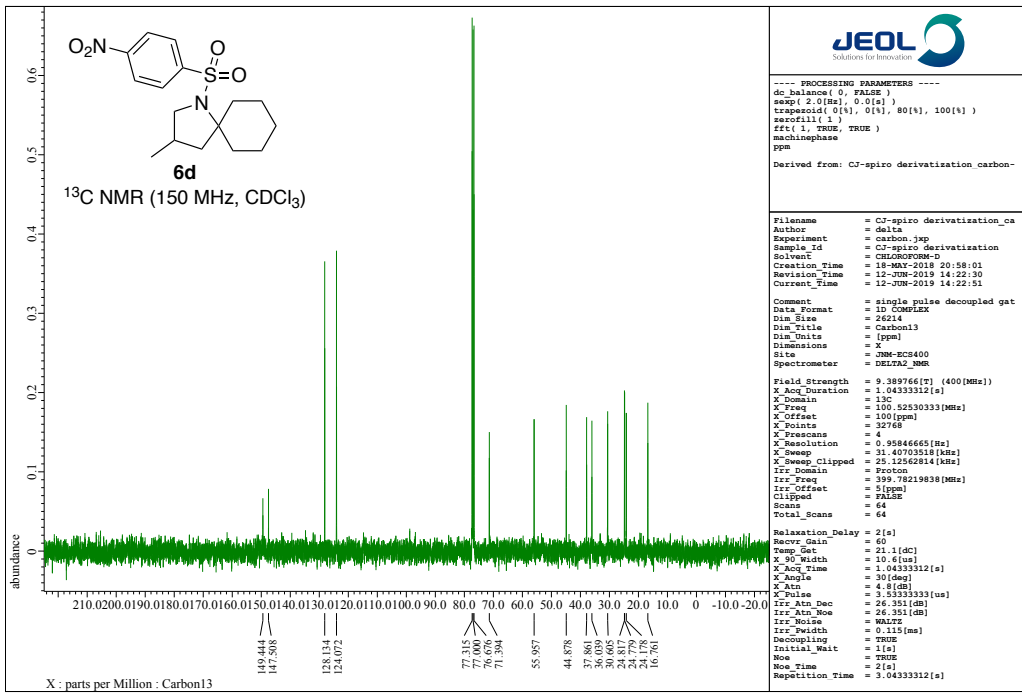


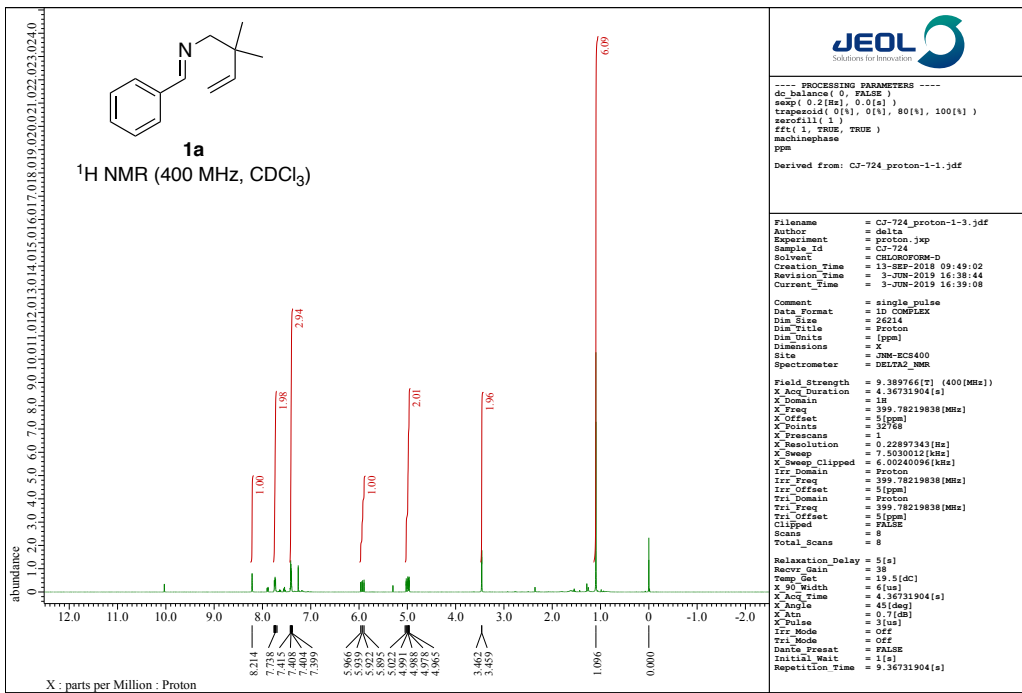
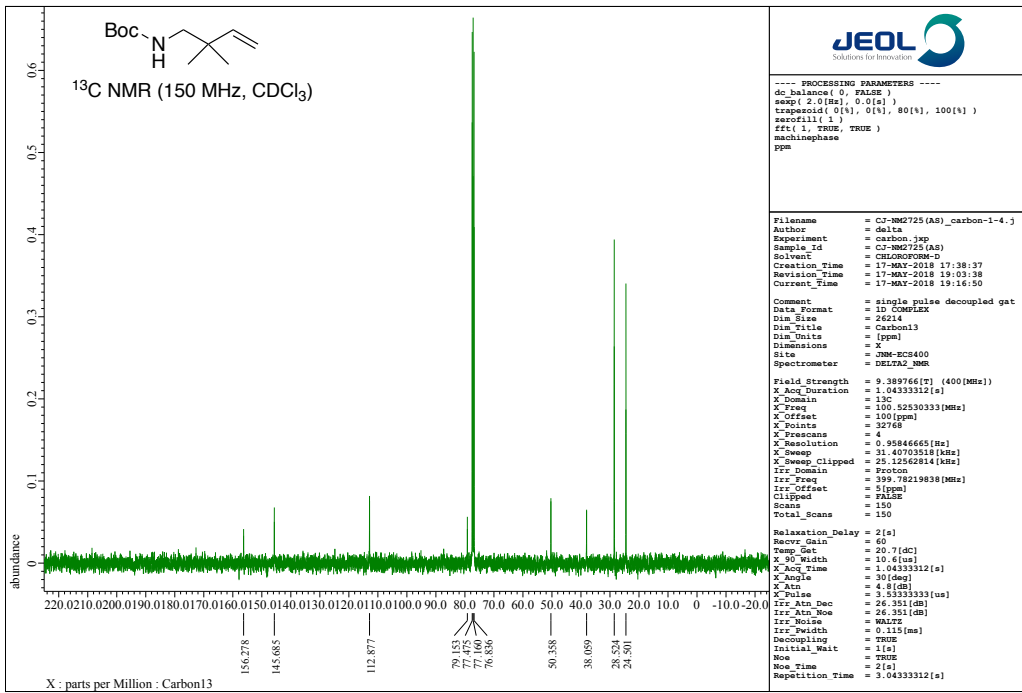


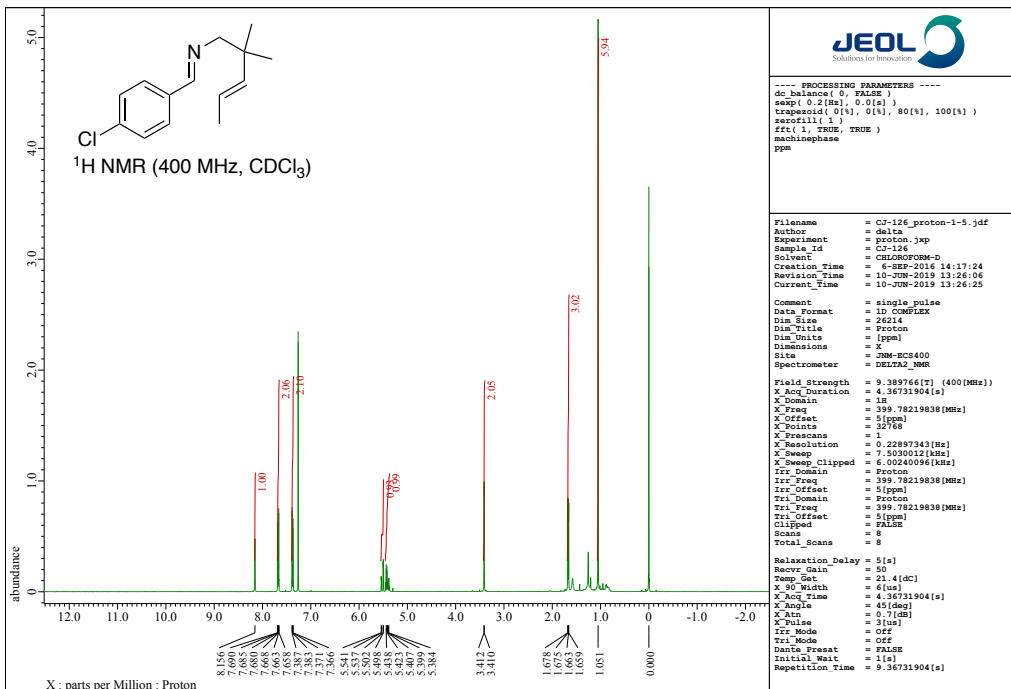
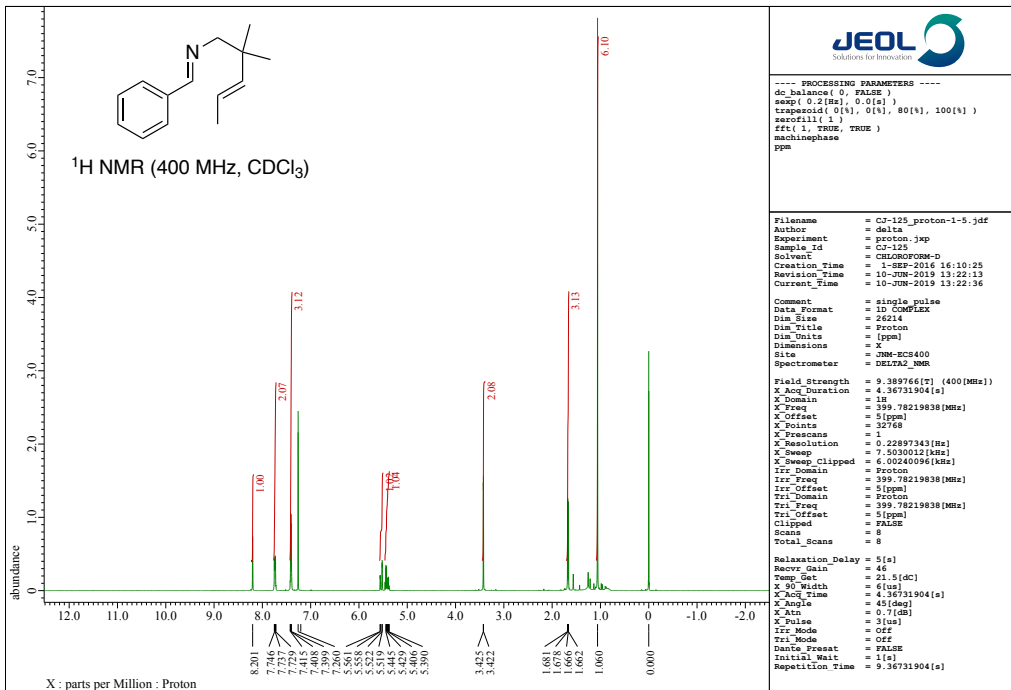


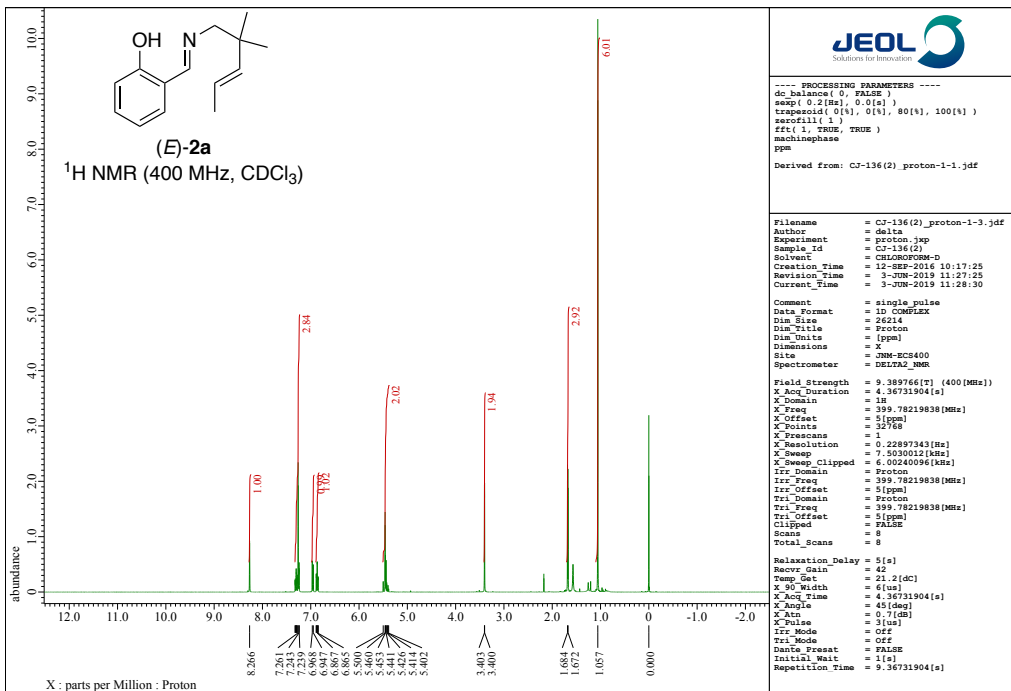
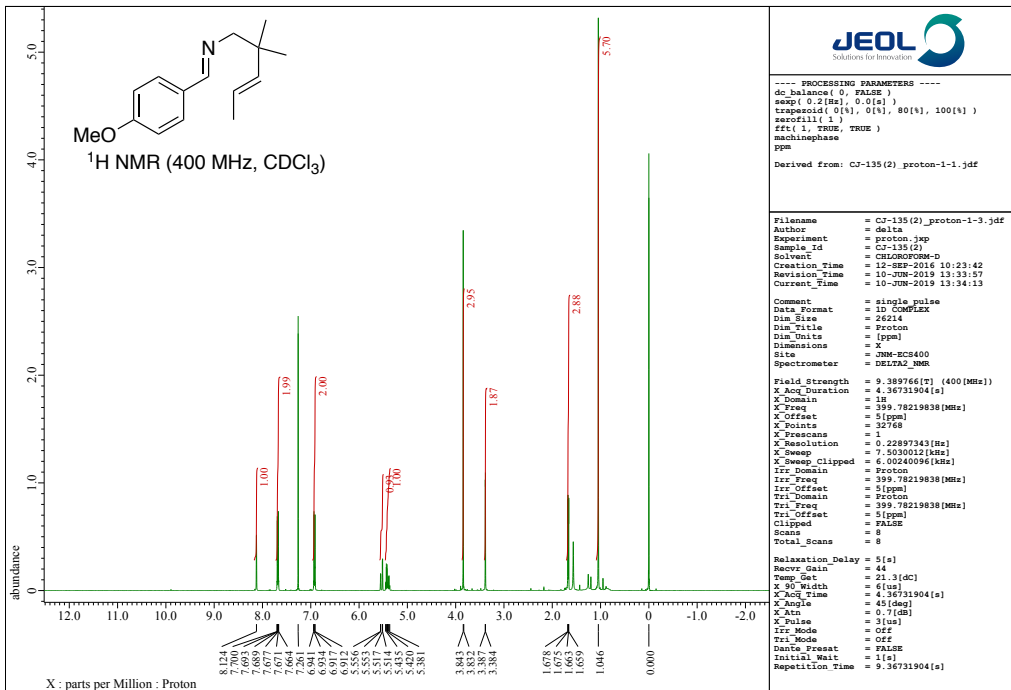


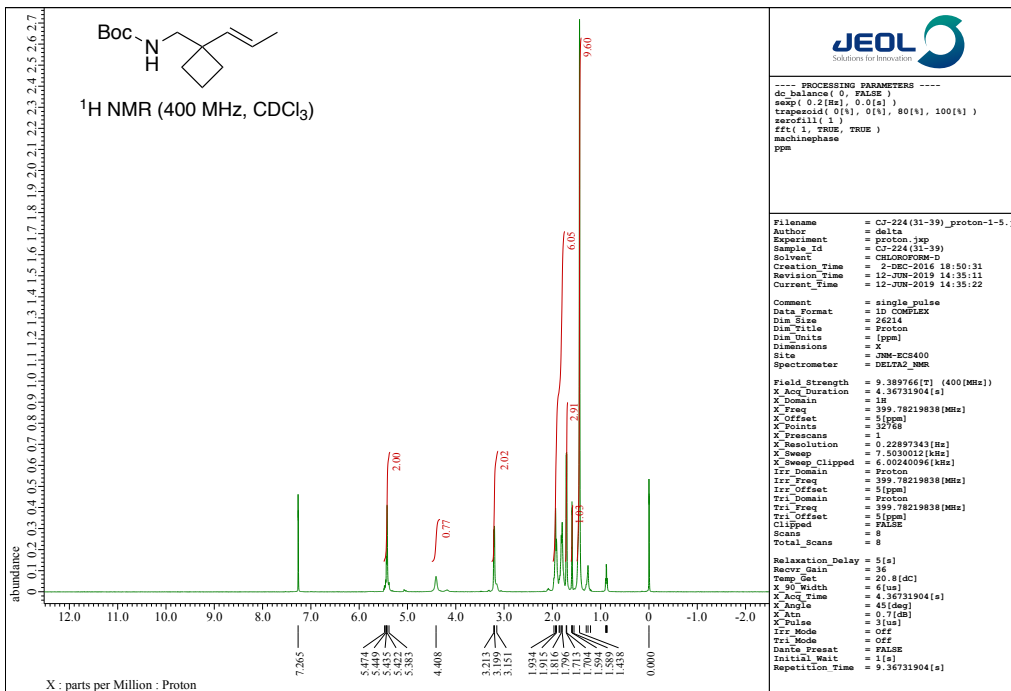
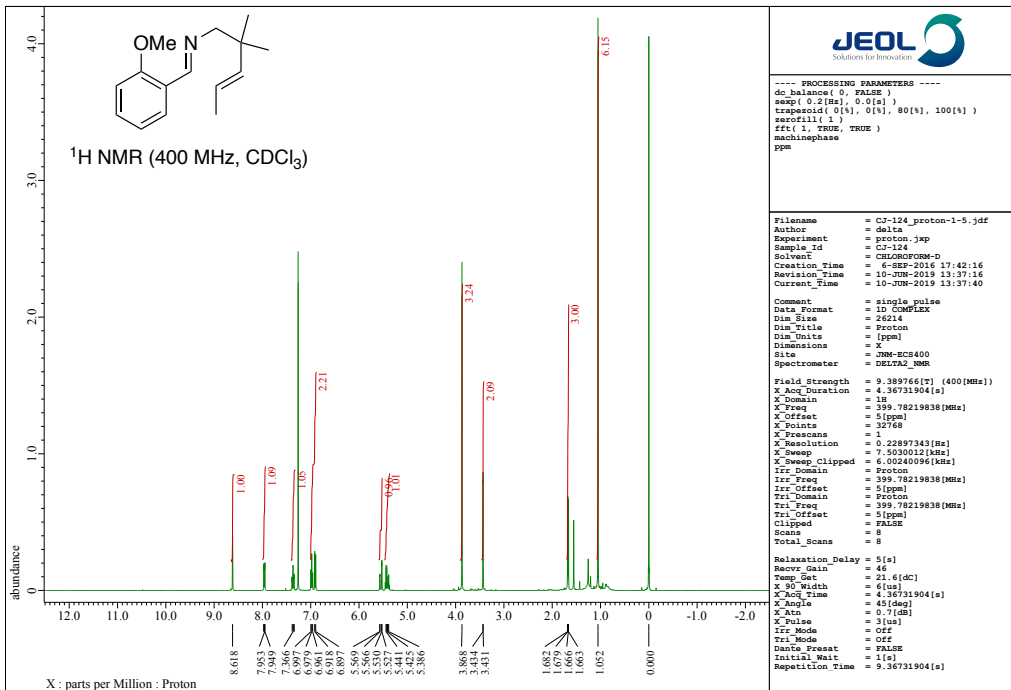


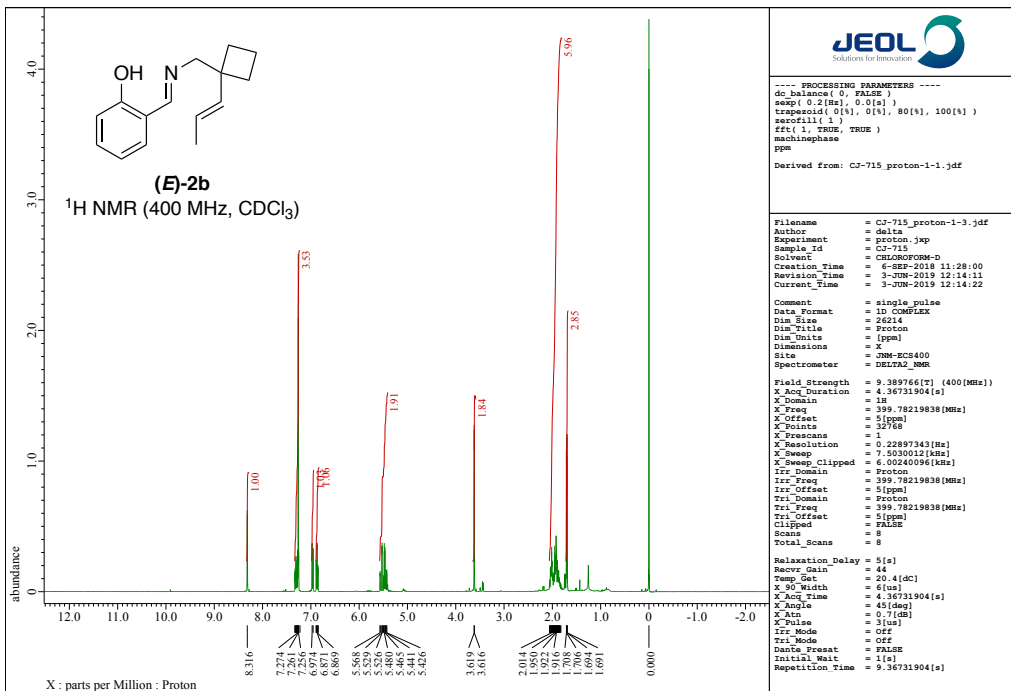
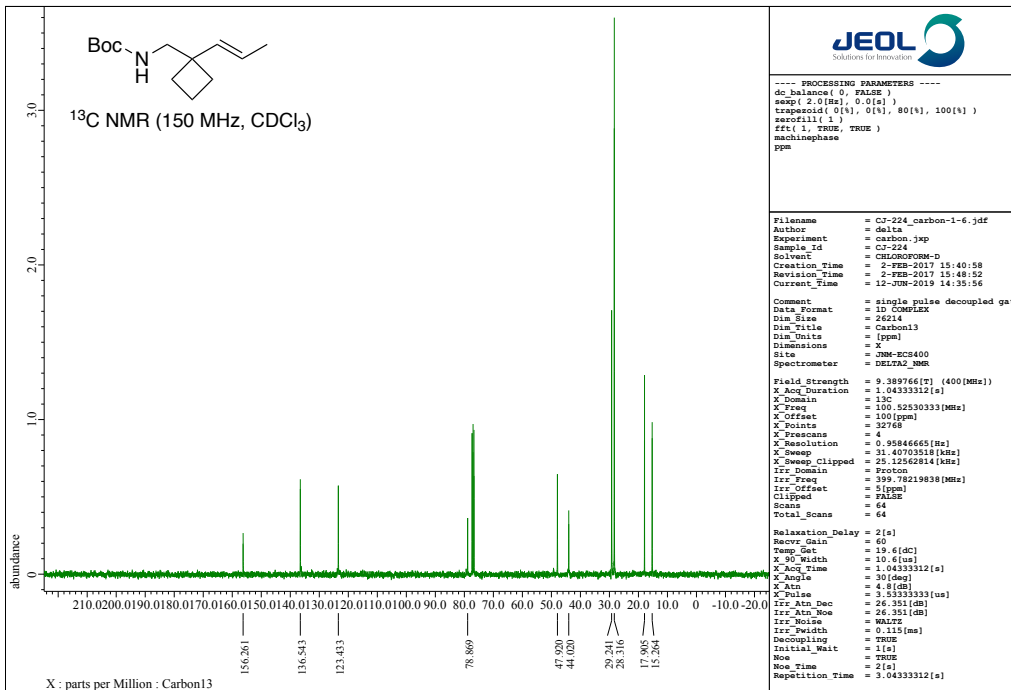


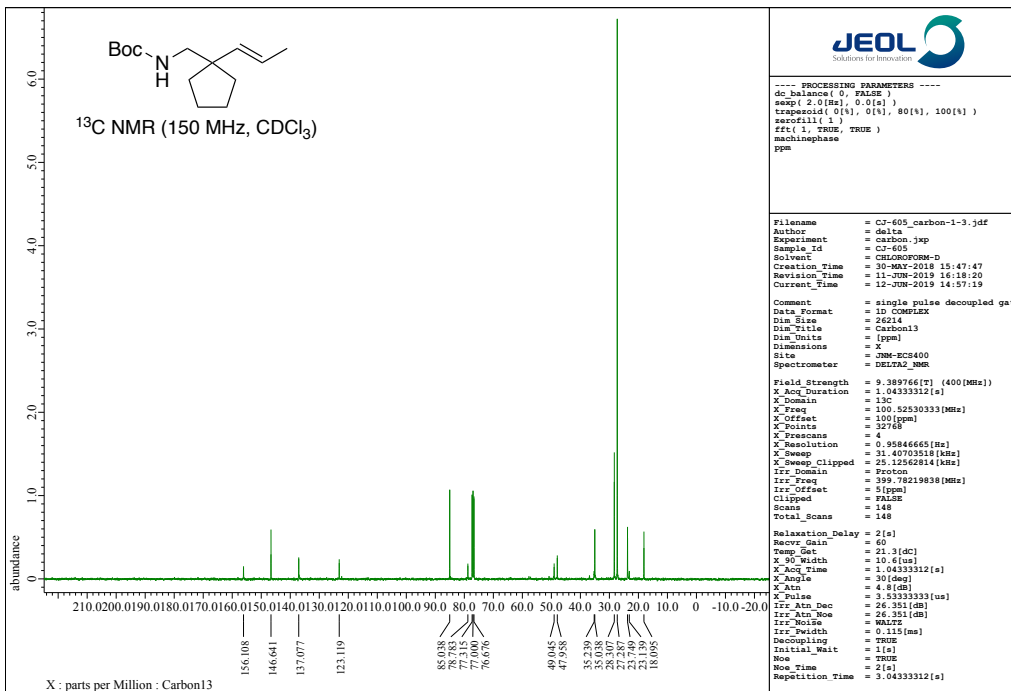
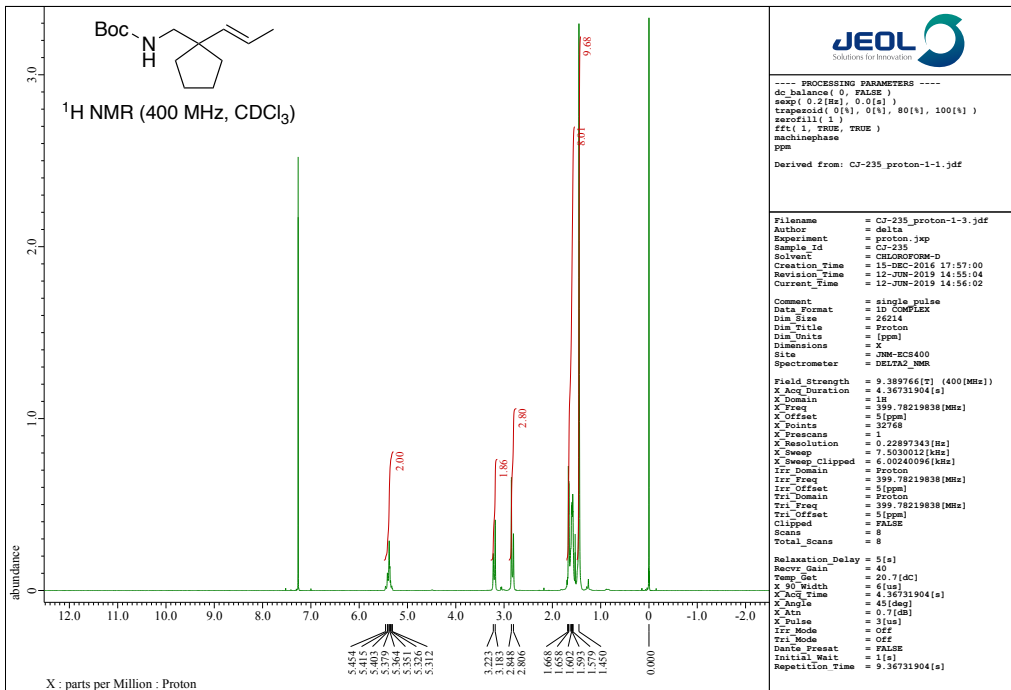


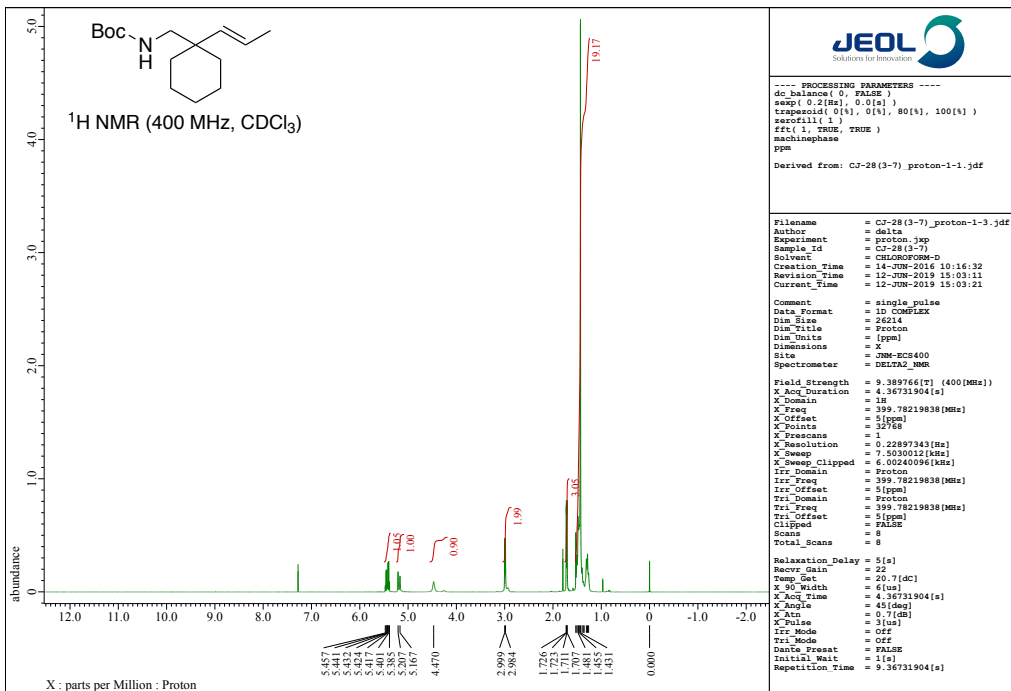
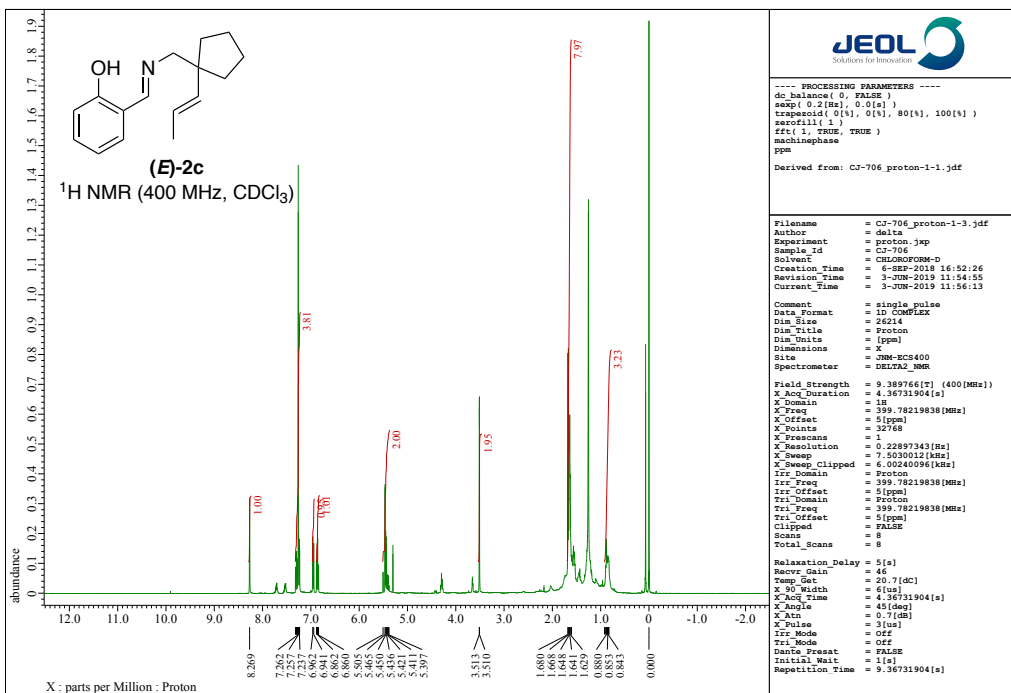


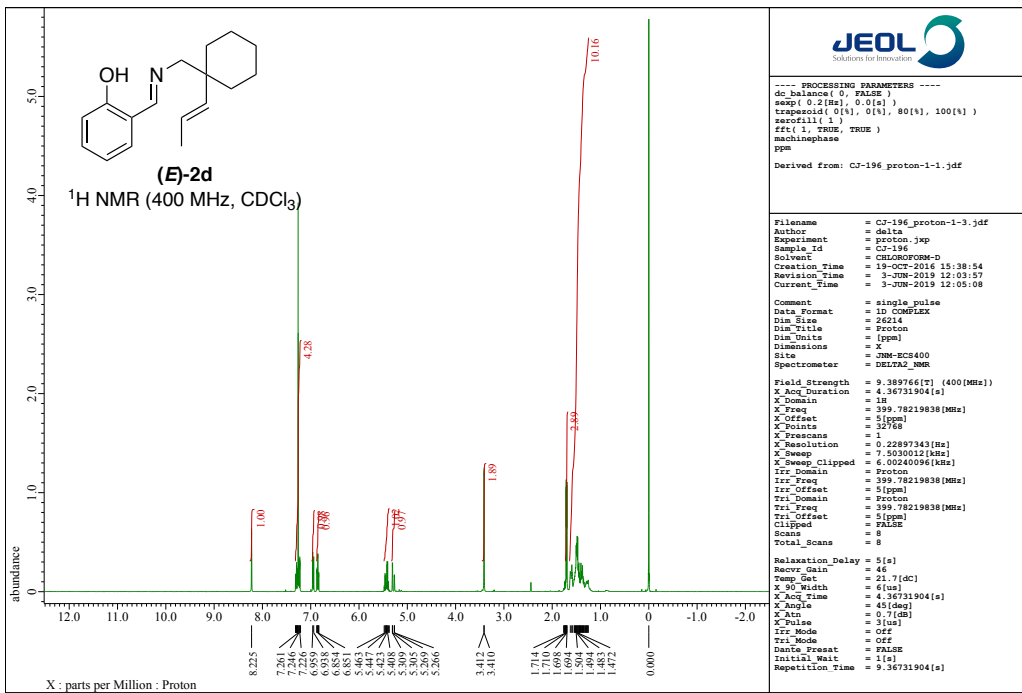
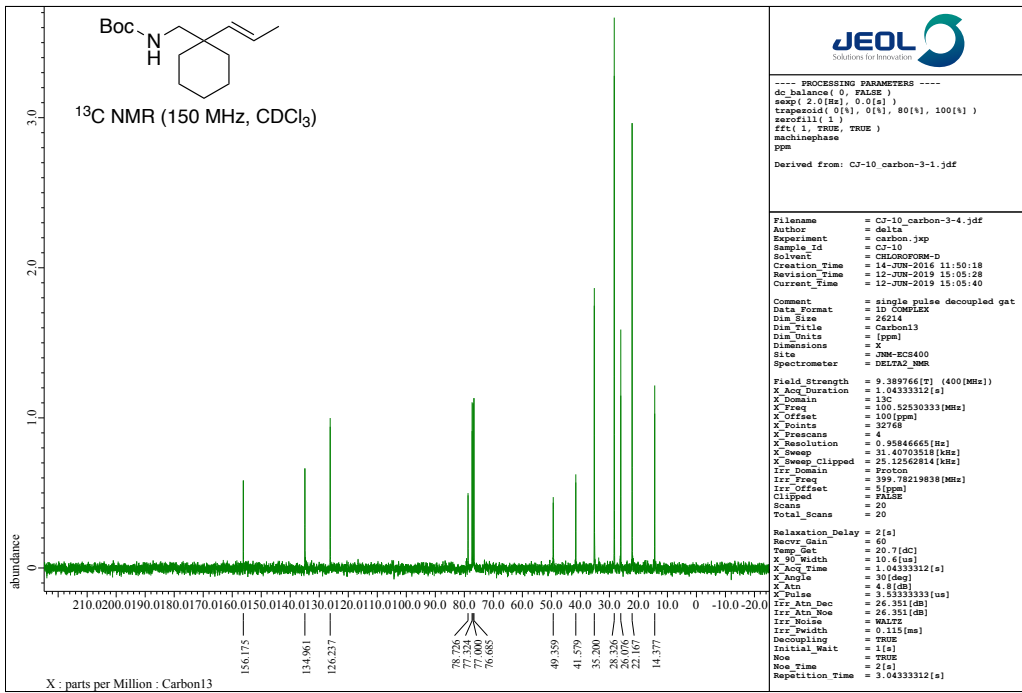


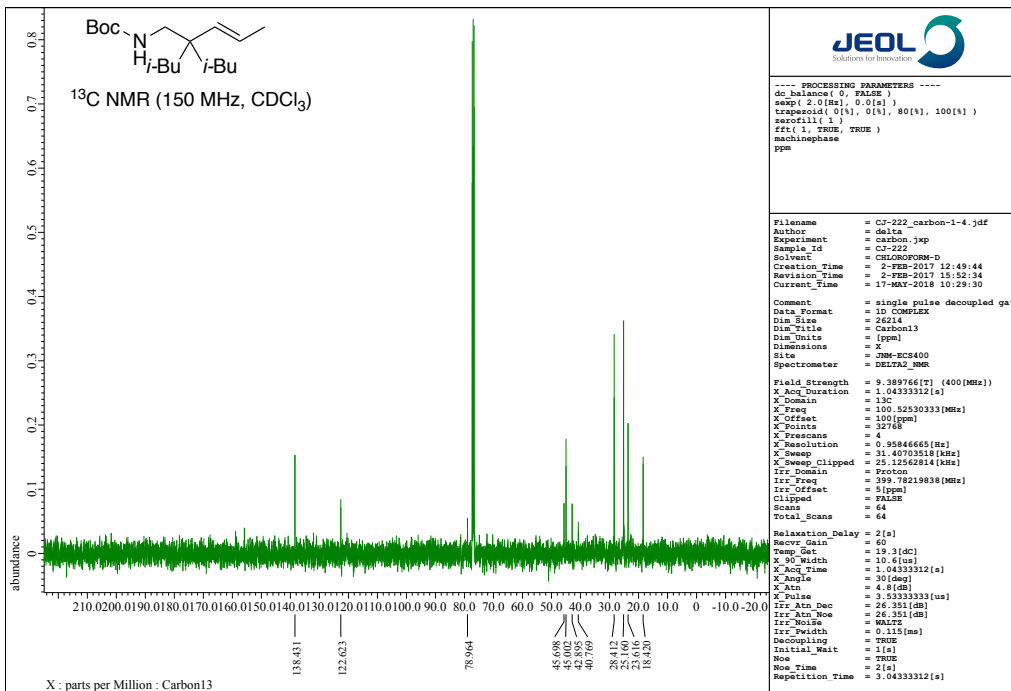
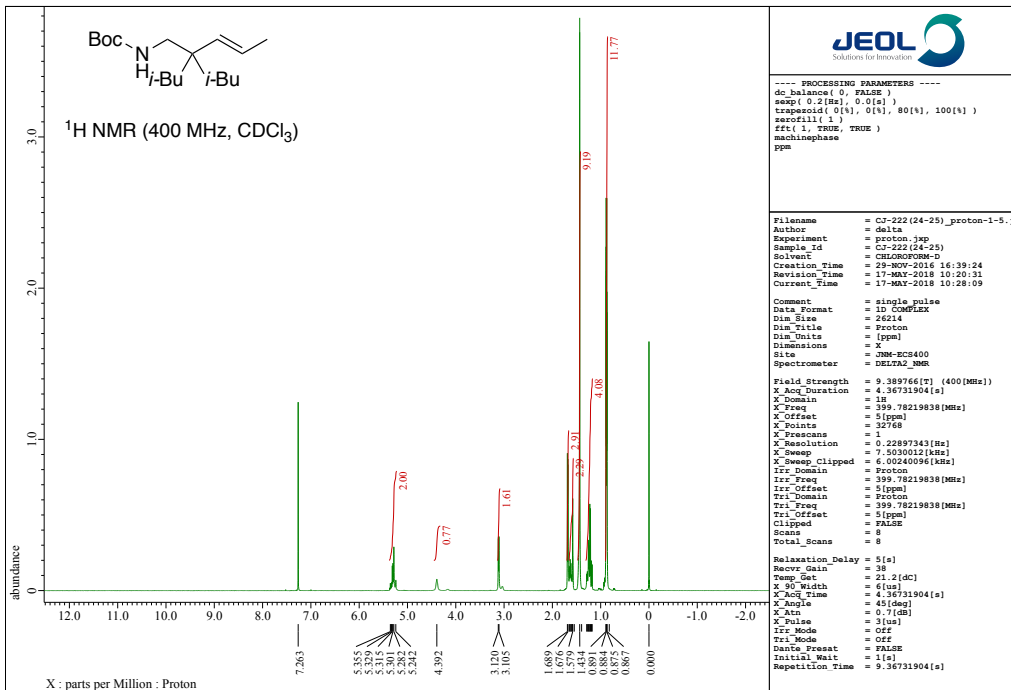


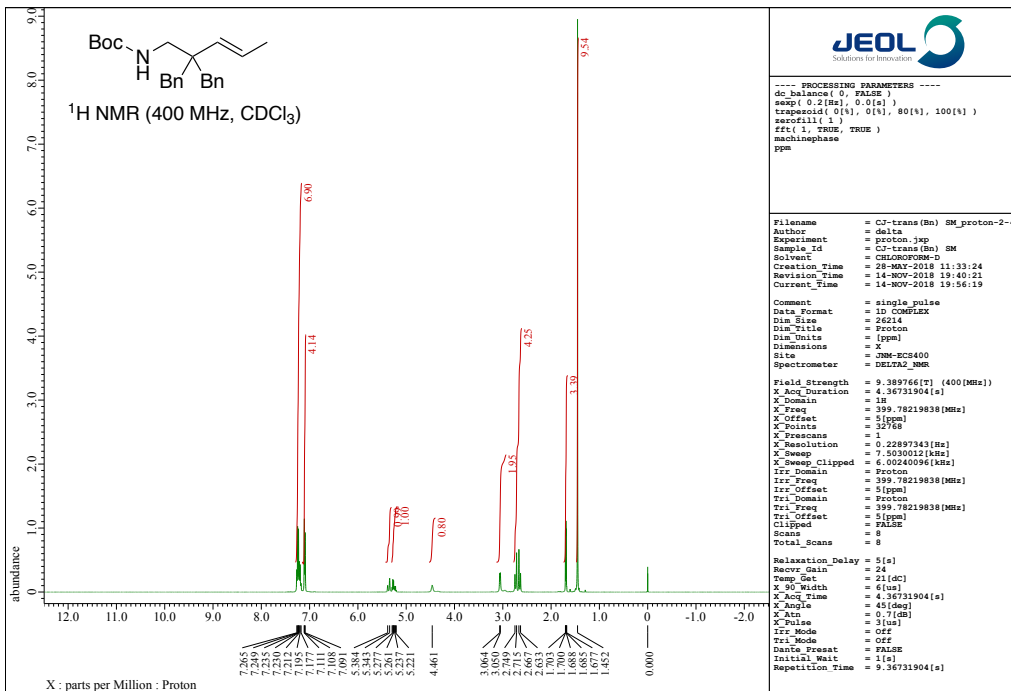
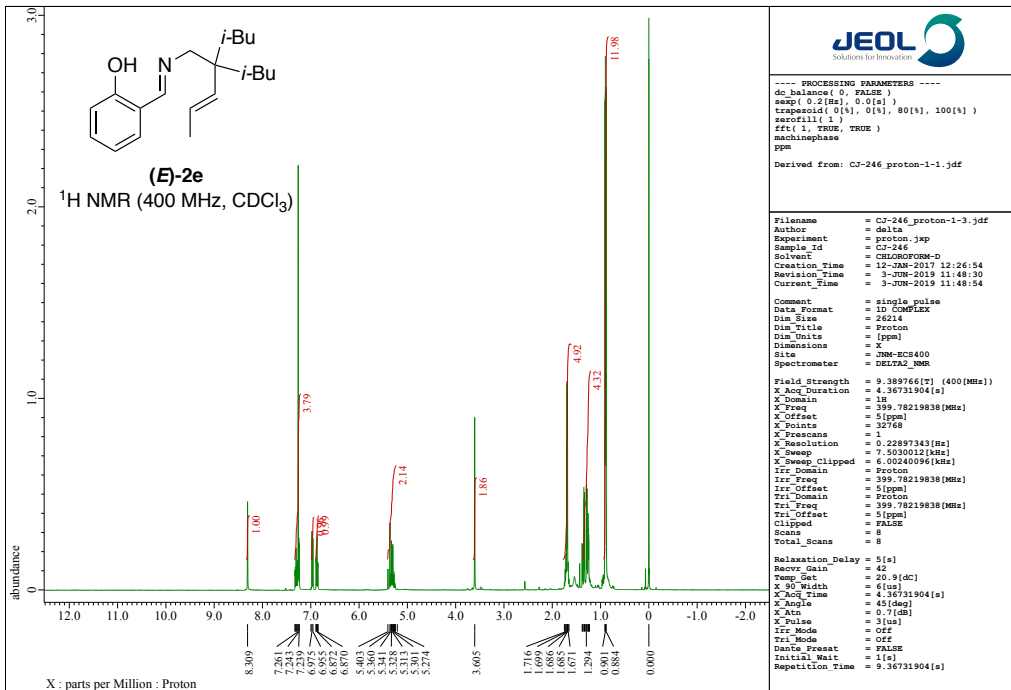


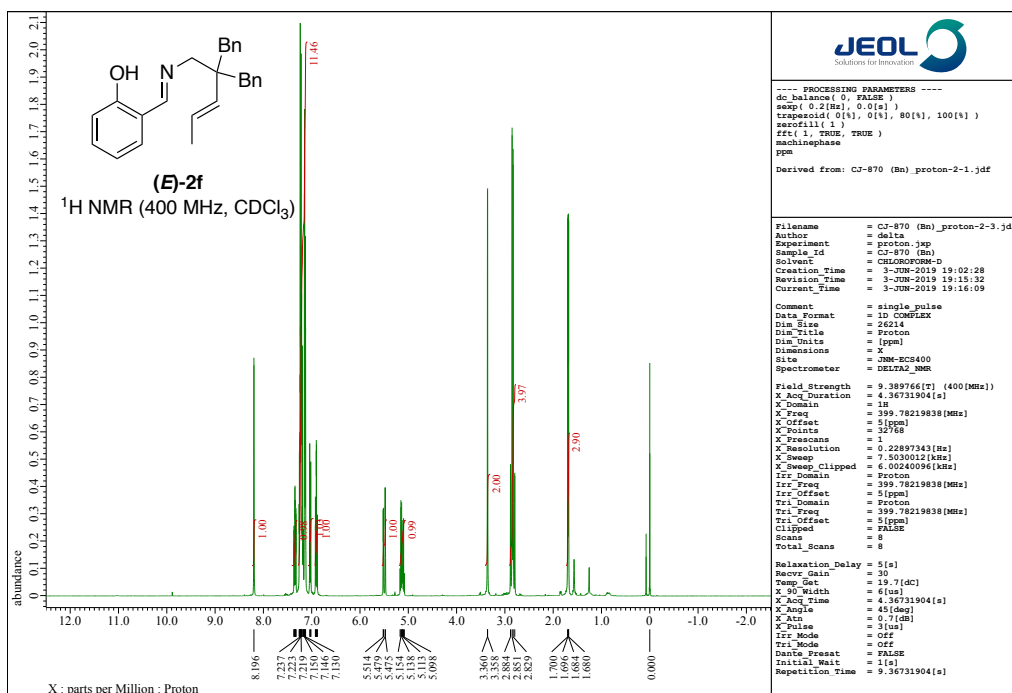
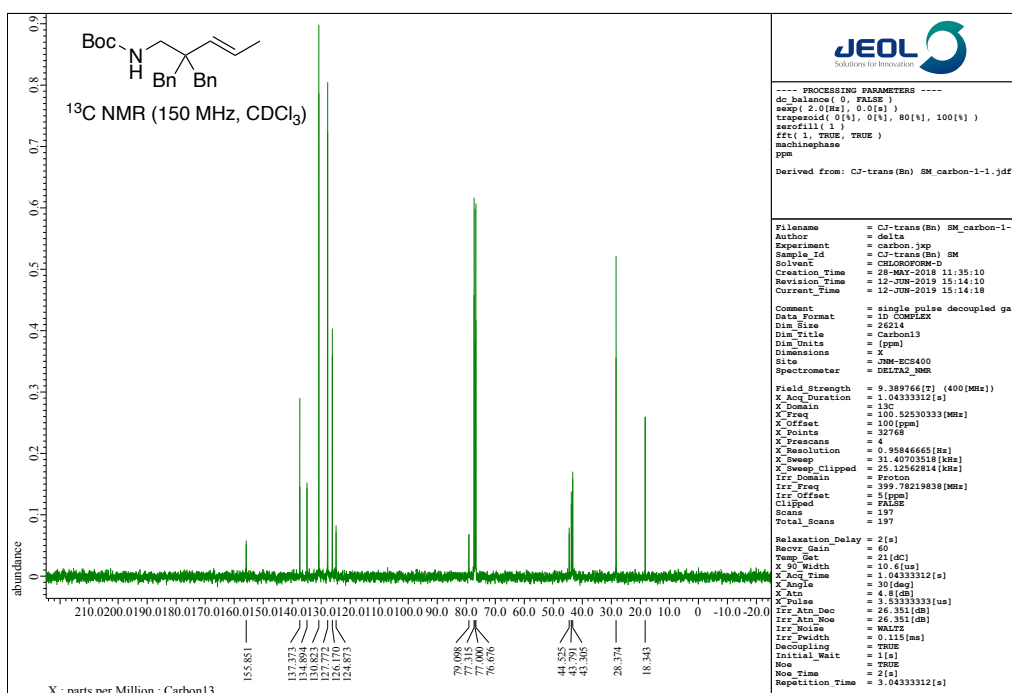


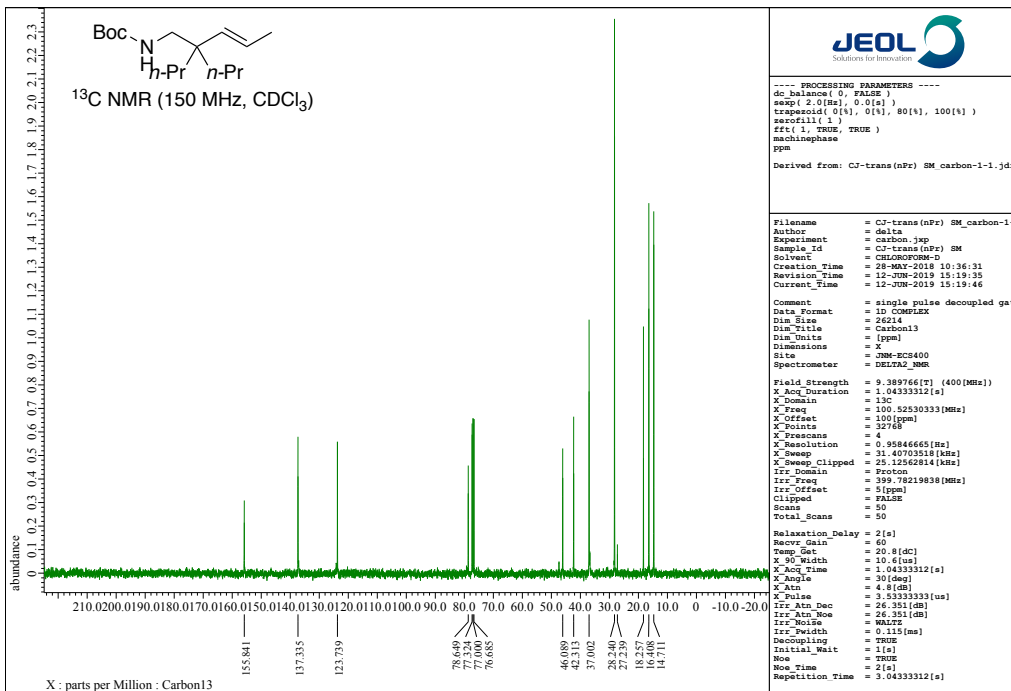
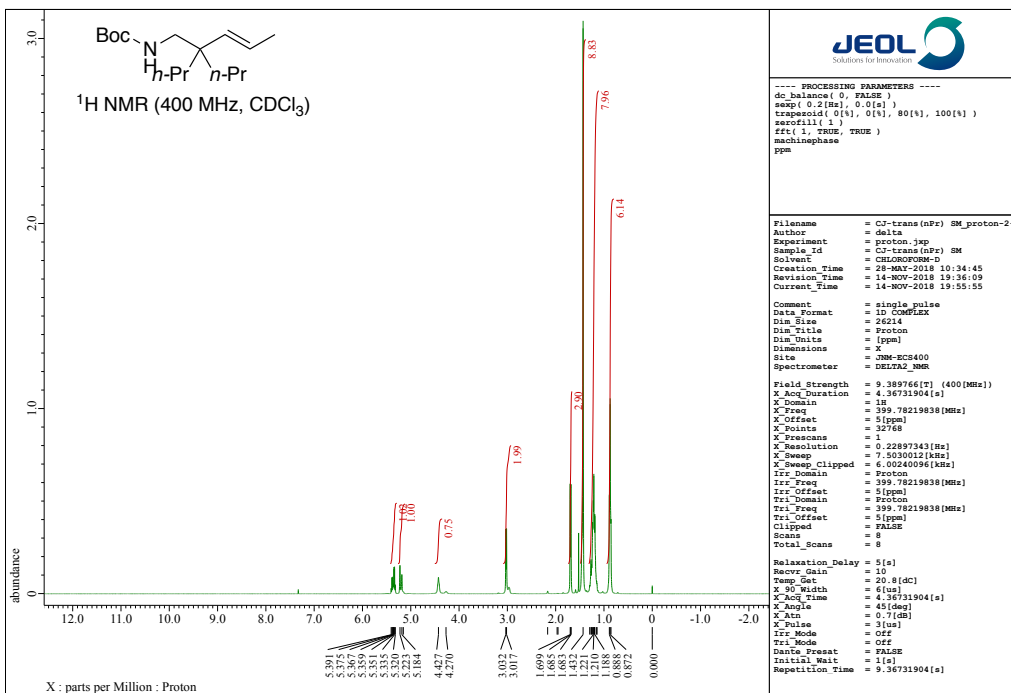


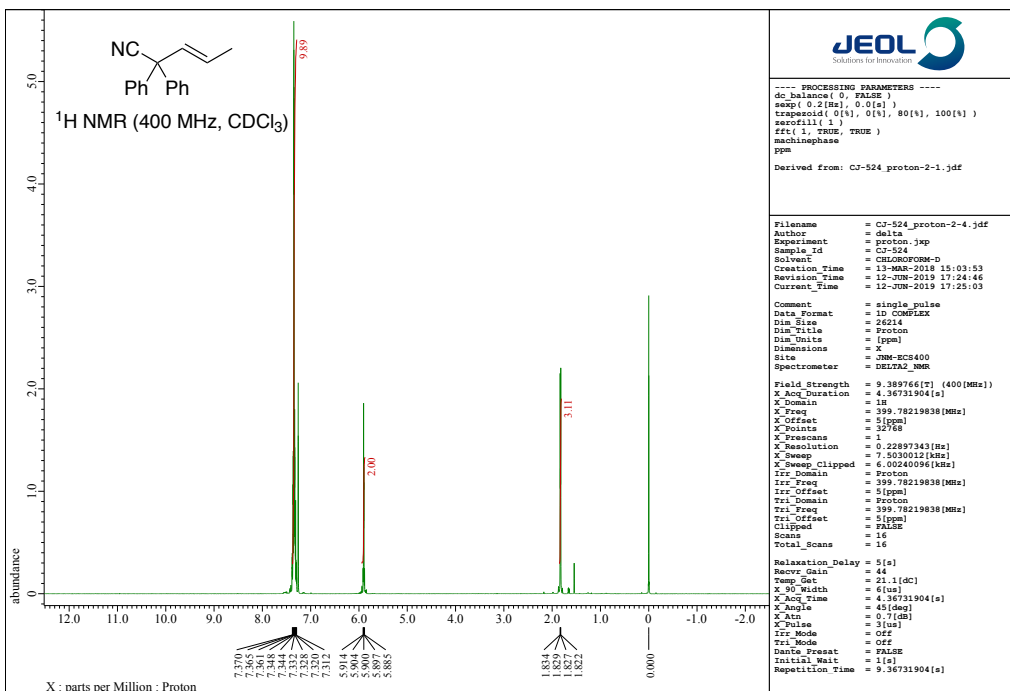
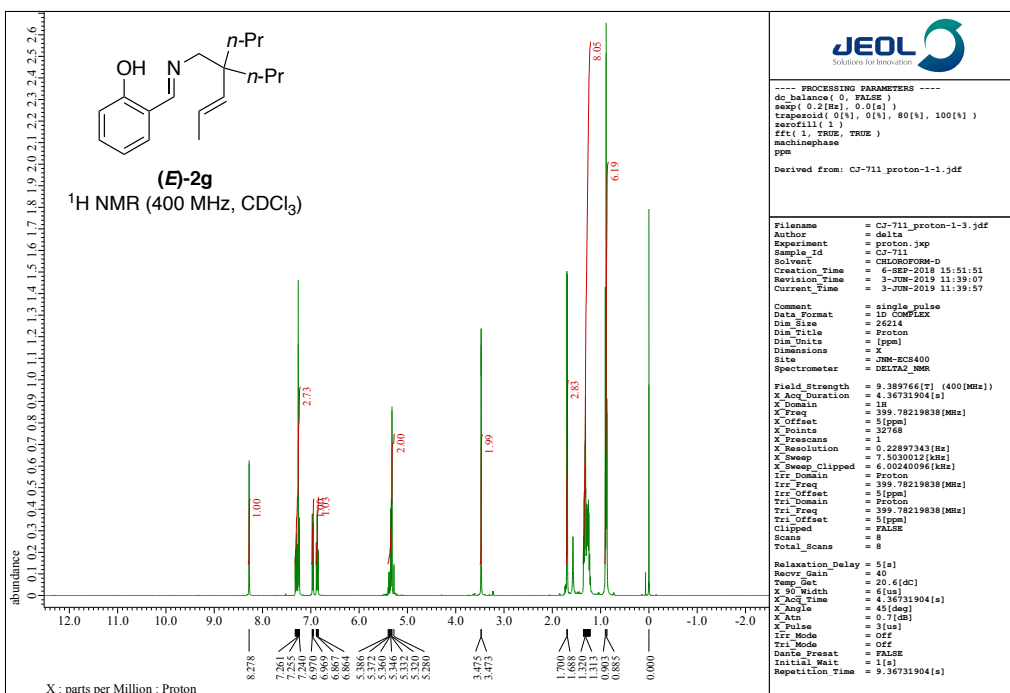


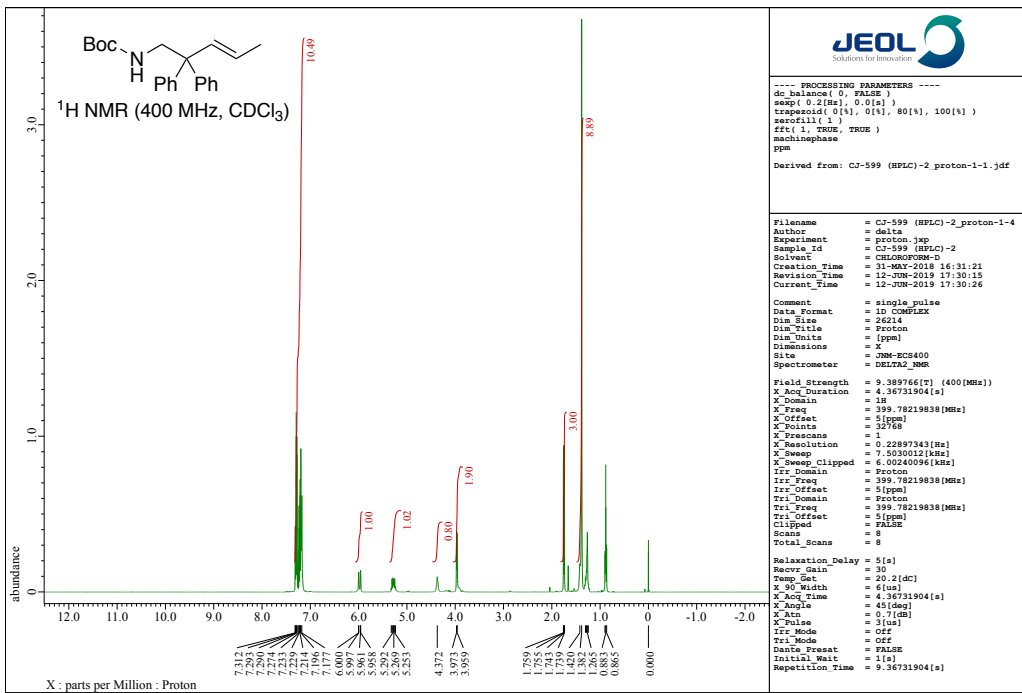
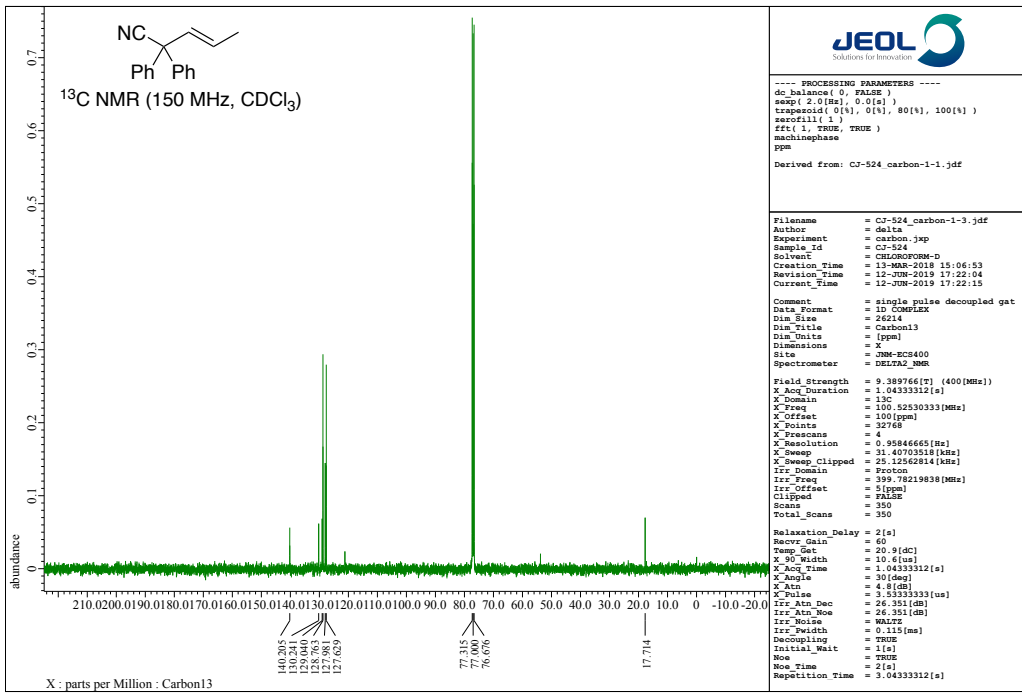


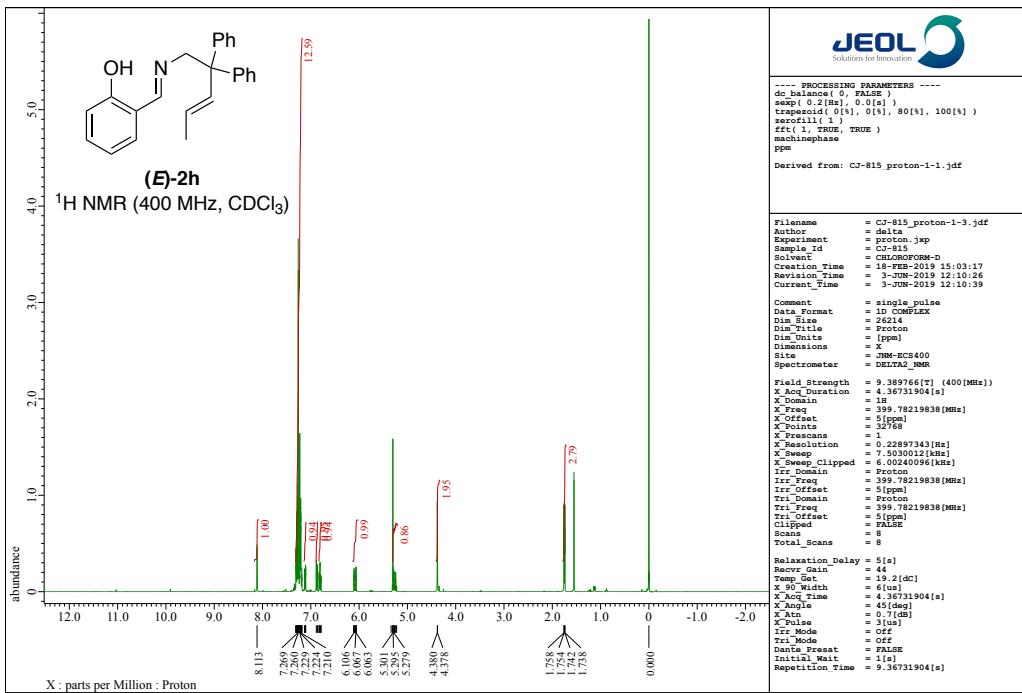
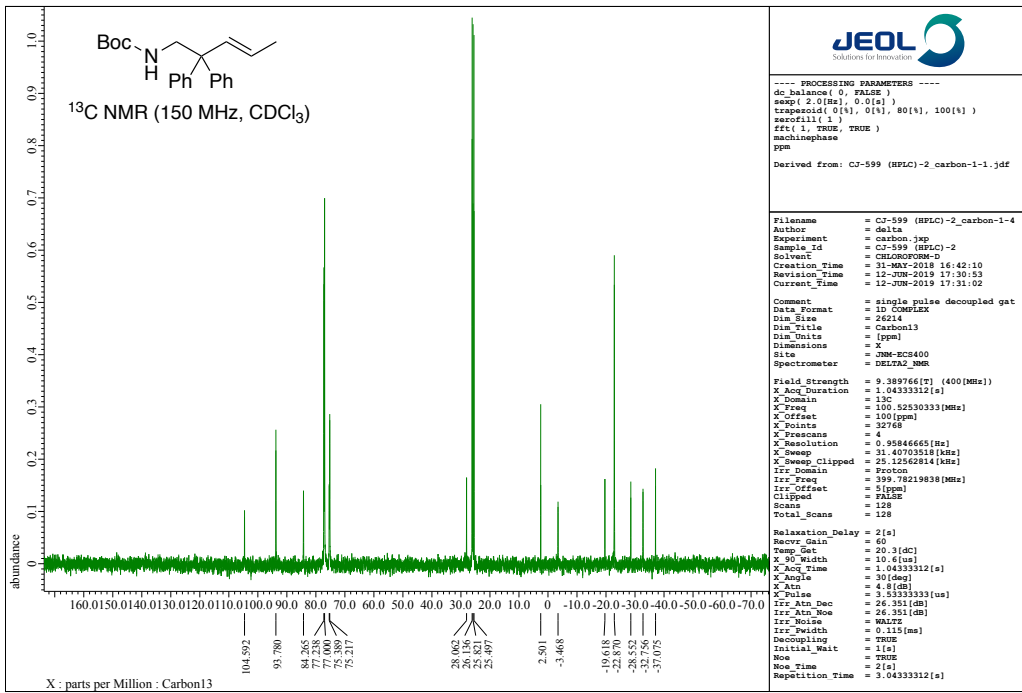


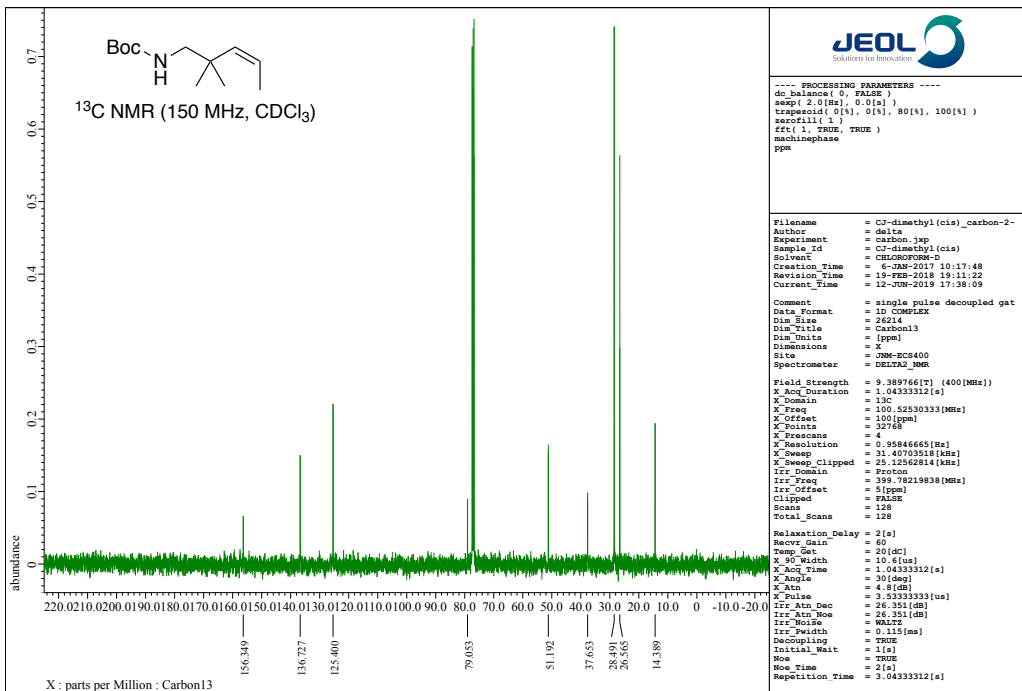
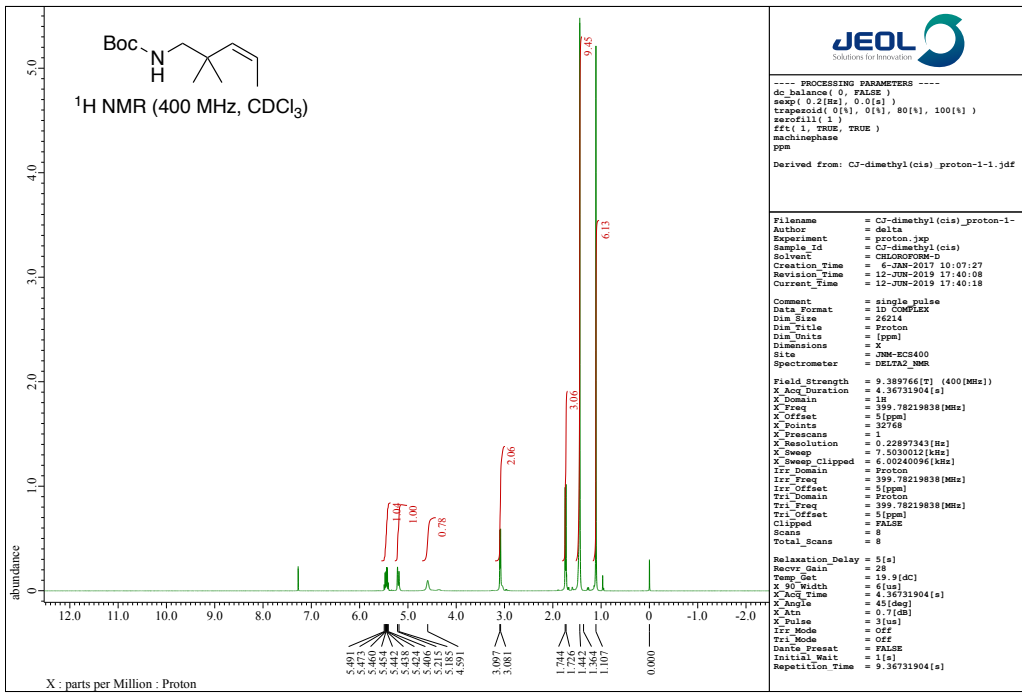


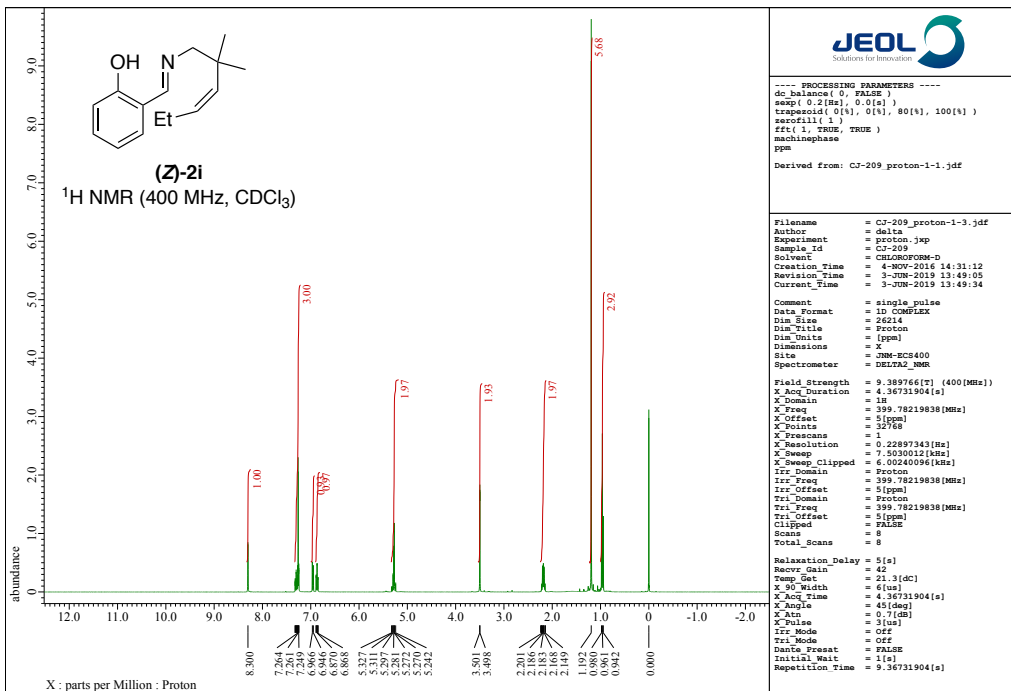
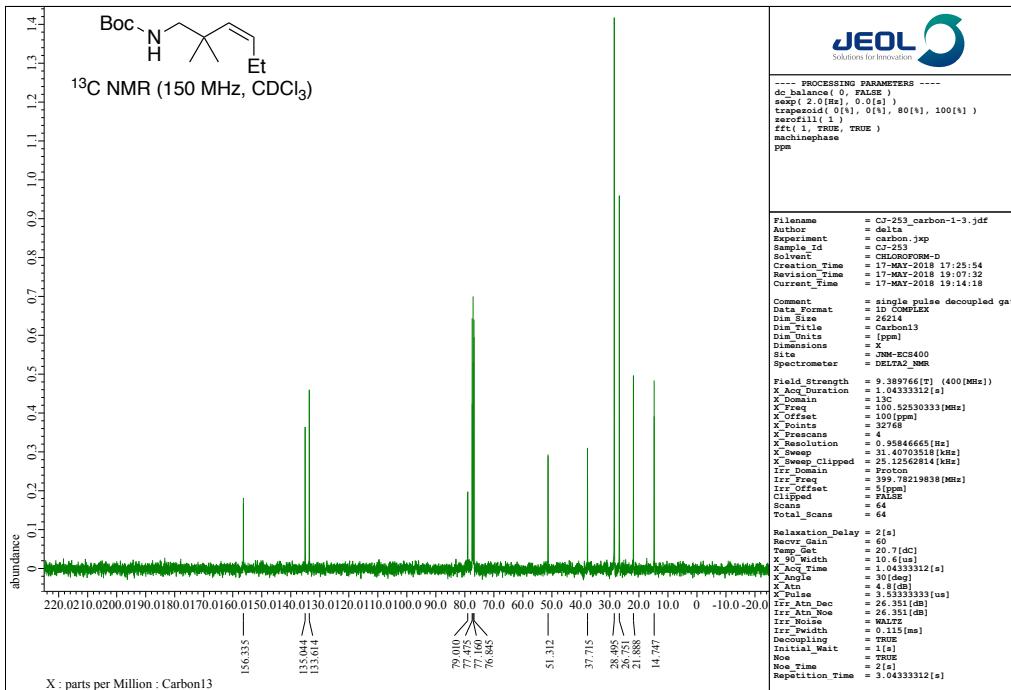


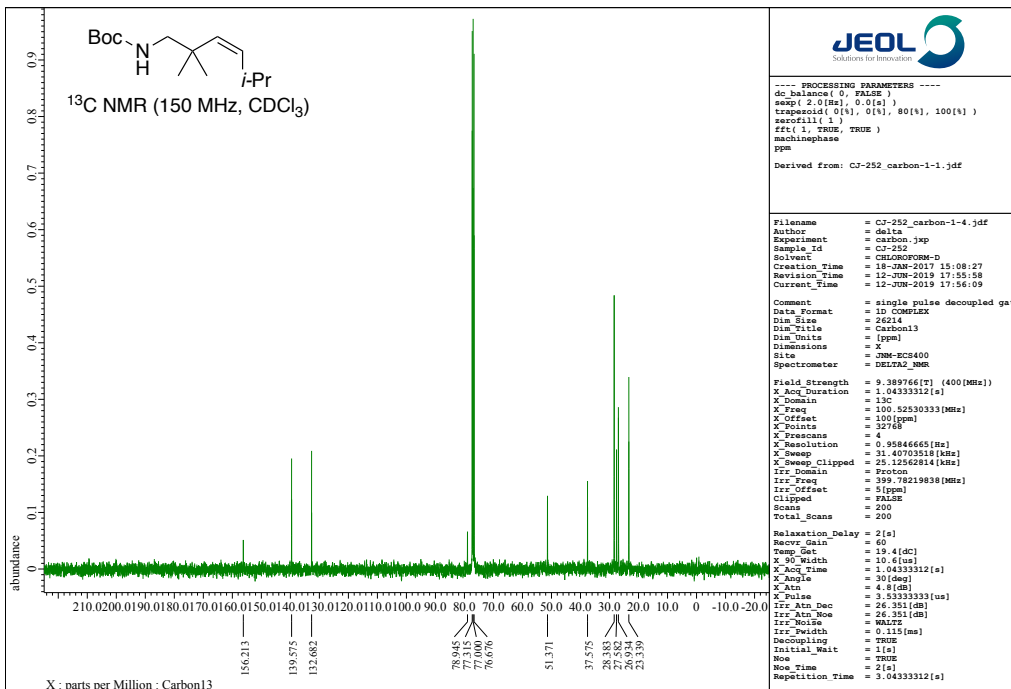
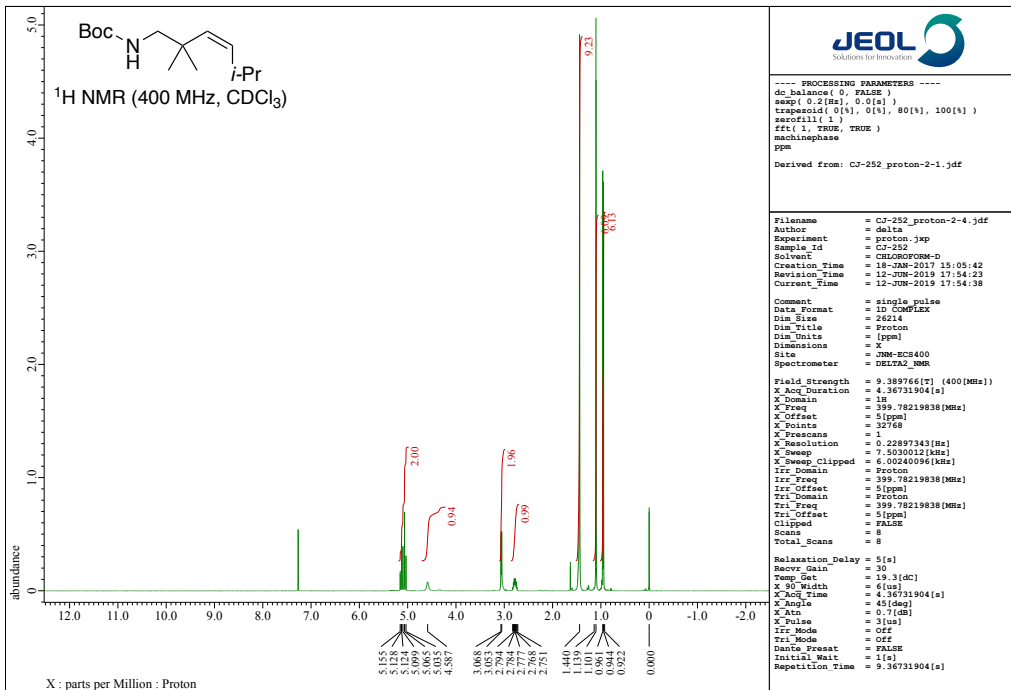


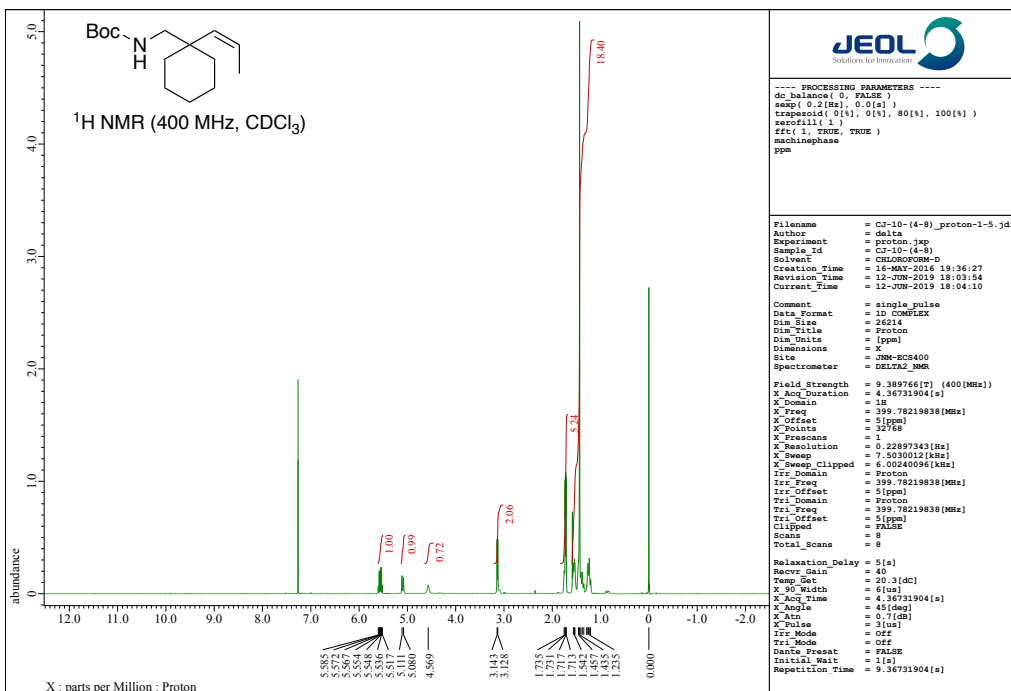
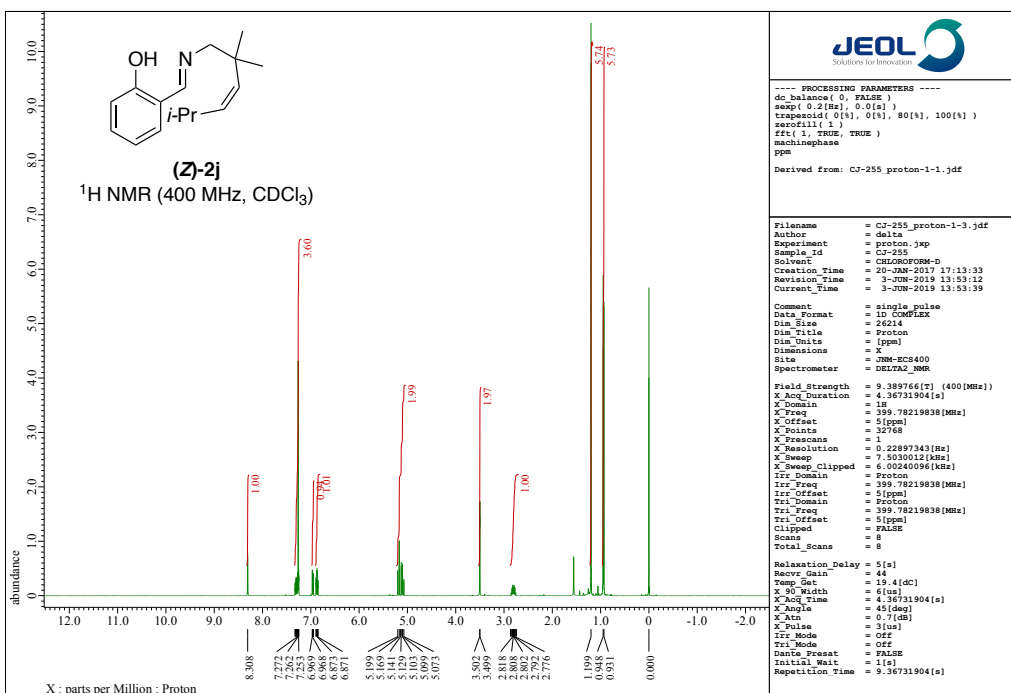


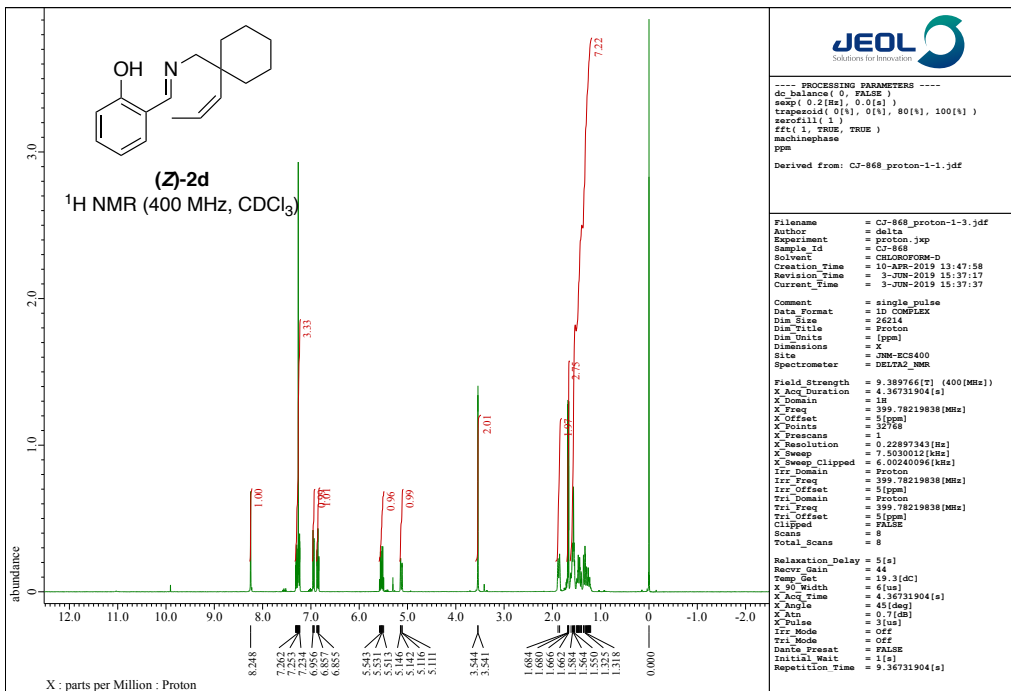
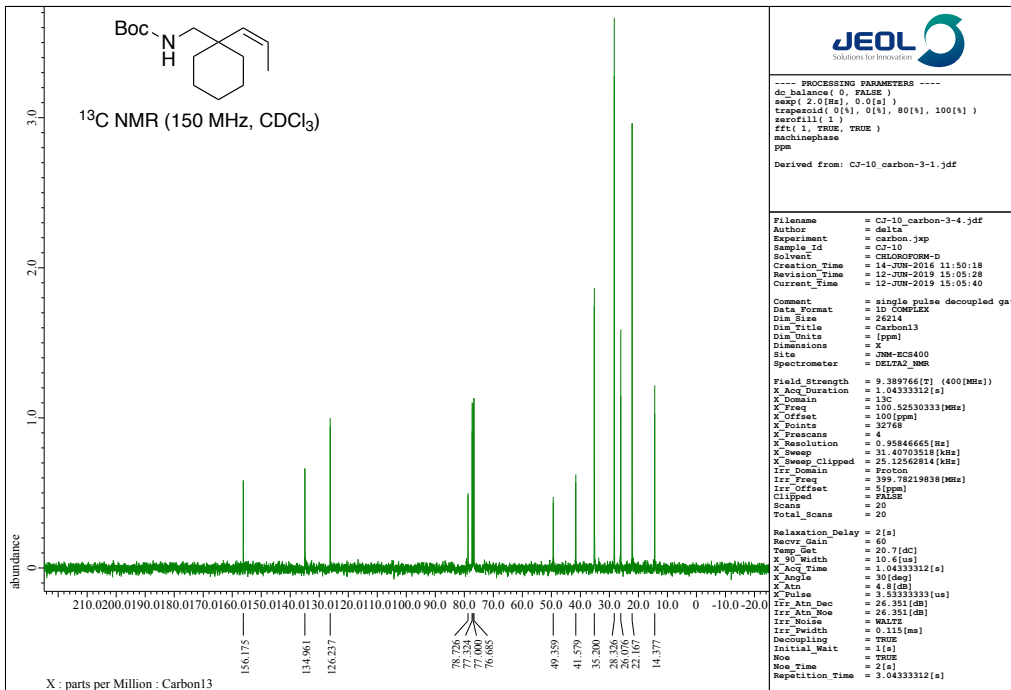


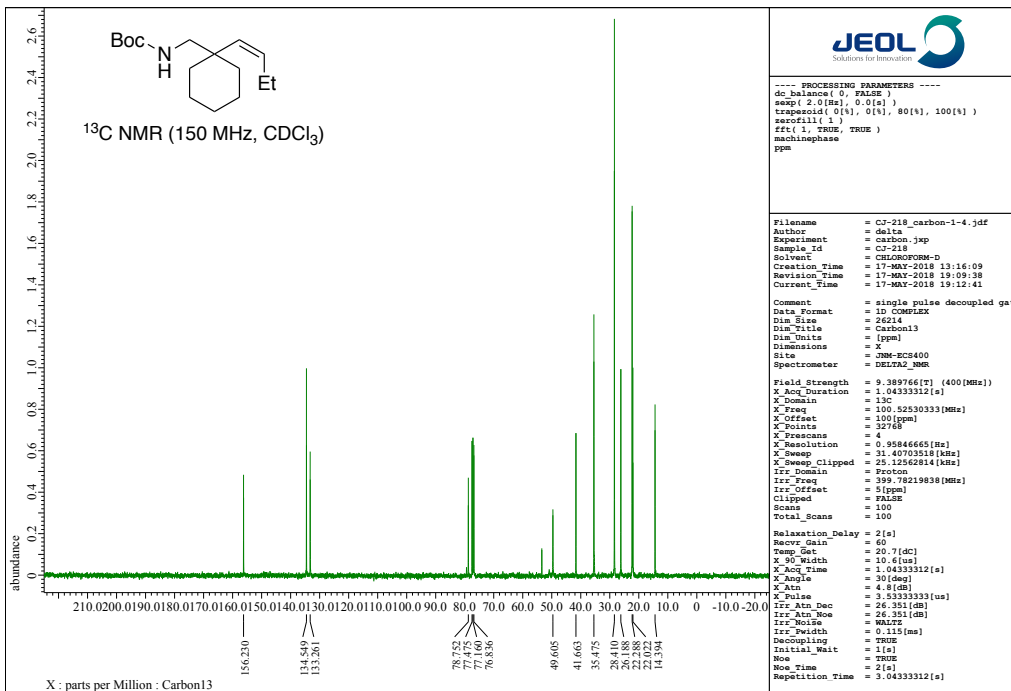
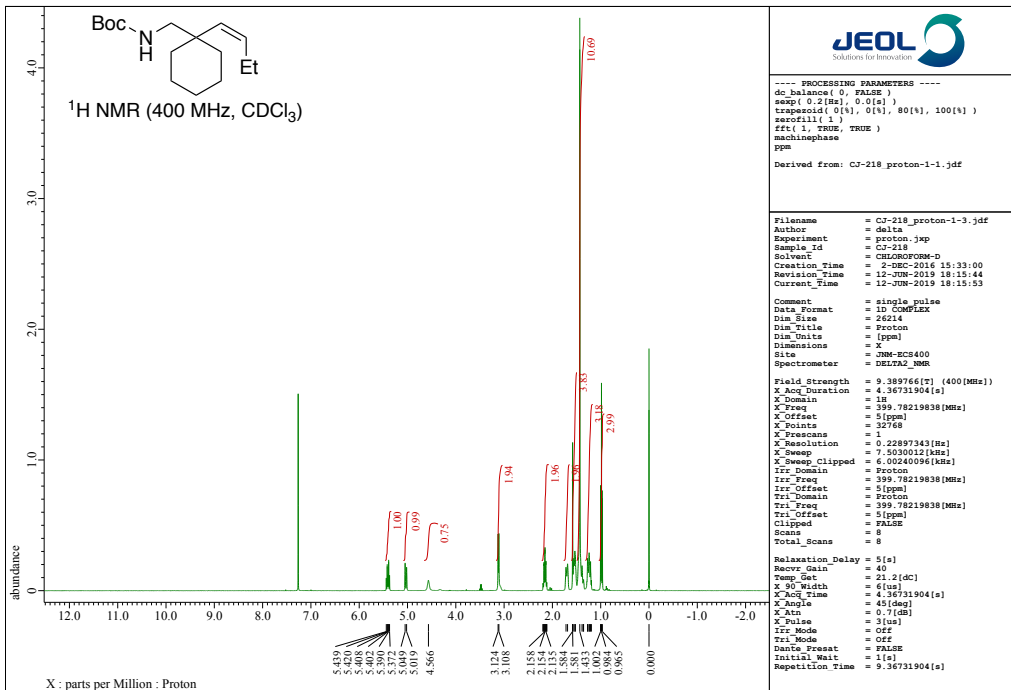


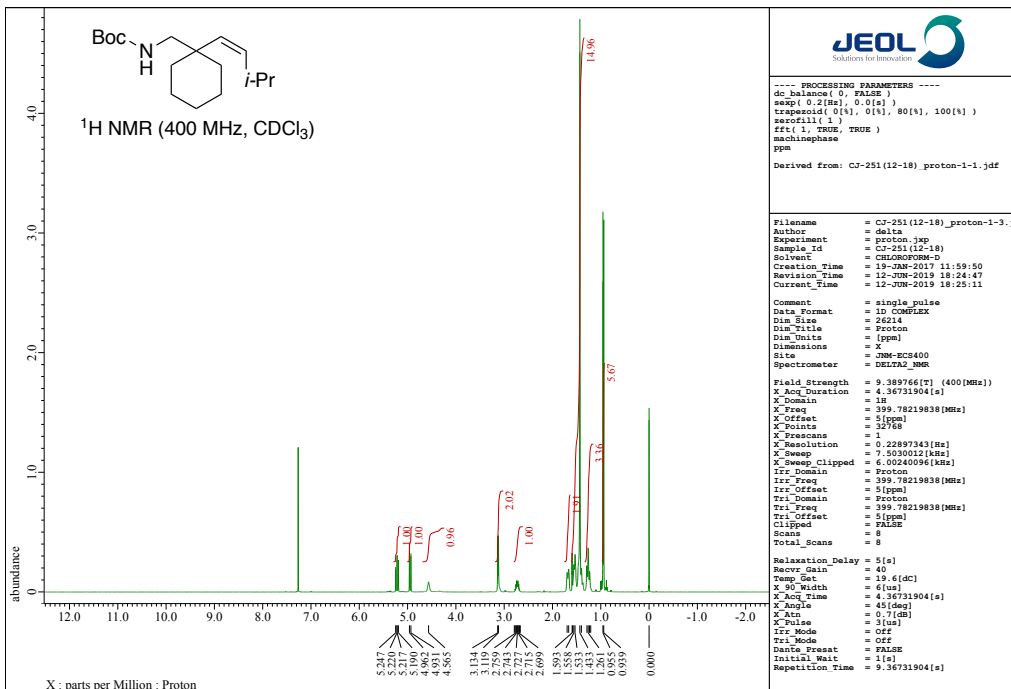
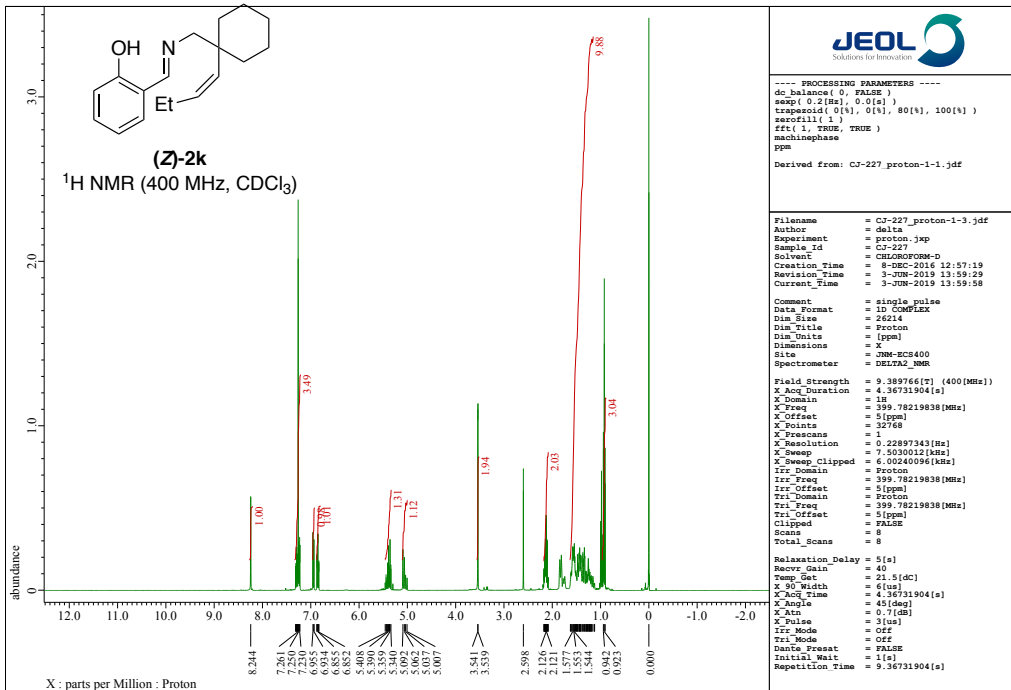


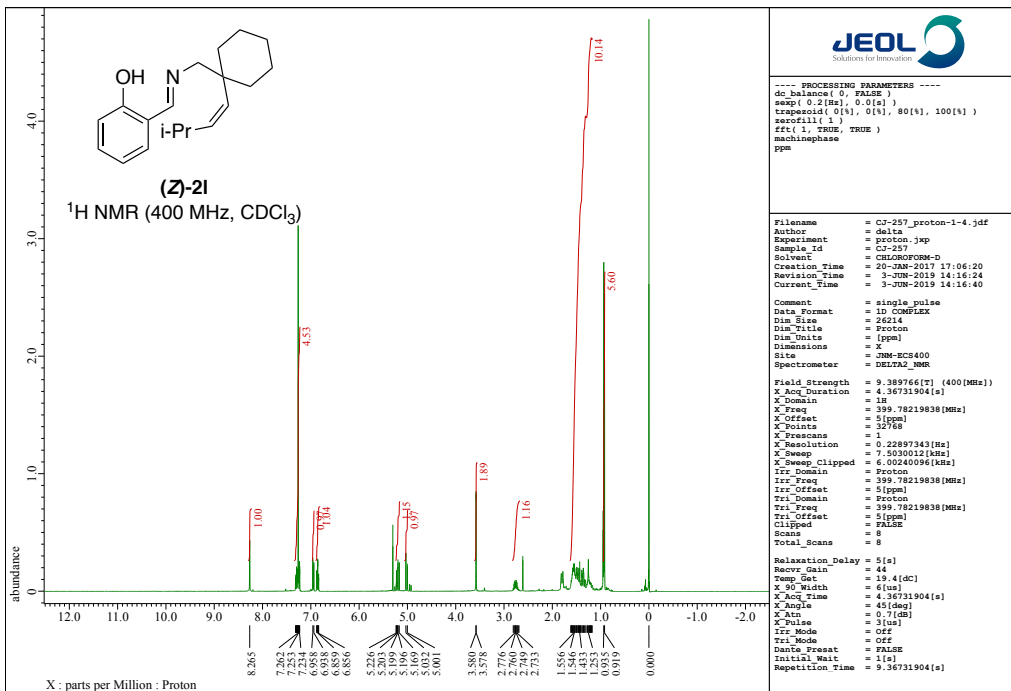
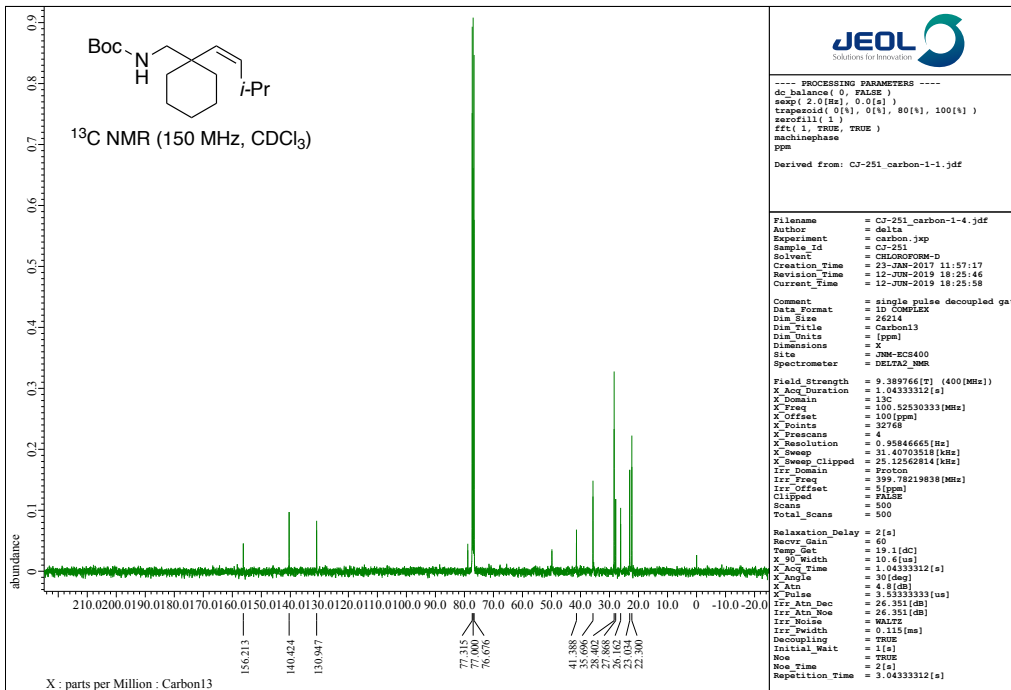


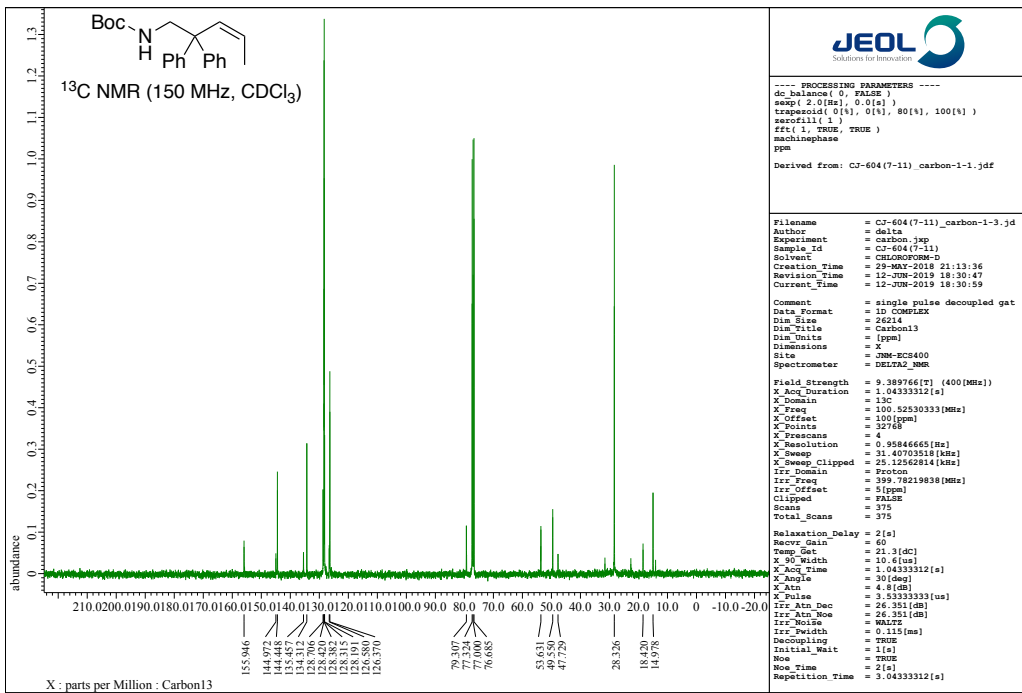
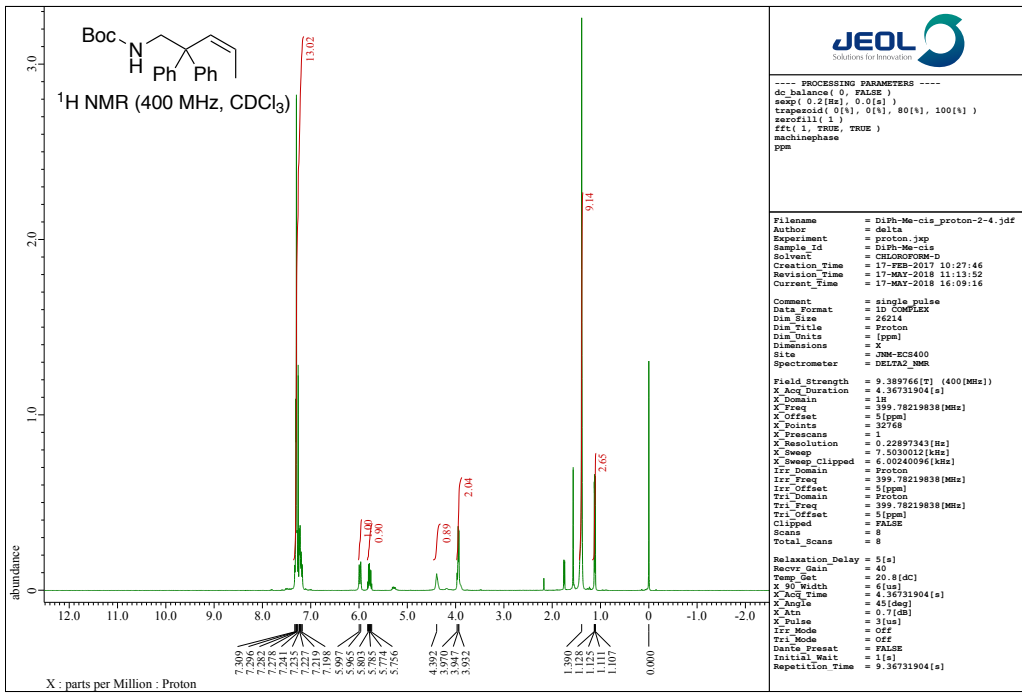


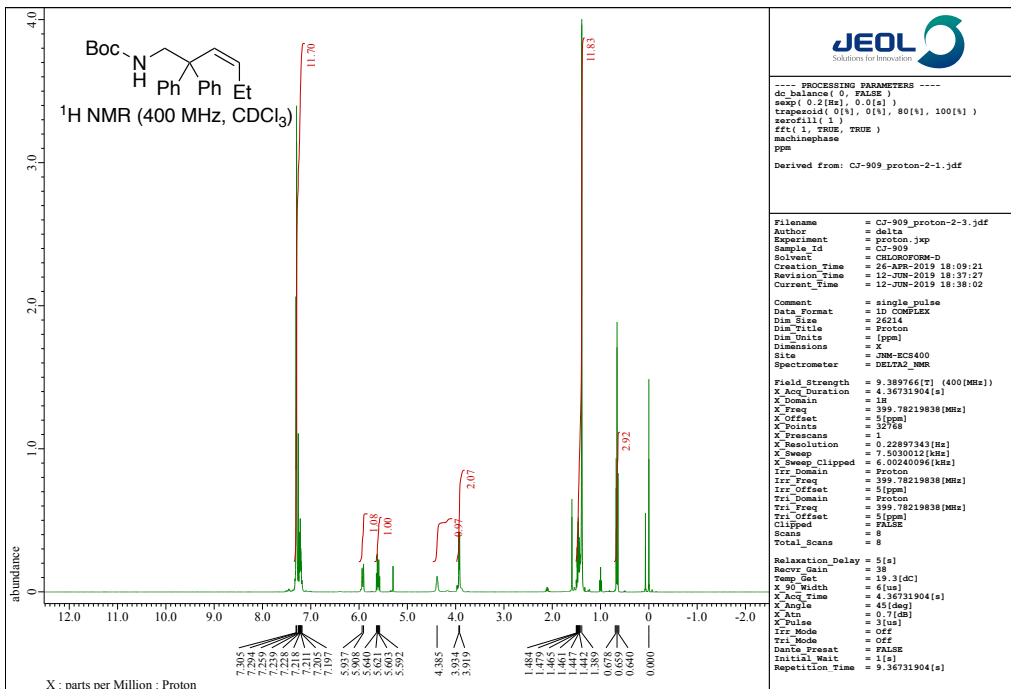
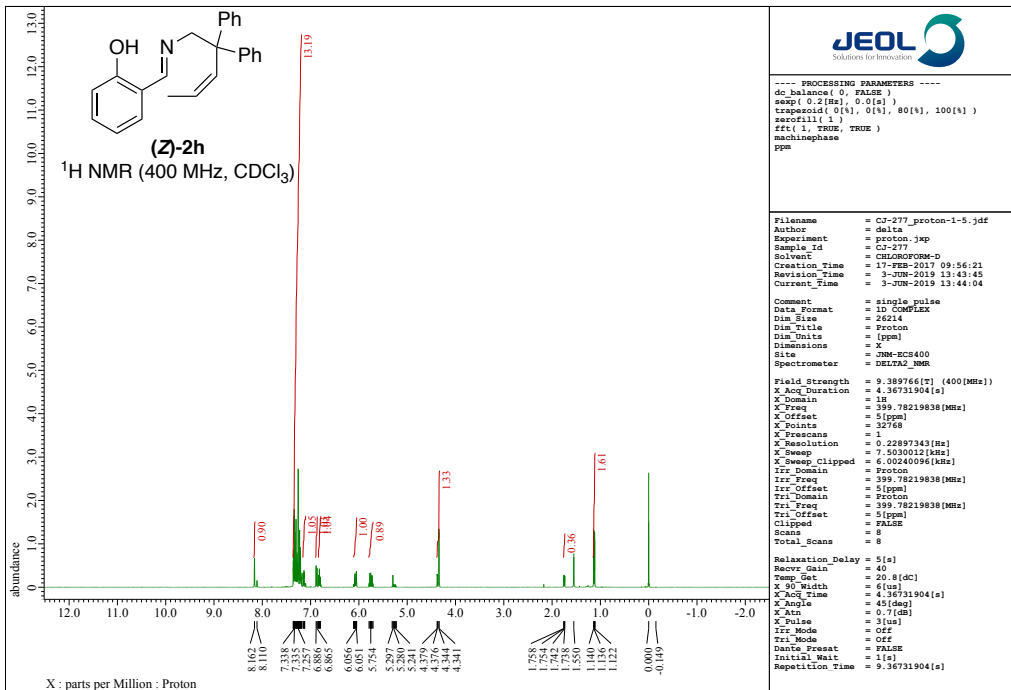


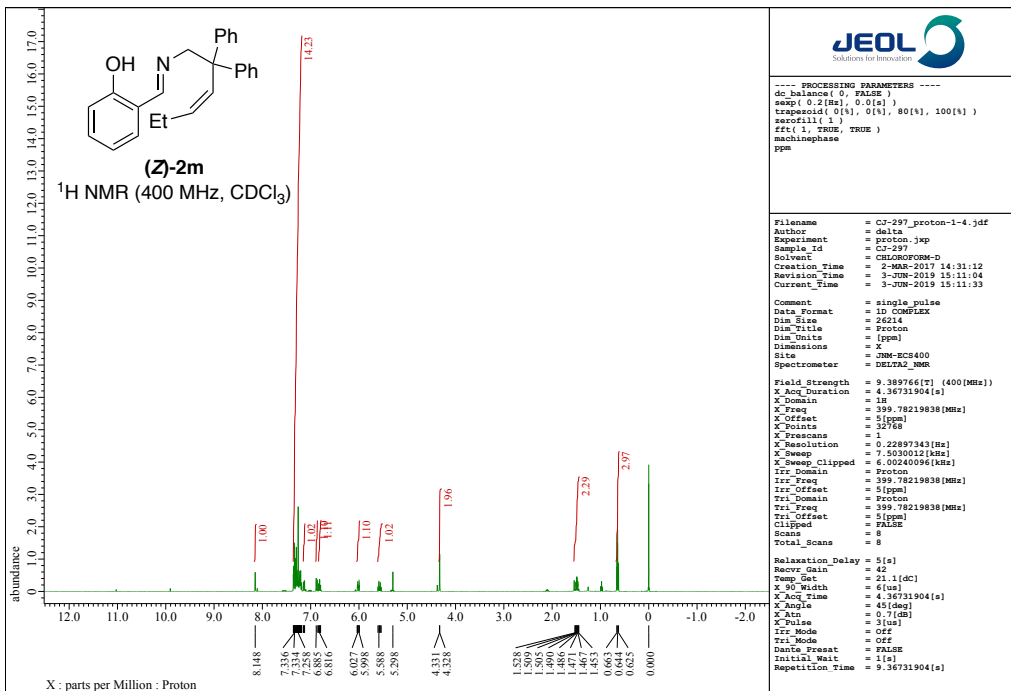
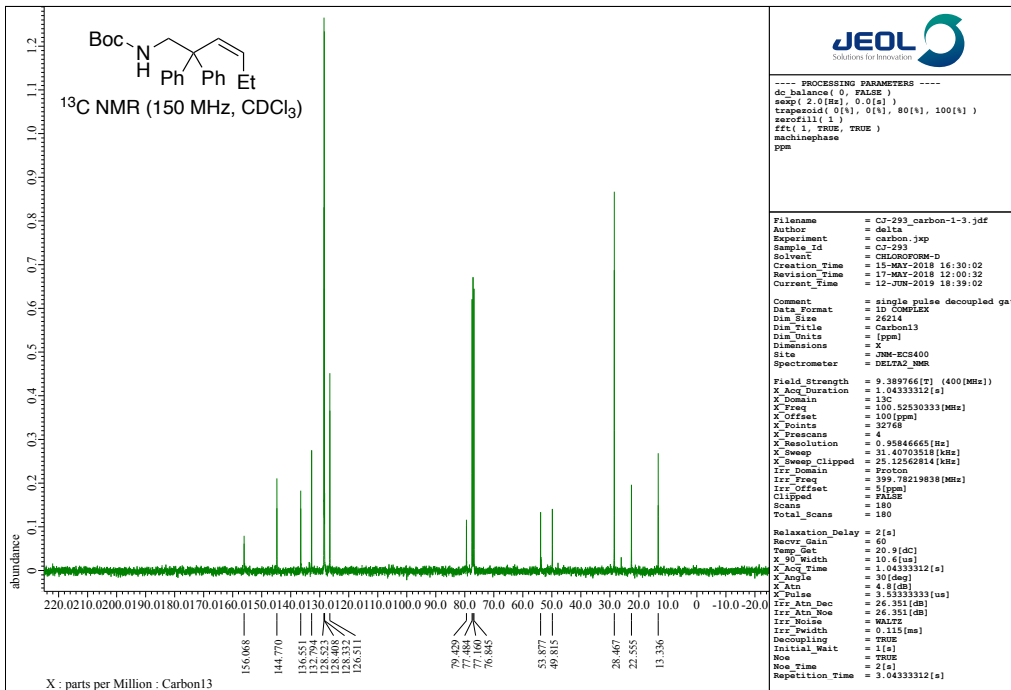




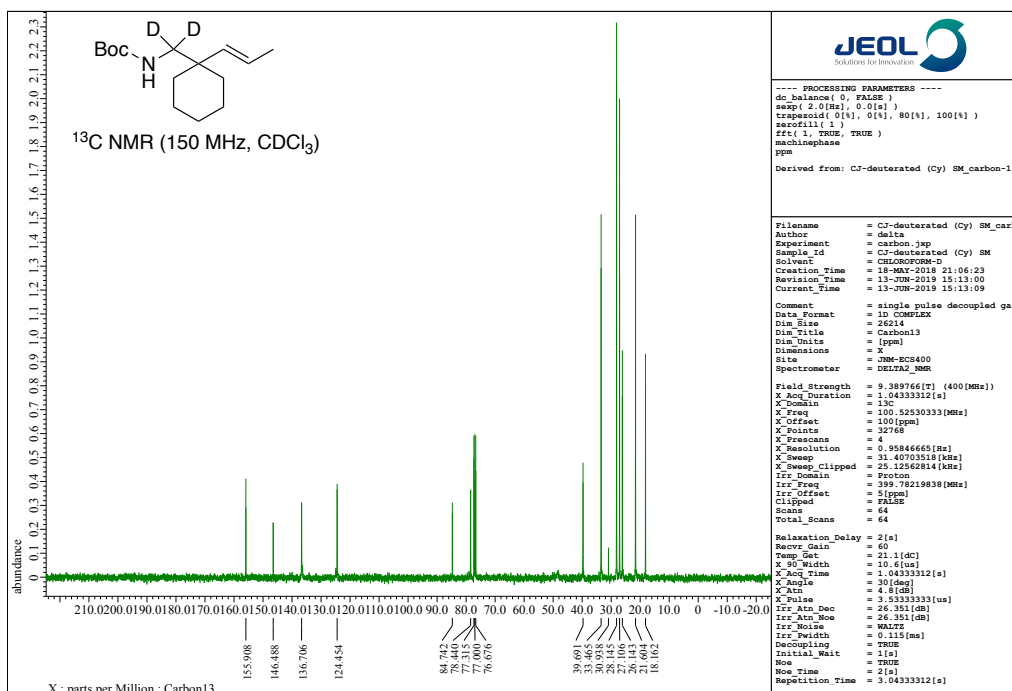
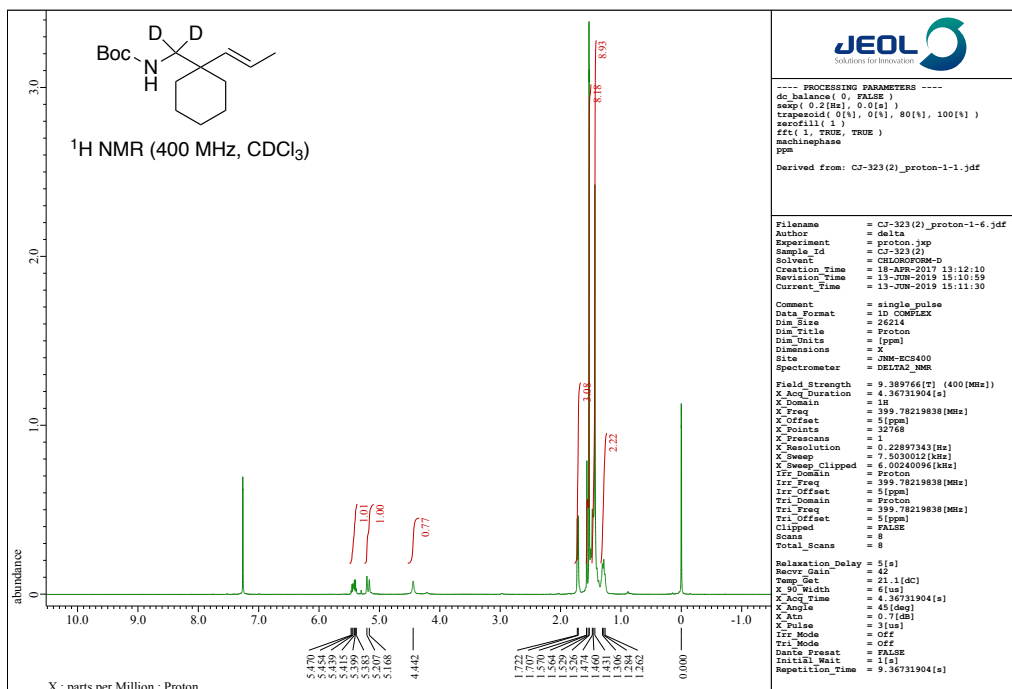


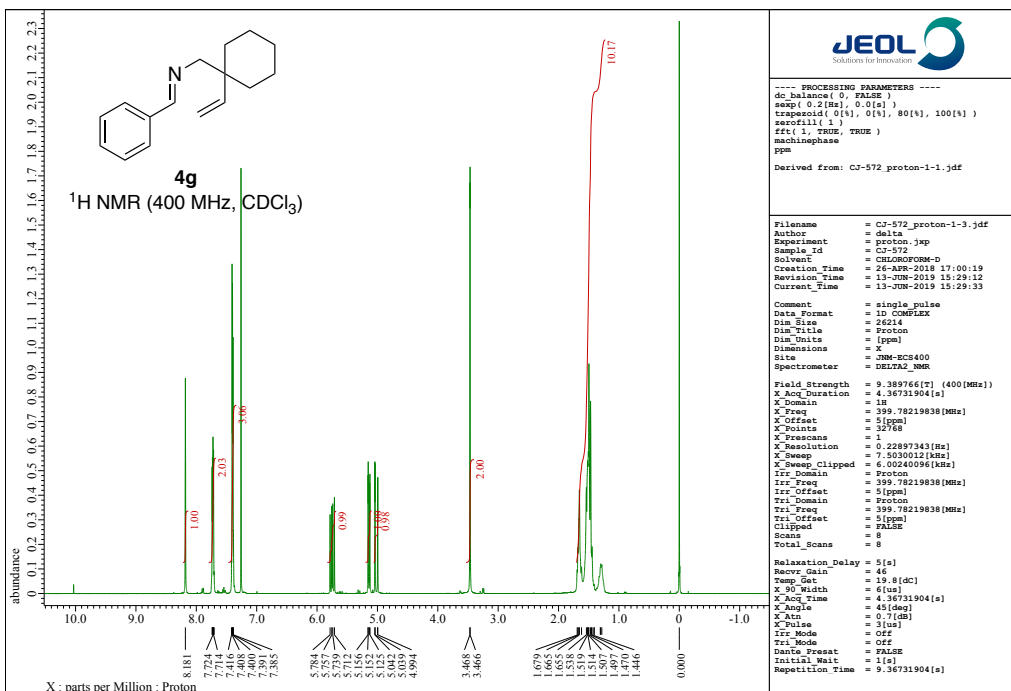
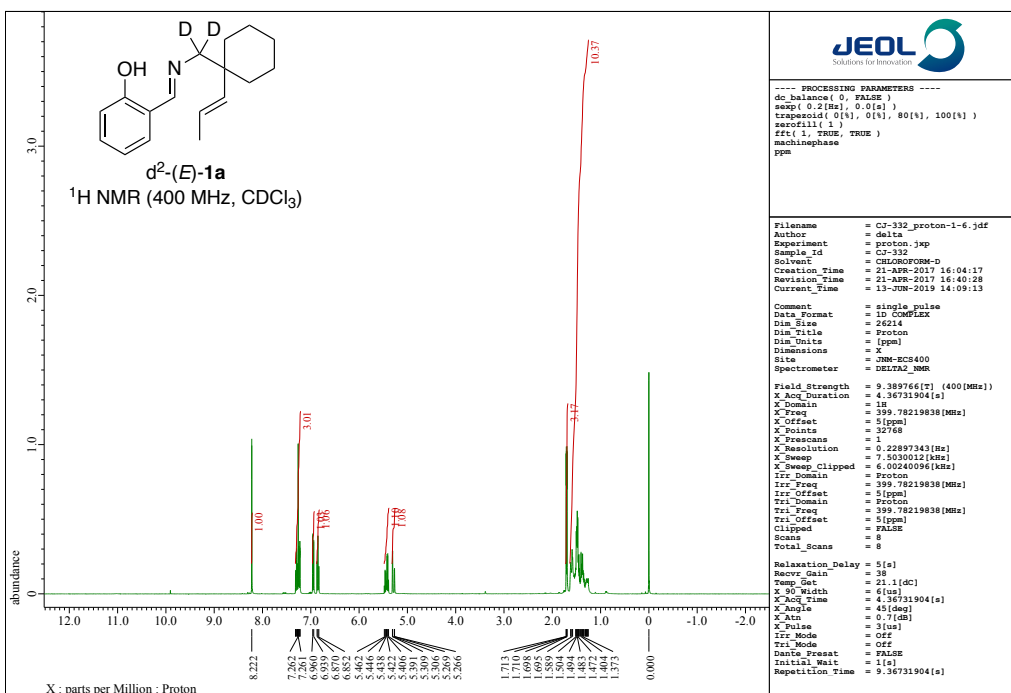


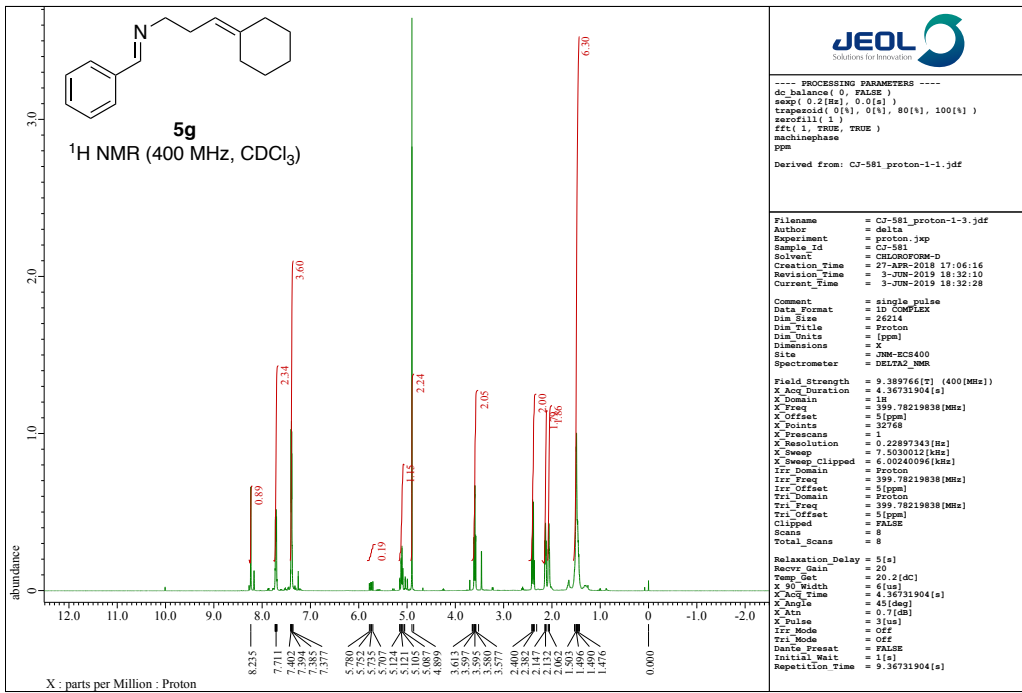




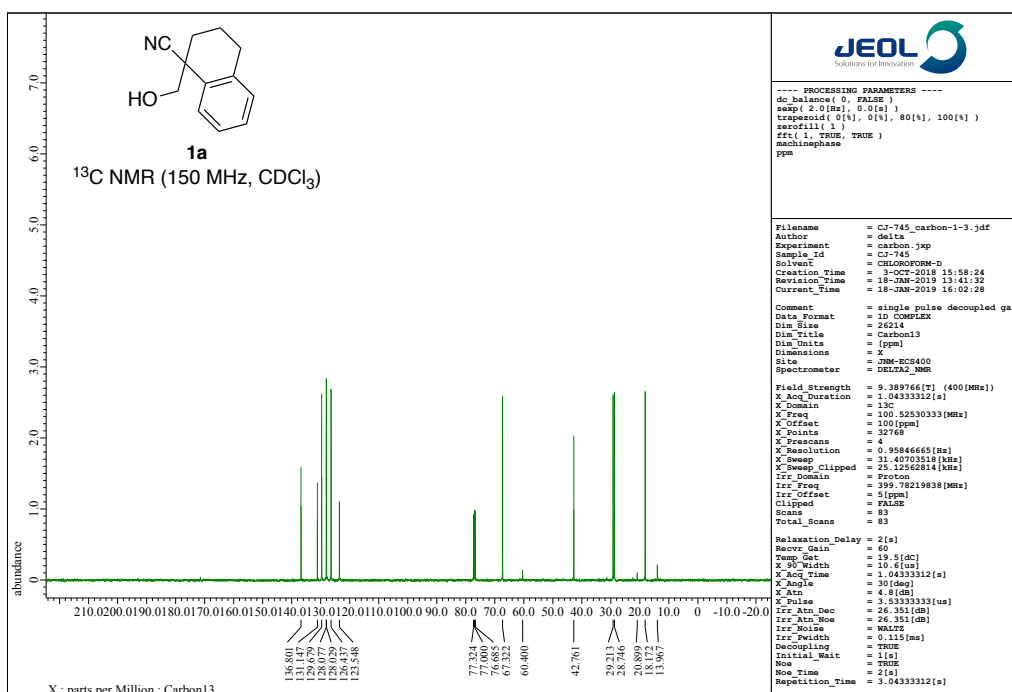
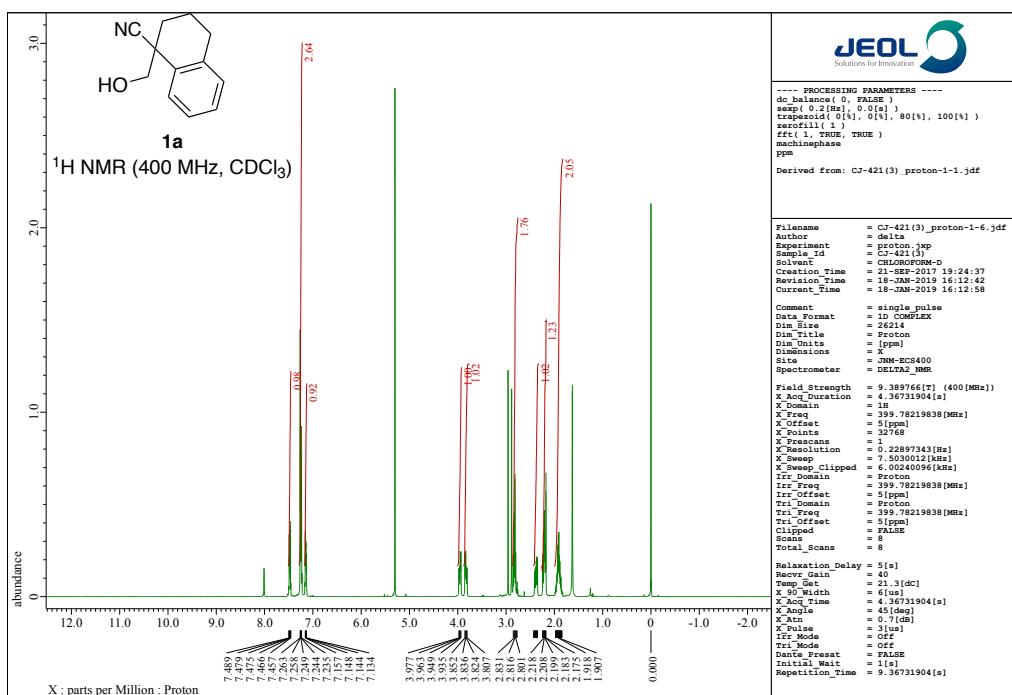
Chapter 3

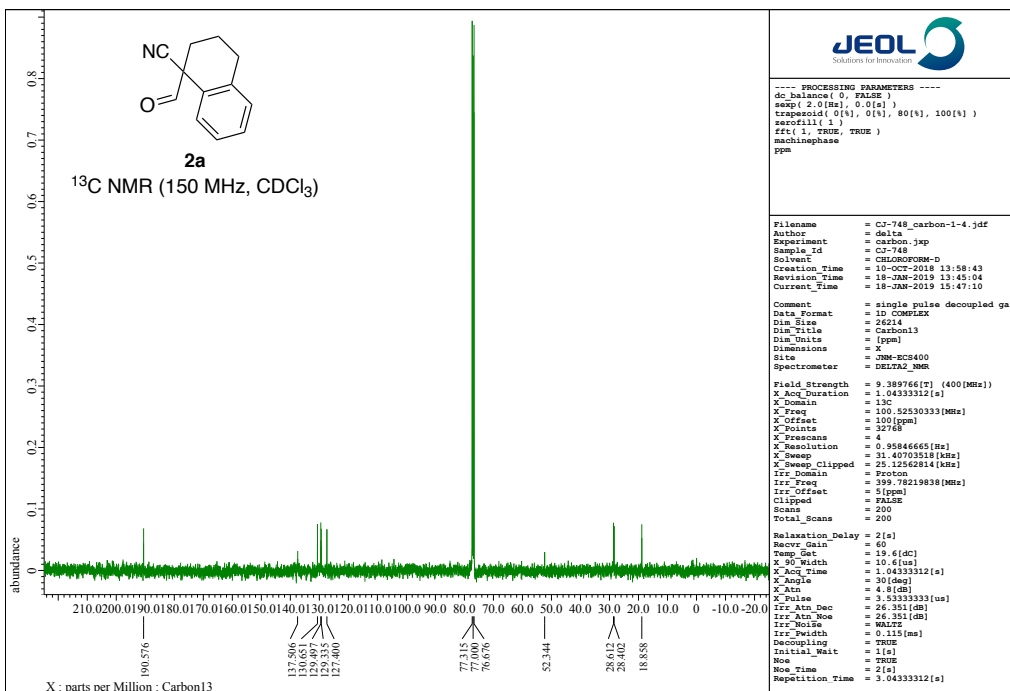
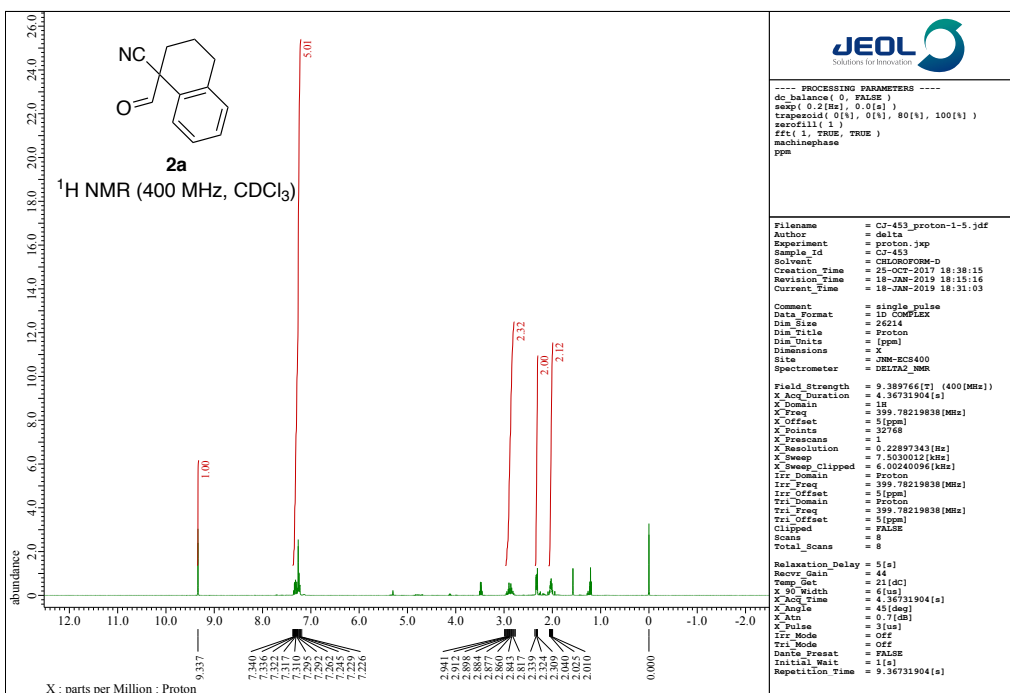


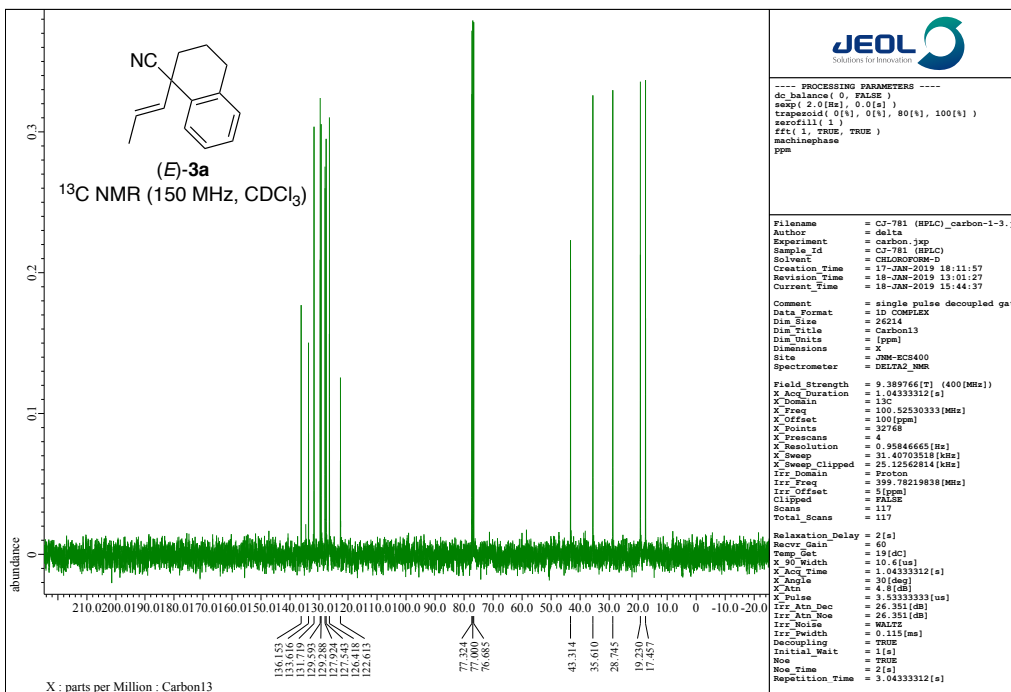
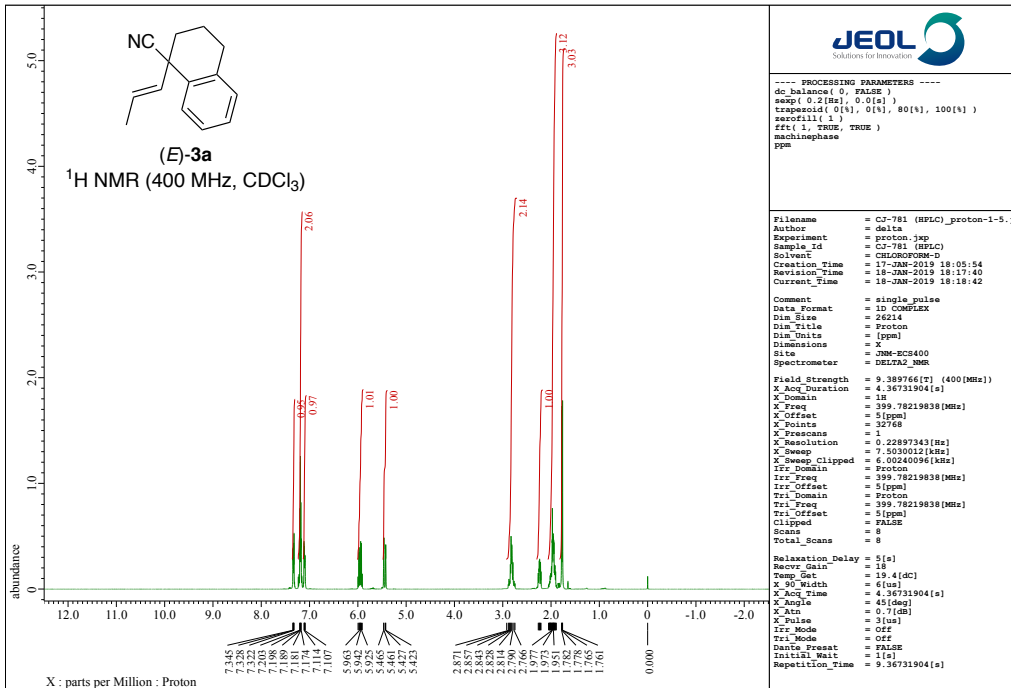


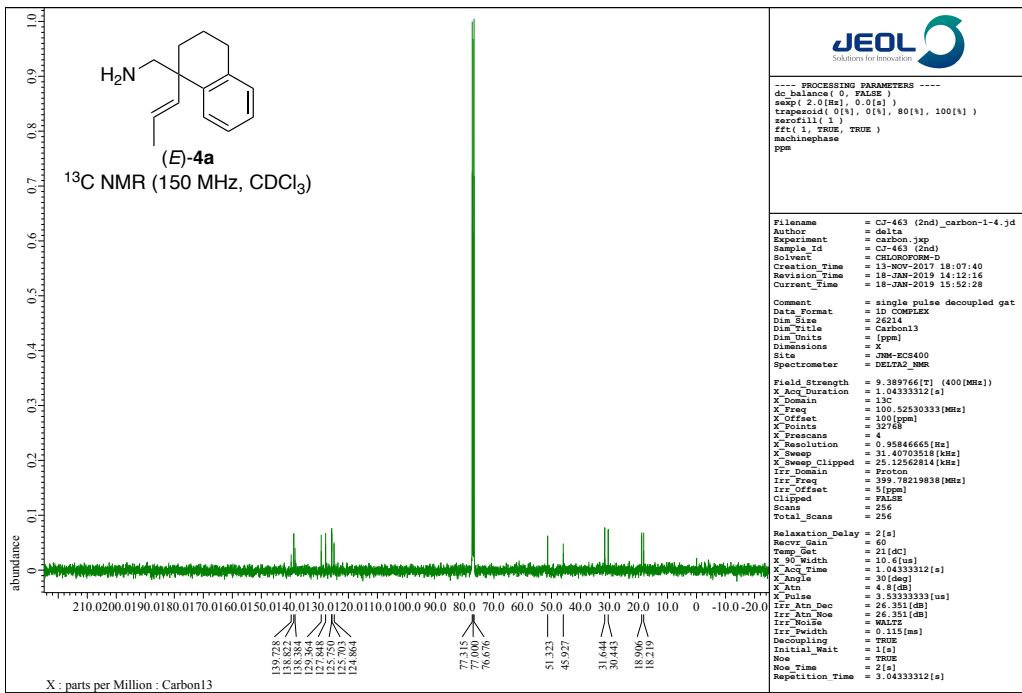
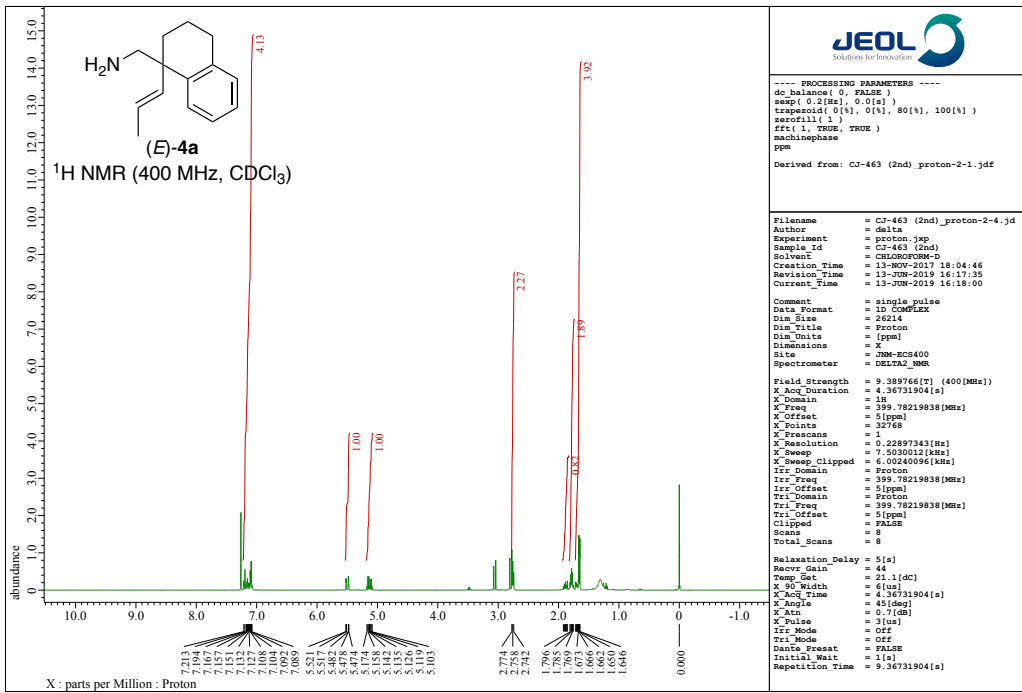


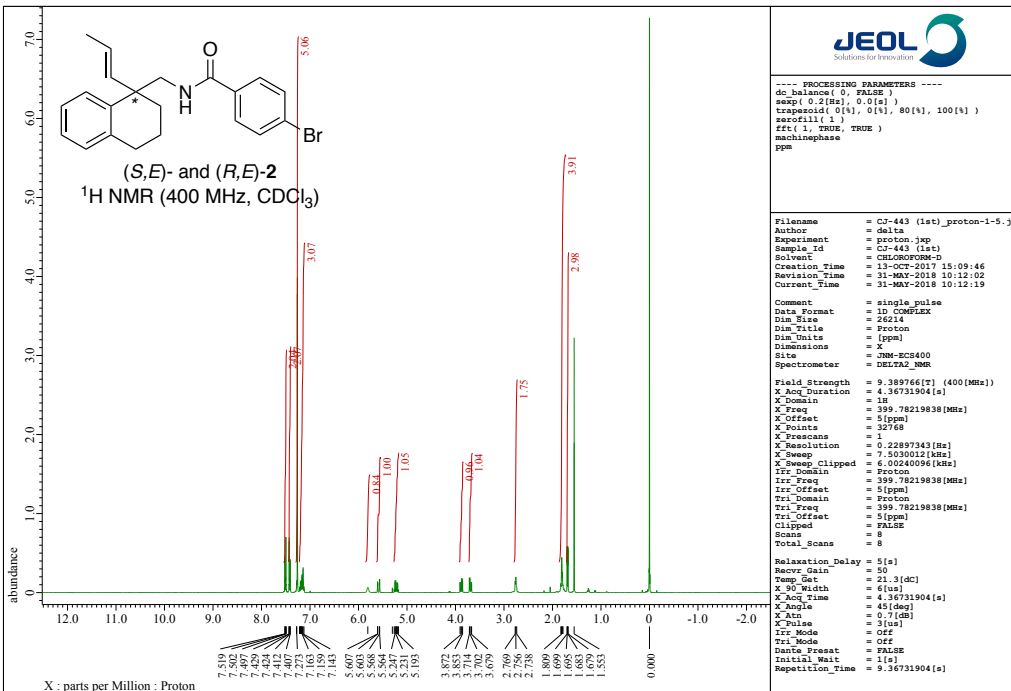
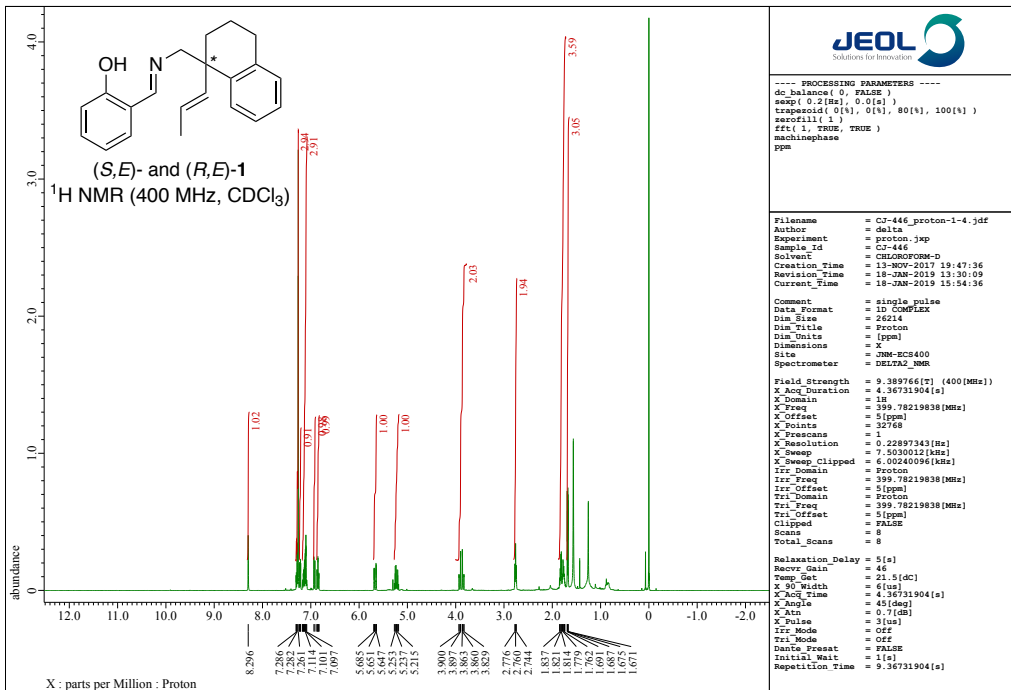
Chapter 4

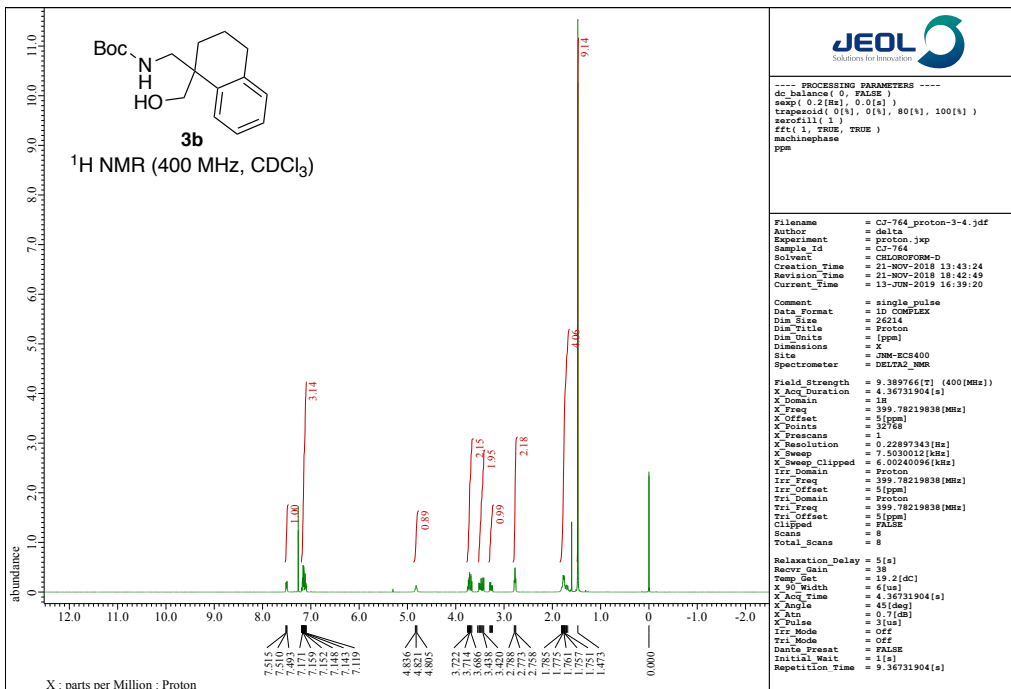
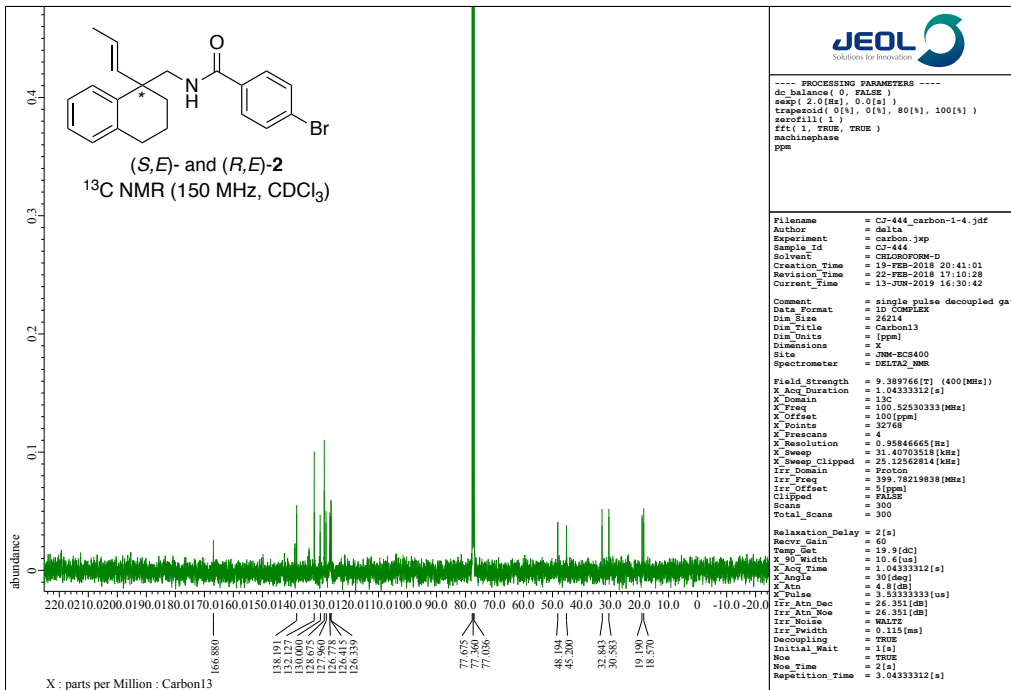


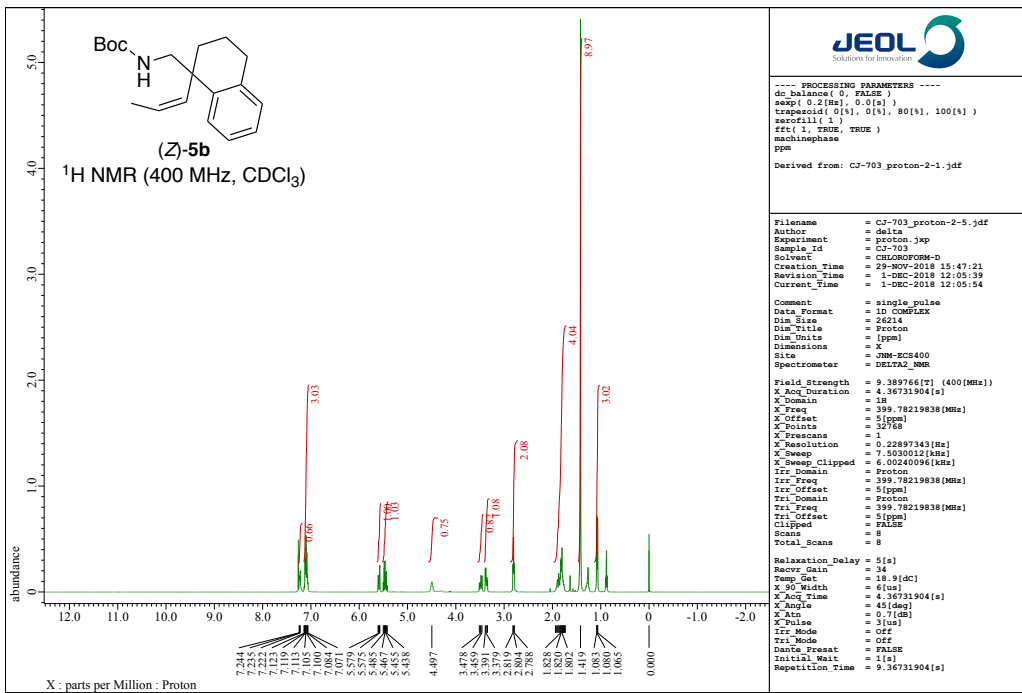
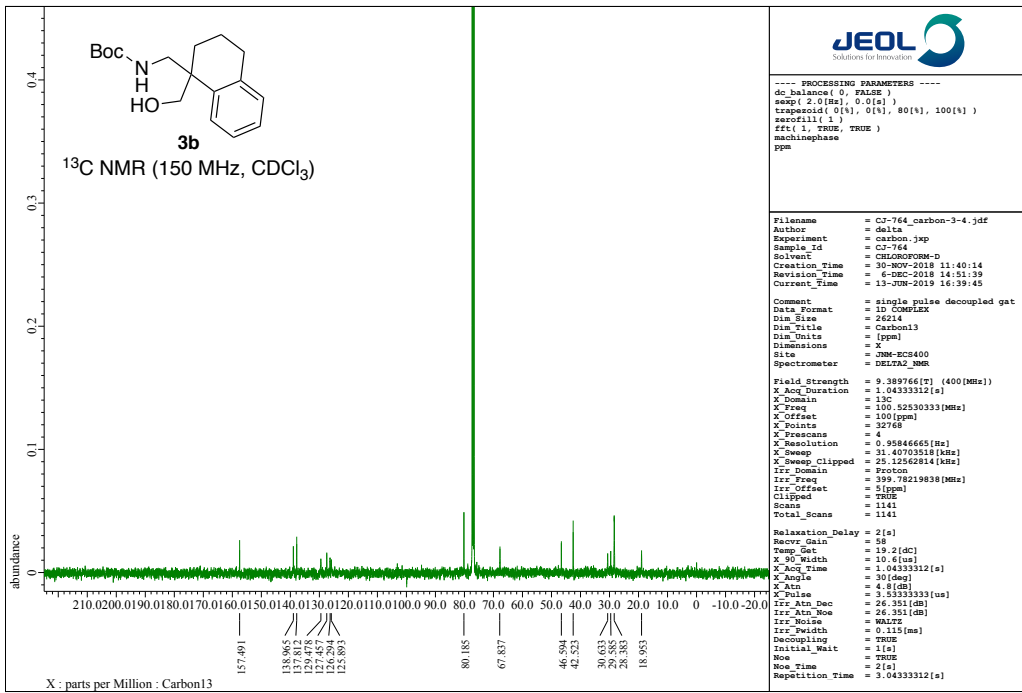


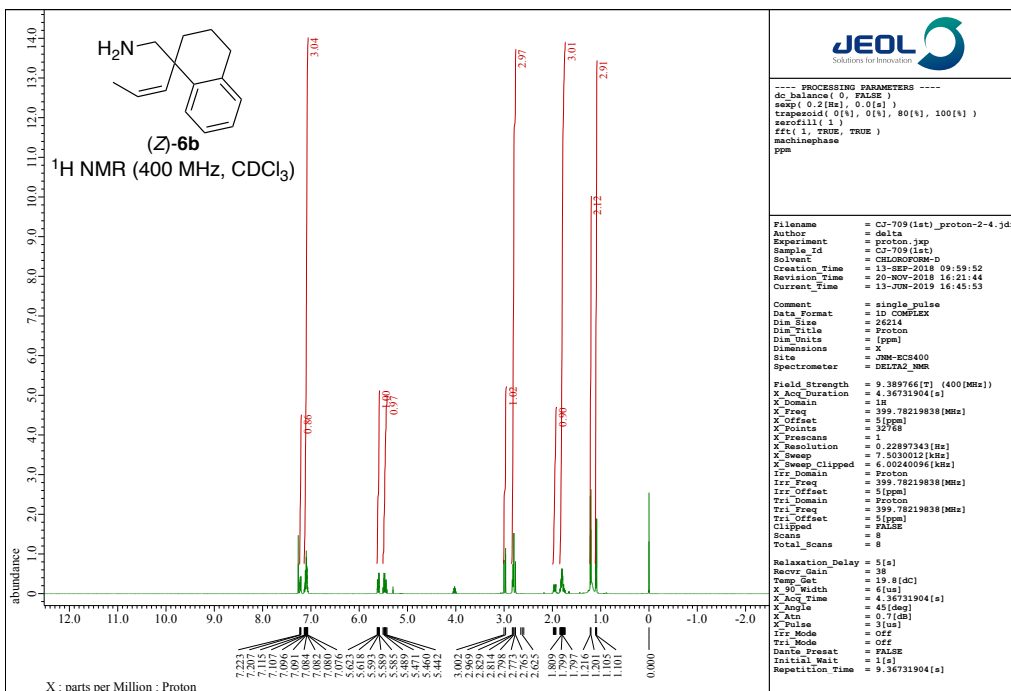
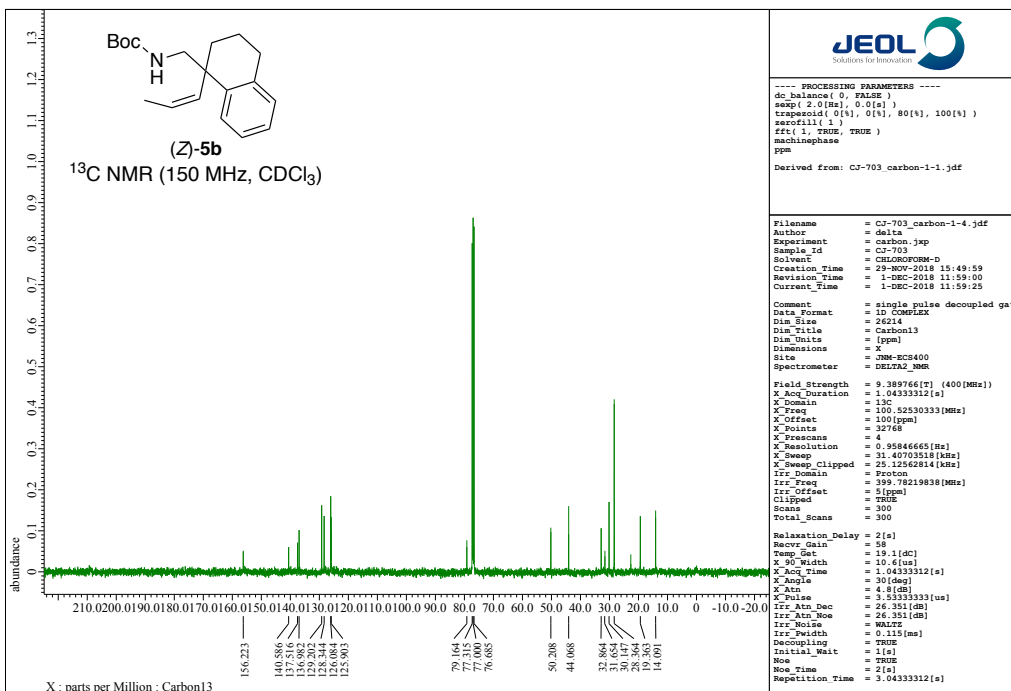


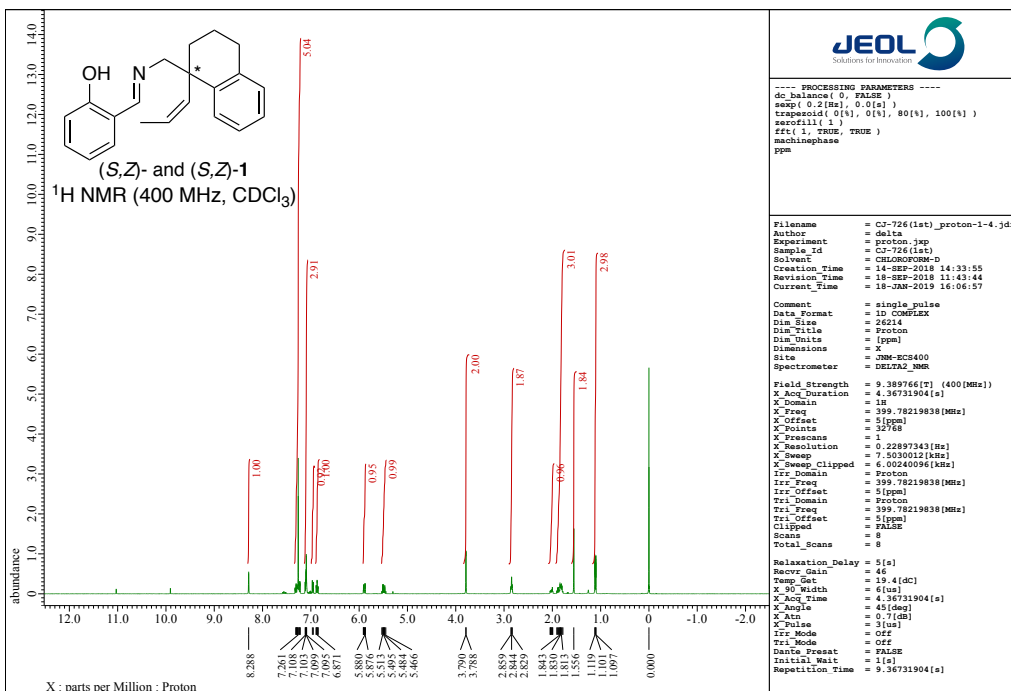
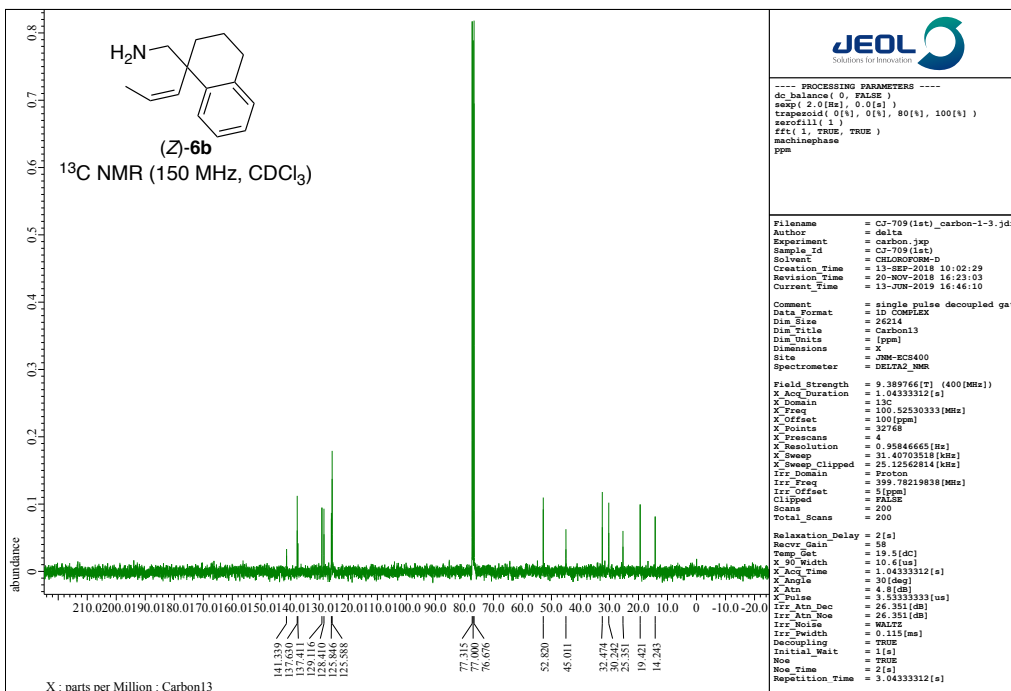


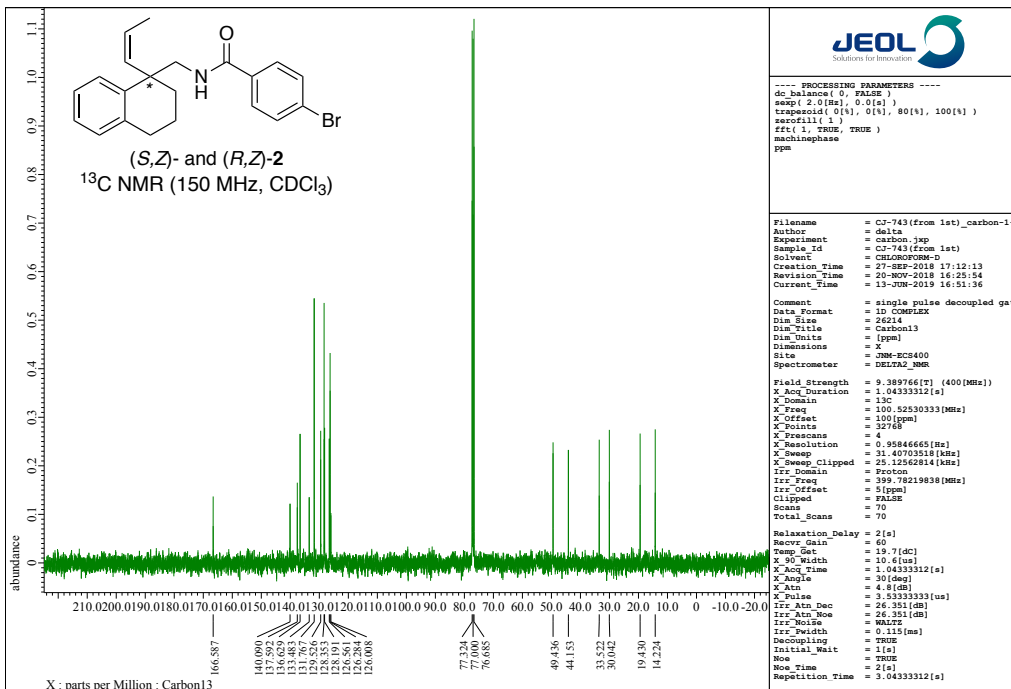
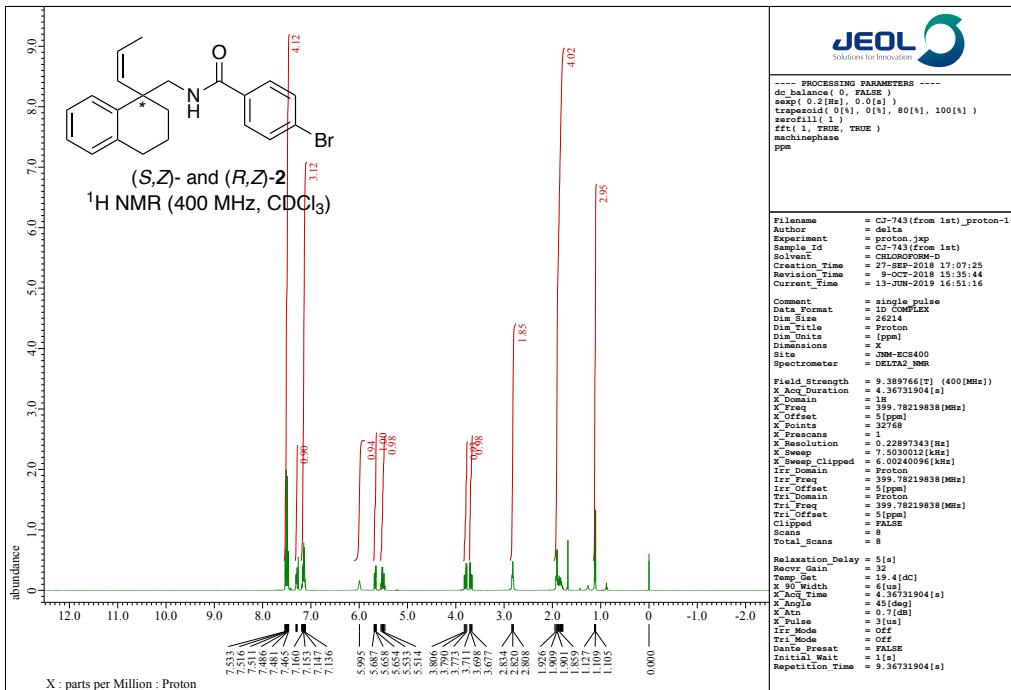


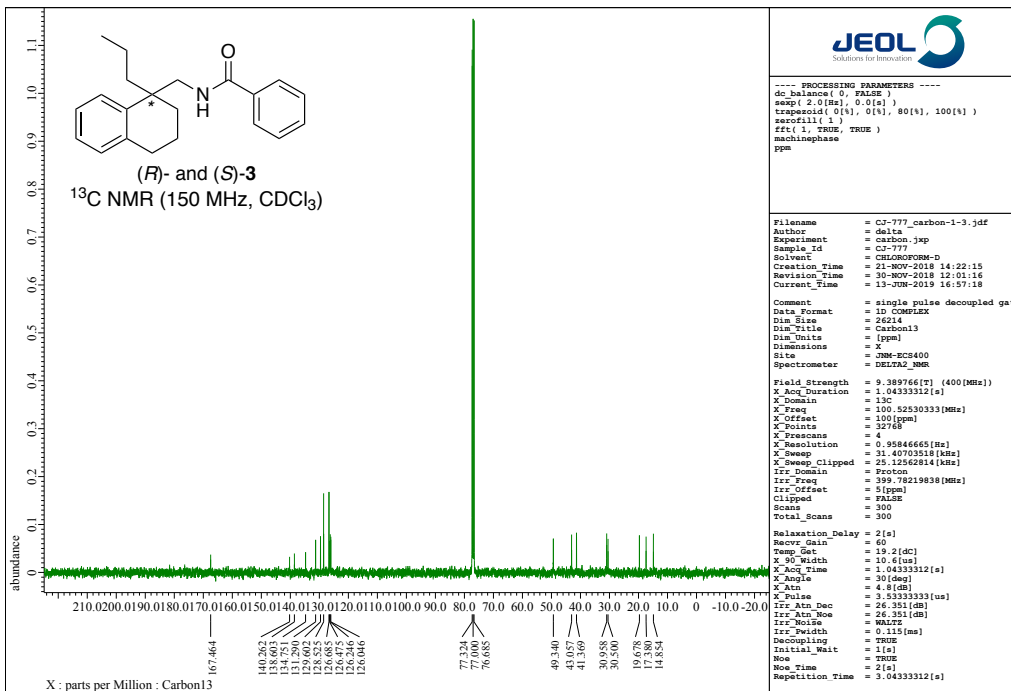
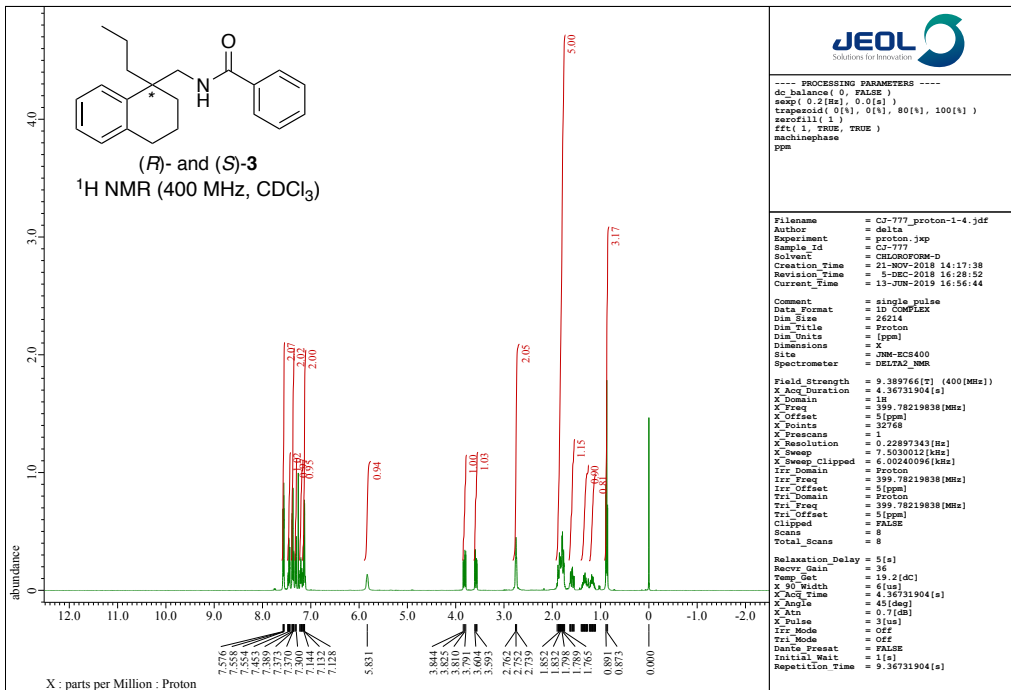


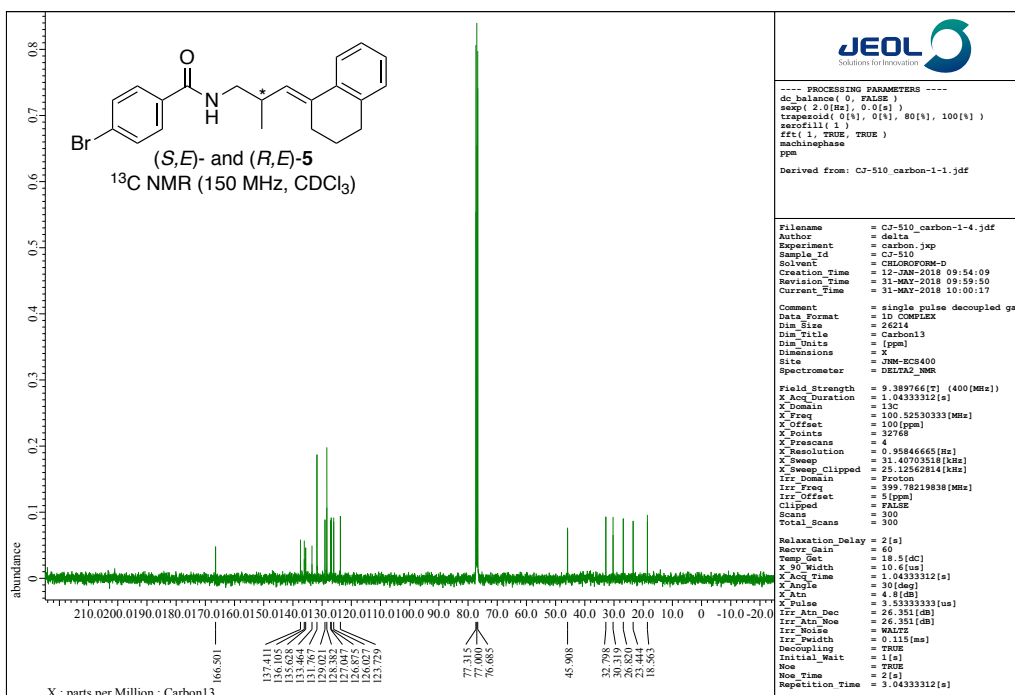
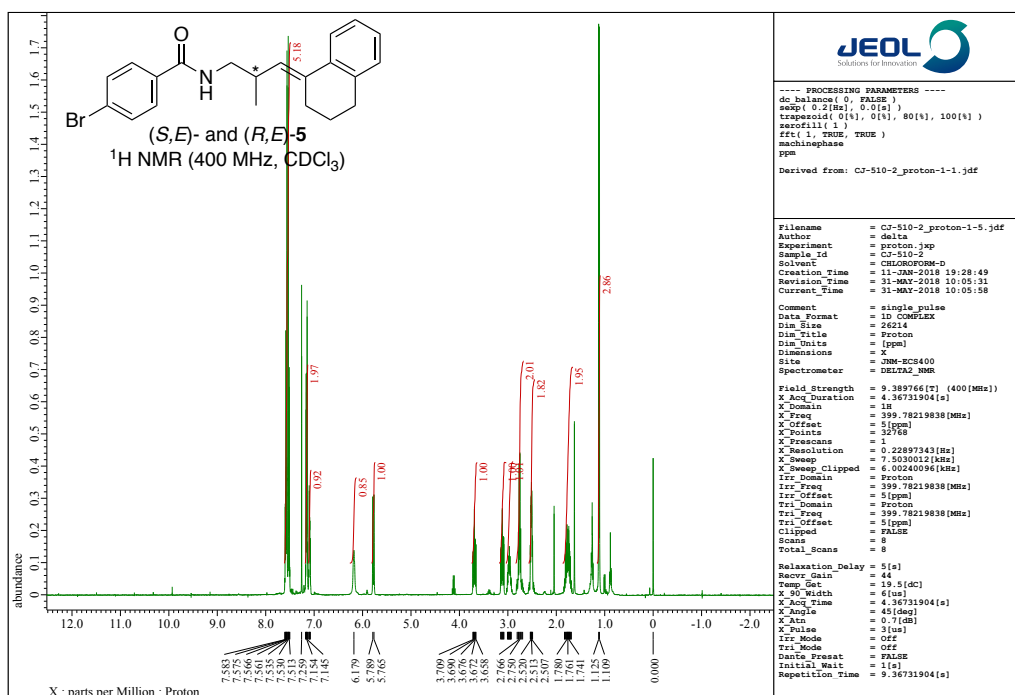




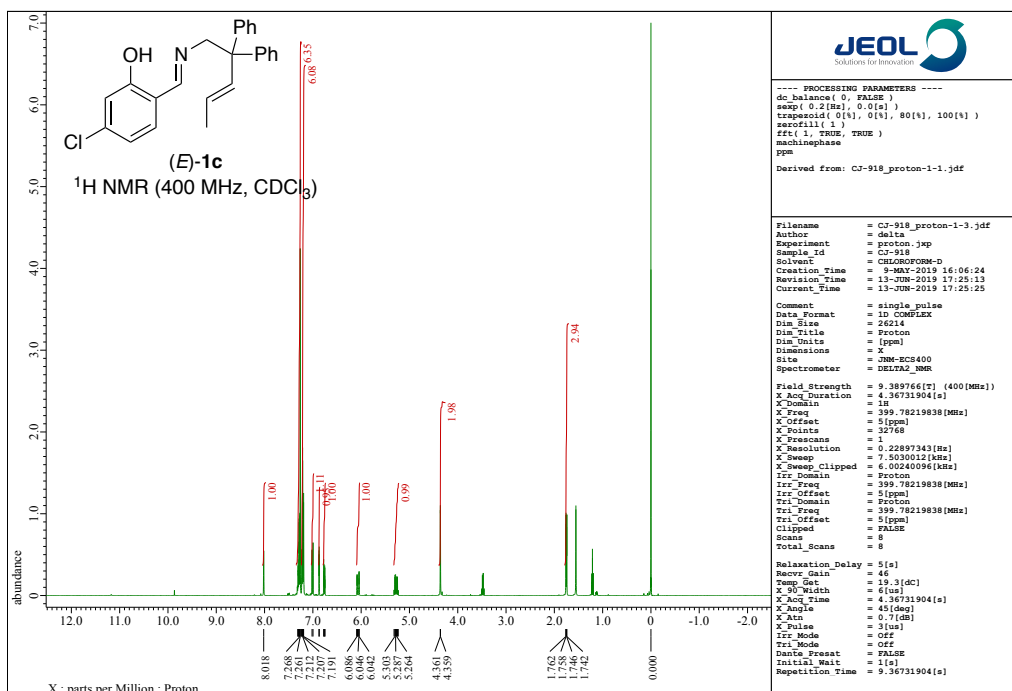
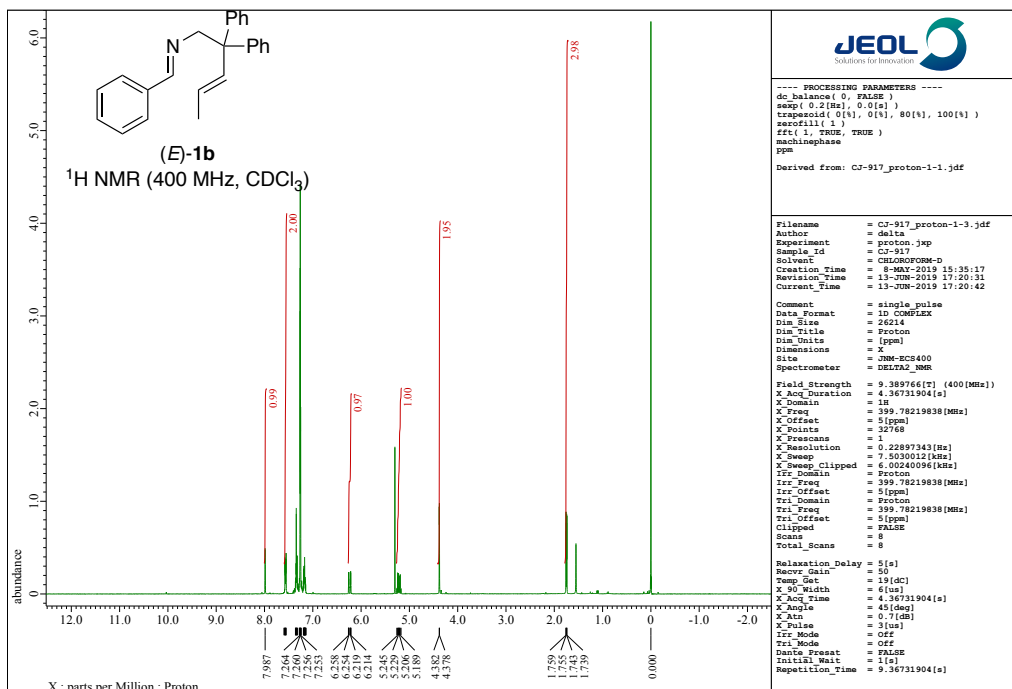


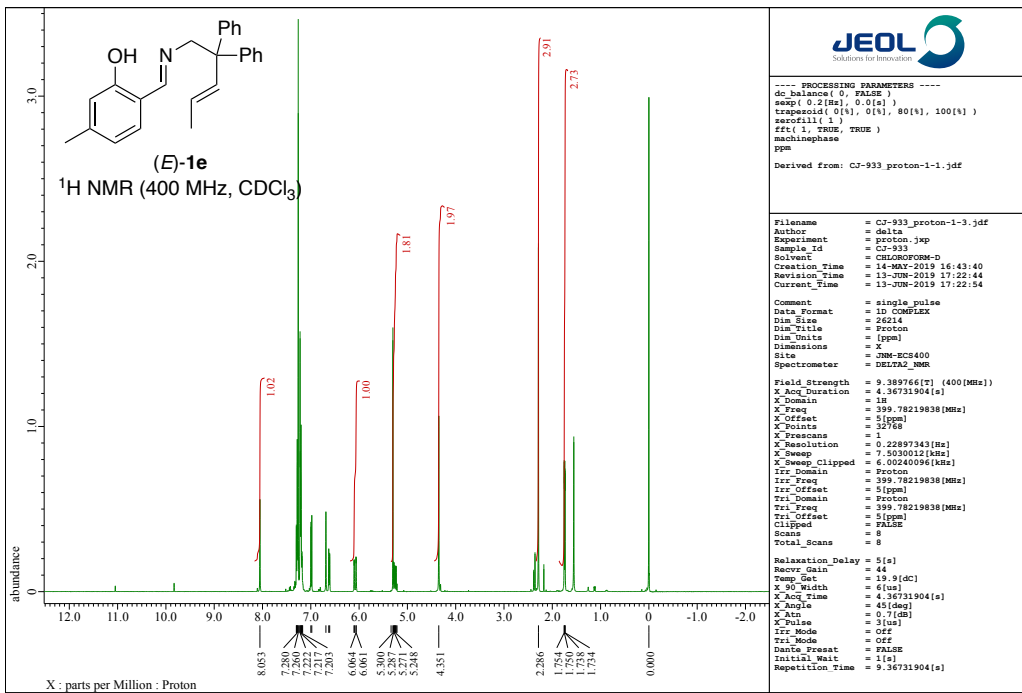
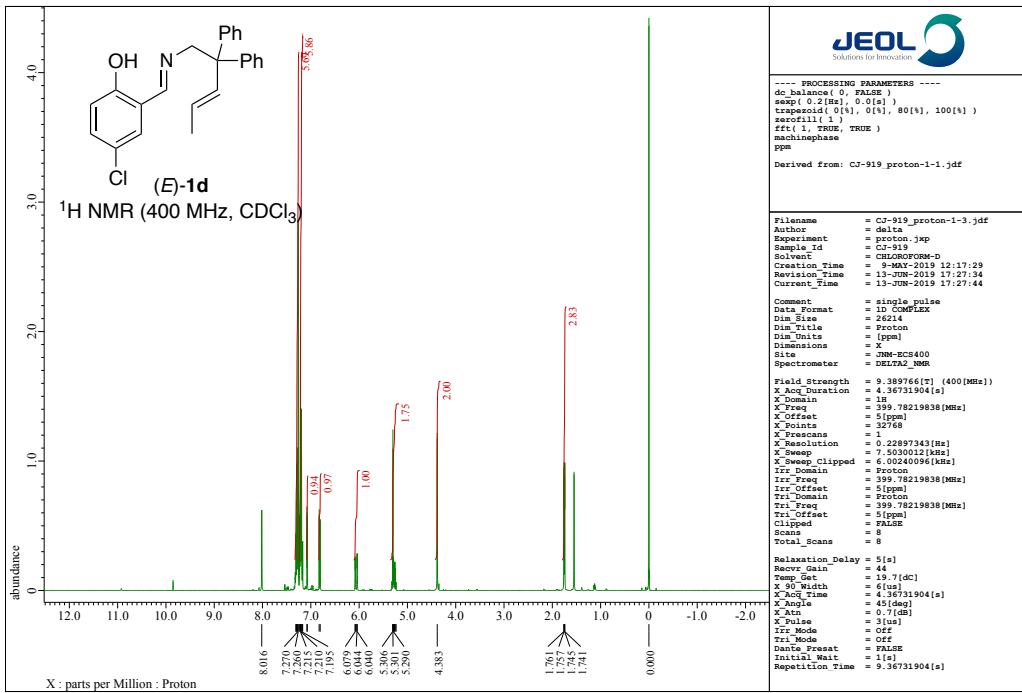


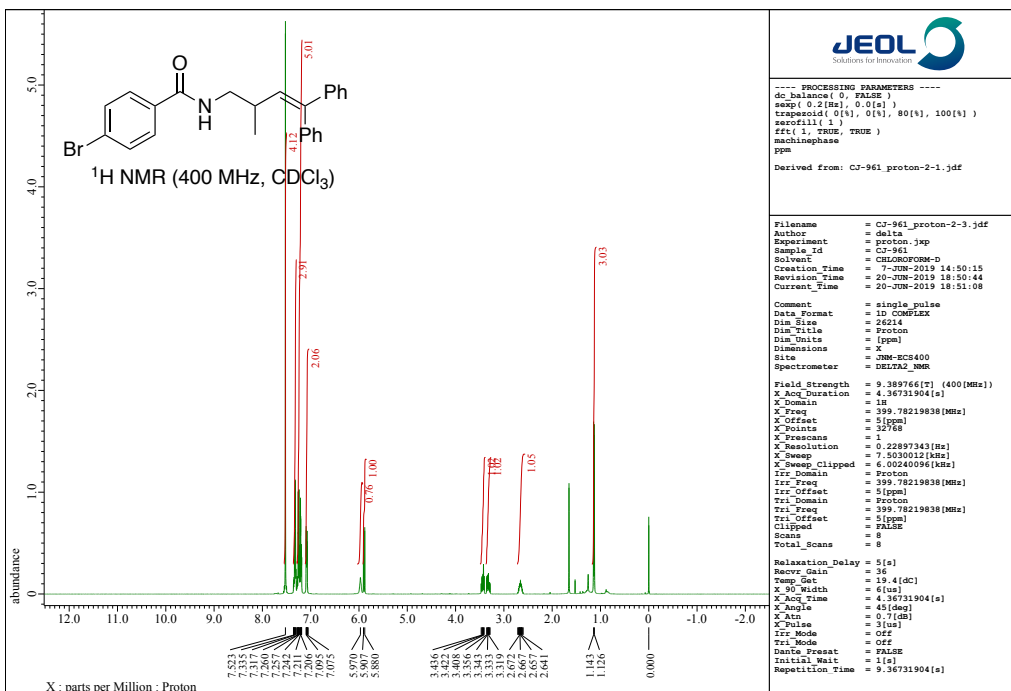
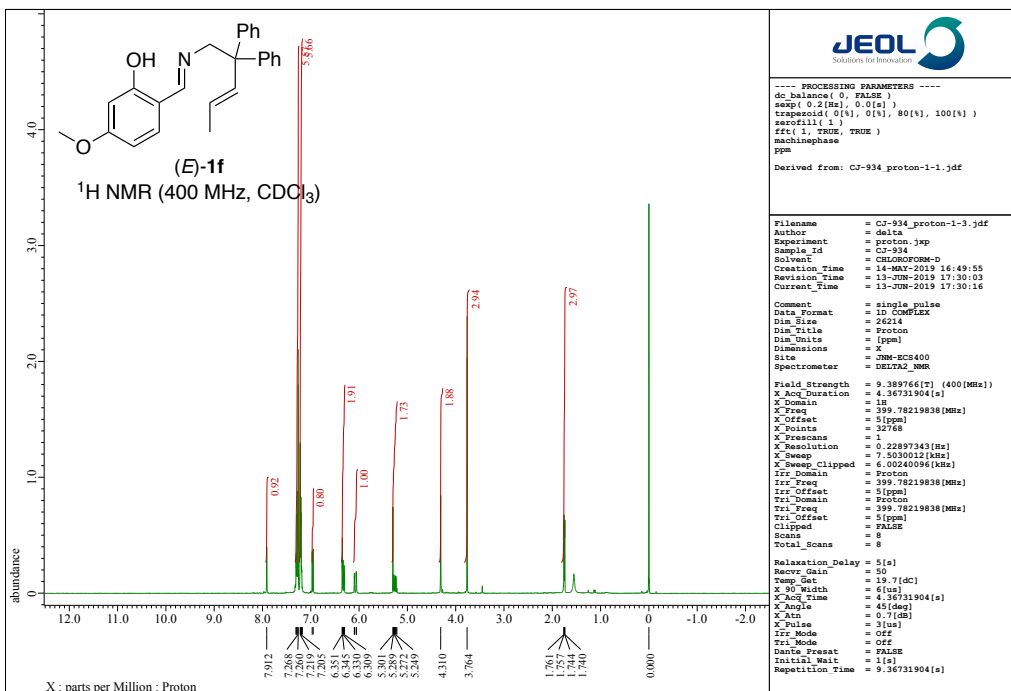


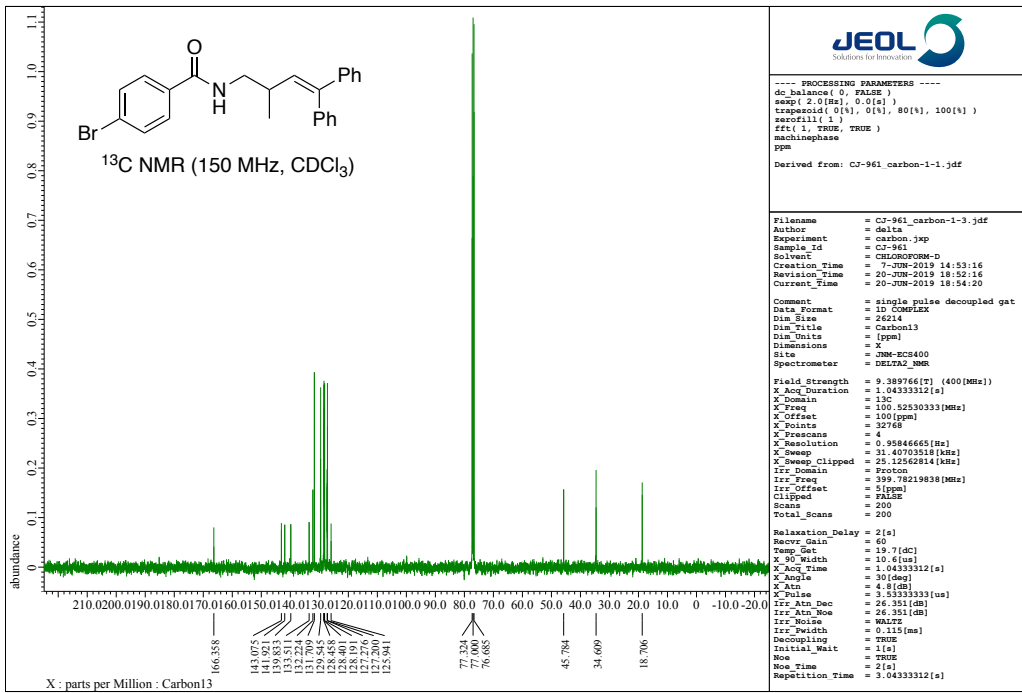


Chapter 5









B. DFT CALCULATIONS

Chapter 3

Table B1. Protonation of R1 (1a) with CSA.

structure	<i>E</i>	<i>H</i>	<i>G</i>	ΔG
CSA	-1089.6692452	-1089.392560	-1089.457192	
CSA ⁻	-1089.2111636	-1088.946593	-1089.011573	

CSA \cdots R1 (1a)	-1766.660002	-1766.025501	-1766.138629	0.00
CSA \cdots R1-H ⁺ (1a)	-1766.662992	-1766.026056	-1766.144933	-3.96

Table B2. 2-Azonia-[3,3]-sigmatropic rearrangement of R1-H⁺.

structure	<i>E</i>	<i>H</i>	<i>G</i>	ΔG
AC1	-677.4222199	-677.051055	-677.124263	0.00
TS-ac1	-677.3929236	-677.023357	-677.089522	21.80
AC2	-677.4278451	-677.056605	-677.127905	-2.29

Table B3. H1–N and C1–N distances (Å) between N1 and R1 in TS10-syn.

Short contacts less than the sum of van der Waals radii (H–N, 2.75 Å; C–N, 3.25 Å) are shown in red. These distances correlate well with ΔG s (kcal/mol).

TS10-syn	H1–N	C1–N	ΔG
<i>1b</i>	2.26	3.12	0.00
<i>1a</i>	2.18	3.13	0.61
<i>2b</i>	2.47	3.20	0.94
<i>2a</i>	2.88	3.45	1.09
<i>3b</i>	4.05	4.93	3.92
<i>3a</i>	4.00	4.87	4.17

Table B4. Ene-aldimines and their products.

structure	<i>E</i>	<i>H</i>	<i>G</i>	ΔG
4b (1a)	-674.7972744	-674.474627	-674.547269	0.00
5b (1b)	-674.8003797	-674.477074	-674.549133	-1.17

4f (1b)	-712.8686753	-712.538693	-712.612493	0.00
5f (1b)	-712.8696253	-712.539572	-712.611182	0.82

4g (1b)	-752.2022724	-751.841100	-751.918047	0.00
5g (1b)	-752.2084318	-751.847265	-751.921086	-1.91

4h (1b)	-791.5160191	-791.124440	-791.202694	0.00
---------	--------------	-------------	-------------	------

5h (<i>Ib-2</i>)	-791.5209020	-791.128719	-791.205433	-1.72
--------------------	--------------	-------------	-------------	-------

4h (<i>Ib</i>)	-791.5160191	-791.124440	-791.202694	0.00
5h (<i>Ib-2</i>)	-791.5209020	-791.128719	-791.205433	-1.72

4i (<i>Ib</i>)	-714.1013707	-713.748423	-713.826298	0.00
5i (<i>Ib</i>)	-714.1051095	-713.751580	-713.827539	-0.78

4k (<i>Ib</i>)	-753.4083513	-753.025530	-753.105315	0.00
5k (<i>Ib</i>)	-753.4093112	-753.026277	-753.106637	-0.83

Chapter 4

CSA and 2-azonia-[3,3]-sigmatropic rearrangement.

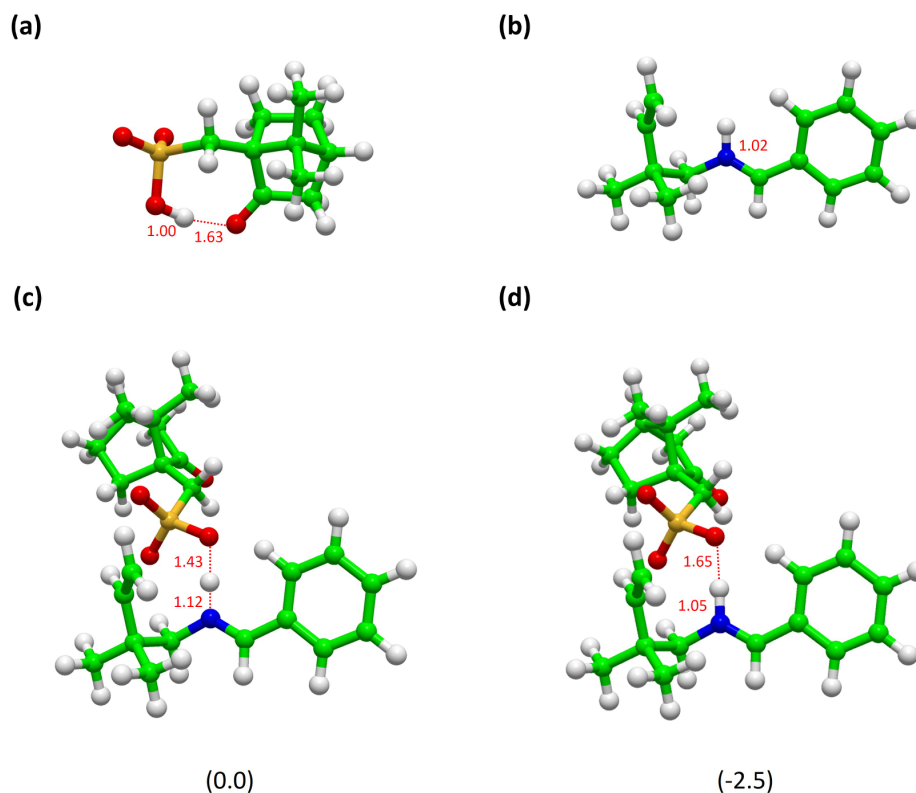


Figure B1. Protonation of R1(1a) with CSA. (a) CSA, (b) $\mathbf{R1-H}^+(1a)$, (c) CSA and $\mathbf{R1}(1a)$ without SMD, and (d) with SMD (DCE). The O–H and N–H distances are given in Å. Although protonation is not complete in vacuum (c), an ion pair of CSA^- and $\mathbf{R1-H}^+(1a)$ with a hydrogen bond (1.65 Å) is formed in DCE (d). Optimized geometries and the Gibbs free energies in parentheses (ΔG , in kcal/mol) were calculated at the SMD(DCE)/M06-2X-D3/6-311+G(d,p) level at 333 K for (a), (b), and (d). For (c), SMD(DCE)/M06-2X-D3/6-311+G(d,p)//M06-2X-D3/6-311+G(d,p) level was used at 333 K (Table B5).

Table B5. Protonation of R1 (1a) with CSA.

structure	E	H	G	ΔG
CSA	-1089.6692452	-1089.392560	-1089.457192	
CSA^-	-1089.2111636	-1088.946593	-1089.011573	

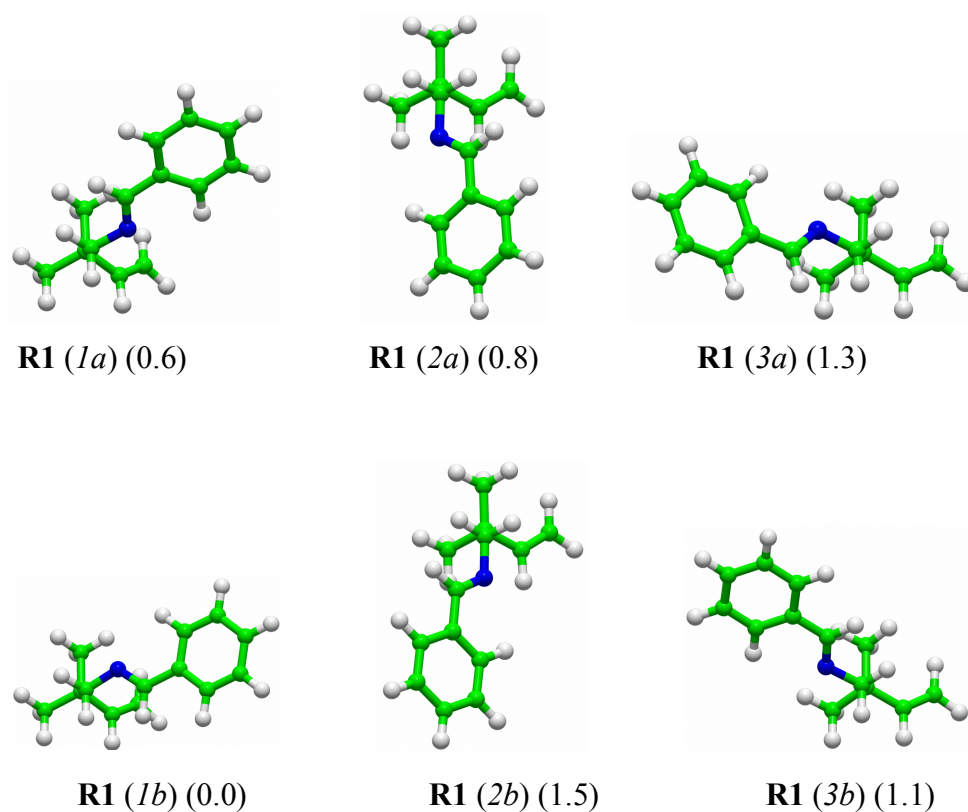


Figure B2. 3D Structure for conformations of **R1**. Imino groups are located at the equatorial position. Optimized geometries and the Gibbs free energies in parentheses (ΔG , in kcal/mol) were calculated at the SMD(DCE)/M06-2X-D3/6-311+G(d,p) level at 333 K (Table B6).

Table B6. 3D Structure for Conformations of **R1**

structure	E	H	G	ΔG
R1 (1b)	-676.9673460	-676.611224	-676.683192	0.00
R1 (3b)	-676.9663795	-676.610300	-676.682570	0.39
R1 (1a)	-676.9669579	-676.610862	-676.682418	0.49
R1 (3a)	-676.9663040	-676.610197	-676.682251	0.59
R1 (2a)	-676.9666553	-676.610392	-676.682134	0.66
R1 (2b)	-676.9665543	-676.610357	-676.682079	0.70

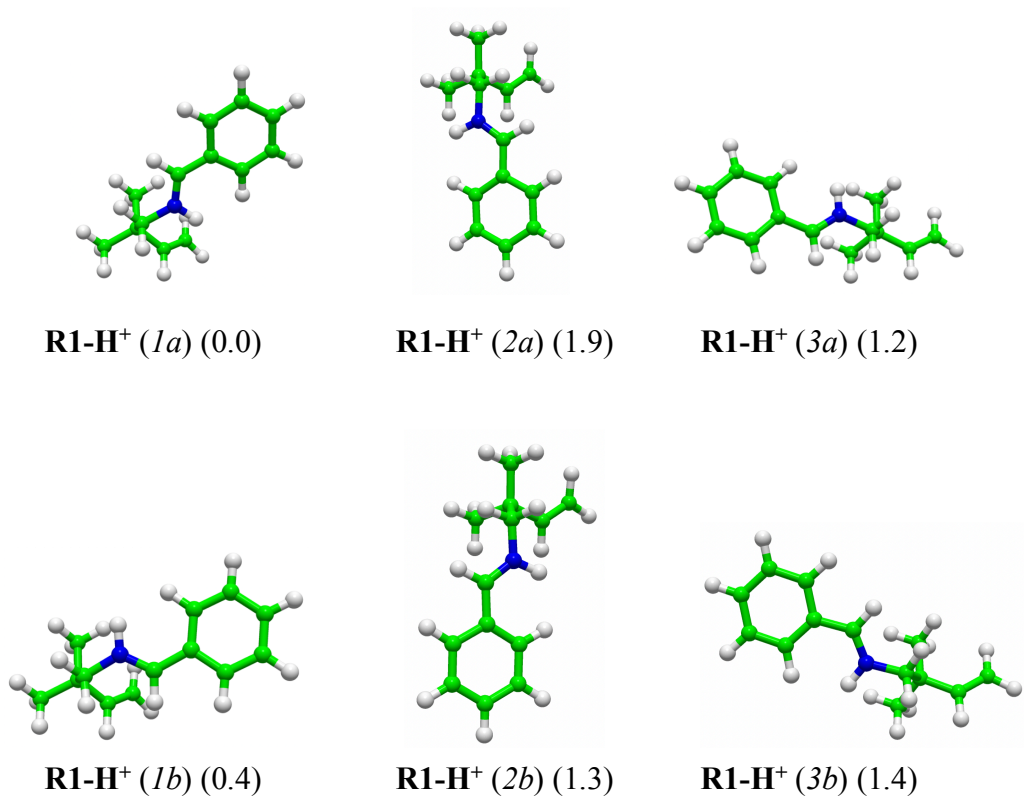


Figure B3. 3D structure for conformations of R1-H⁺. Imino groups are located at the equatorial position. Optimized geometries and the Gibbs free energies in parentheses (ΔG , in kcal/mol) were calculated at the SMD(DCE)/M06-2X-D3/6-311+G(d,p) level at 333 K (Table B7).

Figure B7. 3D Structure for Conformations of R1-H⁺.

structure	<i>E</i>	<i>H</i>	<i>G</i>	ΔG
R1-H ⁺ (1a)	-560.7005877	-560.397996	-560.463721	0.00
R1-H ⁺ (1b)	-560.7005420	-560.397918	-560.463164	0.35
R1-H ⁺ (2a)	-560.6985432	-560.395546	-560.460624	1.94
R1-H ⁺ (2b)	-560.6983543	-560.395621	-560.461674	1.28
R1-H ⁺ (3a)	-560.6984492	-560.395926	-560.461837	1.18
R1-H ⁺ (3b)	-560.6985125	-560.395921	-560.461444	1.43

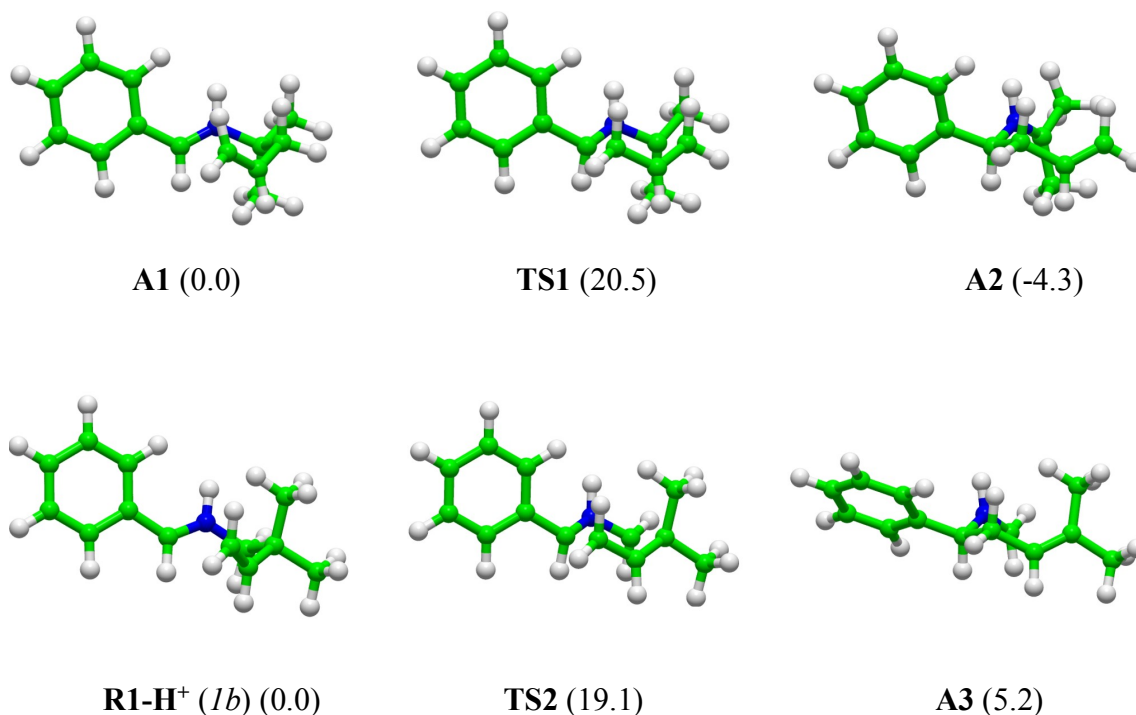


Figure B4. 2-Azonia-[3,3]-sigmatropic rearrangement *via* concerted chair transition states. (a) α -Substituted ene-aldimine and (b) β -substituted ene-aldimine. Optimized geometries and the Gibbs free energies in parentheses (ΔG , in kcal/mol) were calculated at the SMD(DCE)/M06-2X-D3/6-311+G(d,p) level at 333 K (Table B8).

Table B8. 2-Azonia-[3,3]-Sigmatropic Rearrangement *via* Concerted Chair Transition States

structure	<i>E</i>	<i>H</i>	<i>G</i>	ΔG
A1	-560.7030206	-560.400999	-560.466866	0.00
TS1	-560.6740695	-560.373280	-560.434191	20.5
A2	-560.7075684	-560.405470	-560.473745	-4.32
R1-H ⁺ (<i>Ib</i>)	-560.7005420	-560.397918	-560.463164	0.00
TS2	-560.6721483	-560.371404	-560.432681	19.1
A3	-560.6896152	-560.387469	-560.454827	5.23

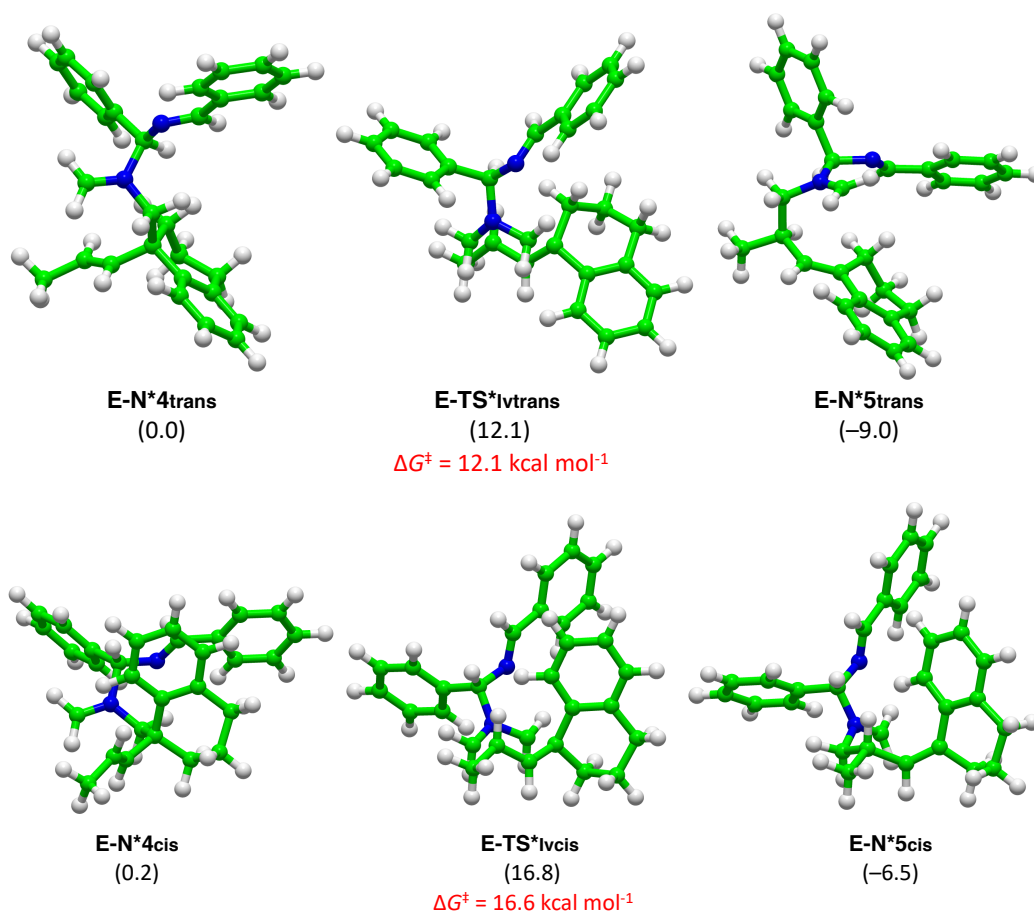


Figure B5. DFT calculation for 2-azonia-[3,3]-sigmatropic rearrangement step in asymmetric formal [1,3]-rearrangement of (*R,E*)-ene-aldimine substrate. The Gibbs free energies in parentheses (ΔG , in kcal/mol) were calculated at the SMD(DCE)/M06-2X-D3/6-311+G(d,p) level at 333 K. Compound name of “cis” and “trans” is based on the relative configuration of the allyl group to the benzo group of tetrahydronaphthalene (Table B9).

Table B9. 2-Azonia-[3,3]-Sigmatropic Rearrangement of E-N*4trans to E-TS*5trans

structure	<i>E</i>	<i>H</i>	<i>G</i>	ΔG
E-N*4trans	-1232.8784638	-1232.309218	-1232.414375	0.00
E-TS*IVtrans	-1232.8617322	-1232.293608	-1232.395089	12.10
E-N*5trans	-1232.8936525	-1232.323971	-1232.428676	-8.97
E-N*4cis	-1232.8781095	-1232.310042	-1232.414110	0.17
E-TS*IVcis	-1232.8527388	-1232.285760	-1232.387679	16.75
E-N*5cis	-1232.8894494	-1232.320015	-1232.424762	-6.52

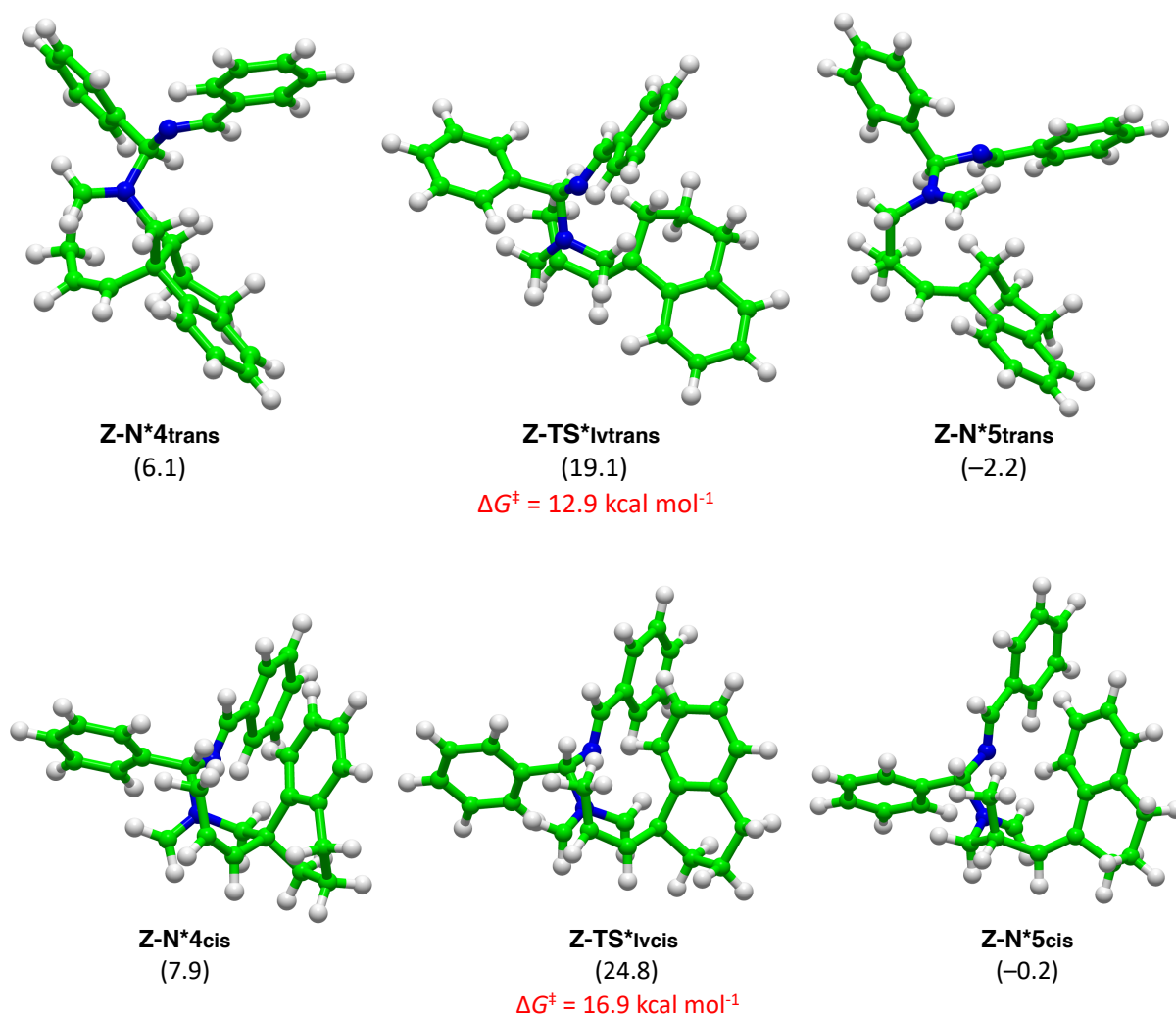


Figure B6. DFT calculation for 2-azonia-[3,3]-sigmatropic rearrangement step in asymmetric formal [1,3]-rearrangement of (*R,Z*)-ene-aldimine substrate. The Gibbs free energies in parentheses (ΔG , in kcal/mol) were calculated at the SMD(DCE)/M06-2X-D3/6-311+G(d,p) level at 333 K. Compound name of “cis” and “trans” is based on the relative configuration of the allyl group to the benzo group of tetrahydronaphthalene (Table B10).

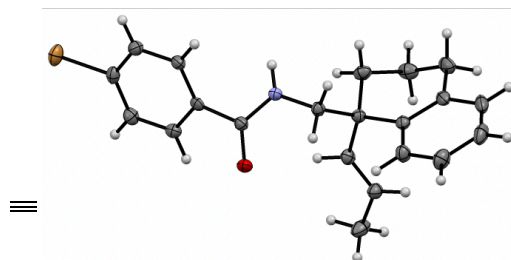
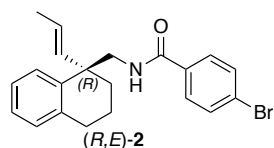
Table B10. 2-Azonia-[3,3]-Sigmatropic Rearrangement of Z-N*4 to Z-TS*5trans

structure	<i>E</i>	<i>H</i>	<i>G</i>	ΔG
Z-N*4trans	-1232.8726928	-1232.302816	-1232.404622	6.12
Z-TS*IVtrans	-1232.8505636	-1232.282687	-1232.384016	19.05
Z-N*5trans	-1232.8844443	-1232.314190	-1232.417935	-2.23
Z-N*4cis	-1232.8664020	-1232.297356	-1232.401758	7.92
Z-TS*IVcis	-1232.8420455	-1232.274295	-1232.374870	24.79
Z-N*5cis	-1232.8802710	-1232.311046	-1232.414670	-0.19

C. CRYSTAL DATA REPORTS

Chapter 4

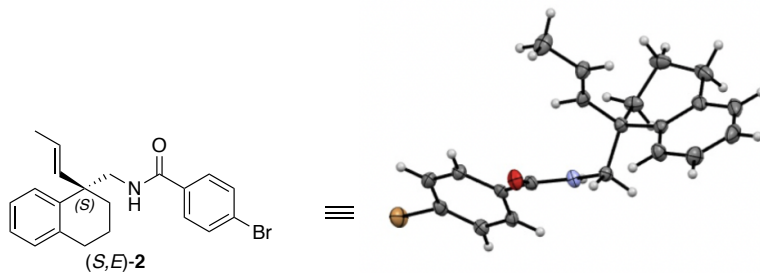
1. X-ray diffraction analysis for (*R,E*)-2 (CCDC 1847527)



Empirical formula	C ₂₁ H ₂₂ BrNO
Formula weight	384.31
Temperature/K	123
Crystal system	orthorhombic
Space group	<i>P</i> 2 ₁ 2 ₁ 2
<i>a</i> /Å	9.8209(2)
<i>b</i> /Å	11.2922(3)
<i>c</i> /Å	16.3132(2)
$\alpha = \beta = \gamma$ /°	90
Volume/Å ³	1809.23(7)
<i>Z</i>	4
ρ_{calc} g/cm ³	1.411
μ /mm ⁻¹	2.285
<i>F</i> (000)	792.00

Crystal size/mm ³	0.300 × 0.300 × 0.300
Radiation	Mo Ka (λ = 0.71073 Å)
2θ range for data collection/°	6.038 to 54.866
Index ranges	-12 ≤ h ≤ 10, -14 ≤ k ≤ 14, -21 ≤ l ≤ 21
Reflections collected	16722
Independent reflections	3958 [R _{int} = 0.0182]
Data/restraints/parameters	4872/0/218
Goodness-of-fit on F ²	1.072
Final R indexes [I ≥ 2σ(I)]	R ₁ = 0.0186, wR ₂ = 0.0474
Final R indexes [all data]	R ₁ = 0.0201, wR ₂ = 0.0479
Largest diff. peak/hole / e Å ⁻³	0.23/-0.46
Flack parameter	0.028(4)

2. X-ray diffraction analysis for (*S,E*)-2 (CCDC 1847529)



Empirical formula	C ₂₁ H ₂₂ BrNO
Formula weight	384.31
Temperature/K	123
Crystal system	orthorhombic
Space group	<i>P</i> 2 ₁ 2 ₁ 2
<i>a</i> /Å	9.8257(5)
<i>b</i> /Å	11.2965(6)
<i>c</i> /Å	16.2909(10)
$\alpha = \beta = \gamma^\circ$	90
Volume/Å ³	1808.23(17)
<i>Z</i>	4
ρ_{calc} g/cm ³	1.412
μ /mm ⁻¹	2.287
<i>F</i> (000)	792.00
Crystal size/mm ³	0.300 × 0.300 × 0.300

Radiation	Mo Ka ($\lambda = 0.71073 \text{ \AA}$)
2Θ range for data collection/ $^\circ$	6.038 to 54.940
Index ranges	$-12 \leq h \leq 12, -14 \leq k \leq 14, -19 \leq l \leq 21$
Reflections collected	17226
Independent reflections	3958 [$R_{\text{int}} = 0.0452$]
Data/restraints/parameters	4105/0/218
Goodness-of-fit on F^2	1.070
Final R indexes [$I \geq 2\sigma(I)$]	$R_1 = 0.0251, wR_2 = 0.0577$
Final R indexes [all data]	$R_1 = 0.0285, wR_2 = 0.0587$
Largest diff. peak/hole / $e \text{ \AA}^{-3}$	0.46/-0.46
Flack parameter	0.028(4)

3. X-ray diffraction analysis for (*R,Z*)-2

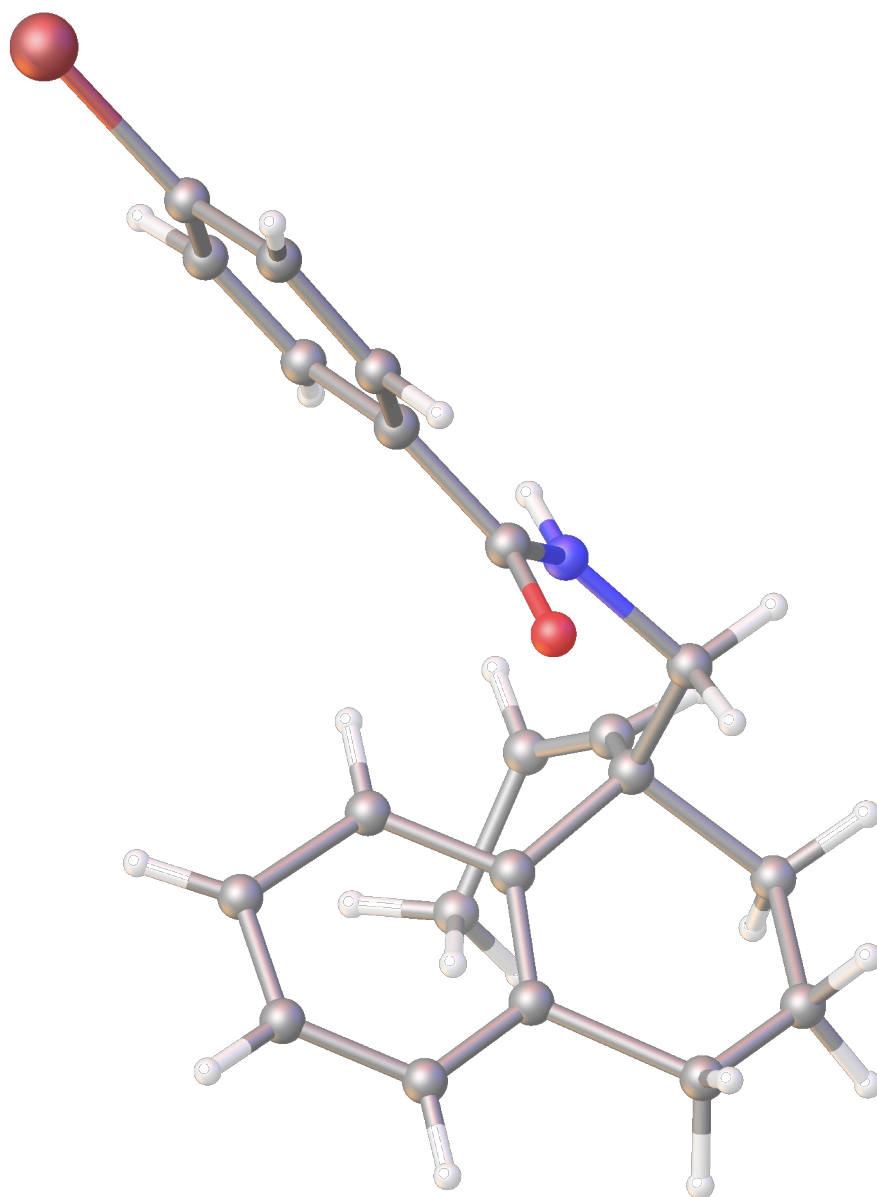
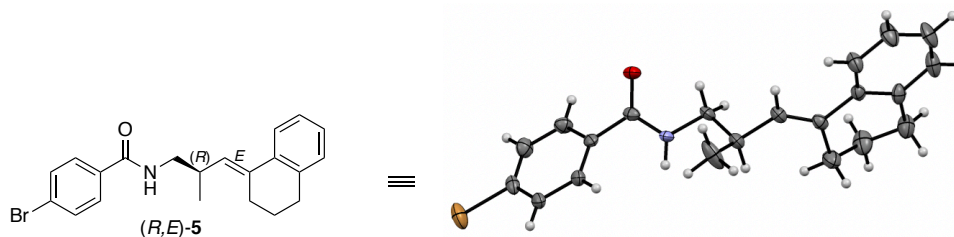


Figure C1. ORTEP diagram of (*R,Z*)-2 substrate by Sponge X-ray analysis

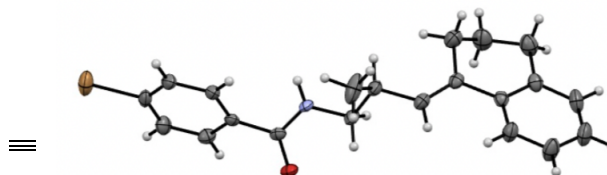
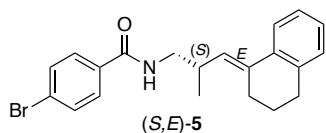
4. X-ray diffraction analysis for (*R,E*)-5 (CCDC 1847526)



Empirical formula	C ₂₁ H ₂₂ BrNO
Formula weight	384.31
Temperature/K	123
Crystal system	orthorhombic
Space group	<i>P</i> 2 ₁ 2 ₁ 2
<i>a</i> /Å	17.6389(6)
<i>b</i> /Å	21.2175(7)
<i>c</i> /Å	4.9308(3)
$\alpha = \beta = \gamma$	90
Volume/Å ³	1845.37(14)
<i>Z</i>	4
ρ_{calc} g/cm ³	1.383
μ /mm ⁻¹	2.241
<i>F</i> (000)	792.00
Crystal size/mm ³	0.356 × 0.272 × 0.150
Radiation	Mo K α (λ = 0.71073 Å)

2 Θ range for data collection/ $^{\circ}$	4.480 to 54.966
Index ranges	$-22 \leq h \leq 18$, $-26 \leq k \leq 27$, $-4 \leq l \leq 6$
Reflections collected	9247
Independent reflections	4130 [$R_{\text{int}} = 0.0233$, $R_{\text{sigma}} = 0.0236$]
Data/restraints/parameters	4130/0/217
Goodness-of-fit on F^2	1.081
Final R indexes [$I \geq 2\sigma(I)$]	$R_1 = 0.0343$, $wR_2 = 0.0820$
Final R indexes [all data]	$R_1 = 0.0442$, $wR_2 = 0.0858$
Largest diff. peak/hole / e \AA^{-3}	0.39/-0.52
Flack parameter	-0.010(4)

5. X-ray diffraction analysis for (S,E)-5 (CCDC 1847528)

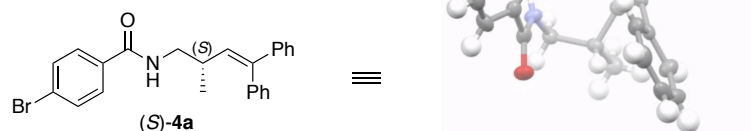


Empirical formula	C ₂₁ H ₂₂ BrNO
Formula weight	384.31
Temperature/K	123
Crystal system	orthorhombic
Space group	<i>P</i> 2 ₁ 2 ₁ 2
<i>a</i> /Å	17.6276(9)
<i>b</i> /Å	21.2274(9)
<i>c</i> /Å	4.9342(2)
$\alpha = \beta = \gamma$ °	90
V olume/Å ³	1846.32(14)
<i>Z</i>	4
ρ_{calc} g/cm ³	1.382
μ /mm ⁻¹	2.240
<i>F</i> (000)	792.00
Crystal size/mm ³	0.333 × 0.298 × 0.123
Radiation	Mo K α (λ = 0.71073 Å)

2 Θ range for data collection/ $^{\circ}$	4.480 to 62.504
Index ranges	$-23 \leq h \leq 22$, $-27 \leq k \leq 22$, $-6 \leq l \leq 7$
Reflections collected	12666
Independent reflections	4872 [$R_{\text{int}} = 0.0397$, $R_{\text{sigma}} = 0.0571$]
Data/restraints/parameters	4872/0/217
Goodness-of-fit on F^2	1.036
Final R indexes [$I \geq 2\sigma(I)$]	$R_1 = 0.0382$, $wR_2 = 0.0724$
Final R indexes [all data]	$R_1 = 0.0581$, $wR_2 = 0.0769$
Largest diff. peak/hole / e \AA^{-3}	0.33/-0.42
Flack parameter	-0.017(6)

Chapter 5

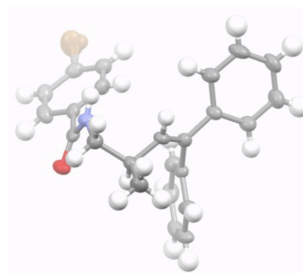
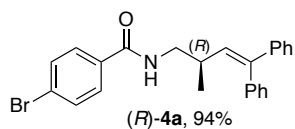
6. X-ray diffraction analysis for (S)-4a



Empirical formula	C ₂₄ H ₂₂ BrNO
Formula weight	420.35
Temperature/K	123
Crystal system	orthorhombic
Space group	<i>P</i> 2 ₁ 2 ₁ 2 ₁
<i>a</i> /Å	9.5491(5)
<i>b</i> /Å	10.0701(5)
<i>c</i> /Å	21.5141(11)
$\alpha = \beta = \gamma$ °	90
Volume/Å ³	2068.7(2)
<i>Z</i>	4
ρ_{calc} g/cm ³	1.349
μ /mm ⁻¹	2.005
<i>F</i> (000)	864.00

Crystal size/mm ³	0.464 × 0.424 × 0.261
Radiation	Mo Ka (λ = 0.71073 Å)
2θ range for data collection/°	4.666 to 54.968
Index ranges	-9 ≤ h ≤ 12, -13 ≤ k ≤ 9, -27 ≤ l ≤ 27
Reflections collected	4389
Independent reflections	4389 [R _{int} = 0.0979, R _{sigma} = 0.1096]
Data/restraints/parameters	4389/0/253
Goodness-of-fit on F ²	0.965
Final R indexes [I ≥ 2σ(I)]	R ₁ = 0.0564, wR ₂ = 0.1039
Final R indexes [all data]	R ₁ = 0.0859, wR ₂ = 0.1136
Largest diff. peak/hole / e Å ⁻³	0.39/-0.26
Flack parameter	-0.010(13)

7. X-ray diffraction analysis for (R)-4a



Empirical formula	C ₂₄ H ₂₂ BrNO
Formula weight	420.35
Temperature/K	123
Crystal system	orthorhombic
Space group	<i>P</i> 2 ₁ 2 ₁ 2 ₁
<i>a</i> /Å	9.5545(5)
<i>b</i> /Å	10.0690(7)
<i>c</i> /Å	21.5034(10)
$\alpha = \beta = \gamma$	90
Volume/Å ³	2068.7(2)
<i>Z</i>	4
ρ_{calc} g/cm ³	1.350
μ /mm ⁻¹	2.005
<i>F</i> (000)	864.00
Crystal size/mm ³	0.648X 0.490X 0.321
Radiation	Mo Ka ($\lambda = 0.71073$ Å)

2 Θ range for data collection/ $^{\circ}$	5.704 to 54.962
Index ranges	$-12 \leq h \leq 9$, $-13 \leq k \leq 12$, $-22 \leq l \leq 67$
Reflections collected	4451
Independent reflections	4451 [$R_{\text{int}} = 0.0856$, $R_{\text{sigma}} = 0.0822$]
Data/restraints/parameters	4451/0/253
Goodness-of-fit on F^2	0.978
Final R indexes [$I \geq 2\sigma(I)$]	$R_1 = 0.0511$, $wR_2 = 0.1001$
Final R indexes [all data]	$R_1 = 0.0780$, $wR_2 = 0.1092$
Largest diff. peak/hole / e \AA^{-3}	0.29/-0.27
Flack parameter	-0.006(11)